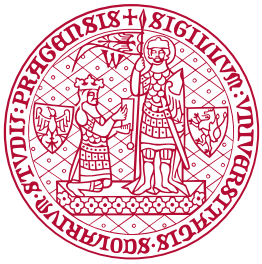

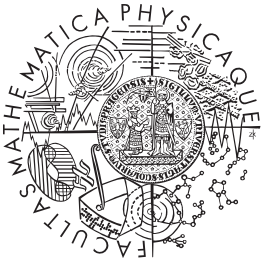

CHARLES UNIVERSITY
Faculty of mathematics
and physics

DOCTORAL THESIS

Vojtěch Kulvait

Mathematical analysis and computer simulations of deformation of nonlinear elastic bodies in the small strain range.

Mathematical Institute of Charles University

Supervisor of the thesis:	prof. RNDr. Josef Málek CSc., DSc.
Study programme:	Physics
Specialization:	Mathematical and Computer Modelling

Prague 2017

I am not sure exactly what heaven will be like, but I do know that when we die and it comes time for God to judge us, He will not ask, "How many good things have you done in your life?," rather He will ask, "How much love did you put into what you did?"

Mother Teresa

I declare that I carried out this doctoral thesis independently, and only with the cited sources, literature and other professional sources.

I understand that my work relates to the rights and obligations under the Act No. 121/2000 Sb., the Copyright Act, as amended, in particular the fact that the Charles University in Prague has the right to conclude a license agreement on the use of this work as a school work pursuant to Section 60 subsection 1 of the Copyright Act.

Prague, June 9, 2017

Vojtěch Kulvait

Moje díky patří **Josefu Málkovi** za vedení práce, mamince **Libuši** a přítelkyni **Pavle**.

Josef Málek si vždy našel čas, aby mi pomohl dělat věci lépe. Díky němu jsem se naučil psát odborné publikace. Děkuju mu za vedení, pomoc s přípravou práce, přečtení práce a poznámky k ní.

Libuše Kulvaitová, maminka, mě podporuje v průběhu celého života i studia. Děkuju.

Pavla Jumrová, přítekyně, provedla pečlivou jazykovou korekturu práce. Děkuju jí za podporu ve své práci a v životě.

I'd like to give special thanks to **Josef Málek** for supervision. I wish to thank my mother **Libuše** and my girlfriend **Pavla** for support.

Title: Mathematical analysis and computer simulations of deformation of nonlinear elastic bodies in the small strain range.

Author: Vojtěch Kulvait

Department: Mathematical Institute of Charles University

Supervisor: prof. RNDr. Josef Málek CSc., DSc.

Abstract: Implicit constitutive theory provides a suitable theoretical framework for elastic materials that exhibit a nonlinear relationship between strain and stress in the range of small strains. We study a class of power-law models, where the nonlinear dependence of strain on the deviatoric part of the stress tensor and its trace are mutually separated. We show that these power-law models are capable to describe the response of a wide variety of beta phase titanium alloys in the small strain range and that these models fit available experimental data exceedingly well. We also develop a mathematical theory regarding the well-posedness of boundary value problems for the considered class of power-law solids. In particular, we prove the existence of weak solutions for power law exponents in the range $(1, \infty)$. Finally, we perform computer simulations for these problems in the anti-plane stress setting focusing on the V-notch type geometry. We study the dependence of solutions on the values of power law exponents and on the V-notch opening angle. We achieve satisfactory results regarding the global stability of computed solutions.

Keywords: elasticity, small strain, nonlinear model, titanium alloy, mathematical analysis, existence of weak solution, computer simulations

Contents

Nomenclature **3**

1 Introduction **7**
1.1 Formulation of the problem 7
1.2 Main results 8
1.3 Structure of the thesis 10

2 Studied models of material response **13**
2.1 History of Mathematical modeling in continuum mechanics 13
2.2 One dimensional nonlinear material responses 15
2.3 New class of elastic models 18
2.4 Studied constitutive models 22
2.4.1 Separation of non-isochoric part from isochoric parts of deformation 22
2.4.2 Power-law model with separated response 24
2.4.3 Strain-limiting models 26

3 Modeling of Gum Metal and other newly developed titanium alloys . **31**
3.1 Experimental data 32
3.2 Existing models 33
3.3 Approximation of elastic moduli 36
3.3.1 Voigt, Reuss and Voigt-Reuss-Hill approximations 37
3.4 Modeling elastic response of titanium alloys 39
3.4.1 Power-law models 40
3.4.2 Algorithm to estimate model parameters 41
3.5 Results 44
3.5.1 Character of response of power-law model 44
3.5.2 Discussion and concluding remarks 56

4 Existence of solutions **59**
4.1 Auxiliary results 60
4.1.1 Proper function spaces 61
4.2 Variational formulation of boundary value problem 66
4.3 Existence of solutions 68
4.4 Existence of solutions for power-law models 77

5 Computer simulations **83**
5.1 Boundary value problem 84
5.1.1 Compatibility conditions 85
5.1.2 Airy's function 85

5.2 Asymptotic solutions for notched domains . . . 86
5.2.1 Cylindrical coordinate system . . . 86
5.2.2 Linear constitutive relation . . . 87
5.2.3 Power law materials . . . 87
5.3 Setting of finite element simulations . . . 89
5.3.1 Computational domains . . . 89
5.3.2 Boundary conditions . . . 91
5.3.3 Variational problem on the space of finite elements . . . 92
5.3.4 Parameters of models for simulations of titanium alloys . . . 93
5.4 Results . . . 93
5.4.1 Global convergence of solutions . . . 94
5.4.2 Local convergence and asymptotic behavior of solutions for V geometry . . . 101
5.4.3 Comparison of solutions in V domains . . . 101
5.4.4 Comparison of solutions in VO and VC domains . . . 104
5.4.5 Dependence on α and r_c . . . 114
5.5 Discussion . . . 125

A Review of the theory . . . **127**
A.1 Vector spaces, tensor algebra and notation . . . 127
A.2 Analysis of PDEs . . . 132
A.2.1 Real analysis, Topology . . . 132
A.2.2 Functional analysis . . . 135
A.2.3 Lebesque spaces and Sobolev spaces . . . 137
A.2.4 Monotone operators . . . 139
A.2.5 Important inequalities . . . 140
A.2.6 Finite element method . . . 141
A.3 Solid mechanics . . . 142
A.3.1 Kinematics . . . 143
A.3.2 Cauchy stress and equations of equilibrium . . . 145
A.3.3 Constitutive theory . . . 146
A.3.4 Linearized elasticity . . . 147

B Supplementary materials . . . **153**

List of Figures . . . **157**

List of Tables . . . **159**

Acronyms . . . **161**

Bibliography . . . **163**

Nomenclature

Vector, matrix and tensor operations

$|.|$ Let $c \in \mathbb{R}$ be a scalar, $\mathbf{v} \in \mathbb{R}^n$ be an n dimensional vector, $\mathbf{A} \in \mathbb{R}^{n \times m}$ be a real matrix and $\mathbf{T} \in \mathbb{R}^{n \times n}$ be a matrix representation of a second order tensor. Then $|c|$ denotes the absolute value of c, $|\mathbf{v}|$ denotes Euclidean norm of $\mathbf{v}$, $|\mathbf{A}|$ denotes Frobenius norm of $\mathbf{A}$ and $|\mathbf{T}|$ denotes Frobenius norm of $\mathbf{T}$.

$$|\mathbf{v}| = \sqrt{\sum_{i=1}^{n} v_i^2}, \quad |\mathbf{A}| = \sqrt{\sum_{i=1}^{n}\sum_{j=1}^{m} A_{ij}^2}, \quad |\mathbf{T}| = \sqrt{\sum_{i=1}^{n}\sum_{j=1}^{n} T_{ij}^2}.$$

$\mathbf{I}$ Identity matrix $\mathbf{I} \in \mathbb{R}^{n \times n}$.

δ_{ij} Kronecker delta,

$$\delta_{ij} = \begin{cases} 1, & i = j, \\ 0, & i \neq j. \end{cases}$$

tr Trace of a second order tensor or a square matrix $\mathbf{T} \in \mathbb{R}^{n \times n}$,

$$\mathrm{tr}\,\mathbf{T} = \sum_{i=1}^{n} T_{ii}.$$

vol Volumetric part of a second order tensor or a square matrix $\mathbf{T} \in \mathbb{R}^{n \times n}$,

$$\mathrm{vol}\,\mathbf{T} = \frac{\mathrm{tr}\,\mathbf{T}}{3}\mathbf{I}.$$

$\mathbf{T}^d$ Deviatoric part of a second order tensor or a square matrix $\mathbf{T} \in \mathbb{R}^{n \times n}$,

$$\mathbf{T}^d = \mathbf{T} - \frac{\mathrm{tr}\,\mathbf{T}}{3}\mathbf{I}.$$

$\mathbf{A}^\top$ Transposition of a matrix $\mathbf{A} \in \mathbb{R}^{n \times m}$.

Differential operators

div Divergence operator. Let $\mathbf{g} : \mathbb{R}^n \to \mathbb{R}^n$ be a vector-valued function, let $\mathbf{J} : \mathbb{R}^n \to \mathbb{R}^{n\times n}$ be a square matrix valued function then

$$\operatorname{div} \mathbf{g} = \operatorname{div} \mathbf{g}(\mathbf{x}) = \sum_{i=1}^{n} \frac{\partial g_i(\mathbf{x})}{\partial x_i},$$

$$\operatorname{div} \mathbf{J} = \operatorname{div} \mathbf{J}(\mathbf{x}), \quad (\operatorname{div} \mathbf{J})_i = \sum_{j=1}^{n} \frac{\partial J_{ij}(\mathbf{x})}{\partial x_j}.$$

∇ Gradient operator. Let $f : \mathbb{R}^n \to \mathbb{R}$ be a scalar valued function and $\mathbf{g} : \mathbb{R}^n \to \mathbb{R}^n$ be a vector-valued function, then

$$\nabla f = \nabla f(\mathbf{x}), \quad (\nabla f)_i = \frac{\partial f(\mathbf{x})}{\partial x_i},$$

$$\nabla \mathbf{g} = \nabla \mathbf{g}(\mathbf{x}), \quad (\nabla \mathbf{g})_{ij} = \frac{\partial g_i(\mathbf{x})}{\partial x_j}.$$

Δ Laplace operator. Let $f : \mathbb{R}^n \to \mathbb{R}$ be a scalar valued function and $\mathbf{g} : \mathbb{R}^n \to \mathbb{R}^n$ be a vector-valued function, then

$$\Delta f = \operatorname{div} \nabla f(\mathbf{x}) = \sum_{i=1}^{n} \frac{\partial^2 f(\mathbf{x})}{\partial x_i^2},$$

$$\Delta \mathbf{g} = \operatorname{div} \nabla \mathbf{g}(\mathbf{x}), \quad (\Delta \mathbf{g})_i = \sum_{j=1}^{n} \frac{\partial^2 g_i(\mathbf{x})}{\partial x_j^2}.$$

$\mathcal{E}$ Symmetric gradient operator. Let $\mathbf{u} : \mathbb{R}^n \to \mathbb{R}^n$ be a vector-valued function, then

$$\mathcal{E}\,\mathbf{u} = \frac{1}{2}\left(\nabla \mathbf{u} + (\nabla \mathbf{u})^\top\right), \quad (\mathcal{E}\,\mathbf{u})_{ij} = \frac{1}{2}\left(\frac{\partial u_i}{\partial x_j} + \frac{\partial u_j}{\partial x_i}\right).$$

$\operatorname{div}_{\mathbf{X}}$ Divergence operator in the refference configuration.

$\nabla_{\mathbf{X}}$ Gradient operator in the reference configuration.

$\Delta_{\mathbf{X}}$ Laplace operator in the reference configuration.

Solid mechanics

$\mathcal{B}$ Material body that is studied.

$\kappa_R(\mathcal{B})$ Reference configuration of an undeformed state, $\mathbf{X} \in \kappa_R(\mathcal{B})$ denotes a material point of the body $\mathcal{B}$ in the reference coordinate system.

$\kappa_\infty(\mathcal{B})$ Configuration of a deformed steady state, $\mathbf{x} \in \kappa_\infty(\mathcal{B})$ denotes a point of the body $\mathcal{B}$ in the spatial coordinate system.

χ Deformation mapping,

$$\chi : \kappa_R(\mathcal{B}) \to \kappa_\infty(\mathcal{B}), \quad \chi = \chi(\mathbf{X}).$$

$\mathbf{u}$ Displacement vector,

$$\mathbf{u} = \chi(\mathbf{X}) - \mathbf{X}.$$

$\mathbf{F}$ Deformation gradient,

$$\mathbf{F} = \nabla_{\mathbf{X}} \chi = \mathbf{I} + \nabla_{\mathbf{X}} \mathbf{u}.$$

$\mathbf{B}$ Left Cauchy-Green strain tensor,

$$\mathbf{B} = \mathbf{F}\mathbf{F}^\top.$$

$\mathbf{C}$ Right Cauchy-Green strain tensor,

$$\mathbf{C} = \mathbf{F}^\top\mathbf{F}.$$

ε Small strain tensor,

$$\varepsilon = \frac{1}{2}\left(\nabla\mathbf{u} + (\nabla\mathbf{u})^\top\right).$$

$\mathbf{T}$ Cauchy stress tensor.

$\mathbf{P_I}$ The first Piola Kirchoff stress tensor,

$$\mathbf{P_I} = \mathbf{T}\mathbf{F}^{-T} \det \mathbf{F}.$$

$\mathbf{P_{II}}$ The second Piola Kirchoff stress tensor,

$$\mathbf{P_{II}} = \mathbf{F}^{-1}\mathbf{P_I}.$$

Constitutive relations

$\widehat{\mathbf{G}}$ Tensor function characterising the constitutive relation between the stress tensor $\bar{\mathbf{T}}$ and strain tensor $\bar{\mathbf{E}}$ of the type $\widehat{\mathbf{G}}(\bar{\mathbf{T}}, \bar{\mathbf{E}}) = \mathbf{0}$.

$\widetilde{\mathbf{G}}$ Tensor function characterising the constitutive relation between the stress tensor $\bar{\mathbf{T}}$ and strain tensor $\bar{\mathbf{E}}$ of the type $\bar{\mathbf{T}} = \widetilde{\mathbf{G}}(\bar{\mathbf{E}})$.

$\mathbf{G}$ Tensor function characterising the constitutive relation between the stress tensor $\bar{\mathbf{T}}$ and strain tensor $\bar{\mathbf{E}}$ of the type $\bar{\mathbf{E}} = \mathbf{G}(\bar{\mathbf{T}})$.

1. Introduction

In this thesis, we study a new class of nonlinear elastic materials that arise from the theory for implicitly constituted non-dissipative solids developed under the additional assumption that the norm of the gradient of deformation is supposed to be small. First of all, we study the potential of these models in capturing the available experimental data for beta titanium alloys. Then, we aim to develop a mathematical theory for boundary value problems relevant to this class of elastic materials. Finally, we study these boundary value problems computationally focusing on the V-notch geometry and the behavior of stress and strain near the tip of the V-notch.

More specifically, the objective of this thesis is to study the following boundary value problem.

1.1 Formulation of the problem

Definition 1.1 (Problem (P)). *Let $\Omega \subset \mathbb{R}^n$, $n = 2$ or 3 be an open, bounded, connected set with the boundary $\partial\Omega$ consisting of two smooth disjoint parts Γ_D and Γ_N such that $\partial\Omega = \overline{\Gamma_D \cup \Gamma_N}$, see Figure 1.1, where $\boldsymbol{\nu} = \boldsymbol{\nu}(\mathbf{x})$ denotes the unit outward normal vector at $\mathbf{x} \in \partial\Omega$. Let $\mathbf{G} : \mathbb{R}^{n\times n}_{sym} \to \mathbb{R}^{n\times n}_{sym}$, $\mathbf{u_0} : \Omega \to \mathbb{R}^n$, $\mathbf{f} : \Omega \to \mathbb{R}^n$ and $\mathbf{g} : \Gamma_N \to \mathbb{R}^n$ be given. We say that the pair of functions $(\mathbf{u}, \mathbf{T}) : \Omega \to \mathbb{R}^n \times \mathbb{R}^{n\times n}_{sym}$ solves the Problem (P) if*

$$
\begin{aligned}
-\operatorname{div} \mathbf{T} &= \mathbf{f} && \text{in } \Omega, && \text{(1.1a)}\\
\mathcal{E}\,\mathbf{u} &= \mathbf{G}(\mathbf{T}) && \text{in } \Omega, && \text{(1.1b)}\\
\mathbf{u} &= \mathbf{u_0} && \text{on } \Gamma_D, && \text{(1.1c)}\\
\mathbf{T}\boldsymbol{\nu} &= \mathbf{g} && \text{on } \Gamma_N, && \text{(1.1d)}
\end{aligned}
$$

where

$$
\mathcal{E}\,\mathbf{u} = \frac{1}{2}\left(\nabla\mathbf{u} + (\nabla\mathbf{u})^\top\right).
$$

The above problem describes the state of the elastic body occupying the set Ω at equilibrium characterized by the equation (1.1a), where $\mathbf{T}$ is the stress tensor and $\mathbf{f}$ stands for external body forces. The body obeys the nonlinear constitutive equation (1.1b) that relates the linearized strain $\mathcal{E}\,\mathbf{u}$, which is a symmetric gradient

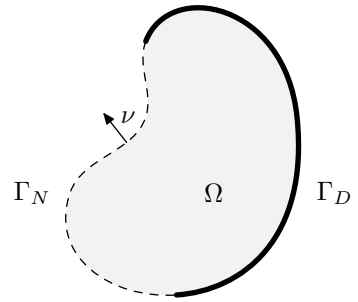

Figure 1.1: Domain illustration.

of the displacement $\mathbf{u}$, and the stress tensor $\mathbf{T}$ by means of a nonlinear function $\mathbf{G}$. The equation (1.1c) prescribes the displacement $\mathbf{u_0}$ on the Dirichlet part of the boundary Γ_D, and the equation (1.1d) prescribes the boundary traction $\mathbf{g}$ on the Neumann part of the boundary Γ_N. The state of the body is subject to an additional assumption that the square of the norm of the displacement gradient can be neglected in comparison to the norm of the displacement gradient itself.

We are interested in the responses where the nonlinear dependence of strain on the deviatoric part of stress and its trace are mutually separated in the way that

$$\begin{aligned} \operatorname{tr}\boldsymbol{\varepsilon} &= \sigma_1(\operatorname{tr}\mathbf{T})\operatorname{tr}\mathbf{T}, \\ \boldsymbol{\varepsilon}^d &= \sigma_2(|\mathbf{T}^d|)\mathbf{T}^d, \end{aligned} \tag{1.2}$$

where σ_1 and σ_2 are nondecreasing scalar functions such that $\sigma_1(0) = 0$ and $\sigma_2(0) = 0$. The formulation (1.2) enables one to divide non-isochoric part of deformation from isochoric parts of deformation to capture these two responses separately. In addition, these responses need not be of the same type, e.g. they could have different polynomial growth. Finally, (1.2) seems to be more appropriate for capturing experimental data as the experiments measure the effect of shear, dilation, etc. separately, see Criscione et al. (2000). Upon substituting (1.2) into (1.1b), the constitutive function $\mathbf{G}$ takes the following form:

$$\mathbf{G}(\mathbf{T}) = \frac{\operatorname{tr}\mathbf{T}}{3}\sigma_1(\operatorname{tr}\mathbf{T})\mathbf{I} + \sigma_2(|\mathbf{T}^d|)\mathbf{T}^d.$$

Power-law response

A natural example of nonlinear constitutive function, which can capture a range of responses and yet is reasonably simple, is the power-law model. In this thesis, we consider power-law models where the constitutive function $\mathbf{G}(\mathbf{T})$ varies as the power of the stress $\mathbf{T}$. Using the setting (1.2), we consider the model

$$\begin{aligned} \operatorname{tr}\boldsymbol{\varepsilon} &= \frac{1}{3K}\left(\frac{\tau_K^2 + |\operatorname{tr}\mathbf{T}|^2}{\tau_K^2}\right)^{\frac{s'-2}{2}}\operatorname{tr}\mathbf{T}, \\ \boldsymbol{\varepsilon}^d &= \frac{1}{2\mu}\left(\frac{\tau_\mu^2 + |\mathbf{T}^d|^2}{\tau_\mu^2}\right)^{\frac{q'-2}{2}}\mathbf{T}^d, \end{aligned} \tag{1.3}$$

where $s' \in (1,\infty)$, $q' \in (1,\infty)$, $K > 0$, $\tau_K > 0$, $\mu > 0$, $\tau_\mu > 0$ are material moduli. The response to the mean normal stress has the power-law exponent s' while the isochoric response has the power-law exponent q', where in general $s' \neq q'$.

1.2 Main results

A recently developed framework of implicit constitutive theory due to Rajagopal (2003, 2007, 2016) provides justification for a number of fluid and solid models, which were previously proposed without a proper reasoning. In this thesis we focus on one specific area of this theory, namely the theory of nonlinear responses in the range of small strains, see Rajagopal (2010, 2011a). This theory provides a rigorous justification for nonlinear constitutive relations of the type (1.1b) in the small

displacement gradient range. That would be impossible within the context of any Cauchy elastic model where the linearization of a nonlinear constitutive expression for the stress leads to Hooke's law, which is a linear relationship between the stress and the linearized strain.

Modeling beta phase titanium alloys

Many materials, including beta phase titanium alloys and concrete, exhibit nonlinear stress strain response in the range of small strains, see Saito et al. (2003); Talling et al. (2009); Sakaguch et al. (2004); Hao et al. (2005); Hou et al. (2010). Gum Metal, which is a beta phase titanium alloy when cold swagged, exhibits reversible elastic response up to the strain magnitude of 2.5%, which is often referred to as superelasticity, see Saito et al. (2003). In Rajagopal (2014), an exponential model within implicit constitutive theory that is able to capture tensile loading response of Gum Metal was proposed. In Devendiran et al. (2017), two exponential models were proposed to capture the tensile loading response of three different beta phase titanium alloys. We have found out that the power law models (1.3) are able to describe tensile loading behavior of Gum Metal and other beta phase titanium alloys in the full range of nonlinear elastic response. From the direct comparison, we conclude that the power-law model (1.3) when fitting tensile loading data is better than the previous models in terms of the quality of fit. When having an additional information, in the form of Voigt-Reuss-Hill estimates of single crystal data, by employing maximalization of an obective function based on these data, we have identified a model with physically realistic material moduli, which fits the available tensile loading data.

Mathematical analysis

In this thesis, we establish the existence of the weak solutions to the Problem (P) from Definition 1.1 when using the power-law model (1.3). We use the notation of the exponents with primes, s' and q', to emphasize their meaning for the weak formulation of the Problem (P). Let s and q be Hölder conjugates of the exponents s' and q'

$$s = \frac{s'}{s'-1}, \quad q = \frac{q'}{q'-1},$$

then the natural Lebesque space for the trace of the small strain $\operatorname{tr}\varepsilon$ is L^s and the natural space for the deviatoric part of the small strain ε^d is L^q. The natural space for the trace of the stress $\operatorname{tr}\mathbf{T}$ is $L^{s'}$ and the natural space for the deviatoric part of the stress $\mathbf{T}^d$ is $L^{q'}$. The spaces for the weak solutions with this structure were introduced in the context of the analysis of Norton-Hoff materials in Geymonat et al. (1986).

The proof of the existence of solutions works with a system of two coupled first order partial differential equations and it does not invert or assume invertibility of the constitutive function $\mathbf{G}$. We divide the proof into two parts. First, we introduce an ε regularized problem with a proper smoothing operator and show the existence of the weak solution to the ε regularized problem. Then, we show that as $\varepsilon \to 0$, the sequence of the solutions to the ε regularized problem converges to the weak solution of the original Problem (P).

In the spatial dimension $n \in \{2, 3\}$, for $s, q \in (1, \infty)$, where Hölder conjugates s' and q' are exponents of the power law dependence (1.3), we show the existence

of the solution $(\mathbf{u}, \mathbf{T})$ so that

$$\mathbf{u} \in L^{min(s,q)}(\Omega)^n, \quad (\mathcal{E}\,\mathbf{u})^d \in L^q(\Omega)^{n\times n}_{sym}, \quad \operatorname{div}\mathbf{u} \in L^s(\Omega), \tag{1.4}$$

and

$$\mathbf{T}^d \in L^{q'}(\Omega)^{n\times n}_{sym}, \quad \operatorname{tr}\mathbf{T} \in L^{s'}(\Omega),$$

whereas

$$Tr\,\mathbf{u} \in W^{1-\frac{1}{min(s,q)},min(s,q)}(\partial\Omega)^n. \tag{1.5}$$

For $n = 3$, we use the generalized Korn's inequality, see Schirra (2012), to further improve regularity of the solution spaces (1.4) and (1.5).

Computer simulations

Computer simulations of the most implicit models in solid mechanics are yet to be made. Simulations regarding the strain-limiting model can be found in Ortiz et al. (2012, 2014); Kulvait et al. (2013). In Devendiran et al. (2017), there are some illustrative simulations of behavior of exponential models.

In the thesis, we focus on the singular behavior of stress around cracks, edges and notches, which is a known phenomenon, see Neuber (1961); Rice (1967). In the anti-plane stress setting, asymptotic solutions of the stress distribution for the linear response in unbounded domains are known for geometries of the V-notch and the V-notch with an end hole, see Jun – Yuqiu (1992); Zappalorto – Lazzarin (2011). Asymptotic solutions for the V-notch geometry in unbounded domains exists also for power-law models, see Bassani (1984). Since these results are valid only in the close vicinity of singularity, in the thesis, we study to what extent these analytical solutions correspond to numerical solutions in finite domains.

We systematically study the response of the power-law models in different geometries of the anti-plane stress setting, where stress concentration can occur. The anti-plane stress setting enables us to reformulate the Problem (P) as a variational problem for an unknown potential called Airy-stress function. We study finite element approximations to the given problem. More precisely, we construct triangulation $\mathcal{T}_h$ of the computational domain, and use the space of piece-wise quadratic functions

$$X^2_h = \{u_h \subset C^0(\overline{\Omega}), u_h|_T \in P^2(T), \forall T \in \mathcal{T}_h\}.$$

On adaptively refined triangular meshes, we perform computer simulations of the power-law models for titanium alloys, which were proposed in Chapter 3. We study differences in stress and strain distributions depending on the power-law exponent. We systematically study stress and strain distributions in the anti-plane stress setting for 194 different geometries of a square plate with a V-notch with various opening angles α and levels of tip smoothening. Computer simulations in this thesis complement the simulations that were performed in Kulvait et al. (2013) for the strain-limiting model.

1.3 Structure of the thesis

The thesis is organized as follows.

Chapter 2 describes in detail constitutive models used in this thesis. After historical remarks, it summarizes important results from implicit constitutive theory regarding modeling of solids in the small strain range. It proposes a hierarchy of models of the form (1.1b). The power-law model of the type (1.3) is put into the context of proposed models. We also introduce strain-limiting models and show that they can be understood as a borderline case of power-law models.

In chapter 3, we show that the power-law models (1.3) are capable of modeling response of many beta phase titanium alloys. First, we estimate material moduli of the studied titanium alloys. Then, we fit the tensile loading experiments with the cold swagged Gum Metal and three other beta phase titanium alloys to the power-law model presented in the thesis. We obtain optimal model parameters for each studied alloy using an algorithm based on the linear regression. Among the models available in the literature, the models proposed and studied in this thesis seems to be the best in corroborating the experimental data.

In Chapter 4, we establish the existence of the weak solution to the Problem (P) with the power-law response (1.3). We derive the variational formulation of the problem and define the proper function spaces. The proof of the existence of weak solutions is divided into two parts. First, we introduce an ε regularized problem with a proper smoothing operator and show the existence of the weak solution to the regularized problem. Using the Galerkin method, we prove the existence of a sequence of solutions in finite-dimensional subspaces of the appropriate functional space. We obtain apriori estimates and show the convergence of solutions for the Galerkin system to the limit in $\mathbf{T}$ and in $\mathbf{u}$. Applying this procedure, we get the solution of the ε regularized problem. Then we show that, as ε converges to zero, the weak solution of the regularized problem converges to the weak solution of the original problem. We prove the existence of weak solutions for power law exponents $p', q' \in (1, \infty)$. We then improve the spaces in which the solution is. In $n = 2$, we employ the compact embedding of the Sobolev spaces to the Lebesque spaces to improve integrability of the solution. In the spatial dimension $n = 3$, we utilize generalized Korn's inequality where only the deviatoric part of the symmetric gradient is used instead of the full symmetric gradient, see Schirra (2012).

In Chapter 5, we present the results of computer simulations for exactly the same models that are proposed in Chapter 3 to obtain a very good fit of the behavior of three different titanium alloys. In the anti-plane stress setting, we set up a discrete variational formulation of the Problem (P). We solve this problem by the Finite element method using the damped Newton method on 872 different geometries of a square plate with a V-notch with various opening angles α and levels of tip smoothening. For each geometry, we use a hierarchy of 6 nested triangular meshes. We compare solutions to the asymptotic solutions for the linear and power-law models. We study global stability of solutions with respect to a refinement level with very satisfying results. We conclude the chapter by showing differences between the linear model and the power-law models with different exponents of power-law relationship. Results are complementary to the work Kulvait et al. (2013) where we studied the strain-limiting model. Source code that implements computer simulations and utilizes FEniCS software library, see Logg et al. (2012), is a part of the supplementary material of this thesis.

In appendix A, we briefly survey notation and basic results from tensor algebra and calculus. We review important results from functional analysis and analysis of

Partial differential equations (PDEs) and we summarize the basic facts regarding the solid mechanics, focusing on small strain elastostatics.

2. Studied models of material response

When we think about elastic bodies from the scientific perspective, we think about their deformation, stress and strain distribution caused by the action of internal or external forces on it. Response of an elastic solid to the deformation is described by the constitutive relation. The quality and accuracy of the constitutive model is thus an important prerequisite for trustworthy predictions of the material response.

In this chapter, we briefly describe historical context of mathematical modeling in solid mechanics. We discuss three main scientific fields on which the thesis is focused. These are *solid mechanics* as a theory of constructing material models, *computational mechanics* which involve solving these models numerically and *mathematical analysis* of related boundary value problems. Then we discuss one dimensional phenomenological models that are frequently used to describe material responses and that motivate the use of power-law models in the thesis. One section is devoted to a new class of elastic solids defined in the context of the implicit constitutive theory, which complements the classical theory of Cauchy elasticity. We also show important implications of implicit constitutive theory for the small strain elasticity. In constitutive models that we study small strain is an isotropic nonlinear function of Cauchy stress. We define, describe and further classify these models by introducing their subclasses that posses less complexity but are still rich enough to describe a variety of responses. Particularly, we define and show important properties of power-law models and strain-limiting models.

2.1 History of Mathematical modeling in continuum mechanics

In the 17th century, Robert Hooke published his work 'Ute tensio, sic vis' (1678) that means 'As the extension, so the force', which is now recognized as a foundation of the theory of elasticity. Another milestone was reached when in 1687, Newton published his 'Principia' that includes three Newton laws of motion. In the 18th century, the works of Leonhard Euler set the foundation for the calculus of variations and the proper mathematical description of continuous media. In the 19th century, the theory was further extended by works of Siméon Denis Poisson and Augustin Louis Cauchy. Cauchy was the first who used the continuum description formalism as is known today. He introduced the concept of the 3×3 symmetric matrix describing the stress state of the body, see Cauchy (1827), which is now referred to as Cauchy stress tensor. In his treatment of continuum mechanics, he also used the displacement vector and the strain tensor and he can be regarded as the author of the modern theory of elasticity. At the beginning of the 20th century, despite the advent of the quantum mechanics, particle physics and the atomistic description of the matter, the attention of the scientific community to the continuum mechanics did not fully disappear. It was evident that, as stated in Little (2007): *'we are surrounded by matter in the form of continuous media; deformable solids, fluids and gases. We will need a science that describes the responses of these materials to the*

external forces imposed upon them until, if ever, the science of particles can be developed such that it predicts the response of the aggregate'. The book Love (1927) includes a complete description of the theory of small strain elasticity with an extensive list of references and the historical background. Up to the half of the 20th century, the models that were used to model the response of elastic solids were mainly linear. However, it was yet evident that materials under particular conditions behave nonlinearly, see Ramberg – Osgood (1943). The theory of large deformations including nonlinear constitutive relations is to a great extent built upon the work of Ronald Samuel Rivlin. He was primarily focused on the rubber deformation and rupture, see Rivlin – Thomas (1951). By studying these phenomena, he built the basis for the theory of nonlinear continuum mechanics. The modern highly abstract treatment of nonlinear models in continuum mechanics was disseminated through the work of Clifford Truesdell and his collaborators. The classical continuum mechanics books, Truesdell – Toupin (1960) and Truesdell – Noll (1969), include rigorous mathematical description of the theory of elasticity. The latter book, Truesdell – Noll (1969), focuses primarily on nonlinear models. A relation that describes deformation response of an elastic material to the applied force, so called constitutive relation, was understood from the early works of Cauchy as an equation where the stress at a given point is a function of the configuration (e.g. deformation gradient or strain). In the definition of elastic material in Truesdell – Noll (1969), we can find : '*A change in stress arises solely in response to a change in configuration, and the material is outright oblivious to the manner in which the change of configuration has occurred in space and time.*' In contrast to that definition, works of Rajagopal on constitutive relations admit implicit stress strain relations for the constitution of an elastic solid, see Rajagopal (2003, 2007, 2011a). These works are referred to in this thesis as **implicit constitutive theory**. They can be seen as complementary to the classical theory of Cauchy elasticity. Implicit constitutive theory has its strong implications for small strain elasticity where it provides the theoretical background for models where the relation between the linearized strain and stress is nonlinear.

The problems that arise in continuum mechanics lead to the boundary value problems for solutions of PDEs. These PDEs are in general nonlinear and their mathematical properties, such as existence, uniqueness and smoothness of solutions, may present open mathematical problems. One of the most famous problems is smoothness of solutions to the Navier-Stokes equations in the fluid dynamics, see Fefferman (2000). Properties of the solutions are important also in the context of convergence of numerical methods to the solutions of original problems. The modern theory of PDEs and its applications to continuum mechanics originates in the 20th century and was influenced by works of Jean Leray, Sergej Sobolev, Jacques-Louis Lions, Olga Ladyzhenskaya and many others. Mathematical analysis of the boundary value problems in continuum mechanics is an ongoing work with a broad community of scientists involved.

Computational mechanics. as a field that involves solving problems arising in continuum mechanics using computers, has evolved in the second half of the 20th century. It was the development of computers and computing technology that has provided a momentum for the growth of computational mechanics and its applications. Computational mechanics is deeply connected with the Finite element method (FEM). The central idea of the FEM is to construct discretization of the computational domain by dividing it into simple elements (e.g. triangles). Solutions

of the boundary value problems are then sought on the finite dimensional spaces constructed using this finite element discretization. Finite element problems are typically constructed in a way that leads to the linear systems with sparse matrices. Theoretical background for these approaches was set in Courant (1943). First works that developed FEM as a method of computational mechanics were motivated by the demand for material strength models in aerospace industry. In the former work Argyris (1955), structural analysis models that use finite elements are described and studied. Actual implementation of FEM for the structural analysis was performed by Turner and Clough in Boeing company, see Turner (1956). The method was initially called Direct Stiffness Method, the term Finite element method was first used in Clough (1960). One of the first books about FEM is Zienkiewicz – Cheung (1967). From the advent of FEM, there was a strong cooperation between the applications (Turner, Clough - Boeing company) and the formal mathematical development of the theory itself (Argyris - Royal Aeronautical Society, Clough - Berkeley University, Zienkiewicz - Northwestern University), see Clough (2004). Computational mechanics has gained new applications over the decades in the areas including industry, biology and medicine. With the drop of the price of computational power, increase of the computer speed and accessible cloud technologies finite element method can be now applied to solve systems of tremendous complexity, see Ayachit (2016). In recent years, there has been a noticeable trend to open software to the public, and its development to the communities of interested people. In the thesis, we use the FEniCS Project[1], which is '*a collection of free software with an extensive list of features for automated, efficient solution of differential equations*', see Logg et al. (2012). FEniCS is written in C++ and Python programming languages. It includes an open source framework for writing variational formulation of boundary value problems for PDEs and solving it using FEM.

Solid mechanics as a theory of constructing material models, formulation of Boundary value problems (BVPs) and their *mathematical analysis*, and *computational mechanics*, which involve solving these problems numerically, are overlapping fields that should work together to create accurate, stable and reliable models. Further integration of these three fields is one of the challenges for the next generation of scientists. This thesis is going in that direction by integrating the study of new models of elastic materials, performing computer simulations and conducting the mathematical analysis of underlying boundary value problems.

2.2 One dimensional nonlinear material responses

In this section, we review the basic approaches for the treatment of nonlinear responses studied in the context of elasticity. For the purpose of providing motivation, we use one dimensional models where σ represents a stress measure (e.g. tensile loading stress) and e represents a strain measure (e.g. relative elongation).

As we study monotone responses, we divide the nonlinear responses in terms of strain stress relationship into two categories of superlinear and sublinear response. The superlinear response is the behavior that the strain grows faster than linearly with respect to stress. This effect is observed in stainless steel and numerous alloys, see Rasmussen (2003). The sublinear response is the oposite behavior, where

[1]For an overview of available finite element packages, see Wikipedia (2017a).

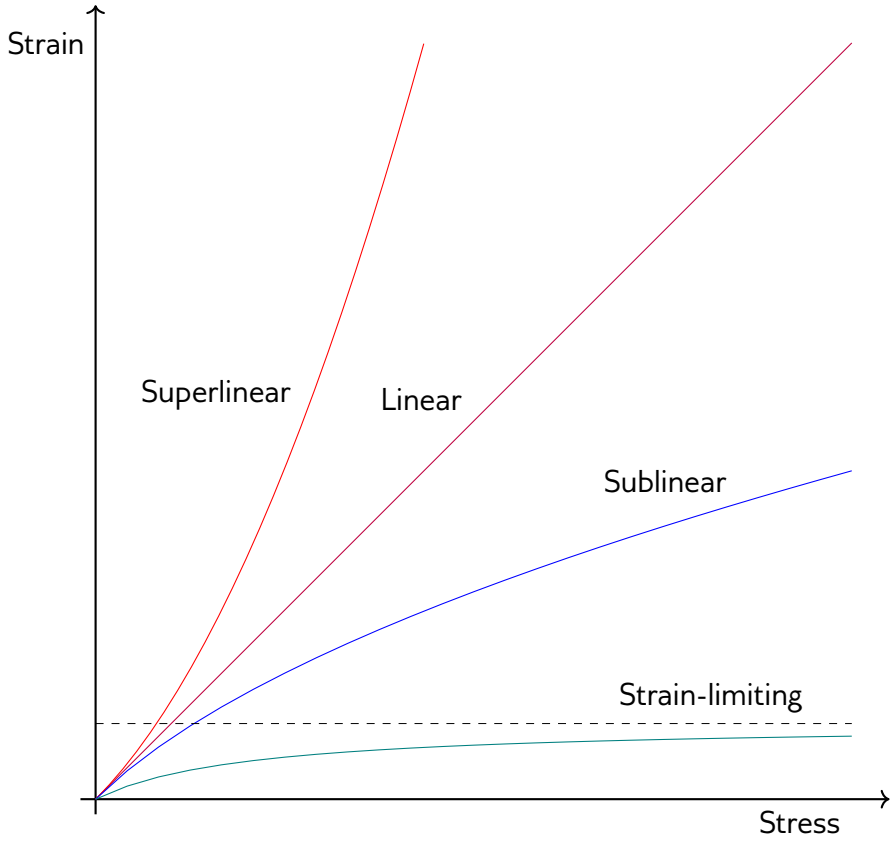

Figure 2.1: One dimensional diagram of stress strain responses.

the strain grows slower than linearly with respect to stress. Sublinear response is sometimes called strain stiffening[2]. It is attributed to materials such as plastics, rubber or biological tissues, see Horgan – Saccomandi (2002, 2006). An extreme case of sublinear response is captured by models where the strain remains bounded as the stress grows into the infinity. This class of models is referred to as strain-limiting models. In the theory of finite strain elasticity, similar models are called limiting chain extensibility models. For the schematic diagram of the described types of material responses, see Figure 2.1.

Power-law responses

Power-law model is a phenomenological model where one quantity varies proportionally to the power of another quantity (in our case, these quantities are stress and strain). Power-law model is capable to capture both superlinear and sublinear responses.

The power-law model, which was proposed to model nonlinear behavior of the aircraft construction materials when subject to high stresses, so called Ramberg-Osgood model, is of the form

$$e = \frac{\sigma}{E} + K\left(\frac{\sigma}{E}\right)^n, \tag{2.1}$$

[2]According to Erk et al. (2010), strain stiffening is defined as *increase in a material's elastic modulus with applied strain*.

where E, K and n are model parameters. The model (2.1) was formulated due to the inadequacy of linear relationship to capture material response prior to plastic deformation range. The Ramberg-Osgood model was able to capture behavior of aluminium alloy, stainless steel and carbon-steel[3], see Ramberg – Osgood (1943). Mathematical analysis of a three dimensional model of this type can be found in Knees – Sändig (2004).

The Knowles model is another power-law model proposed to study stress and strain distribution around the crack tip for the incompressible hyperelastic materials in the anti-plane strain setting, see Knowles (1977). The strain energy density function of the Knowles model leads to the representation where stress is a power-law function of strain such that as one dimensional analogue, we have model

$$\sigma = \mu \left(1 + ce^2\right)^{n-1} e,$$

where μ and c are material parameters and n is a power-law exponent, see Horgan – Saccomandi (2001).

Exponential responses

Exponential models, where one quantity varies exponentially with respect to other quantity, are another phenomenological models used to model nonlinear material responses. One of the well known exponential models is the Fung model, which was proposed to model sublinear response of muscles, skin and soft tissues, see Fung (1967)[4]. One dimensional analogue of the Fung model takes the form

$$\sigma = \mu \exp\left(be^2\right) e,$$

where μ and b are material parameters, see Horgan – Saccomandi (2001).

Exponential models were also used in the context of implicit constitutive theory to fit response of Gum Metal alloy in Rajagopal (2014). Aforementioned model is of the form

$$e = 2\lambda \exp\left(\eta\sigma\right)\sigma,$$

where λ and η are model parameters.

Strain-limiting responses

The class of models of special interest is a class, where the strain is bounded for arbitrary stress, so called strain-limiting models. The first model of this type was proposed in Neuber (1961). These models were studied in the context of implicit constitutive theory in Rajagopal (2011b); Kulvait et al. (2013). One dimensional analogue of the model from Kulvait et al. (2013) takes the form

$$e = \frac{\tau_\mu}{2\mu} \frac{\sigma}{\sqrt{\tau_\mu^{\,a} + |\sigma|^2}}, \tag{2.2}$$

[3]Materials such as steel present plastic deformation when subject to high stresses. Thus for high stresses they can not be accurately modelled by purely elastic models.

[4]Fung accents the importance of considering full stress strain response and using nonlinear models for modeling biological materials. In Fung (1967), the author states that *'It is necessary, however, to give up the usual practice of trying to characterize the elasticity of a tissue by a representative Young's modulus, because this modulus varies over a very wide range.'*

where $\mu > 0$ and $\tau_\mu > 0$ are model parameters. We can see that as the stress σ in (2.2) approaches infinity, the strain e remains bounded by $\tau_\mu/(2\mu)$. Analogous models in the context of finite strain elasticity are known as limiting chain extensibility models, see for example Gent (1996); Horgan – Saccomandi (2003).

2.3 New class of elastic models

In this section, we describe implicit constitutive theory, see Rajagopal (2003, 2007, 2011a) and its implications for the theory of elasticity in the small strain range. The classical definition of an elastic solid is a definition by Cauchy. It requires that the stress tensor $\mathbf{T}$ at a given point is an explicit function of the deformation gradient $\mathbf{F}$ at a given point.

Definition 2.1 (Cauchy elastic solid). *Cauchy elastic solid is a generally anisotropic material with a constitutive relation of the type*

$$\mathbf{T} = \widetilde{\mathbf{G}}(\mathbf{F}). \tag{2.3}$$

The constitutive function behaves under the action of arbitrary orthogonal transformation given by matrix $\mathbf{Q} \in OG(n)$ in the way that (objectivity, frame indifference)

$$\widetilde{\mathbf{G}}(\mathbf{QF}) = \mathbf{Q}\widetilde{\mathbf{G}}(\mathbf{F})\mathbf{Q}^\top, \quad \widetilde{\mathbf{G}}(\mathbf{0}) = \mathbf{0}.$$

In the equation (2.3), the stress $\mathbf{T}$ is a function of a kinematic quantity, namely the deformation gradient $\mathbf{F}$, not vice versa. We might justify an unequal status of these quantities by the definition of hyperelastic (Green elastic) solid in finite strain theory. Hyperelastic solid is defined by its particular form of Hemholtz free energy W, called strain energy density function, which describes energy stored in a given deformation state of the body $W = W(\mathbf{F})$. The constitutive equation is then derived by utilizing the Clausius-Planck equation which is a form of the second law of thermodynamics under the natural requirement that *there is no dissipation and all the energy stored in the body can be recovered in a purely mechanical process*, see Rajagopal (2003). Energy dissipation is understood as an irreversible process of converting a part of mechanical energy into the heat. By the Coleman-Noll procedure, it is possible to derive a constitutive equation of the form

$$\mathbf{P_I} = \frac{\partial W}{\partial \mathbf{F}}, \tag{2.4}$$

where $\mathbf{P_I}$ is the First Piola-Kirchoff stress tensor. For details of the Coleman-Noll procedure, see (Holzapfel, 2000, p. 208). Thus, by thermodynamical reasoning, we have a constitutive relation (2.4) that is of the form (2.3) in the sense that a measure of stress is a function of a measure of deformation. Green elastic solid is a special case of Cauchy elastic solid, see Truesdell – Noll (1969). The open question was whether the zero energy dissipation of a material would guarantee that the constitutive relation for that material must be of the form (2.4). The answer is negative. In the work Rajagopal (2007), the author discusses the natural meaning of elasticity and argues that when we consider an elastic body defined as the material incapable of energy dissipation, then we don't need to restrict ourselves to the Green's type constitutive relation. Rajagopal – Srinivasa (2007, 2009) proposed rate

type models for solids incapable of dissipation, which are not Green elastic. For further thermodynamic discussion of these models, see Bridges – Rajagopal (2014)[5].

Implicitly constituted solids

The fact that all non dissipative materials do not have a constitutive relation of the form (2.4) leaves unjustified why the basic definition of elastic material should be Cauchy's definition. It is natural to use a fully implicit model of elastic materials that extends Cauchy's model and prefers neither stress nor strain. Implicit models for describing constitutive relations were first considered in Morgan (1966). In the context of elasticity of isotropic materials, these models were reinvented in Rajagopal (2007). The most general implicit constitutive model relates Cauchy stress $\mathbf{T}$ to the left Cauchy-Green stress tensor $\mathbf{B}$ by means of the following definition.

Definition 2.2 (Isotropic implicitly constituted solid). *The isotropic implicitly constituted solid is a body with a constitutive relation of the type*

$$\widehat{\mathbf{G}}(\mathbf{B}, \mathbf{T}) = \mathbf{0}, \tag{2.5}$$

the constitutive function behaves under the action of arbitrary orthogonal transformation given by matrix $\mathbf{Q} \in OG(n)$ in the way that (objectivity, frame indifference, isotropy)

$$\widehat{\mathbf{G}}(\mathbf{Q}\mathbf{B}\mathbf{Q}^\top, \mathbf{Q}\mathbf{T}\mathbf{Q}^\top) = \mathbf{Q}\widehat{\mathbf{G}}(\mathbf{B}, \mathbf{T})\mathbf{Q}^\top.$$

The materials with the constitutive relation (2.5) are classified as a new class of elastic solids. Fully implicit models are however difficult to work with. Even though there is an intention to decipher their structure, see Sfyris – Bustamante (2014), the implicit nature of the constitutive relations makes it harder to fit experimental data to these models and to work with these models in numerical schemes. The class (2.5) of isotropic implicitly constituted solids has two important explicit subclasses.

Stress as function of strain

A classical sub-class of the bodies defined through (2.5) is the isotropic compressible Cauchy elastic solid.

Definition 2.3 (Isotropic Cauchy elastic solid). *The isotropic Cauchy elastic solid is a material with a constitutive relation of the type*

$$\mathbf{T} = \widetilde{\mathbf{G}}(\mathbf{B}), \tag{2.6}$$

the constitutive function behaves under the action of arbitrary orthogonal transformation given by matrix $\mathbf{Q} \in OG(n)$ in the way that (objectivity, frame indifference, isotropy)

$$\widetilde{\mathbf{G}}(\mathbf{Q}\mathbf{B}\mathbf{Q}^\top) = \mathbf{Q}\widetilde{\mathbf{G}}(\mathbf{B})\mathbf{Q}^\top, \quad \widetilde{\mathbf{G}}(\mathbf{0}) = \mathbf{0}.$$

From the Rivlin Ericksen Representation Theorem A.35, (p. 132) the function $\widetilde{\mathbf{G}}(\mathbf{B})$ can be rewritten to the form

$$\widetilde{\mathbf{G}}(\mathbf{B}) = \alpha_1\mathbf{I} + \alpha_2\mathbf{B} + \alpha_3\mathbf{B}^2,$$

[5]For applications of these models in biomechanics, see Freed – Einstein (2013); Freed et al. (2013).

where the material moduli α_i, $i \in \{0, 1, 2\}$ depend on the principal invariants of the left Cauchy-Green strain tensor $\mathrm{I}_{\mathbf{B}}$, $\mathrm{II}_{\mathbf{B}}$ and $\mathrm{III}_{\mathbf{B}}$. We also require $\widetilde{\mathbf{G}}(\mathbf{0}) = \mathbf{0}$ to assure zero strain for zero stress. This condition takes the form $\alpha_1(0, 0, 0) = 0$.

Linearization

There is a plenty of settings where the assumption of the norm of the displacement gradient being small is perfectly reasonable, while at the same time, the linear relationship between stress and strain is quite often too restrictive. However, the only known rigorous way to approximate a constitutive relation of the isotropic Cauchy elastic solid (2.6) using small strain tensor $\boldsymbol{\varepsilon}$ is a linearization that leads to Hooke's law

$$\mathbf{T} = \lambda(\operatorname{tr}\boldsymbol{\varepsilon})\mathbf{I} + 2\mu\boldsymbol{\varepsilon}. \tag{2.7}$$

Here, $\boldsymbol{\varepsilon}$ is linearized strain and λ and μ are material moduli. For details, see Proposition A.133 (p. 127).

Strain as function of stress

To use nonlinear models consistently with a theory, we use the following class of elastic solids that is different from the class of the isotropic Cauchy elastic solids (2.6). It is another subclass of isotropic implicitly constituted solid models (2.5), which has not been studied until recently, see Rajagopal (2007).

Definition 2.4 (Isotropic material where strain is a function of stress). *An isotropic material where strain is a function of stress is a material with a constitutive relation of the type*

$$\mathbf{B} = \mathbf{G}(\mathbf{T}), \tag{2.8}$$

the constitutive function behaves under the action of arbitrary orthogonal transformation given by matrix $\mathbf{Q} \in OG(n)$ in the following way (objectivity, frame indifference, isotropy)

$$\mathbf{G}(\mathbf{Q}\mathbf{T}\mathbf{Q}^{\top}) = \mathbf{Q}\mathbf{G}(\mathbf{T})\mathbf{Q}^{\top}, \quad \mathbf{G}(\mathbf{0}) = \mathbf{0}. \tag{2.9}$$

From the Rivlin Ericksen Representation Theorem and (2.9), we obtain the representation

$$\mathbf{G}(\mathbf{T}) = \beta_1\mathbf{I} + \beta_2\mathbf{T} + \beta_3\mathbf{T}^2,$$

where material moduli β_i, $i \in \{0, 1, 2\}$ are functions of the invariants of Cauchy stress I_T, II_T and III_T and $\beta_1(0, 0, 0) = 0$.

Constitutive relations of the type (2.8) are complimentary to the constitutive relations for the Cauchy elastic solid (2.5). The role of stress and strain is flipped as strain is an explicit function of stress. This is coherent with the classical Newtonian concept of causality, where force represented by stress is the cause for kinematic phenomena of deformation, see Rajagopal (2010). Fitting the experimental data to the models (2.8) is of a similar difficulty as fitting the data to models of the type (2.5). For example, in Criscione – Rajagopal (2013), the authors use a particular model of the type (2.8) to obtain a very good fit of the experimental data for large deformations of rubber, published in Penn (1970).

Linearization

When assuming that the norm of displacement gradient is small, that is $|\nabla_{\mathbf{X}}\mathbf{u}| < \delta \ll 1$, then we can easily approximate the constitutive equation (2.8) by the model working with a small strain tensor $\boldsymbol{\varepsilon}$. We can estimate $\mathbf{B} \approx \mathbf{I} + 2\boldsymbol{\varepsilon}$, see Proposition A.121 (p 144). From (2.8), we have that

$$\mathbf{I} + 2\boldsymbol{\varepsilon} = \mathbf{G}(\mathbf{T}). \tag{2.10}$$

The equation (2.10) leads to the following definition of isotropic solid where small strain is a function of stress.

Definition 2.5 (Isotropic solid where small strain is a function of stress). *The isotropic material where strain is a function of stress is a material with a constitutive relation of the type*

$$\boldsymbol{\varepsilon} = \mathbf{G}(\mathbf{T}). \tag{2.11}$$

The constitutive function behaves under the action of arbitrary orthogonal transformation given by matrix $\mathbf{Q} \in OG(n)$ in the way that (objectivity, frame indifference, isotropy)

$$\mathbf{G}(\mathbf{Q}\mathbf{T}\mathbf{Q}^{\top}) = \mathbf{Q}\mathbf{G}(\mathbf{T})\mathbf{Q}^{\top}, \quad \mathbf{G}(\mathbf{0}) = \mathbf{0}.$$

Using Rivlin Ericksen Representation Theorem and (2.12), the equation (2.11) takes the form

$$\mathbf{G}(\mathbf{T}) = \gamma_1\mathbf{I} + \gamma_2\mathbf{T} + \gamma_3\mathbf{T}^2. \tag{2.12}$$

The material moduli γ_i, $i = 1 \dots 3$ are functions of the invariants of Cauchy stress I_T, II_T and III_T and $\gamma_1(0,0,0) = 0$. It should be noted that the small strain tensor $\boldsymbol{\varepsilon}$ is not objective. However, under the small displacement gradient assumption, $\boldsymbol{\varepsilon}$ should be understood as an approximation of the objective tensor $(\mathbf{B} - \mathbf{I})/2$, which is constituted by the relation (2.11) and fulfils (2.12).

Models (2.11) can only be rigorously justified within the newly developed framework of implicit constitutive relations, see Rajagopal (2003, 2007); Rajagopal – Srinivasa (2007). In the classical theory, using linearized strain and at the same time admitting nonlinear response would lead to inconsistency of the model, see Rajagopal (2007); Criscione – Rajagopal (2013). Therefore the models from Definition 2.5 extend significantly the admissible range of material responses. In general, models of the type (2.11) are useful for modeling situations and regimens where strain remains small[6] and at the same time where nonlinear response occurs during the studied process. There are no restrictions on the stress magnitude. It can even be very high. In particular, these models are suitable for numerous materials, which exhibit nonlinear relationship between stress and strain in the small displacement gradient range, see Rajagopal (2014); Saito et al. (2003); Zhang et al. (2009); Penn (1970).

In Chapter 3, we study models of the type (2.11) for describing responses of beta phase titanium alloys, namely Gum Metal, *Ti-30Nb-10Ta-5Zr* alloy, *Ti-24Nb-4Zr-7.9Sn* alloy and *Ti-30Nb-12Zr* alloy.

[6] According to Rajagopal (2014), the strain can be regarded as small when $\|\boldsymbol{\varepsilon}\| < 0.1$.

2.4 Studied constitutive models

The representation (2.12) is relatively complex. In the thesis we restrict ourselves to the particular subclasses of (2.12). We define a reduced constitutive model as follows.

Definition 2.6 (Reduced constitutive model). *In the thesis, we study a subclass of materials constituted by Definition 2.5 for which*

$$\boldsymbol{\varepsilon} = \gamma_1(\mathrm{I}_T, \mathrm{II}_T)\mathbf{I} + \gamma_2(\mathrm{I}_T, \mathrm{II}_T)\mathbf{T}, \tag{2.13}$$

where γ_1 and γ_2 are scalar functions that depend on the first two invariants of Cauchy stress I_T and II_T and $\gamma_1(0,0) = 0$.

In the scientific literature, sometimes $\gamma_i(\operatorname{tr}\mathbf{T}, |\mathbf{T}|)$ is used instead of $\gamma_i(\mathrm{I}_T, \mathrm{II}_T)$. We will show that these representations are equivalent.

Lemma 2.7. *Let $\mathbf{T}$ be a symmetric second order tensor. The trace $\operatorname{tr}\mathbf{T}$ and the norm $|\mathbf{T}|$ can be expressed as a functions of the first two invariants of $\mathbf{T}$.*

Proof. Recall that

$$\mathrm{I}_T = \operatorname{tr}\mathbf{T}, \quad \mathrm{II}_T = \frac{1}{2}\left((\operatorname{tr}\mathbf{T})^2 - |\mathbf{T}|^2\right), \quad \text{where} \quad |\mathbf{T}| = \sqrt{\operatorname{tr}\mathbf{T}^2}. \tag{2.14}$$

By a simple manipulation with (2.14), we get

$$\operatorname{tr}\mathbf{T} = \mathrm{I}_T, \quad |\mathbf{T}| = \sqrt{\mathrm{I}_T^2 - 2\mathrm{II}_T},$$

that finishes the proof. □

Therefore it is possible to write coefficients γ_i, $i \in \{1, 2\}$ in (2.13) equivalently in the form

$$\gamma_1 = \gamma_1(\operatorname{tr}\mathbf{T}, |\mathbf{T}|), \qquad \gamma_2 = \gamma_2(\operatorname{tr}\mathbf{T}, |\mathbf{T}|),$$

where $\gamma_1(0,0) = 0$.

2.4.1 Separation of non-isochoric part from isochoric parts of deformation

Shearing deformation is an isochoric response. That means that the deformation preserves volume of the deformed body. Bulk deformation is a response to the mean normal stress that changes volume. In Hooke's law, the shearing deformation is described by the shear modulus μ and the non-isochoric deformation by the bulk modulus K, see Section A.3.4, (p. 148). The ratio of the shear modulus to the bulk modulus differs from material to material. Some materials such as rubber are usually modeled as incompressible due to the fact that the ratio of shear modulus to bulk modulus is of order 10^4, see Horgan – Saccomandi (2004). Another materials such as steel are much more compressible and their shear modulus is of the same order as the bulk modulus. Moreover, as the measurement of the non-isochoric response is in the most cases independent from the measurement of shear or tensile response, it seems to be more appropriate to separate these responses also on the level of the

model, see Criscione et al. (2000); Fook et al. (1976). In the following definition, we employ such separation of non-isochoric part of deformation from isochoric parts of deformation to model the response of the isotropic solid where small strain is a function of the stress.

Definition 2.8 (Reduced model with separated non-isochoric and isochoric responses). *The constitutive model defined by relations between deviatoric parts and traces of the small strain tensor ε and Cauchy stress $\mathbf{T}$.*

$$\begin{aligned} \operatorname{tr}\varepsilon &= \sigma_1(\operatorname{tr}\mathbf{T})\operatorname{tr}\mathbf{T}, \\ \varepsilon^d &= \sigma_2(|\mathbf{T}^d|)\mathbf{T}^d, \end{aligned} \tag{2.15}$$

where σ_1 and σ_2 are scalar functions, $\sigma_1(0) = 0$ and $\sigma_2(0) = 0$.

The following Lemma shows that the models with non-isochoric part of deformation separated from the isochoric parts of deformation (2.15) are a special subclass of the models from Definition 2.6.

Lemma 2.9. *Constitutive relation for the material from Definition 2.8 can be expressed as a special case of the constitutive relation from Definition 2.6.*

Proof. The term $|\mathbf{T}^d|$ can be expressed as

$$|\mathbf{T}^d| = |\mathbf{T} - \frac{\operatorname{tr}\mathbf{T}}{3}\mathbf{I}| = \sqrt{|\mathbf{T}|^2 - \frac{1}{3}(\operatorname{tr}\mathbf{T})^2}, \tag{2.16}$$

thus from Lemma 2.7, $|\mathbf{T}^d|$ is a function of invariants I_T and II_T. From (2.15),

$$\varepsilon = \gamma_1(\operatorname{tr}\mathbf{T}, |\mathbf{T}|)\mathbf{I} + \gamma_2(\operatorname{tr}\mathbf{T}, |\mathbf{T}|)\mathbf{T}, \tag{2.17}$$

where

$$\begin{aligned} \gamma_1(\operatorname{tr}\mathbf{T}, |\mathbf{T}|) &= \frac{\sigma_1(\operatorname{tr}\mathbf{T})\operatorname{tr}\mathbf{T}}{3} - \frac{\operatorname{tr}\mathbf{T}}{3}\sigma_2\left(\sqrt{|\mathbf{T}|^2 - \frac{1}{3}(\operatorname{tr}\mathbf{T})^2}\right), \\ \gamma_2(\operatorname{tr}\mathbf{T}, |\mathbf{T}|) &= \sigma_2\left(\sqrt{|\mathbf{T}|^2 - \frac{1}{3}(\operatorname{tr}\mathbf{T})^2}\right). \end{aligned} \tag{2.18}$$

When $\operatorname{tr}\mathbf{T} = 0$ and $|\mathbf{T}| = 0$, we have that

$$\sigma_1(\operatorname{tr}\mathbf{T}) = 0, \quad \sigma_2(\sqrt{|\mathbf{T}|^2 - (\operatorname{tr}\mathbf{T})^2/3}) = 0$$

and thus $\gamma_1(\operatorname{tr}\mathbf{T}, |\mathbf{T}|) = 0$. We see that the model from Definition 2.8 is a subclass of the model from Definition 2.6. □

The reduced model with separated non-isochoric and isochoric responses, see Definition 2.8 is a special case of the model from Definition 2.6. This model still includes linear Hooke's law, see (A.30) (p. 149). The only restriction is that the non-isochoric response and the shearing response have to be modeled independently.

2.4.2 Power-law model with separated response

Power-law models were introduced in Section 2.2 as elegant tools to describe material response phenomenologically. We mention Generalized Ramberg-Osgood model proposed in Knees – Sändig (2004).

Definition 2.10 (Generalized Ramberg-Osgood model). *The constitutive model defined by relations between deviatoric parts and traces of the small strain tensor ε and Cauchy stress $\mathbf{T}$ in the form*

$$\begin{aligned} \operatorname{tr}\varepsilon &= \frac{1}{3K}\operatorname{tr}\mathbf{T}, \\ \varepsilon^d &= \frac{1}{2\mu}\mathbf{T}^d + C\left(\frac{|\mathbf{T}^d|}{\tau_\mu}\right)^{q'-2}\mathbf{T}^d, \end{aligned} \tag{2.19}$$

where $K > 0$, $\mu > 0$, $C > 0$, $\tau_\mu > 0$, $q' \in [2, \infty)$ are material moduli.

In this thesis, we study a more general model of the power-law response justified by Definition 2.8, which uses the separation of the non-isochoric part from the isochoric parts of the deformation and admits independent power-law exponents in those two parts of the response.

Definition 2.11 (Power-law solid). *The constitutive model defined by relations between deviatoric parts and traces of the small strain tensor ε and Cauchy stress $\mathbf{T}$ in the form*

$$\begin{aligned} \operatorname{tr}\varepsilon &= \frac{1}{3K}\left(\frac{\tau_K^2 + |\operatorname{tr}\mathbf{T}|^2}{\tau_K^2}\right)^{\frac{s'-2}{2}}\operatorname{tr}\mathbf{T}, \\ \varepsilon^d &= \frac{1}{2\mu}\left(\frac{\tau_\mu^2 + |\mathbf{T}^d|^2}{\tau_\mu^2}\right)^{\frac{q'-2}{2}}\mathbf{T}^d, \end{aligned} \tag{2.20}$$

where $q' \in (1, \infty)$, $s' \in (1, \infty)$, $K > 0$, $\tau_K > 0$, $\mu > 0$, $\tau_\mu > 0$ are material moduli.

We wish to remark that the model (2.20) can be put in the appropriate thermodynamic setting, see Rajagopal – Srinivasa (2007, 2009); Bridges – Rajagopal (2014). In particular, there is a (Gibbs) potential $\mathcal{G}(\mathbf{T})$, see Bulíček et al. (2014), of the form

$$\mathcal{G}(\mathbf{T}) = \frac{1}{2}\int_0^{|\operatorname{tr}\mathbf{T}|^2}\frac{1}{9K}\left(\frac{\tau_K^2+\xi}{\tau_K^2}\right)^{\frac{s'-2}{2}}\mathrm{d}\xi + \frac{1}{2}\int_0^{|\mathbf{T}^d|^2}\frac{1}{2\mu}\left(\frac{\tau_\mu^2+\xi}{\tau_\mu^2}\right)^{\frac{q'-2}{2}}\mathrm{d}\xi, \tag{2.21}$$

so that (2.20) can be written in the form

$$\varepsilon = \frac{\partial\mathcal{G}}{\partial\mathbf{T}}.$$

Lemma 2.12 (Linearization of power-law solid). *By linearizing the constitutive relation* (2.20) *from Definition 2.11 around $\mathbf{T} = \mathbf{0}$, we obtain Hooke's law, see* (A.34) *(p. 151) with bulk modulus K and shear modulus μ.*

Proof. Using classical linearization, we approximate $\operatorname{tr}\varepsilon$ around $\operatorname{tr} T = 0$ and ε^d around $\mathbf{T}^d = \mathbf{0}$ by linear functions $L\operatorname{tr}\varepsilon$ and $L\varepsilon^d$ so that

$$\begin{aligned} L\operatorname{tr}\varepsilon(\operatorname{tr}\mathbf{T}) &= \operatorname{tr}\varepsilon(0) + \left.\frac{d\operatorname{tr}\varepsilon}{d\operatorname{tr}\mathbf{T}}\right|_{\operatorname{tr}\mathbf{T}=0} \operatorname{tr} T, \\ L\varepsilon_{ij}^d(\mathbf{T}) &= \varepsilon^d(\mathbf{0}) + \sum_{k,l} \left.\frac{\partial\varepsilon_{ij}^d}{\partial T_{kl}^d}\right|_{\mathbf{T}^d=\mathbf{0}} T_{kl}^d. \end{aligned} \tag{2.22}$$

To compute derivatives in (2.22), first recall that

$$\frac{\partial|\mathbf{A}|}{\partial A_{ij}} = \frac{A_{ij}}{|\mathbf{A}|}. \tag{2.23}$$

Combining (2.22) with (2.20), the derivative of $\operatorname{tr}\varepsilon$ with respect to $\operatorname{tr}\mathbf{T}$ is of the form

$$\frac{d\operatorname{tr}\varepsilon}{d\operatorname{tr}\mathbf{T}} = \frac{s'-2}{3K\tau_K^2}\left(\frac{\tau_K^2 + |\operatorname{tr}\mathbf{T}|^2}{\tau_K^2}\right)^{\frac{s'-4}{2}} (\operatorname{tr}\mathbf{T})^2 + \frac{1}{3K}\left(\frac{\tau_K^2 + |\operatorname{tr}\mathbf{T}|^2}{\tau_K^2}\right)^{\frac{s'-2}{2}} \tag{2.24}$$

and partial derivatives of $\varepsilon^d(\mathbf{T}^d)$ with respect to $\mathbf{T}^d$ take the form

$$\frac{\partial\varepsilon_{ij}^d(\mathbf{T}^d)}{\partial T_{kl}^d} = \frac{q'-2}{2\mu\tau_\mu^2}\left(\frac{\tau_\mu^2 + |\mathbf{T}^d|^2}{\tau_\mu^2}\right)^{\frac{q'-4}{2}} T_{kl}^d T_{ij}^d + \frac{1}{2\mu}\left(\frac{\tau_\mu^2 + |\mathbf{T}^d|^2}{\tau_\mu^2}\right)^{\frac{q'-2}{2}} \delta_{ik}\delta_{jl}. \tag{2.25}$$

We rewrite (2.24) and (2.25) using $\varepsilon^d(\mathbf{0}) = \mathbf{0}$, $\operatorname{tr}\varepsilon^d(\mathbf{0}) = \mathbf{0}$ to get that

$$\left.\frac{d\operatorname{tr}\varepsilon}{d\operatorname{tr}\mathbf{T}}\right|_{\operatorname{tr}\mathbf{T}=0} = \frac{1}{3K}, \tag{2.26}$$

$$\left.\frac{\partial\varepsilon_{ij}^d(\mathbf{T}^d)}{\partial T_{kl}^d}\right|_{\mathbf{T}^d=0} = \frac{1}{2\mu}\delta_{ik}\delta_{jl}. \tag{2.27}$$

We conclude that the linearization (2.22) leads to the Hooke's law, where

$$\begin{aligned} L\operatorname{tr}\varepsilon(\operatorname{tr}\mathbf{T}) &= \frac{1}{3K}\operatorname{tr} T, \\ L\varepsilon_{ij}^d(\mathbf{T}) &= \frac{1}{2\mu}T_{ij}^d, \end{aligned} \tag{2.28}$$

and the material moduli K and μ have the meaning of bulk modulus and shear modulus. □

In Chapter 3, we estimate material moduli using the model (2.20) for four different beta phase titanium alloys that behave nonlinearly in the small strain range. We show that these sets of material moduli fit the experimental data from tensile loading experiment very well. In chapter 4, we derive the weak formulation of Problem (P), see Definition 1.1, (p. 7). Then we prove the existence of the weak solution to the Problem (P) when using the constitutive model (2.20). In chapter 5, we study the behavior of the power-law solids by computer simulation.

2.4.3 Strain-limiting models

In this thesis, we are mostly interested in studying the power law model (2.20), which can have different polynomial growth in the non-isochoric part and in the isochoric parts of the response. For the sake of completeness, we also include important results for the so called strain-limiting response, which can be understood as a borderline case of power-law response, where we admit to set $q' = 1$ and $s' = 1$ in the model (2.20).

Definition 2.13 (Basic strain-limiting solid). *The constitutive model defined by relations between deviatoric parts and traces of the small strain tensor ε and Cauchy stress $\mathbf{T}$ in the form*

$$\begin{aligned} \operatorname{tr}\varepsilon &= \frac{\tau_K}{3K}\frac{\operatorname{tr}\mathbf{T}}{\sqrt{\tau_K^2+|\operatorname{tr}\mathbf{T}|^2}}, \\ \varepsilon^d &= \frac{\tau_\mu}{2\mu}\frac{\mathbf{T}^d}{\sqrt{\tau_\mu^2+|\mathbf{T}^d|^2}}, \end{aligned} \tag{2.29}$$

where $K > 0$, $\tau_K > 0$, $\mu > 0$, $\tau_\mu > 0$ are model parameters.

A model of this type was first proposed in Neuber (1961). When setting $q' = 1$ and $s' = 1$ in the model (2.20), we obtain exactly the model (2.29) and therefore we can use Lemma 2.12 to show that upon its linearization we get Hooke's law with the bulk modulus K and the shear modulus μ. Next lemma shows that the strain-limiting model (2.29) represents a sublinear response where strain is bounded for any stress.

Lemma 2.14. *Let $K > 0$, $\tau_K > 0$, $\mu > 0$, $\tau_\mu > 0$ be parameters of the model (2.29), then there exists a constant $C > 0$ such that $\forall \mathbf{T} \in \mathbb{R}^{3\times3}_{sym} : |\varepsilon(\mathbf{T})| < C$.*

Proof. By rewriting (2.29) into the form

$$|\operatorname{tr}\varepsilon| = \frac{\tau_K}{3K}\sqrt{\frac{|\operatorname{tr}\mathbf{T}|^2}{\tau_K^2+|\operatorname{tr}\mathbf{T}|^2}} \le \frac{\tau_K}{3K}, \tag{2.30}$$

and

$$\left|\varepsilon^d\right| = \frac{\tau_\mu}{2\mu}\sqrt{\frac{|\mathbf{T}^d|^2}{\tau_\mu^2+|\mathbf{T}^d|^2}} \le \frac{\tau_\mu}{2\mu}, \tag{2.31}$$

we immediately get the claim of the Lemma. □

Rajagopal strain-limiting solid

In the context of the implicit constitutive theory, another strain limiting model was proposed in Rajagopal (2011b); Rajagopal – Walton (2011) to study brittle materials and problems in fracture mechanics.

Definition 2.15 (Rajagopal strain-limiting solid). *The constitutive model defined by relations between small strain tensor ε and Cauchy stress $\mathbf{T}$ in the form*

$$\varepsilon = -\beta\left(1-\exp\frac{-\gamma\operatorname{tr}\mathbf{T}}{1+|\mathbf{T}|}\right)\mathbf{I} + \frac{\tau_\mu}{2\mu}\frac{\mathbf{T}}{\left(\tau_\mu^{\,a}+|\mathbf{T}|^{\,a}\right)^{1/a}}, \tag{2.32}$$

where $\beta \geq 0$, $\gamma > 0$, $\mu > 0$, $\tau_\mu > 0$, $a > 0$ *are material moduli*[7].

The model (2.32) does not have the non-isochoric part separated from the isochoric parts of deformation and therefore it does not belong to the class of models given by the Definition 2.8. However, we can propose a strain-limiting model that is similar to (2.32) that separates aforementioned parts of the deformation.

Definition 2.16 (Strain-limiting solid with non-isochoric response separated from isochoric response). *The constitutive model defined by relations between deviatoric parts and traces of the small strain tensor* $\boldsymbol{\varepsilon}$ *and Cauchy stress* $\mathbf{T}$ *in the form*

$$\begin{aligned} \operatorname{tr} \boldsymbol{\varepsilon} &= 3\beta \left(1 - \exp \frac{-\gamma \operatorname{tr} \mathbf{T}}{1 + |\operatorname{tr} \mathbf{T}|}\right), \\ \boldsymbol{\varepsilon}^d &= \frac{\tau_\mu}{2\mu} \frac{\mathbf{T}^d}{\left(\tau_\mu^a + |\mathbf{T}^d|^a\right)^{1/a}}, \end{aligned} \tag{2.33}$$

where $\beta \geq 0$, $\gamma > 0$, $\mu > 0$, $\tau_\mu > 0$, $a > 0$ *are material moduli.*

Following results documents that models of the type (2.32) and (2.33) has bounded stains for arbitrary stress and that they can be linearized around $\mathbf{T} = \mathbf{0}$ to obtain Hooke's law.

Lemma 2.17. *Let* $\beta \geq 0$, $\gamma > 0$, $\mu > 0$, $\tau_\mu > 0$, $a > 0$ *be material moduli of the model* (2.32). *Then there exists a constant* $C > 0$ *such that* $\forall \mathbf{T} \in \mathbb{R}^{3\times 3}_{sym} : |\boldsymbol{\varepsilon}(\mathbf{T})| < C$.

Proof. We begin by noticing that

$$|T_{ii}| \leq \sqrt{T_{11}^2 + T_{22}^2 + T_{33}^2}, \quad i \in \{1, 2, 3\}, \tag{2.34}$$

and that

$$|\mathbf{T}| \geq \sqrt{T_{11}^2 + T_{22}^2 + T_{33}^2}. \tag{2.35}$$

From the previous inequalities, we establish the inequality

$$\frac{|\operatorname{tr} \mathbf{T}|}{1 + |\mathbf{T}|} \leq \frac{|T_{11}| + |T_{22}| + |T_{33}|}{1 + \sqrt{T_{11}^2 + T_{22}^2 + T_{33}^2}} \leq 3. \tag{2.36}$$

By similar reasoning, we obtain

$$\frac{\tau_\mu}{2\mu} \frac{|T_{ij}|}{\left(\tau_\mu^a + |\mathbf{T}|^a\right)^{1/a}} \leq \frac{\tau_\mu}{2\mu} \frac{|T_{ij}|}{|\mathbf{T}|} \leq \frac{\tau_\mu}{2\mu}. \tag{2.37}$$

Setting a bound on $|\varepsilon_{ij}|$ will be divided into two parts. First, when $i \neq j$, we combine (2.32) and (2.37) to obtain

$$-\frac{\tau_\mu}{2\mu} \leq \varepsilon_{ij} \leq \frac{\tau_\mu}{2\mu} \quad \text{for } i \neq j. \tag{2.38}$$

[7]The former strain-limiting model from Rajagopal (2010) has $\beta < 0$, but it would lead to $\hat{\lambda}$ being always negative in the linearized relation, see Lemma 2.18 To avoid this in Definition 2.15, we change the sign of β.

When $i = j$, we have to deal with the first term in (2.32). From (2.36) and (2.32), we derive an additional estimate

$$\left| -\beta \left(1 - \exp \frac{-\gamma \operatorname{tr} \mathbf{T}}{1 + |\operatorname{tr} \mathbf{T}|} \right) \right| \leq \beta(1 + e^{3\gamma}). \tag{2.39}$$

Combining results from (2.38) and (2.39), we can set a bound on the ε_{ij} for all $i, j \in \{1 \dots 3\}$ such that

$$-\beta(1 + e^{3\gamma}) - \frac{\tau_\mu}{2\mu} \leq \varepsilon_{ij} \leq \beta(1 + e^{3\gamma}) + \frac{\tau_\mu}{2\mu},$$

therefore we can conclude that $|\boldsymbol{\varepsilon}(\mathbf{T})|$ is bounded for an arbitrary $\mathbf{T} \in \mathbb{R}^{3\times3}_{sym}$. □

Lemma 2.18 (Linearization of strain-limiting model). *When we linearize the constitutive relation* (2.32) *from Definition 2.15 around* $\mathbf{T} = \mathbf{0}$*, we obtain Hooke's law, see* (A.30) *(p. 149) with Lamé parameters* $\hat{\lambda}$*,* $\hat{\mu}$*, where*

$$\hat{\lambda} = \frac{4\beta\gamma\mu^2}{1 - 6\beta\gamma\mu}, \quad \hat{\mu} = \mu.$$

Proof. Recall that the derivatives of tensor invariants take the form

$$\frac{\partial \operatorname{tr} \mathbf{A}}{\partial A_{ij}} = \delta_{ij}, \quad \frac{\partial |\mathbf{A}|}{\partial A_{ij}} = \frac{A_{ij}}{|\mathbf{A}|}. \tag{2.40}$$

Using (2.40), we compute derivatives of $\boldsymbol{\varepsilon}(\mathbf{T})$ with respect to $\mathbf{T}$ for the constitutive relation (2.32). We have that

$$\frac{\partial \varepsilon_{ij}(\mathbf{T})}{\partial T_{kl}} = -\delta_{ij}\beta\gamma \exp\left(\frac{-\gamma \operatorname{tr} \mathbf{T}}{1 + |\mathbf{T}|}\right) \left(\frac{\delta_{kl}}{1 + |\mathbf{T}|} - \frac{\operatorname{tr} \mathbf{T}\, T_{kl}}{|\mathbf{T}|(1 + |\mathbf{T}|)^2} \right) + \frac{\tau_\mu \delta_{ik}\delta_{jl}}{2\mu \left(\tau_\mu^a + |\mathbf{T}|^a\right)^{1/a}} - \frac{\tau_\mu T_{ij} T_{kl} |\mathbf{T}|^{a-2}}{2\mu \left(\tau_\mu^a + |\mathbf{T}|^a\right)^{\frac{a+1}{a}}},$$

from which is easy to show that

$$\left.\frac{\partial \varepsilon_{ij}}{\partial T_{kl}}\right|_{\mathbf{T}=\mathbf{0}} = -\delta_{ij}\delta_{kl}\beta\gamma + \frac{\delta_{ik}\delta_{jl}}{2\mu}. \tag{2.41}$$

Using linearization, we approximate $\boldsymbol{\varepsilon}(\mathbf{T})$ around $\mathbf{T} = \mathbf{0}$ by linear function $L\varepsilon_{ij}(\mathbf{T})$ such that

$$L\varepsilon_{ij}(\mathbf{T}) = \boldsymbol{\varepsilon}(\mathbf{0}) + \sum_{k,l} \left.\frac{\partial \varepsilon_{ij}}{\partial T_{kl}}\right|_{\mathbf{T}=\mathbf{0}} T_{kl}. \tag{2.42}$$

When we substitute the equation (2.41) into (2.42) and utilize that $\boldsymbol{\varepsilon}(\mathbf{0}) = \mathbf{0}$, we have that

$$L\varepsilon_{ij}(\mathbf{T}) = -\sum_{k,l} \delta_{ij}\delta_{kl}\beta\gamma\, T_{kl} + \sum_{k,l} \frac{\delta_{ik}\delta_{jl}}{2\mu} T_{kl} = -\beta\gamma\delta_{ij} \operatorname{tr} \mathbf{T} + \frac{T_{ij}}{2\mu}. \tag{2.43}$$

It is a simple matter to rewrite (2.43) into the form

$$L\boldsymbol{\varepsilon}(\mathbf{T}) = -\beta\gamma \operatorname{tr} \mathbf{T}\mathbf{I} + \frac{\mathbf{T}}{2\mu}.$$

Comparing the last equation to Hooke's law (A.30) with Lamé parameters $\hat{\lambda}$ and $\hat{\mu}$, we get

$$\beta\gamma = \frac{\hat{\lambda}}{2\hat{\mu}(3\hat{\lambda} + 2\hat{\mu})}, \quad \mu = \hat{\mu},$$

which yields

$$\hat{\lambda} = \frac{4\beta\gamma\mu^2}{1 - 6\beta\gamma\mu}, \quad \hat{\mu} = \mu.$$

□

In Kulvait et al. (2013), computer simulations relevant to the strain-limiting solid (2.32) in a plate with a V-notch, subject to the state of anti-plane stress, are presented. In particular, the existence of stress concentration near the V-notch tip and the boundedness of strain is computationally documented therein. The asymptotic behavior of stress near the V-notch tip is further studied in Gou et al. (2015); Zappalorto – Lazzarin (2011). Numerical studies regarding stress and strain distributions in a tensile loaded finite rectangular plate with an elliptic hole were published in Ortiz et al. (2012, 2014).

3. Modeling of Gum Metal and other newly developed titanium alloys

Titanium is the 9th most abundant element in the Earth's crust, see Neal et al. (2011). At temperature of 882.5 °C, it undergoes allotropic transformation from the close packed hexagonal alpha phase to the body centered cubic beta phase. Transformation temperature can be altered by addition of some elements. Alpha stabilisers are elements that increase transformation temperature, such as Aluminium (Al), Oxygen (O), Nitrogen (N) or Carbon (C). Elements that decrease transformation temperature, such as Molybdenum (Mo), Vanadium (V), Niobium (Nb), Cooper (Cu) or Silicon (Si), are called beta stabilisers. Titanium alloys are metals that consists of a mixture of titanium, as a dominant component, and other chemical elements. In general, there are three types of titanium alloys, alpha alloys with alpha stabilisers where titanium is in alpha phase, alpha-beta alloys where titanium exists in both phases and beta alloys with beta stabilisers where titanium is in beta phase, see Machado – Wallbank (1990). We follow a notation, where a titanium alloy is denoted by the chemical symbol of Titanium (Ti) followed by chemical symbols of other elements in the mixture preceded by their relative abundance in the alloy. For example, Titanium alloy with a composition of 6% Alluminium (Al) and 4% Vanadium (V) is denoted by *Ti-6Al-4V*. Titanium alloys provide extraordinary material properties such as high strength, resistance to corrosion and resistance to high temperatures. They are expensive to manufacture and thus their main areas of application are high tech industries (automotive industry, aerospace industry, premium electronics), military equipment and medical materials, see Wikipedia (2017b).

In material science, there is an ongoing effort to develop new titanium alloys in virtue of their beneficial properties. An illustrative example is Gum Metal[1], a material that has been developed by Toyota central R&D labs. Gum Metal is a designation for a class of beta titanium alloys with unique elastic properties that include low Young's modulus, high strength and high yield strain relative to the other conventionally used materials and titanium alloys, see Nagasako et al. (2013) and Figure 3.1. Cold swagged Gum Metal has reversible nonlinear elastic response up to strains of 2.5 %, which is referred to as super elasticity, see Talling et al. (2009); Saito et al. (2003).

Gum Metal, however, is not the only titanium alloy that exhibits nonlinear response between the strain and the stress in the elastic regime, which can be considered small strain. Such nonlinear elastic behavior seems to be typical for many beta phase titanium alloys, see Sakaguch et al. (2004); Hao et al. (2005); Hou et al. (2010). Therefore, in addition to Gum Metal, we study the following beta phase titanium alloys: *Ti-30Nb-10Ta-5Zr* alloy, see Sakaguch et al. (2004), *Ti-24Nb-4Zr-7.9Sn* alloy, see Hao et al. (2005) and *Ti-30Nb-12Zr* alloy, see Hou et al. (2010). We show that these beta phase titanium alloys in their elastic regime can be modeled using power-law models (2.20).

[1]GUMMETAL is a trademark owned by TOYOTSU MATERIAL INCORPORATED company (as of 2017).

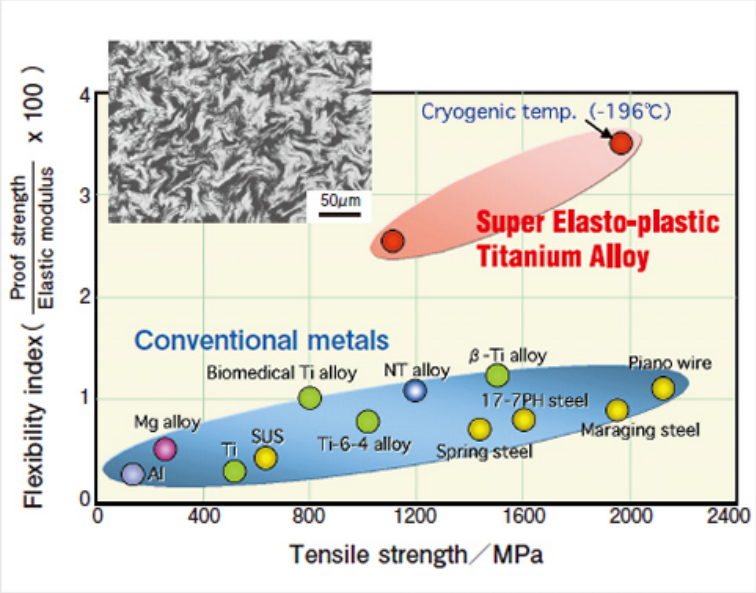

Figure 3.1: Unique elastic properties of the Gum Metal alloy. Image source: http://www.tytlabs.com/tech/tec2.html

3.1 Experimental data

We use the power-law models (2.20) to capture behavior of beta phase titanium alloys. For comparison, we are using the same experimental data as the works Rajagopal (2014) and Devendiran et al. (2017). These data originate from uniaxial tensile loading experiments.

A tensile loading experiment is described by the set of pairs (σ^i, η^i), $i = \{1 \dots N\}$. Each pair contains the value of strain η^i corresponding to the loading stress σ^i. There is no loss of generality in assuming that the tensile stress is applied along the direction of the first Cartesian coordinate. Therefore, the stress tensor takes the form

$$\mathbf{T} = (\mathbf{e}_1 \otimes \mathbf{e}_1)\sigma = \begin{pmatrix} \sigma & 0 & 0 \\ 0 & 0 & 0 \\ 0 & 0 & 0 \end{pmatrix}, \tag{3.1}$$

where $T_{11} = \sigma$ is its only nonzero component[2]. We shall also identify the normal strain components $(\varepsilon_{11}, \varepsilon_{22}, \varepsilon_{33})$ with (η, γ, γ), i.e. we assume that $\varepsilon_{22} = \varepsilon_{33}$. Note that to our best knowledge there are no data regarding the transverse strain γ.

Experiments describing tensile loading behavior of Gum Metal, *Ti-30Nb-10Ta-5Zr* alloy, *Ti-24Nb-4Zr-7.9Sn* alloy and *Ti-30Nb-12Zr* alloy can be found in the following works Saito et al. (2003); Sakaguch et al. (2004); Hao et al. (2005); Hou et al. (2010). We use the data from the elastic regime of these experiments as they were presented in Rajagopal (2014) and Devendiran et al. (2017). Data describing tensile loading of cold swagged Gum Metal are from (Rajagopal, 2014, Figure 1). Data for *Ti-30Nb-10Ta-5Zr* alloy were obtained from (Devendiran et al., 2017, Figure 1, top). Data for *Ti-24Nb-4Zr-7.9Sn* alloy are from (Devendiran et al., 2017, Figure 1, middle). Data that

[2]Symbol $\mathbf{e}_1$ denotes the unit vector in the direction of the first Cartesian coordinate and symbol $\otimes$ denotes the tensor product.

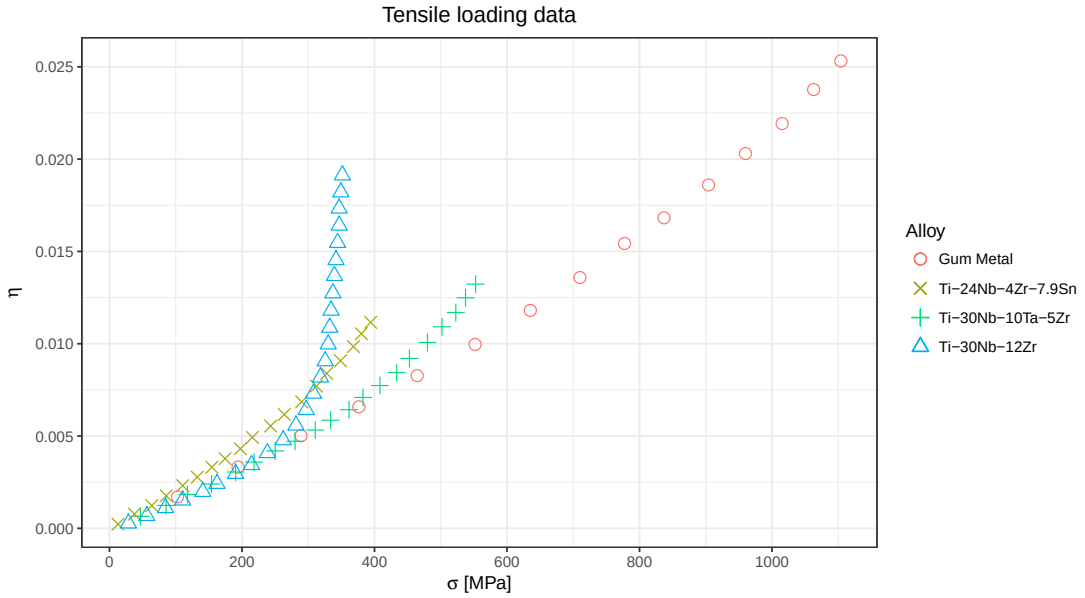

Figure 3.2: A tensile loading data of beta phase titanium alloys, see also Tables 3.1–3.4.

describe *Ti-30Nb-12Zr* alloy originate from (Devendiran et al., 2017, Figure 1, bottom). We extracted data from the referenced figures using Plot Digitizer[3]. These data can be found in Tables 3.1–3.4, they are summarized in Figure 3.2.

3.2 Existing models

The reversible elastic response of cold swagged Gum Metal can be observed up to strains of 2.5 %, see Saito et al. (2003) and Figure 3.2. Since the elastic response of Gum Metal and many other titanium alloys is in the range $|\varepsilon| < 0.025$, such strains could be regarded as large by experimentalists because most metals exceed elastic regime for this magnitude of strain. On the other hand, from the modeling point of view we can use a small displacement gradient approximation and model the response using a small strain tensor since the displacement gradient is small enough that its square can be neglected, see Rajagopal (2014). Therefore existing models proposed in Rajagopal (2014) and Devendiran et al. (2017) use small strain to predict response of beta phase titanium alloys in their elastic regime.

Modeling Gum Metal

Two models were proposed in Rajagopal (2014) to fit the experimental data for cold swagged Gum Metal, see Table 3.1. The first model is a power-law model wherein the strain is given by

$$\varepsilon = \lambda_1 \mathbf{I} \operatorname{tr} \mathbf{T} + \lambda_2 (1 + \alpha \operatorname{tr} \mathbf{T}^2)^n \mathbf{T},$$

[3]Plot Digitizer is an open source software for digitizing scanned plots of functional data, see http://plotdigitizer.sourceforge.net. Plot Digitizer is written in Java and licensed under the GNU General Public License.

Point #	Stress σ [MPa]	Strain η
1	102.8	0.0017
2	194.1	0.0033
3	289.1	0.0050
4	376.4	0.0066
5	464.5	0.0083
6	551.8	0.0100
7	635.2	0.0118
8	710.1	0.0136
9	777.4	0.0154
10	837.0	0.0168
11	904.2	0.0186
12	960.0	0.0203
13	1015.2	0.0219
14	1062.8	0.0238
15	1103.9	0.0253

Table 3.1: Uniaxial tensile loading data of the cold swagged Gum Metal alloy, see Saito et al. (2003). Data were extracted from (Rajagopal, 2014, Figure 1).

where λ_1, λ_2, α and n are the material moduli. The second is an exponential model of the form

$$\boldsymbol{\varepsilon} = \lambda_1 \mathbf{I} \operatorname{tr} \mathbf{T} + \lambda_2 \mathbf{T} \exp(\beta \operatorname{tr} \mathbf{T}), \tag{3.2}$$

where λ_1, λ_2 and β are the material moduli. For the uniaxial loading, when setting $\lambda_1 = 0$, the model (3.2) reduces to

$$\eta = \lambda_2 \sigma \exp(\beta \sigma). \tag{3.3}$$

Actual material parameters that were used in Rajagopal (2014) are

$$\lambda_2 = 1.57 \times 10^{-11}\,\mathrm{Pa}^{-1}, \qquad \beta = 3.22 \times 10^{-10}\,\mathrm{Pa}^{-1}. \tag{3.4}$$

The model (3.3) with parameters (3.4) provides a very good agreement with experimental data, see Figure 3.3. If we linearize this model around $\sigma = 0$, we obtain an estimate for Young's modulus

$$\frac{1}{E} = \frac{d\eta}{d\sigma}(0) = \lambda_2,$$

which yields $E = 63.7$ GPa.

Modeling beta phase titanium alloys

In Devendiran et al. (2017), two models to capture the response of beta phase titanium alloys were proposed. The first is an implicit model

$$\begin{aligned}\boldsymbol{\varepsilon} - \alpha_1((\operatorname{tr}\mathbf{T} + \operatorname{tr}\mathbf{T}\operatorname{tr}\boldsymbol{\varepsilon} - 2\operatorname{tr}(\mathbf{T}\boldsymbol{\varepsilon}))\mathbf{I} + 2(\operatorname{tr}\mathbf{T})\boldsymbol{\varepsilon}) - \\ (\alpha_2 + \alpha_3 \exp(1 + \alpha_4(\operatorname{tr}\mathbf{T}^2 + 2\operatorname{tr}(\mathbf{T}^2)\operatorname{tr}\boldsymbol{\varepsilon} + 4\operatorname{tr}(\mathbf{T}^2\boldsymbol{\varepsilon})))^{\frac{n}{2}})\mathbf{T} = \mathbf{0},\end{aligned} \tag{3.5}$$

Point#	Stress σ [MPa]	Strain η
1	46.7	0.0007
2	85.4	0.0012
3	117.6	0.0018
4	153.9	0.0024
5	190.4	0.0030
6	218.2	0.0036
7	250.1	0.0042
8	280.1	0.0047
9	310.6	0.0053
10	333.8	0.0059
11	361.6	0.0064
12	382.6	0.0071
13	408.2	0.0077
14	433.4	0.0084
15	452.8	0.0092
16	479.9	0.0101
17	501.8	0.0109
18	522.7	0.0117
19	537.4	0.0125
20	552.5	0.0132

Table 3.2: Uniaxial tensile loading data of *Ti-30Nb-10Ta-5Zr* alloy, see Sakaguch et al. (2004). Data were extracted from (Devendiran et al., 2017, Figure 1, top).

where α_1, α_2, α_3, α_4 and n are the material moduli. For the uniaxial stress setting (3.1), the model (3.5) can be rewritten as

$$\begin{aligned} \eta &= (\alpha_1(1+\eta+2\gamma)+\alpha_2)\sigma + \alpha_3 \exp\left(1+\alpha_4(1+6\eta+4\gamma)\sigma^2\right)^{\frac{n}{2}}, \\ \gamma &= \alpha_1(1+4\gamma-\eta)\sigma. \end{aligned} \tag{3.6}$$

Young's modulus for the model (3.5) can be estimated as

$$E_\alpha = \frac{1}{\alpha_1+\alpha_2}.$$

The second model is of the form

$$\boldsymbol{\varepsilon} = \beta_1(\operatorname{tr}\mathbf{T})\mathbf{I} + (\beta_2 + \beta_3 \exp\left(1+\beta_4 \operatorname{tr}(\mathbf{T}^2)\right)^{\frac{n}{2}})\mathbf{T}, \tag{3.7}$$

where β_1, β_2, β_3, β_4 and n are the material moduli. For the uniaxial loading of the form (3.1), the model (3.7) simplifies to

$$\begin{aligned} \eta &= (\beta_1+\beta_2+\beta_3 \exp\left(1+\beta_4(\sigma^2)\right)^{\frac{n}{2}})\sigma, \\ \gamma &= \beta_1\sigma. \end{aligned} \tag{3.8}$$

Young's modulus for the model (3.8) can be estimated as

$$E_\beta = \frac{1}{\beta_1+\beta_2+\beta_3 e}.$$

Point #	Stress σ [MPa]	Strain η
1	12.9	0.0002
2	37.8	0.0008
3	63.8	0.0012
4	85.7	0.0018
5	110.5	0.0023
6	132.5	0.0028
7	154.5	0.0033
8	174.4	0.0038
9	197.6	0.0043
10	215.7	0.0049
11	243.2	0.0055
12	263.9	0.0062
13	290.1	0.0069
14	312.3	0.0077
15	327.9	0.0084
16	348.6	0.0091
17	368.2	0.0098
18	380.1	0.0105
19	394.2	0.0112

Table 3.3: Uniaxial tensile loading data of *Ti-24Nb-4Zr-7.9Sn* alloy, see Hao et al. (2005). Data were extracted from (Devendiran et al., 2017, Figure 1, middle).

In Devendiran et al. (2017), models (3.6) and (3.8) were used to fit experimental data of *Ti-30Nb-10Ta-5Zr* alloy, *Ti-24Nb-4Zr-7.9Sn* alloy and *Ti-30Nb-12Zr* alloy, see Table 3.2–3.4. For values of material moduli of these alloys, we refer to (Devendiran et al., 2017, Tables 1 and 2). In Figures 3.4, 3.5 and 3.6, the explicit model (3.8) is included as a dashed line.

3.3 Approximation of elastic moduli

In this section, we estimate basic elastic properties of the studied titanium alloys by providing rough estimates for their bulk modulus, shear modulus and Young's modulus. The roughness is twofold. First, each alloy might differ based on a particular chemical composition and the method of material processing. For example, the term Gum Metal describes a class of materials, and every unique alloy differs in its properties. There are differences in chemical composition as each material might differ in the amount of oxygen in the mixture, and there are differences between the raw material properties and the cold swagged material properties, see Saito et al. (2003). Second, there is nonlinearity in the material response in the elastic regime. Therefore, characterising such complex materials by two independent linearized moduli is inaccurate. Although we are primarily interested in modeling nonlinearity in the elastic response of these alloys, we also feel the need to make this first order estimate just to put studied materials into the context of other materials and their known elastic properties, see Table 3.5.

Point #	Stress σ [MPa]	Strain η
1	28.6	0.0003
2	56.4	0.0007
3	84.5	0.0011
4	110.5	0.0015
5	140.9	0.0020
6	162.4	0.0024
7	190.4	0.0030
8	214.5	0.0034
9	238.4	0.0041
10	262.2	0.0048
11	281.5	0.0056
12	296.9	0.0064
13	307.9	0.0073
14	318.4	0.0082
15	325.7	0.0091
16	330.1	0.0100
17	332.4	0.0109
18	334.5	0.0118
19	337.2	0.0127
20	339.5	0.0137
21	341.9	0.0145
22	344.3	0.0155
23	346.7	0.0164
24	346.6	0.0173
25	349.2	0.0182
26	351.5	0.0191

Table 3.4: Uniaxial tensile loading data of *Ti-30Nb-12Zr* alloy, see Hou et al. (2010). Data were extracted from (Devendiran et al., 2017, Figure 1, bottom).

3.3.1 Voigt, Reuss and Voigt-Reuss-Hill approximations

Titanium alloys that we are interested in are beta phase alloys that form a body centered cubic structure. Following Talling et al. (2008); Rajagopal (2014); Devendiran et al. (2017), we regard them as isotropic polycrystalline materials. Based on the single crystal properties, we use Voigt-Reuss-Hill (VRH) approximation scheme, see Hill (1952), to estimate elastic moduli of isotropic mixture that is composed of these single crystals. VRH scheme combines the Voigt approximation, see Voigt (1928), with the Reuss approximation, see Reuss (1929), to estimate elastic moduli of the material. According to Hill (1952), *the Voigt moduli exceed the Reuss moduli, while the true values should lie between them*.

A linearized elastic model for a body centered cubic crystal is based on the general elastic model for anisotropic materials, see Definition A.132, (p. 148), where

Material	Elastic modulus		
	Shear (μ) [GPa]	Bulk (K)[GPa]	Young's E [GPa]
Silicone Rubber	0.0003–0.02	1.5–2	0.001–0.05
Aluminium Extrusions	25–27	65–71	69–73
Stainless Steel	74–81	134–152	190–203
Diamond	440–470	530–548	1050–1210
Titanium Dioxide	90–112	209–218	230–288
Ti-6Al-4V Alloy	40–45	97–153	110–119
Ti-6Al-7Nb Alloy	36–41	111–142	100–110

Table 3.5: Elastic moduli of various materials. Data were obtained from http://www.azom.com, see AZoNetwork UK Ltd..

the tensor $\mathbf{C}$ has the special form

$$\mathbf{C} = \begin{pmatrix} C_{11} & C_{12} & C_{12} & 0 & 0 & 0 \\ C_{12} & C_{11} & C_{12} & 0 & 0 & 0 \\ C_{12} & C_{12} & C_{11} & 0 & 0 & 0 \\ 0 & 0 & 0 & C_{44} & 0 & 0 \\ 0 & 0 & 0 & 0 & C_{44} & 0 \\ 0 & 0 & 0 & 0 & 0 & C_{44} \end{pmatrix},$$

where C_{11}, C_{12} and C_{44} are three independent elastic moduli.

Elastic moduli of isotropic mixture

The Voigt estimate of the bulk modulus is equal to the Reuss estimate. We have that

$$K_V = K_R = K_{VRH} = \frac{C_{11} + 2C_{12}}{3}. \tag{3.9}$$

For the shear modulus, the Voigt estimate μ_V and the Reuss estimate μ_R differ

$$\mu_V = \frac{C_{11} - C_{12} + 3C_{44}}{5}, \quad \mu_R = \frac{5(C_{11} - C_{12})C_{44}}{4C_{44} + 3(C_{11} - C_{12})}, \tag{3.10}$$

while $\mu_R \leq \mu_V$. The Voigt-Reuss-Hill estimate is an average of these estimates

$$\mu_{VRH} = \frac{\mu_V + \mu_R}{2}. \tag{3.11}$$

To derive Voigt and Reuss estimates for Young's modulus, we can use (3.9), (3.10) and conversions between elastic moduli, see Table A.1, (p. 151). The Voigt estimate

$$E_V = \frac{(C_{11} - C_{12} + 3C_{44})(C_{11} + 2C_{12})}{2C_{11} + 3C_{12} + C_{44}} \tag{3.12}$$

differs from the Reuss estimate

$$E_R = \frac{5(C_{11} + 2C_{12})(C_{11} - C_{12})C_{44}}{(3C_{11} + C_{12})C_{44} + C_{11}^2 + C_{11}C_{12} - 2C_{12}^2}, \tag{3.13}$$

where $E_R \leq E_V$. The Voigt-Reuss-Hill approximation of Young's modulus is then

$$E_{VRH} = \frac{E_V + E_R}{2}. \tag{3.14}$$

We finish this section by deriving Voigt and Reuss estimates for Poisson's ratio. Combining (3.9), (3.12), (3.13) with a formula from Table A.1, (p. 151), yields the Voigt estimate

$$\nu_V = 0.5 - \frac{C_{11} - C_{12} + 3C_{44}}{4C_{11} + 6C_{12} + 2C_{44}}, \tag{3.15}$$

and the Reuss estimate

$$\nu_R = 0.5 - \frac{5(C_{11} - C_{12})C_{44}}{2(3C_{11} + C_{12})C_{44} + 2C_{11}^2 + 2C_{11}C_{12} - 4C_{12}^2}. \tag{3.16}$$

The Voigt-Reuss-Hill approximation of Poisson's ratio is an average of the previous two estimates

$$\nu_{VRH} = \frac{\nu_V + \nu_R}{2}. \tag{3.17}$$

Single crystal properties of studied titanium alloys

Elastic moduli of single crystals are available for two different forms of Gum Metal *Ti-36Nb-2Ta-3Zr-0.3O*. *'The first alloy (PH) was obtained by powder metallurgy, in which arc-melted and plasma-sprayed powder was hot isostatically pressed (HIPed) and solution treated and quenched. The second processing route involved mixing of pure elemental powders (EP) which were then cold pressed, forged, hot rolled, solution treated and quenched.'*, see Talling et al. (2008).

Elastic moduli of single crystals of *Ti-30Nb-10Ta-5Zr* and *Ti-24Nb-4Zr-8Sn* can be found in Obbard et al. (2010) and Zhang et al. (2011) respectively. Elastic moduli of single crystals of *Ti-30Nb-12Zr* are not available.

Table 3.6 summarizes the single crystal moduli of aforementioned beta phase titanium alloys and Table 3.7 lists the estimates of the elastic parameters of the isotropic mixture of these crystals according to Voigt-Reuss-Hill approximation.

Material	C_{11} [GPa]	C_{12} [GPa]	C_{44} [GPa]
Gum Metal (PH)	125.0	90.0	31.0
Gum Metal (EP)	125.0	93.0	28.0
Ti-30Nb-10Ta-5Zr	67.1	39.9	29.8
Ti-24Nb-4Zr-8Sn	57.2	36.1	35.9

Table 3.6: Single crystal moduli of studied beta phase titanium alloys. The elastic moduli C_{11}, C_{12} and C_{44} of single crystals of *Ti-30Nb-10Ta-5Zr* alloy, *Ti-24Nb-4Zr-8Sn* alloy and the two forms of Gum Metal abbreviated PH and EP were obtained from Obbard et al. (2010), Zhang et al. (2011) and Talling et al. (2008) respectively.

3.4 Modeling elastic response of titanium alloys

Young's modulus is defined as a proportion of the tensile stress to tensile strain. Therefore we might estimate Young's modulus from the experimental data using the equation

$$\sigma_i = E\eta_i, \tag{3.18}$$

from which we obtain a least square estimate of Young's modulus E. To demonstrate the extent to which the tensile response deviates from being linear, represented by

Material	K_{VRH}	μ_R	μ_V	μ_{VRH}	E_R	E_V	E_{VRH}	ν_R	ν_V	ν_{VRH}
Gum Metal (PH)	101.7	23.7	25.6	24.6	65.9	70.9	68.4	0.39	0.38	0.39
Gum Metal (EP)	103.7	21.5	23.2	22.4	60.4	64.8	62.6	0.40	0.40	0.40
Ti-30Nb-10Ta-5Zr	49.0	20.2	23.3	21.8	53.2	60.4	56.8	0.32	0.29	0.31
Ti-24Nb-4Zr-8Sn	43.1	18.3	25.8	22.0	48.1	64.4	56.3	0.31	0.25	0.28

Table 3.7: VRH estimates of the elastic parameters of studied titanium alloys. K_{VRH} denotes the VRH approximation of the bulk modulus (3.9). μ_V, μ_R and μ_{VRH} denote the Voigt and the Reuss approximations (3.10) and the VRH approximation (3.11) of the shear modulus. E_R, E_V and E_{VRH} denote the Voigt estimate (3.12), the Reuss estimate (3.13) and the VRH estimate (3.14) of Young's modulus. ν_V, ν_R and ν_{VRH} denote the Voigt approximation (3.15), the Reuss approximation (3.16) and the VRH approximation (3.17) of Poisson's ratio. With the exception of dimensionless Poisson's ratio, all other values are in GPa.

(3.18), we estimate Young's modulus based on different σ_i ranges. Let σ_{max} denote the maximal tensile stress value in the experimental data, which can be understood as the elastic limit. Let $p \in (0, 1]$. Then the E_p is a least square estimate of Young's modulus based on the experimental data pairs (σ_i, η_i), for which $\sigma_i < p\sigma_{max}$.

In Table 3.8, there are values of E_p for studied titanium alloys. The variance of the data, notably in case of *Ti-30Nb-12Zr* alloy, indicates how misleading it could be to characterise the response of these materials by a single number in the whole elastic range without considering the nonlinear nature of the response.

Material	$E_{0.1}$	$E_{0.2}$	$E_{0.3}$	$E_{0.5}$	$E_{0.6}$	$E_{0.7}$	$E_{0.8}$	$E_{0.9}$	E_1
Gum Metal	60.2	58.8	58.1	56.3	55.4	54.4	52.3	50.5	47.8
Ti-30Nb-10Ta-5Zr	71.8	69.4	65.1	61.6	60.2	57.6	55.6	53.1	48.2
Ti-24Nb-4Zr-7.9Sn	49.6	51.1	48.7	47.2	46.0	44.8	43.4	41.7	39.2
Ti-30Nb-12Zr	105.1	86.3	79.4	70.8	68.2	63.7	60.9	51.3	25.5

Table 3.8: Estimates of Young's modulus, E_p, is computed based on a subset of experimental data, for which stress $\sigma_i \leq p\sigma_{max}$. Units are GPa.

3.4.1 Power-law models

In this section, we use the following model to capture response of studied beta phase titanium alloys based on experimental data, see Tables 3.1–3.4

Definition 3.1 (Power-law solid for fitting beta phase titanium alloys). *The constitutive model defined by relations between deviatoric parts and traces of the small strain tensor ε and Cauchy stress $\mathbf{T}$ of the form*

$$\varepsilon = \frac{1}{9K}\left(\frac{\tau_0^2 + |\operatorname{tr}\mathbf{T}|^2}{\tau_0^2}\right)^{\frac{s'-2}{2}} (\operatorname{tr}\mathbf{T})\mathbf{I} + \frac{1}{2\mu}\left(\frac{\tau_0^2 + \frac{3}{2}|\mathbf{T}^d|^2}{\tau_0^2}\right)^{\frac{q'-2}{2}} \mathbf{T}^d, \tag{3.19}$$

where $\tau_0 > 0$, $s' \in (1, \infty)$, $q' \in (1, \infty)$, $K > 0$ and $\mu > 0$ are model parameters.

The parameter s' and the coefficient K describe volume changes in response to the mean normal stress, while the parameter q' and the coefficient μ describe

the isochoric part of deformation. In the remainder of this chapter, we refer to parameters K and μ as to bulk and shear moduli and we call the response to the mean normal stress the bulk response. Note that we obtain Hooke's law (A.31) upon setting $s' = q' = 2$ in (3.19). The parameter τ_0 is chosen in such a manner that we are guaranteed that the response of the nonlinear model is reasonably close to the linearized model if $|\mathbf{T}|$ is small. It means that, upon linearizing the model (3.19) around $\mathbf{T} = \mathbf{0}$, see Lemma 2.12, (p. 24), we obtain the classical linearized elastic model, which provides good approximation of the response as long as

$$|\mathbf{T}| \ll \tau_0. \tag{3.20}$$

Model (3.19) is a special case of the model (2.20) from Definition 2.11, (p. 24), where $\tau_K = \tau_0$ and $\tau_\mu = \sqrt{2/3}\tau_0$.

3.4.2 Algorithm to estimate model parameters

When describing tensile loading experiment, the Cauchy stress tensor $\mathbf{T}$ is of the form (3.1). It immediately follows that

$$\mathbf{T}^d = \begin{pmatrix} \frac{2}{3}\sigma & 0 & 0 \\ 0 & -\frac{1}{3}\sigma & 0 \\ 0 & 0 & -\frac{1}{3}\sigma \end{pmatrix}, \qquad |\mathbf{T}^d| = \sqrt{\frac{2}{3}}\sigma, \qquad \operatorname{tr}\mathbf{T} = \sigma.$$

When fitting tensile loading data to the model (3.19) with parameters (τ_0, s', q', K, μ), the model reduces to

$$\eta = \frac{1}{9K}\left(\frac{\tau_0^2+\sigma^2}{\tau_0^2}\right)^{\frac{s'-2}{2}}\sigma + \frac{1}{3\mu}\left(\frac{\tau_0^2+\sigma^2}{\tau_0^2}\right)^{\frac{q'-2}{2}}\sigma, \tag{3.21a}$$

$$\gamma = \frac{1}{9K}\left(\frac{\tau_0^2+\sigma^2}{\tau_0^2}\right)^{\frac{s'-2}{2}}\sigma - \frac{1}{6\mu}\left(\frac{\tau_0^2+\sigma^2}{\tau_0^2}\right)^{\frac{q'-2}{2}}\sigma. \tag{3.21b}$$

We use two approaches for fixing τ_0 in (3.21a). For all experimental data that we use, $|\mathbf{T}|$ takes values in the range 10^7-10^9 (10 MPa$-$1 GPa), and for $|\mathbf{T}| > 5.10^8$, the response is nonlinear, see Figure 3.2. In the first approach, we set $\tau_0 = 5.10^8$ for all studied materials. In the second approach, we set $\tau_0 = \sigma_{max}$, where σ_{max} represents the maximal loading in the elastic regime. In both approaches, we always meet the assumption (3.20) in the linear regime.

Thus, upon fixing τ_0, our model (3.21a) is completely characterized by four parameters. The model (3.3) used by Rajagopal (2014) to fit tensile response for cold swagged Gum Metal has two parameters, while the explicit model used by Devendiran et al. (2017) to describe the tensile response of three titanium alloys has five parameters.

The equation (3.21a) with the values of parameters (τ_0, s', q') can be understood as a linear model of the form

$$\eta = c_1 f_1(\sigma) + c_2 f_2(\sigma), \tag{3.22}$$

where

$$f_1(\sigma) = \left(\frac{\tau_0^2+\sigma^2}{\tau_0^2}\right)^{\frac{s'-2}{2}}\sigma, \quad f_2(\sigma) = \left(\frac{\tau_0^2+\sigma^2}{\tau_0^2}\right)^{\frac{q'-2}{2}}\frac{2}{3}\sigma.$$

Let (σ^i, η_i), $i \in \{1 \dots N\}$ be the data of a tensile stress experiment, see Tables 3.1–3.4. The values of functions $f_1(\sigma^i)$ and $f_2(\sigma^i)$ are understood as independent variables and the value of strain η^i is understood as an observed value. Using the linear regression, we obtain estimates for the coefficients c_1 and c_2 in (3.22) and derive estimates of the bulk and shear moduli

$$K = \frac{1}{9c_1}, \quad \mu = \frac{1}{2c_2}. \tag{3.23}$$

Using this procedure, we can estimate optimal values of the parameters K and μ for a given (τ_0, s', q'). Since the parameter τ_0 is fixed, we need to estimate optimal values of the exponents s' and q'. We decided to perform this estimation based on comparing quality of fit for many pairs (s', q') from the search space. For measuring quality of fit of the model, we need the following definitions.

Definition 3.2 (Mean of observations).

$$\overline{\eta} = \frac{1}{N} \sum_{i=1}^{N} \eta^i.$$

Definition 3.3 (Total sum of squares[4]).

$$S_{tot} = \sum_{i=1}^{N} (\eta^i - \overline{\eta})^2. \tag{3.24}$$

Definition 3.4 (Residual sum of squares).

$$S_{res} = \sum_{i=1}^{N} (\eta^i - (c_1 f_1(\sigma^i) + c_2 f_2(\sigma^i)))^2.$$

Definition 3.5 (Coefficient of determination R^2).

$$R^2 = 1 - \frac{S_{res}}{S_{tot}}. \tag{3.25}$$

The coefficient of determination $R^2 \leq 1$ is a standard measure of the quality of fit in the linear regression. The closer the value of the coefficient of determination is to 1, the better the fit is.

Implementation

We outline the algorithm used for fitting tensile loading data for an alloy to the model (3.22) as follows:

- We fix some particular value of τ_0, derived from a characteristic magnitude of stress for which the response can be modeled as linear for small strain tending to zero.

[4]For linear models without an intercept, as is the case (3.22), the formula (3.24) for the total sum of squares is often used with $\overline{\eta} = 0$. We decided to use the formula (3.24) involving $\overline{\eta}$ in order to obtain more realistic coefficients of determination R^2.

- We choose an admissible set of the model parameters (s', q'). In particular, we use $s' \in \{1.01, 1.02, \dots, 100\}$, $q' \in \{1.01, 1.02, \dots, 100\}$. The values of s' and q' are discrete values from the finite sequence $\{1.01, 1.02, \dots, 100\}$ of numbers incremented by 0.01.

- For each admissible pair of (s', q'), we compute the estimates of coefficients (c_1, c_2) of the model (3.22) using linear regression of the experimental data. From (3.25), we get the value of the coefficient of determination R^2.

- We choose the pair (s', q') that maximizes the coefficient of determination R^2 among all admissible pairs of the model exponents.

- For the pair (s', q') that maximizes R^2, we substitute the least square estimate of (c_1, c_2) into the equation (3.23) to compute parameters of the model K and μ.

This algorithm yields a set of model parameters (τ_0, s', q', K, μ) that is called **the best fit**. The best fit maximizes the coefficient of determination and minimizes the residual sum of squares among all admissible pairs of (s', q'). Linear regression was performed using function `lm` from the R software environment and language, see R Core Team (2016). For more details about fitting models in R, see Chambers – Hastie (1992). The source code of the algorithm has been deposited to https://bitbucket.org/kulvait/fittingtitaniumalloys. It can also be found in the supplemental material for the thesis.

Apparent ambiguity of the best fit

There is a symmetry in the equation (3.21a) that leads to the existence of two sets of parameters with the same quality of fit. Let us assume that (τ_0, s', q', K, μ) is the best fit with the coefficient of determination R^2. The alternative choice to the best fit $(\tau_0, \hat{s}', \hat{q}', \hat{K}, \hat{\mu})$, where

$$\hat{s}' = q', \quad \hat{q}' = s', \quad \hat{\mu} = 3K, \quad \hat{K} = \frac{\mu}{3}, \tag{3.26}$$

fits the equation identically (3.21a) as the best fit (τ_0, s', q', K, μ). Therefore it also leads to the identical coefficient of determination for the model (3.22). However, the term with exponent s' describes volume changing deformation and the term with exponent q' describes volume preserving deformation. That means that the original model from Definition 3.1 will be different when comparing the original and the alternative set of parameters.

To fix this apparent ambiguity, we have to add an extra condition. One possible option is to set

$$|s' - 2| > |q' - 2|. \tag{3.27}$$

We will refer to the inequality (3.27) as to a highly nonlinear bulk response condition. An alternative condition takes the form

$$|s' - 2| \leq |q' - 2|. \tag{3.28}$$

The inequality (3.28) will be referred as a highly nonlinear shear response condition. In the results section, we show that the condition (3.28) leads to positive strain component γ and negative Poison's ratio

$$\nu = \frac{3K - 2\mu}{2(3K + \mu)}. \tag{3.29}$$

Therefore we have identified the condition (3.27) as being physically more reasonable.

Using an additional physical information, the VRH estimates for the first three alloys, see Table 3.7, we can further improve the properties of the model (3.19). In the outlined algorithm we have maximized the coefficient of determination R^2. Let for a given alloy ν_V and ν_R be Voigt and Reuss estimates of Poisson's ratio. It can be shown that $\nu_V < \nu_R$. Let K and μ be parameters of the fit for a given pair (s', q') and ν be Poisson's ratio given by (3.29). We define an objective function

$$O = \begin{cases} R^2 - (\nu_V - \nu), & \text{if } \nu < \nu_V, \\ R^2, & \text{if } \nu_V \leq \nu \leq \nu_R, \\ R^2 - (\nu - \nu_R), & \text{if } \nu_R < \nu. \end{cases} \tag{3.30}$$

Maximizing the objective function over the whole search space of exponents (s', q') leads to the unique properties of the best fit. Moreover the model is underpinned by additional physical information regarding the single crystal data.

3.5 Results

In Tables 3.9–3.13, the values of the best fit of the tensile loading experiments are presented. Tables 3.9 and 3.10 list the material moduli under the assumption (3.27) of a highly nonlinear bulk response for $\tau_0 = 5.10^8$ and $\tau_0 = \sigma_{max}$ respectively. Tables 3.11 and 3.12 were created under the constraint (3.28) of highly nonlinear shear response for $\tau_0 = 5.10^8$ and $\tau_0 = \sigma_{max}$ respectively. Table 3.13 lists the material moduli, when minimizing the objective function defined by (3.30).

In Figures 3.3–3.6, there is a comparison of the best fit of the power law model (3.21a) for $\tau_0 = 5.10^8$ with the predictions of the explicit models considered in Rajagopal (2014) and Devendiran et al. (2017) when fitting tensile loading experimental data. For the first three alloys, these figures were created based on the data from Table 3.13, for the last alloy, based on the Table 3.9. However, these figures are almost identical when considering different settings of the model.

Table 3.14 lists the coefficients of determination R^2 that were computed for the models (3.3), (3.6) and (3.8) considered in Rajagopal (2014); Devendiran et al. (2017).

3.5.1 Character of response of power-law model

The power-law model (3.19) can be rewritten into the form

$$\operatorname{tr}\boldsymbol{\varepsilon} = \frac{1}{3K}\left(\frac{\tau_0^2 + |\operatorname{tr}\mathbf{T}|^2}{\tau_0^2}\right)^{\frac{s'-2}{2}} \operatorname{tr}\mathbf{T}, \quad \boldsymbol{\varepsilon}^d = \frac{1}{2\mu}\left(\frac{\tau_0^2 + \frac{3}{2}|\mathbf{T}^d|^2}{\tau_0^2}\right)^{\frac{q'-2}{2}} \mathbf{T}^d. \tag{3.31}$$

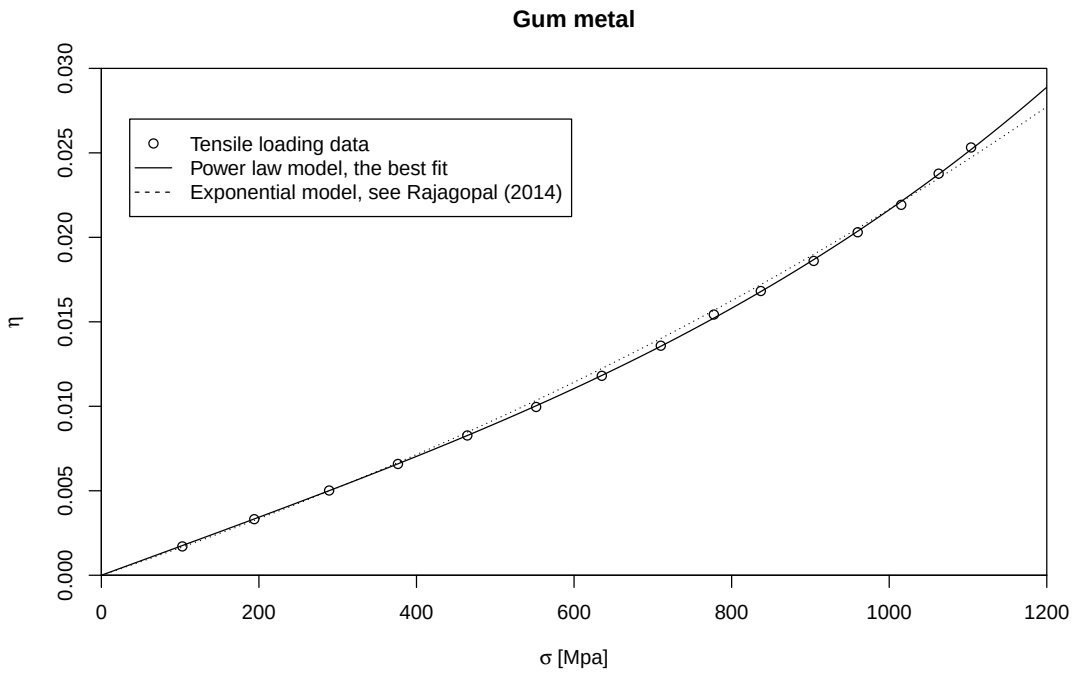

Figure 3.3: Best fit of the model (3.22) compared to (3.3) for Gum Metal.

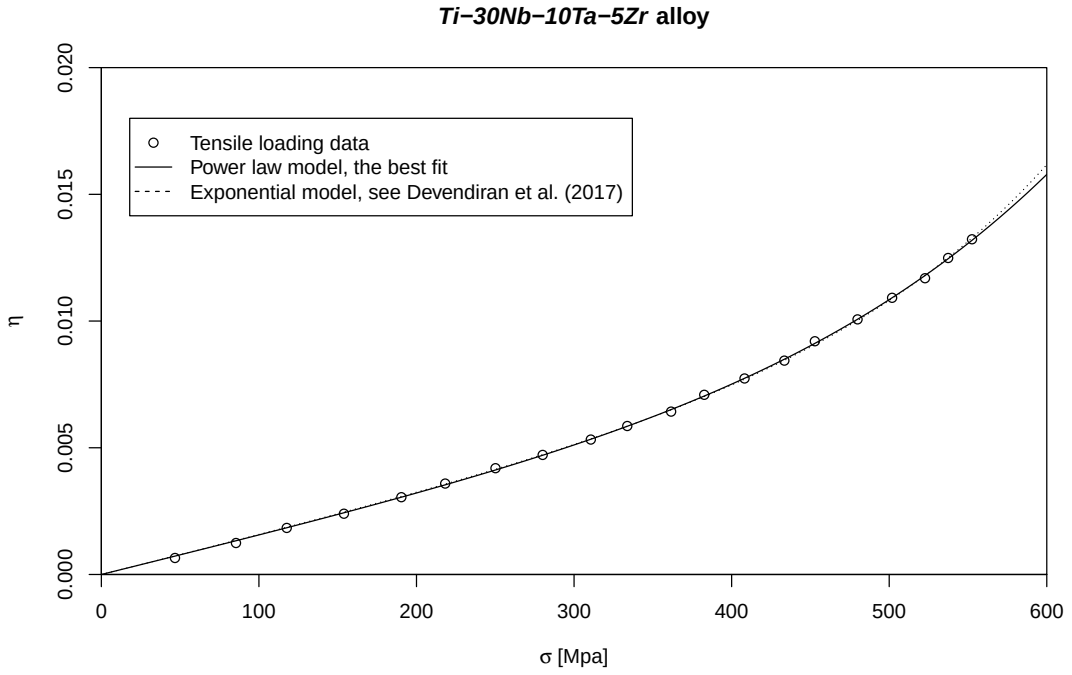

Figure 3.4: Best fit of the model (3.22) compared to (3.8) for *Ti-30Nb-10Ta-5Zr* alloy.

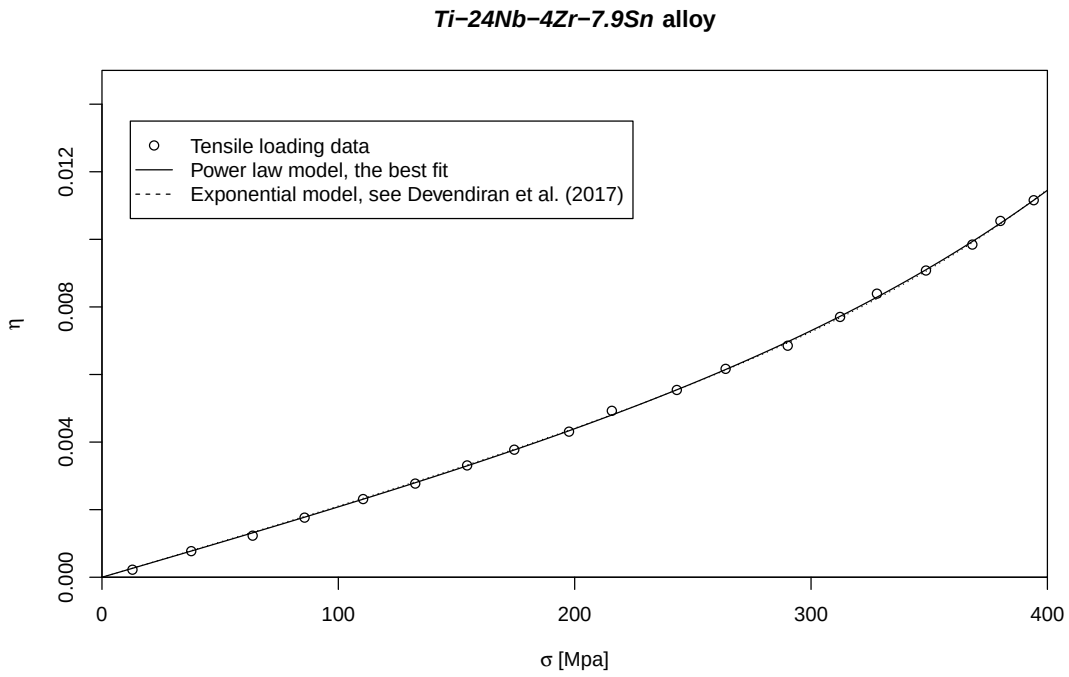

Figure 3.5: Best fit for the model (3.22) compared to (3.8) for *Ti-24Nb-4Zr-7.9Sn* alloy.

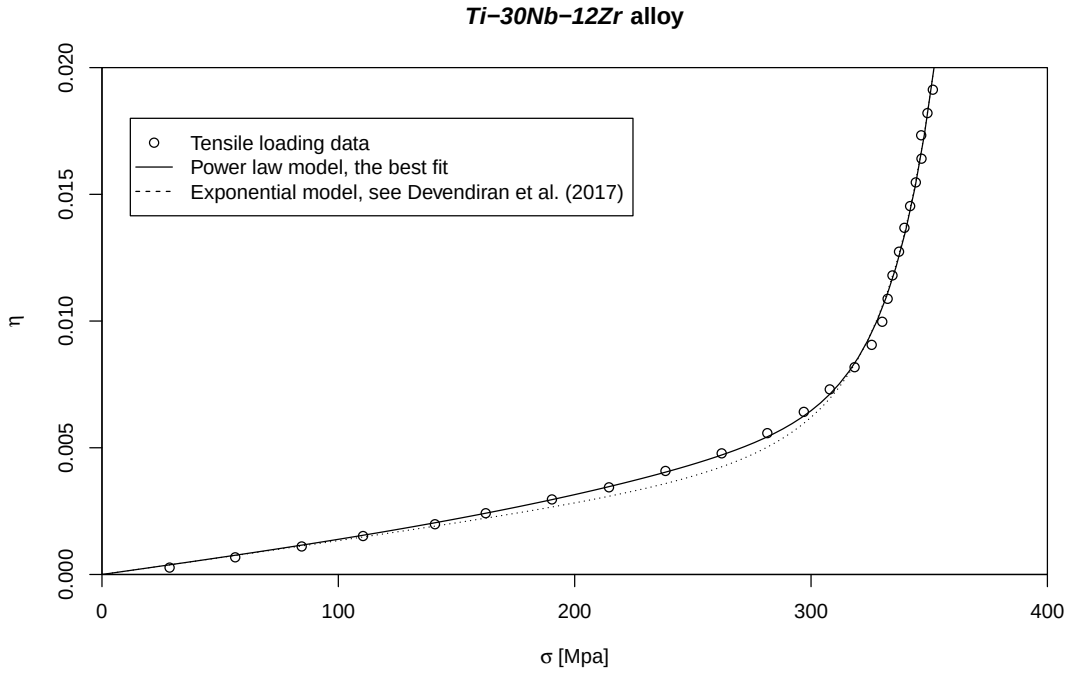

Figure 3.6: Best fit for the model (3.22) compared to (3.8) for *Ti-24Nb-4Zr-7.9Sn* alloy.

Alloy	τ_0	s'	q'	K	μ	R^2	E	ν
Gum Metal	0.5 GPa	7.65	2.23	6223 GPa	20.2 GPa	0.9998	60.5 GPa	0.50
Ti-30Nb-10Ta-5Zr	0.5 GPa	9.15	2.49	334 GPa	22.3 GPa	0.9998	65.6 GPa	0.47
Ti-24Nb-4Zr-7.9Sn	0.5 GPa	15.68	2.99	1126 GPa	16.5 GPa	0.9997	49.3 GPa	0.49
Ti-30Nb-12Zr	0.5 GPa	56.49	4.29	180 252 GPa	25.1 GPa	0.9980	75.4 GPa	0.50

Table 3.9: The values of the best fit, Young's modulus E and Poisson's ratio ν, when $\tau_0 = 0.5$ GPa under the assumption of the highly nonlinear bulk response (3.27). Young's modulus and Poisson's ratio were estimated from the best fit data based on the conversion relationships, see Table A.1, (p. 151).

Alloy	τ_0	s'	q'	K	μ	R^2	E	ν
Gum Metal	1.1 GPa	28.5	2.82	1 283 552 GPa	20.0 GPa	0.9999	60.1 GPa	0.50
Ti-30Nb-10Ta-5Zr	0.6 GPa	9.81	2.58	291 GPa	22.4 GPa	0.9998	65.5 GPa	0.46
Ti-24Nb-4Zr-7.9Sn	0.4 GPa	12.13	2.65	1201 GPa	16.5 GPa	0.9997	49.4 GPa	0.49
Ti-30Nb-12Zr	0.4 GPa	37.89	3.39	804 644 GPa	25.7 GPa	0.9980	77.0 GPa	0.50

Table 3.10: The values of the best fit, Young's modulus E and Poisson's ratio ν, when $\tau_0 = \sigma_{max}$ under the assumption of the highly nonlinear bulk response (3.27). Young's modulus and Poisson's ratio were estimated from the best fit data based on the conversion relationships, see Table A.1, (p. 151).

A set of values (τ_0, s', q', K, μ) associated with the best fit can be used to predict the character of the response for general deformation based on the equation (3.31). The bulk and shear responses take the form

$$B(\operatorname{tr}\mathbf{T}) = \operatorname{tr}\boldsymbol{\varepsilon} = \frac{1}{3K}\left(\frac{\tau_0^2 + |\operatorname{tr}\mathbf{T}|^2}{\tau_0^2}\right)^{\frac{s'-2}{2}} \operatorname{tr}\mathbf{T}, \tag{3.32a}$$

$$S(|\mathbf{T}^d|) = |\boldsymbol{\varepsilon}^d| = \frac{1}{2\mu}\left(\frac{\tau_0^2 + \frac{3}{2}|\mathbf{T}^d|^2}{\tau_0^2}\right)^{\frac{q'-2}{2}} |\mathbf{T}^d|. \tag{3.32b}$$

In Figures 3.7–3.17, there is a comparison of the bulk response (3.32a) with the shear response (3.32b) for the best fit of each alloy. In Figures 3.18, 3.19 and 3.20, we compare the bulk responses (3.32a) in tension and in compression for all alloys. Figures 3.7–3.20 come in triplets. The first figure is for the highly nonlinear bulk response condition (3.27), the second figure is for the highly nonlinear shear response condition (3.28) and the third figure, when available, is for the best fit when maximizing the objective function (3.30). For simplicity, we include these figures only for models, where $\tau_0 = 0.5$ GPa.

In a simple tension, we are interested in the behavior of the ratio $\hat{\nu}(\sigma) = -\gamma/\eta$, which is by (3.21) of the form

$$\hat{\nu}(\sigma) = -\frac{\gamma}{\eta} = -\frac{\frac{1}{9K}\left(\frac{1}{\tau_0}\right)^{s'-2}\left(\tau_0^2+\sigma^2\right)^{\frac{s'-2}{2}} - \frac{1}{6\mu}\left(\frac{1}{\tau_0}\right)^{q'-2}\left(\tau_0^2+\sigma^2\right)^{\frac{q'-2}{2}}}{\frac{1}{9K}\left(\frac{1}{\tau_0}\right)^{s'-2}\left(\tau_0^2+\sigma^2\right)^{\frac{s'-2}{2}} + \frac{1}{3\mu}\left(\frac{1}{\tau_0}\right)^{q'-2}\left(\tau_0^2+\sigma^2\right)^{\frac{q'-2}{2}}}. \tag{3.33}$$

When $\sigma \to 0$, the equation (3.33) yields Poison's ratio (3.29). In Figures 3.21 and 3.22, we depict the graph of function $\hat{\nu}$ from (3.33) for all alloys. Moreover, we include Figure 3.23, which summarizes the behavior of the strain component γ for all considered models in a simple tension.

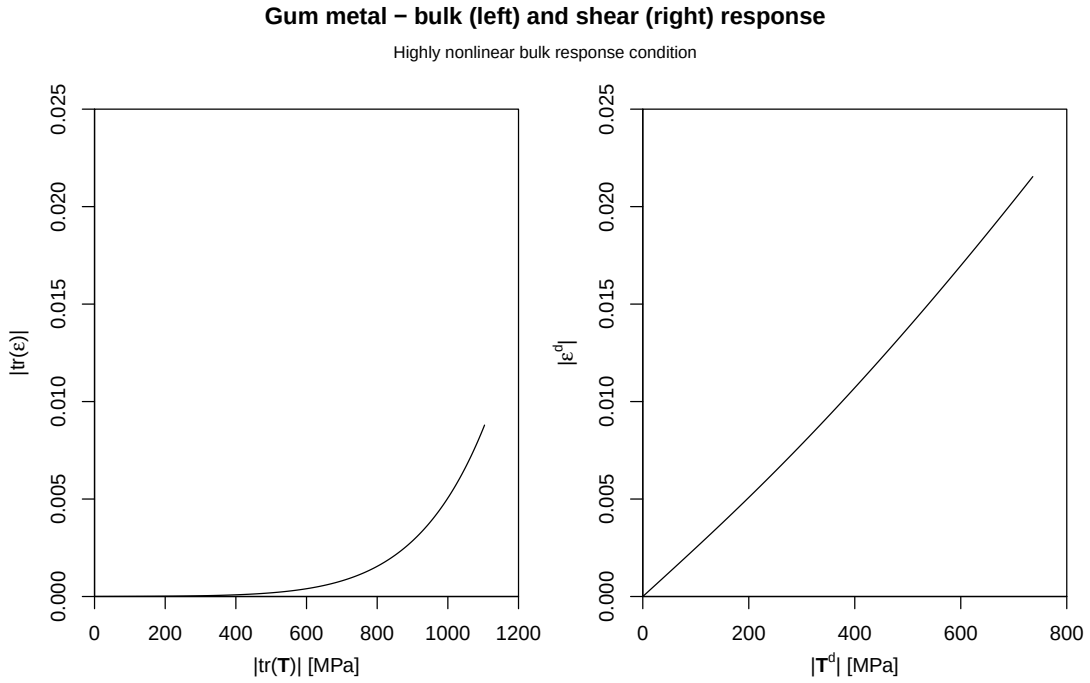

Figure 3.7: Bulk and shear responses (3.32). The power-law model was derived for the values of the best fit for Gum Metal when considering $\tau_0 = 0.5\,\text{GPa}$ and the highly nonlinear bulk response condition (3.27).

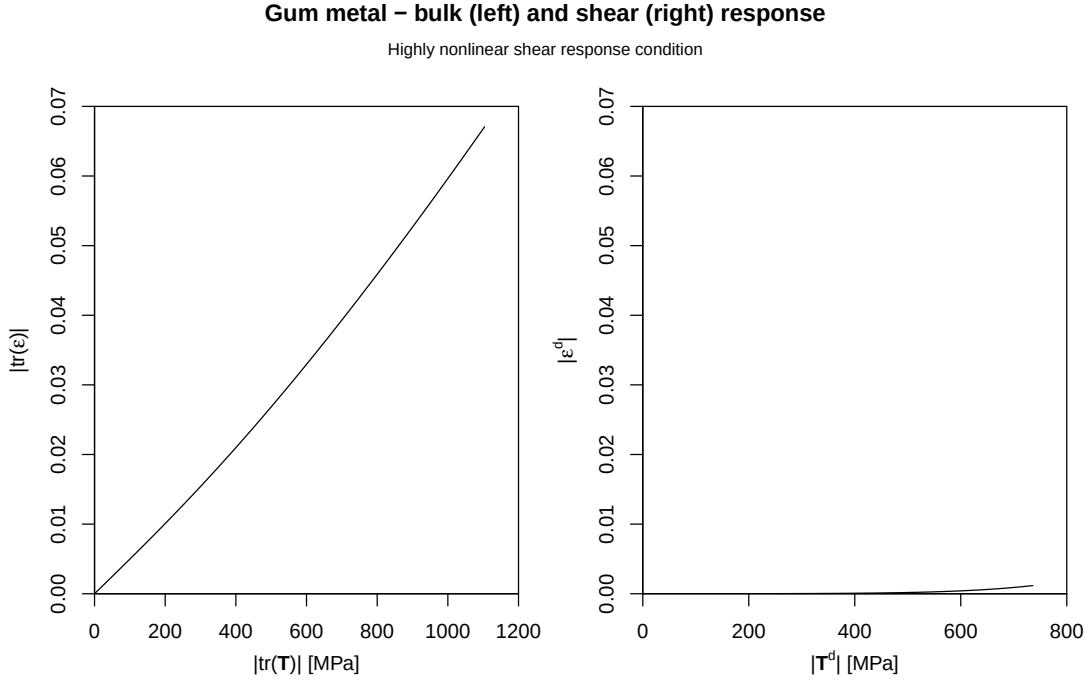

Figure 3.8: Bulk and shear responses (3.32). The power-law model was derived for the values of the best fit for Gum Metal when considering $\tau_0 = 0.5\,\text{GPa}$ and the highly nonlinear shear response condition (3.28).

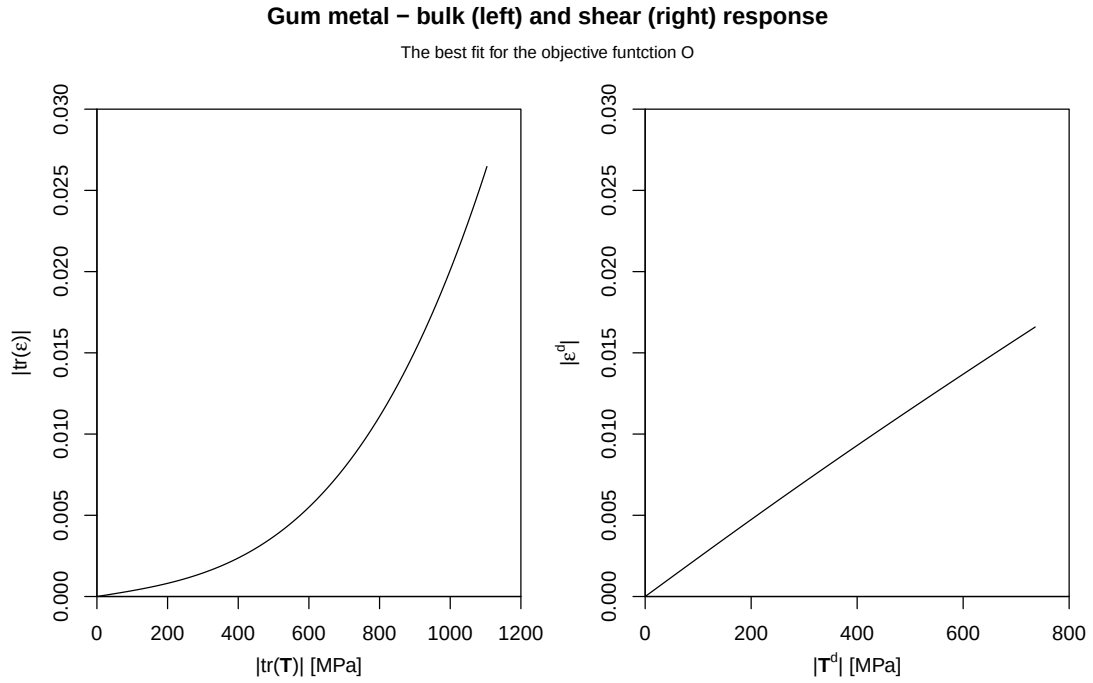

Figure 3.9: Bulk and shear responses (3.32). The power-law model was derived for the values of the best fit for Gum Metal when considering $\tau_0 = 0.5\,\text{GPa}$ and when maximizing the objective function (3.30).

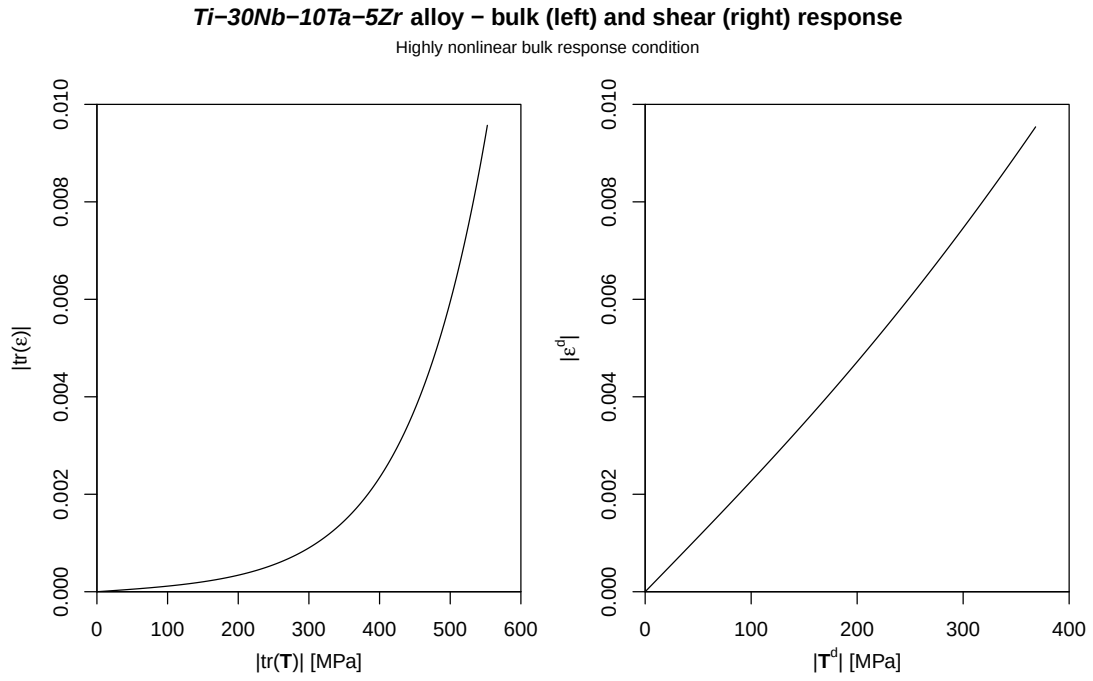

Figure 3.10: Bulk and shear responses (3.32). The power-law model was derived for the values of the best fit for *Ti-30Nb-10Ta-5Zr* alloy when considering $\tau_0 = 0.5\,\text{GPa}$ and the highly nonlinear bulk response condition (3.27).

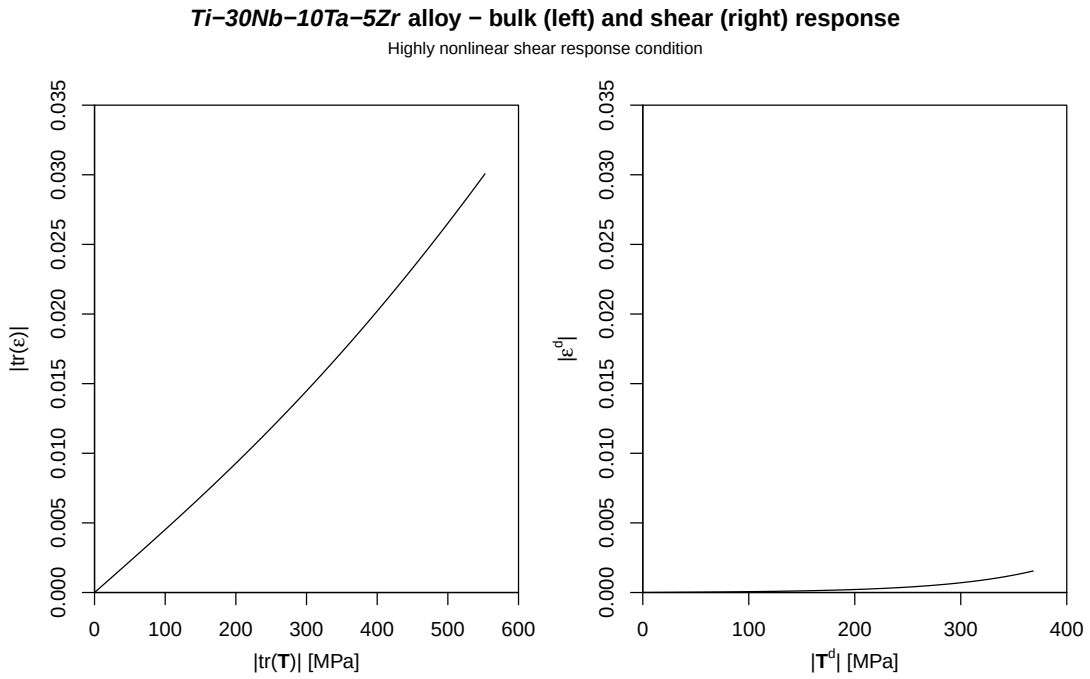

Figure 3.11: Bulk and shear responses (3.32). The power-law model was derived for the values of the best fit for *Ti-30Nb-10Ta-5Zr* alloy when considering $\tau_0 = 0.5\,\text{GPa}$ and the highly nonlinear shear response condition (3.28).

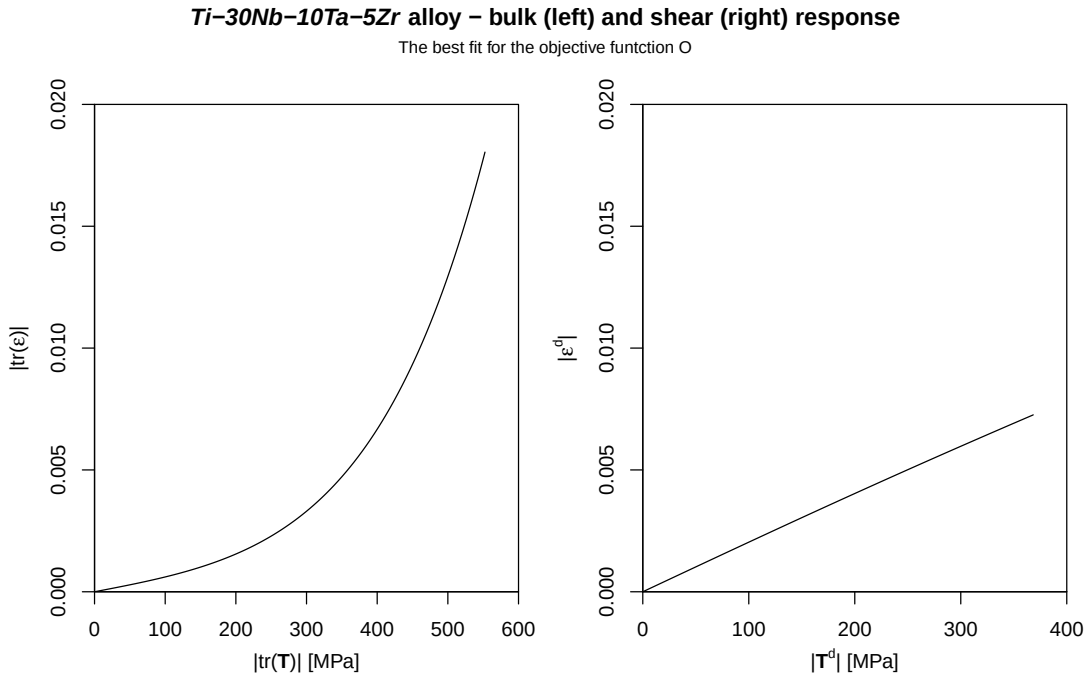

Figure 3.12: Bulk and shear responses (3.32). The power-law model was derived for the values of the best fit for *Ti-30Nb-10Ta-5Zr* alloy when considering $\tau_0 = 0.5\,\text{GPa}$ and when maximizing the objective function (3.30).

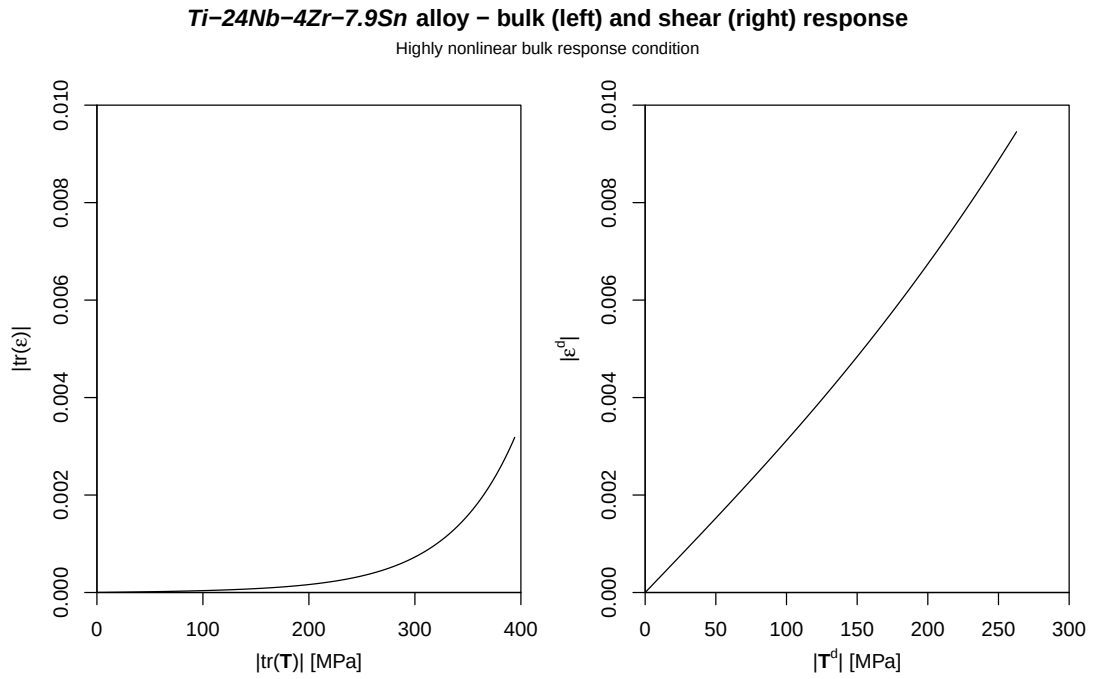

Figure 3.13: Bulk and shear responses (3.32). The power-law model was derived for the values of the best fit for *Ti-24Nb-4Zr-7.9Sn* alloy when considering $\tau_0 = 0.5$ GPa and the highly nonlinear bulk response condition (3.27).

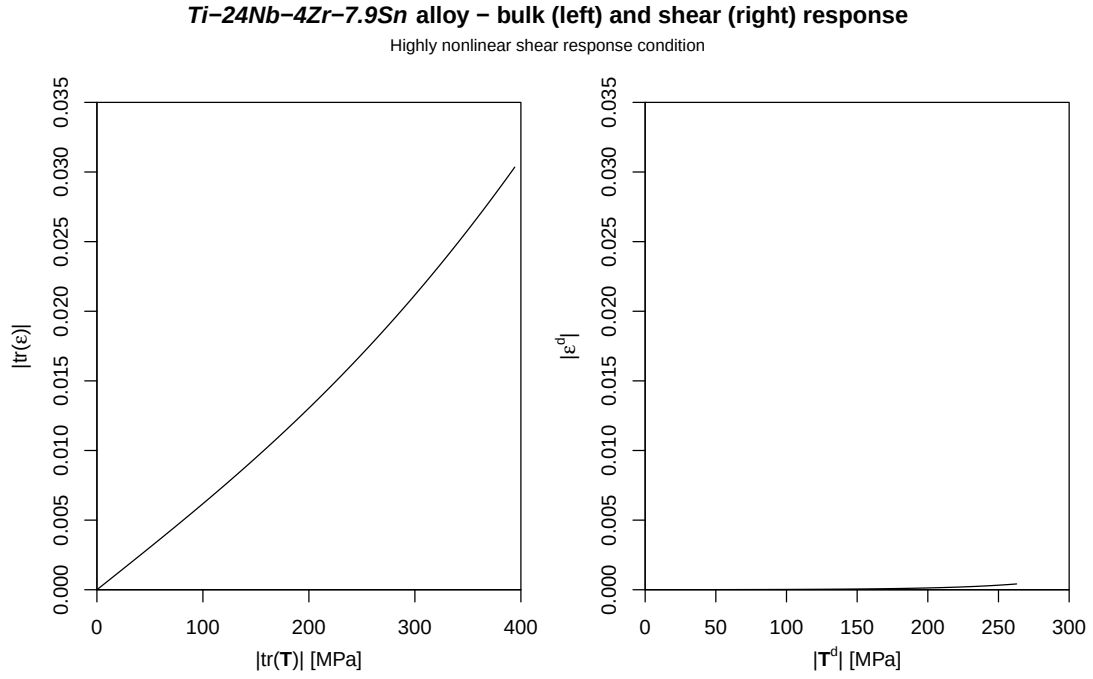

Figure 3.14: Bulk and shear responses (3.32). The power-law model was derived for the values of the best fit for *Ti-24Nb-4Zr-7.9Sn* alloy when considering $\tau_0 = 0.5$ GPa and the highly nonlinear shear response condition (3.28).

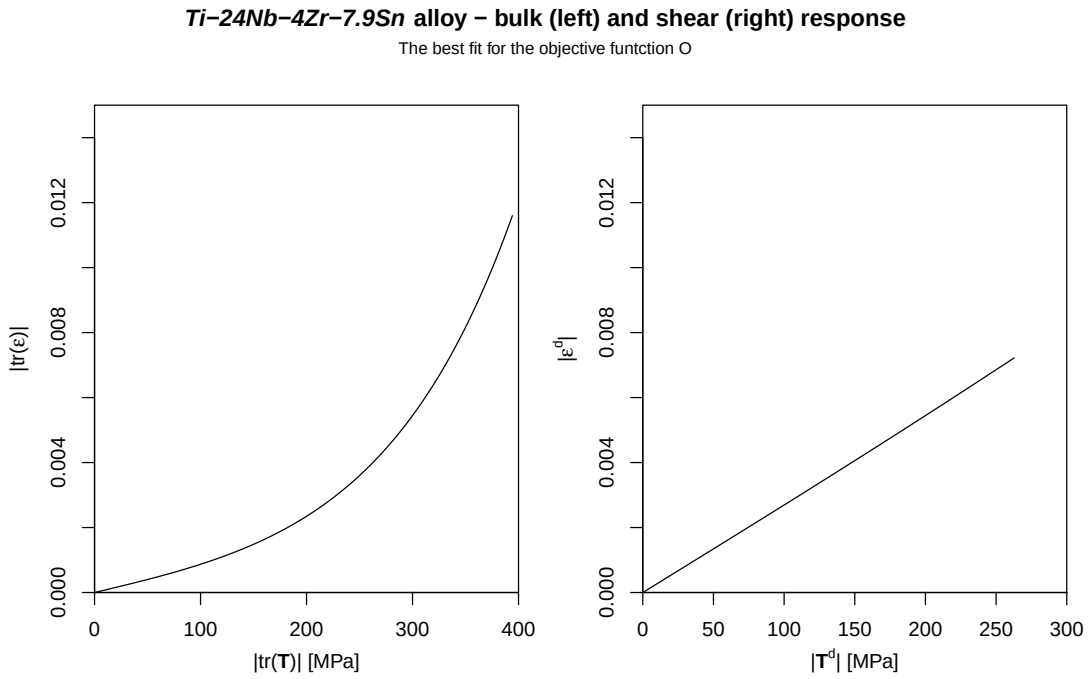

Figure 3.15: Bulk and shear responses (3.32). The power-law model was derived for the values of the best fit for *Ti-24Nb-4Zr-7.9Sn* alloy when considering $\tau_0 = 0.5\,\text{GPa}$ and when maximizing the objective function (3.30).

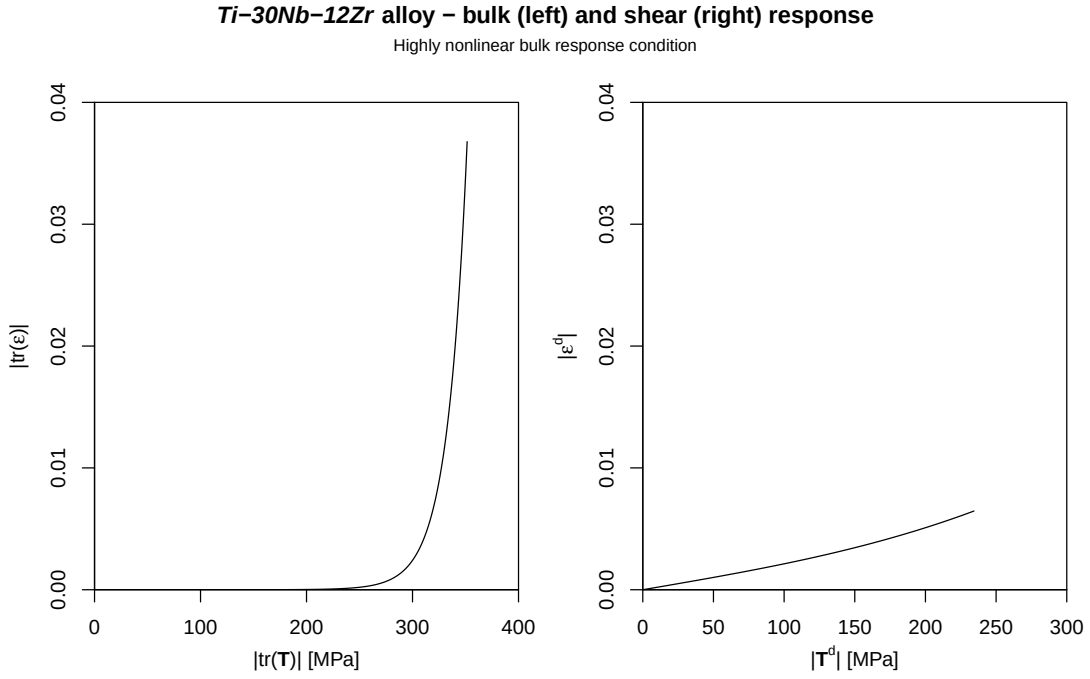

Figure 3.16: Bulk and shear responses (3.32). The power-law model was derived for the values of the best fit for *Ti-30Nb-12Zr* alloy when considering $\tau_0 = 0.5\,\text{GPa}$ and the highly nonlinear bulk response condition (3.27).

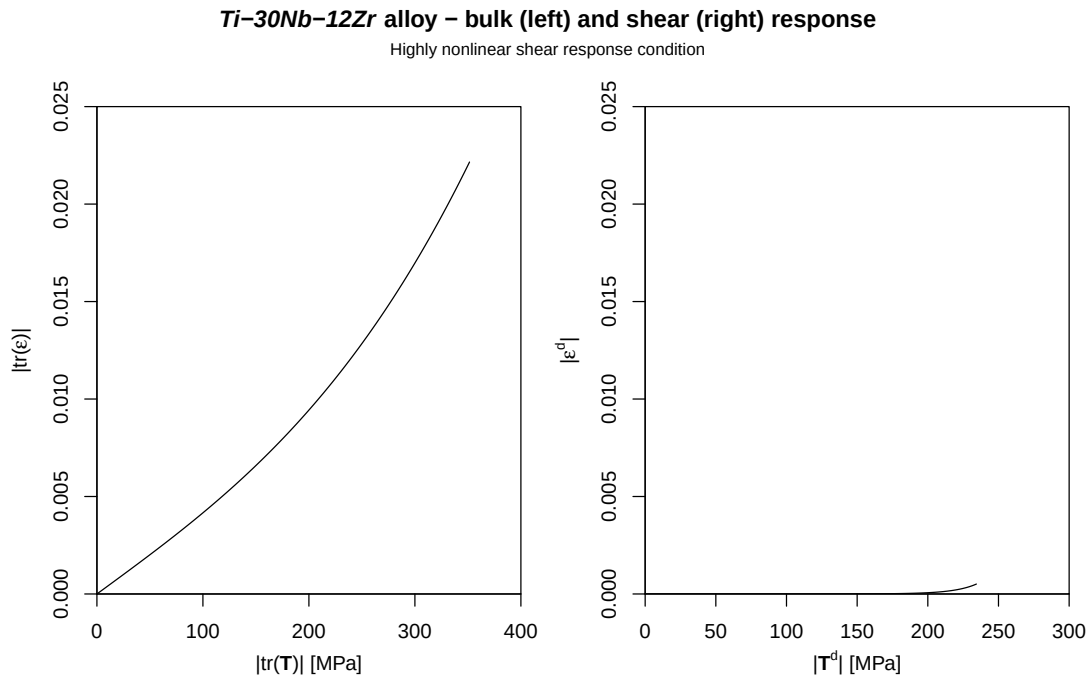

Figure 3.17: Bulk and shear responses (3.32). The power-law model was derived for the values of the best fit for *Ti-30Nb-12Zr* alloy when considering $\tau_0 = 0.5$ GPa and the highly nonlinear shear response condition (3.28).

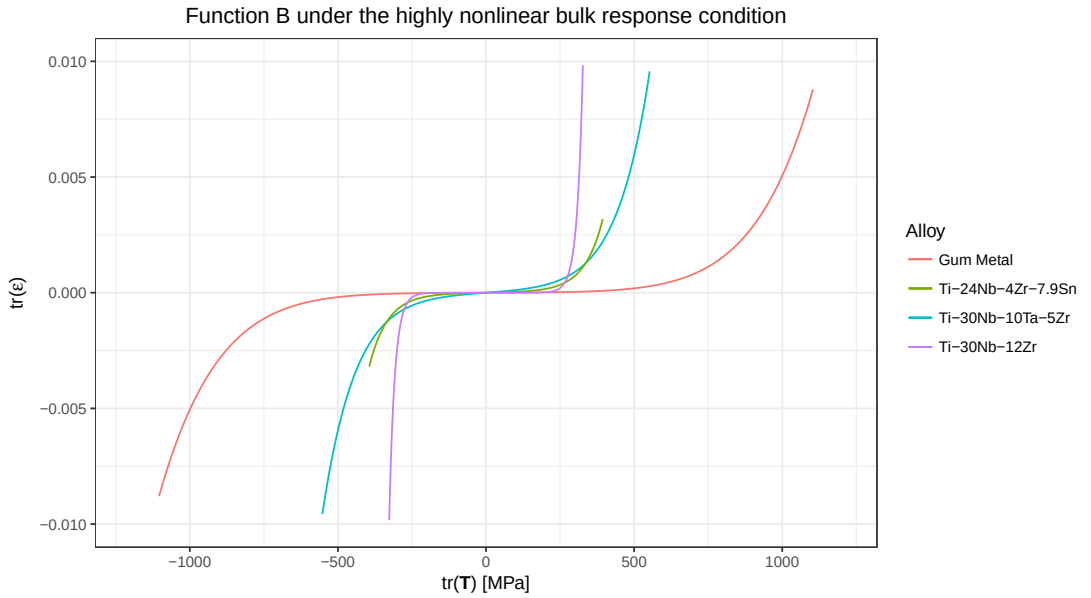

Figure 3.18: Comparison of the bulk responses (3.32a) including compression for all alloys. Model is based on the best fit when considering $\tau_0 = 0.5$ GPa and the highly nonlinear bulk response condition (3.27).

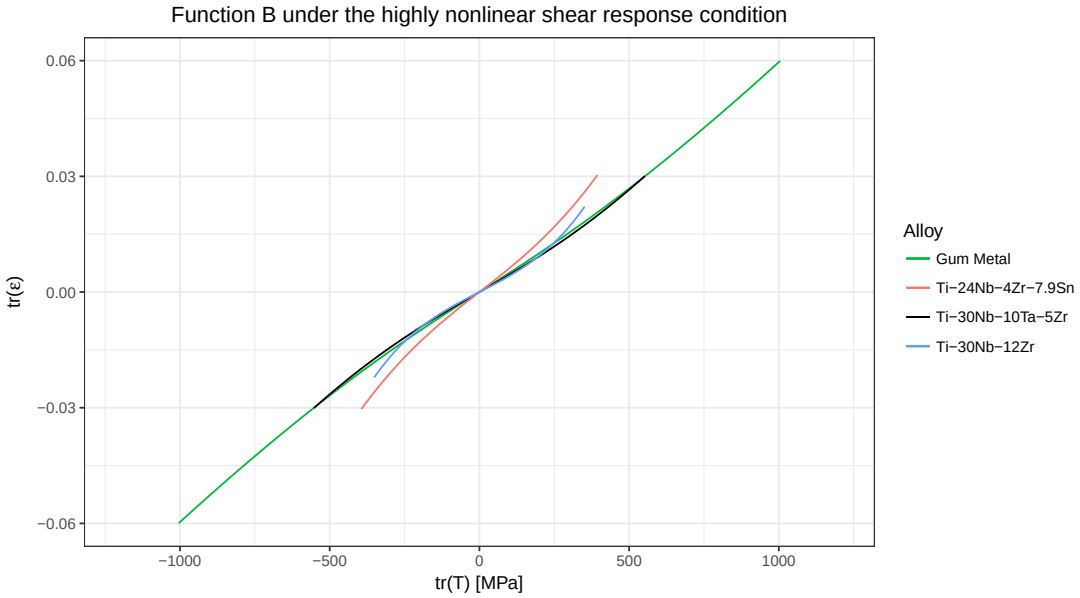

Figure 3.19: Comparison of the bulk responses (3.32a) including compression for all alloys. Model is based on the best fit when considering $\tau_0 = 0.5$ GPa and the highly nonlinear shear response condition (3.28).

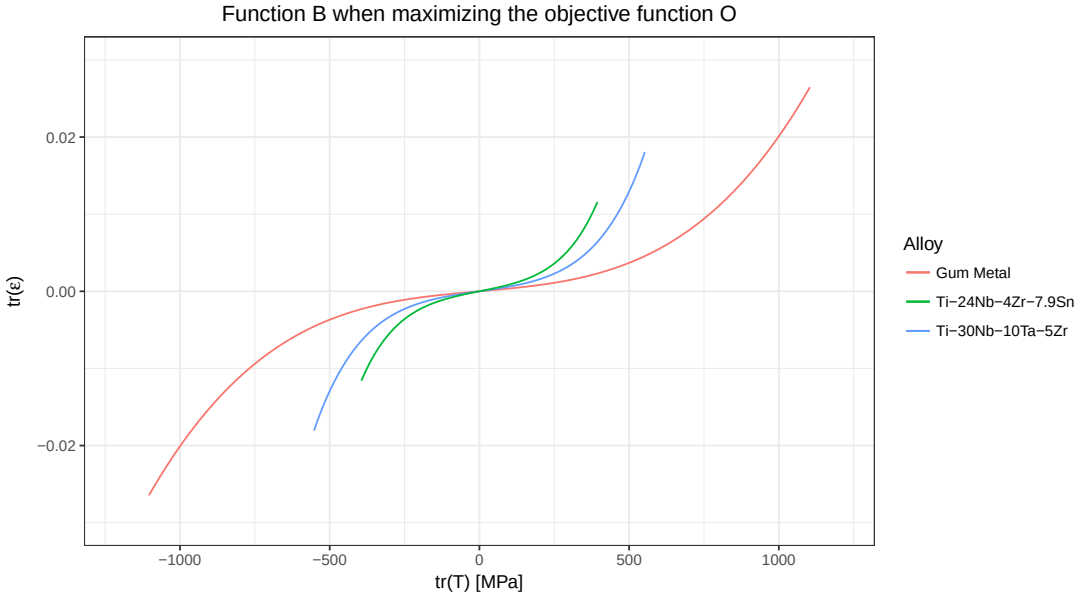

Figure 3.20: Comparison of the bulk responses (3.32a) including compression for all alloys. The model is based on the best fit when considering $\tau_0 = 0.5$ GPa and when maximizing the objective function (3.30).

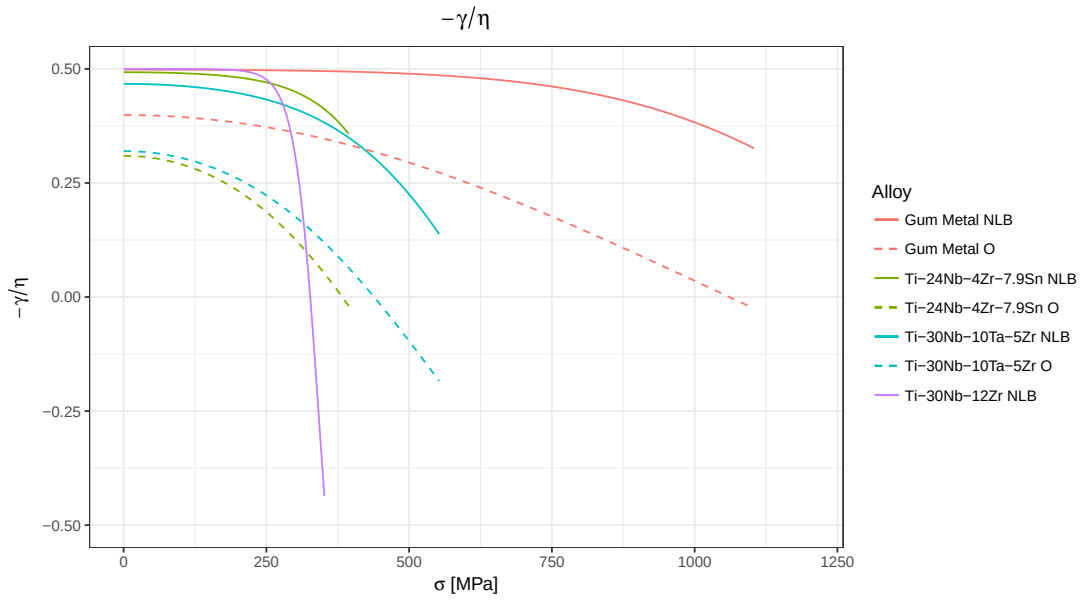

Figure 3.21: Comparison of the ratio $-\gamma/\eta$ of the form (3.33) in a simple tension for all alloys. The model is based on the best fit when considering $\tau_0 = 0.5\,\text{GPa}$. In this graph, we include the best fit data when considering the highly nonlinear bulk response condition (3.27), labelled NLB, and the best fit data obtained by maximizing the objective function (3.30), labelled O.

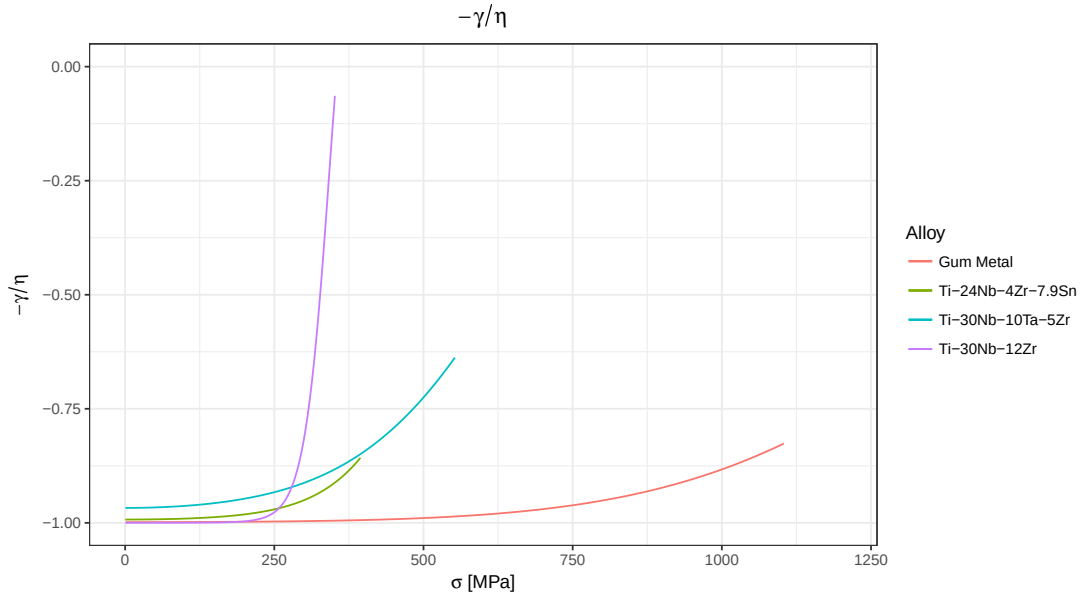

Figure 3.22: Comparison of the ratio $-\gamma/\eta$ of the form (3.33) in a simple tension for all alloys. The model is based on the best fit when considering $\tau_0 = 0.5\,\text{GPa}$ and the highly nonlinear shear response condition (3.28).

Alloy	τ_0	s'	q'	K	μ	R^2	E	ν
Gum Metal	0.5 GPa	2.23	7.65	6.7 GPa	18 668 GPa	0.9998	60.5 GPa	−1.00
Ti-30Nb-10Ta-5Zr	0.5 GPa	2.49	9.15	7.4 GPa	1001 GPa	0.9998	65.6 GPa	−0.97
Ti-24Nb-4Zr-7.9Sn	0.5 GPa	2.99	15.68	5.5 GPa	3378 GPa	0.9997	49.3 GPa	−0.99
Ti-30Nb-12Zr	0.5 GPa	4.29	56.49	8.4 GPa	540 755 GPa	0.9980	75.4 GPa	−1.00

Table 3.11: The values of the best fit, Young's modulus E and Poisson's ratio ν, when $\tau_0 = 0.5$ GPa under the assumption of the highly nonlinear shear response (3.28). Young's modulus and Poisson's ratio were estimated from the best fit data based on the conversion relationships, see Table A.1, (p. 151).

Alloy	τ_0	s'	q'	K	μ	R^2	E	ν
Gum Metal	1.1 GPa	2.82	28.5	6.7 GPa	3 850 656 GPa	0.9999	60.1 GPa	−1.00
Ti-30Nb-10Ta-5Zr	0.6 GPa	2.58	9.81	7.5 GPa	873 GPa	0.9998	65.5 GPa	−0.96
Ti-24Nb-4Zr-7.9Sn	0.4 GPa	2.65	12.13	5.5 GPa	3604 GPa	0.9997	49.4 GPa	−0.99
Ti-30Nb-12Zr	0.4 GPa	3.39	37.89	8.6 GPa	2 413 931 GPa	0.9980	77.0 GPa	−1.00

Table 3.12: The values of the best fit, Young's modulus E and Poisson's ratio ν, when $\tau_0 = \sigma_{max}$ under the assumption of the highly nonlinear shear response (3.28). Young's modulus and Poisson's ratio were estimated from the best fit data based on the conversion relationships, see Table A.1, (p. 151).

3.5.2 Discussion and concluding remarks

All beta phase titanium alloys that have been studied behave nonlinearly in their elastic regime. Thus, it would be inappropriate to describe them using the linearized elastic model. This can be documented by varying estimates of Young's modulus for different stress ranges, see Table 3.8. We have considered a class of power-law models where the nonlinear dependence of the strain on the deviatoric part of the stress and its trace are mutually separated and can have different polynomial growth. Such a decomposition is more appropriate for capturing experimental data as the experiments focus on measuring the effect of shear, dilation, etc. separately, see see Criscione et al. (2000).

We have found out that the power-law models are able to describe tensile loading behavior of Gum Metal and other beta phase titanium alloys in the full range of nonlinear elastic response, see Figures 3.3–3.6. The power-law model (3.19) outperforms or at least is as good as the existing models due to Rajagopal (2014) and Devendiran et al. (2017). The coefficient of determination R^2 is very close to the ideal value of 1 for all the above mentioned models, see Tables 3.9–3.14.

The algorithm to find the best fit for a tensile loading experiment have to be supplied with an extra constraint to yield a unique best fit. The effects of using one of the constraints (3.27) or (3.28) on the bulk and shear responses in (3.19) are mutually inverse. For the constraint (3.27), the shear response is close to the linear one and the bulk response is highly nonlinear, see Figures 3.7, 3.10, 3.13, 3.16, 3.18. Under the constraint (3.28), we have a highly nonlinear shear response and a bulk response that is almost linear, see Figures 3.8, 3.11, 3.14, 3.17, 3.19. When comparing the effects of the reversal of the constraints, exponents of the bulk term s' and the shear term q' are reversed, the bulk and shear moduli change according to the relation (3.26), while Young's modulus is the same for both conditions, see Tables 3.9–3.12.

There are compelling reasons to choose the constraint (3.27), which leads to the

Alloy	τ_0	s'	q'	K	μ	R^2	E	ν
Gum Metal	0.5 GPa	4.19	1.92	96.6 GPa	20.9 GPa	0.9998	58.6 GPa	0.40
Ti-30Nb-10Ta-5Zr	0.5 GPa	6.43	1.88	59.8 GPa	24.5 GPa	0.9998	64.6 GPa	0.32
Ti-24Nb-4Zr-7.9Sn	0.5 GPa	7.49	2.14	42.7 GPa	18.6 GPa	0.9997	48.8 GPa	0.31

Table 3.13: The values of the best fit, Young's modulus E and Poisson's ratio ν, for $\tau_0 = 0.5$ GPa when maximizing the objective function (3.30). Young's modulus and Poisson's ratio were estimated from the best fit data based on the conversion relationships, see Table A.1, (p. 151).

Alloy	R^2_{exp}	E_{exp}	R^2_{imp}	E_{imp}
Gum Metal	0.9982	63.7 GPa	-	-
Ti-30Nb-10Ta-5Zr	0.9997	63.8 GPa	0.9960	67.0 GPa
Ti-24Nb-4Zr-7.9Sn	0.9996	48.1 GPa	0.9993	50.5 GPa
Ti-30Nb-12Zr	0.9966	75.6 GPa	0.9944	61.6 GPa

Table 3.14: Basic parameters of the fits of the tensile loading data to models (3.3), (3.6) and (3.8) that were performed in Rajagopal (2014); Devendiran et al. (2017). We list the coefficients of determination R^2_{exp}, R^2_{imp} and Young's modulus estimates E_{exp}, E_{imp} for these models. For Gum Metal, R^2_{exp} and E_{exp} are the parameters of the model (3.3). For other alloys, R^2_{exp} and E_{exp} are the parameters of the explicit model (3.8) while R^2_{imp} and E_{imp} are parameters of (3.6). For comparison with the power-law model (3.22), see the last columns in Tables 3.9–3.12.

highly nonlinear bulk response, over the constraint (3.28). First, the latter constraint (3.28) yields the positive transverse strain γ in the whole elastic range of tensile loading for all alloys, see Figure 3.23. In turn, that leads to a negative function $\hat{\nu}(\sigma) = -\gamma/\eta$, which in the limit $\sigma \to 0$ leads to negative Poisson's ratio close to -1, see Figure 3.22. In contrast, using the constraint (3.27) yields positive Poisson's ratio for all alloys, see Figure 3.21. Moreover upon using the constraint (3.27), the values of the shear modulus μ, see Table 3.9, are in the range that is close to the VRH estimates of shear moduli of titanium alloys, see Table 3.7.

We now consider the physically more realistic condition (3.27), see Table 3.9. We wish to compare material moduli with the previous works, see Table 3.14, and with the VRH estimates, see Table 3.7. Young's modulus in Table 3.9 for Gum Metal differs by ~ 3 GPa from the estimate by the model (3.3), see Table 3.14. When comparing the value of Young's modulus with the model (3.8), we obtain the difference of ~ 2 GPa in case of *Ti-30Nb-10Ta-5Zr* alloy and the difference that is less than 1 GPa for other two alloys, see Table 3.14. Very good compliance with the VRH estimates, see Table 3.7, was achieved for the values of the shear modulus and Young's modulus from Table 3.9. Young's modulus is within a range of VRH estimates for Gum Metal and *Ti-24Nb-4Zr-7.9Sn* alloy. In case of *Ti-30Nb-10Ta-5Zr* alloy, the power-law model predicts Young's modulus ~ 5 GPa above the VRH range. Shear moduli from Table 3.9 are ~ 3 GPa under the VRH range for Gum Metal and *Ti-24Nb-4Zr-7.9Sn* alloy. In case of *Ti-30Nb-10Ta-5Zr* alloy, shear modulus is in the VRH range. Bulk moduli K and Poisson's ratios ν from Table 3.9 are above the VRH range for all alloys. Our model predicts that these materials behave initially as incompressible (very high bulk modulus and Poison's ratio close to 0.5) while the compressibility and generalized Poisson's ratio (3.33) decrease as the stress grows, see Figures 3.18,

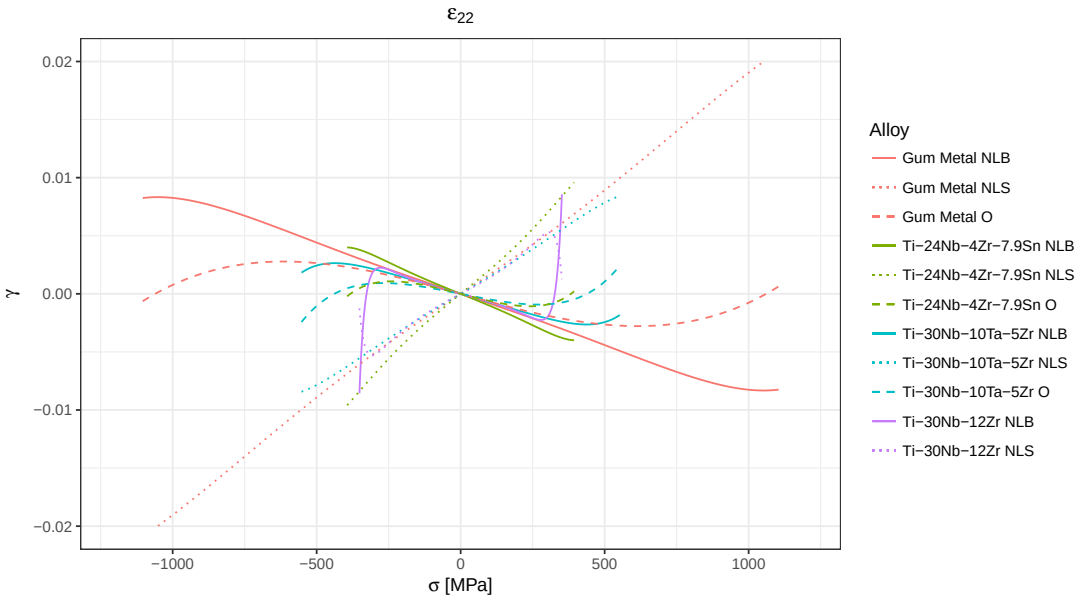

Figure 3.23: Comparison of the strain component γ in a simple tension for all alloys. Model is based on the best fit when considering $\tau_0 = 0.5\,\mathrm{GPa}$. In this graph we include data when considering nonlinear bulk response condition (3.27), labelled NLB, with the opposite condition (3.28), labelled NLS, and with the best fit obtained by maximizing the objective function (3.30), labelled O.

3.21.

To obtain the bulk modulus K and Poisson's ratio ν that are close to VRH estimates (3.9) and (3.17), we introduce an objective function (3.30), which takes into account deviation from the Poisson's ratio given by the VRH estimate. Maximization of the objective function over the search space of power-law exponents leads to an unique set of the best fit parameters. The decrease in the quality of fit for alloys considered is negligible, see Table 3.13. Using the modified algorithm, we were able to obtain very good compliance with VRH estimates in terms of both the bulk modulus K (3.9) and the shear modulus μ (3.17), compare Tables 3.7, 3.13. For *Ti-30Nb-12Zr* alloy, the single crystal data are not available and this approach is not applicable.

The main results of this chapter are considered for publication, see Kulvait et al. (2017).

4. Existence of solutions

There is a growing number of results regarding the mathematical analysis of the BVPs that arise when studying implicitly constituted materials. The strain-limiting model (2.32) in the setting of the anti-plane stress is related to the minimal surface problem. Some existence results, depending on the geometry of Ω, can be found in Bulíček et al. (2015a). In Bulíček et al. (2015b), the existence of solution to the problem with strain-limiting response was established in the spatially periodic setting. The full three-dimensional problem for the strain-limiting model with Dirichlet boundary conditions considered on the whole part of the boundary was investigated in Bulíček et al. (2014), and the authors proved the existence of a weak solution for $a \in (0, 1/3)$. In Bulíček et al. (2014), the authors also established the existence of a renormalized weak solution for any $a > 0$. In Beck et al. (2017), the mixed boundary value problem for the limiting strain model was studied, and the whole theory was strengthened in the sense that the weak solution exists for all $a > 0$ with the caveat that the prescribed traction on the Neumann part of the boundary may not be attained. The existence of solutions to the three-dimensional problem for the strain-limiting model, where cracks and displacement discontinuities are allowed, is studied by means of generalized variational inequalities in Itou et al. (2016). In Knees – Sändig (2004, 2006), the generalised Ramberg-Osgood model (2.19), see Definition 2.10, (p. 24), is studied by means of a minimalization problem for the stress based complementary energy functional of the type (2.21). Regularity results and the existence of solutions are established. These results can be applied to the analysis of power-law models (2.20), see Definition 2.11, (p. 24), with a linear response to the mean normal stress $s' = 2$ and $q' \in [2, \infty)$.

In this chapter, we derive the weak formulation of the Problem (P), see Definition 1.1, (p. 7), which works with anisotropic spaces, studied in Geymonat et al. (1986). We prove the existence of weak solutions to this problem when the constitutive equation is of the form (2.20). We divide the proof into two parts. First, we introduce an ε regularized problem with a proper smoothing operator and show the existence of the weak solution to the ε regularized problem. Using the Galerkin method, we prove the existence of a sequence of solutions in finite-dimensional subspaces of the native space of weak solutions. We obtain apriori estimates and show that we can pass solutions of the Galerkin system to the limit in $\mathbf{T}$ and in $\mathbf{u}$ to obtain the solution of the ε regularized problem. Finally, we show that as $\varepsilon \to 0$, the sequence of the solutions to the ε regularized problem converges to the weak solution of the original problem. The proof of the existence of solutions works with the system of two coupled first order partial differential equations and it does not invert or assume invertibility of the constitutive function $\mathbf{G}$.

In the spatial dimension $n \in \{2, 3\}$, for $s, q \in (1, \infty)$, where Hölder conjugates s' and q' are exponents of the power law dependence (2.20), we show the existence of the solution $(\mathbf{u}, \mathbf{T})$, so that

$$\mathbf{u} \in L^{min(s,q)}(\Omega)^n, \quad (\mathcal{E}\,\mathbf{u})^d \in L^q(\Omega)^{n\times n}_{sym}, \quad \operatorname{div}\mathbf{u} \in L^s(\Omega),$$

and

$$\mathbf{T}^d \in L^{q'}(\Omega)^{n\times n}_{sym}, \quad \operatorname{tr}\mathbf{T} \in L^{s'}(\Omega),$$

where $\mathbf{u}$ has the trace in

$$Tr\,\mathbf{u} \in W^{1-\frac{1}{min(s,q)},min(s,q)}(\partial\Omega)^n. \tag{4.1}$$

For $n = 2$, $q \in (1,\infty)$, $s \in (max(1,\frac{2q}{2+q}),\infty)$, we can improve this result, using compact embedding, to obtain solutions

$$\mathbf{u} \in L^q(\Omega)^2, \quad (\mathcal{E}\,\mathbf{u})^d \in L^q(\Omega)^{2\times 2}_{sym}, \quad \mathrm{div}\,\mathbf{u} \in L^s(\Omega),$$

where the trace of $\mathbf{u}$ is still in the space given by (4.1). In the spatial dimension $n = 3$, we utilize the generalized Korn inequality where only the deviatoric part of the symmetric gradient is used instead of the full symmetric gradient, see Schirra (2012). We get solutions in the space

$$\mathbf{u} \in L^q(\Omega)^3, \quad (\mathcal{E}\,\mathbf{u})^d \in L^q(\Omega)^{3\times 3}_{sym}, \quad \mathrm{div}\,\mathbf{u} \in L^{max(s,q)}(\Omega),$$

where $\mathbf{u}$ has the trace in $W^{1-\frac{1}{q},q}(\partial\Omega)^3$.

4.1 Auxiliary results

In Section A.2 (p. 132), we reviewed the most important results regarding the analysis of PDEs. Here, we list some auxiliary lemmas, definitions and less-known results, which we utilize later when proving the existence of the solution to the variational problem. Unless stated otherwise, by Ω we understand an open, bounded, simply connected subset of $\mathbb{R}^n$, $n \in \{2,3\}$.

Lemma 4.1. *Let $a_1,\dots,a_k \geq 0$, $k \in \mathbb{N}$, $g > 0$. Let $p_1,\dots,p_k \geq 1$. If $a_1 + \dots + a_k \geq g$, then there exists $C = C(k,p_1,\dots,p_k)$ such that*

$$a_1^{p_1} + \dots + a_k^{p_k} \geq C\,\min(g^{p_1},\dots,g^{p_k}).$$

Proof. There is no loss of generality in assuming that $a_1 \leq \dots \leq a_k$. Hence

$$\frac{a_1^{p_1} + \dots + a_k^{p_k}}{\min(g^{p_1},\dots,g^{p_k})} \geq \frac{a_k^{p_k}}{g^{p_k}} \geq \frac{a_k^{p_k}}{(a_1+\dots+a_k)^{p_k}} \geq \frac{a_k^{p_k}}{(ka_k)^{p_k}} \geq \frac{1}{k^{p_k}}. \tag{4.2}$$

Since p_k in (4.2) is the exponent of the largest term a_k, in the full generality we have that

$$\frac{a_1^{p_1} + \dots + a_k^{p_k}}{\min(g^{p_1},\dots,g^{p_k})} \geq \min(\frac{1}{k^{p_1}},\dots,\frac{1}{k^{p_k}}).$$

□

Lemma 4.2. *Let $\mathbf{f} : \mathbb{R}^n \to \mathbb{R}^n$ be a continuous function. If there exists some $r > 0$ such that*

$$\mathbf{f}(\mathbf{x}) \cdot \mathbf{x} > 0, \quad \forall \mathbf{x} \in \mathbb{R}^n : |\mathbf{x}| = r,$$

then there exists $\mathbf{y} \in \mathbb{R}^n$, $|\mathbf{y}| \leq r$, satisfying $\mathbf{f}(\mathbf{y}) = \mathbf{0}$.

Proof. See (Evans, 2010, p. 529). □

Lemma 4.3. *Suppose that $\mathbf{T} \in L^{q'}(\Omega)^{n\times n}_{sym}$, $\mathbf{v} \in W^{1,q}(\Omega)^n$. Then*

$$\int_\Omega \mathbf{T} : \nabla\mathbf{v}\,\mathrm{d}x = \int_\Omega \mathbf{T} : \mathcal{E}\,\mathbf{v}\,\mathrm{d}x.$$

Proof. From the symmetry of $\mathbf{T}$, we have that

$$\mathbf{T} : \frac{1}{2}\left(\nabla\mathbf{v} - (\nabla\mathbf{v})^\top\right) = 0.$$

By splitting $\nabla\mathbf{v}$ into the symmetric and antisymmetric part

$$\mathbf{T} : \nabla\mathbf{v} = \mathbf{T} : \frac{1}{2}\left(\nabla\mathbf{v} + (\nabla\mathbf{v})^\top\right) + \underbrace{\mathbf{T} : \frac{1}{2}\left(\nabla\mathbf{v} - (\nabla\mathbf{v})^\top\right)}_{0} = \mathbf{T} : \mathcal{E}\,\mathbf{v},$$

we establish the formula. □

4.1.1 Proper function spaces

In what follows, we establish the existence of the weak solution to the Problem (P), see Definition 1.1, (p. 7), when subject to the power-law response (2.20), see Definition 2.11, (p. 24). We have been using the notation of the power law exponents with primes, s' and q', to emphasize their meaning for the weak formulation of the Problem (P). Let s and q be Hölder conjugates of exponents s' and q'

$$s = \frac{s'}{s'-1}, \quad q = \frac{q'}{q'-1},$$

then the natural Lebesque space for the trace of the small strain $\operatorname{tr}\varepsilon$ is L^s and the natural space for the deviatoric part of the small strain ε^d is L^q. The natural space for the trace of the stress $\operatorname{tr}\mathbf{T}$ is $L^{s'}$ and the natural space for the deviatoric part of the stress $\mathbf{T}^d$ is $L^{q'}$. Let us define these function spaces. Recall that the deviatoric part of the tensor $\mathbf{T}$ is denoted by $\mathbf{T}^d$.

Definition 4.4. *Let $p, q, s \in (1, \infty)$. The spaces of functions $(L^{(q,s)}(\Omega), \|.\|_{(q,s)})$, $(W^{1,(p,q,s)}(\Omega), \|.\|_{1,(p,q,s)})$, $(W^{1,(q,s)}(\Omega), \|.\|_{1,(q,s)})$, $(W^{1,(q,*)}(\Omega), \|.\|_{1,(q,*)})$ are defined below.*

$$L^{(q,s)}(\Omega) = \{\mathbf{E} : \mathbf{E}^d \in L^q(\Omega)^{n\times n}_{sym}, \operatorname{tr}\mathbf{E} \in L^s(\Omega)\},$$

with the norm

$$\|\mathbf{E}\|_{(q,s)} = \|\mathbf{E}^d\|_q + \|\operatorname{tr}\mathbf{E}\|_s.$$

$$W^{1,(p,q,s)}(\Omega) = \{\mathbf{u} : \mathbf{u} \in L^p(\Omega)^n, (\mathcal{E}\,\mathbf{u})^d \in L^q(\Omega)^{n\times n}_{sym}, \operatorname{div}\mathbf{u} \in L^s(\Omega)\},$$

with the norm

$$\|\mathbf{u}\|_{1,(p,q,s)} = \|\mathbf{u}\|_p + \|(\mathcal{E}\,\mathbf{u})^d\|_q + \|\operatorname{div}\mathbf{u}\|_s.$$

$$W^{1,(q,s)}(\Omega) = W^{1,(q,q,s)}(\Omega),$$

with the norm

$$\|\mathbf{u}\|_{1,(q,s)} = \|\mathbf{u}\|_{1,(q,q,s)}.$$

$$W^{1,(q,*)}(\Omega) = \{\mathbf{u} : \mathbf{u} \in L^q(\Omega)^n, (\mathcal{E}\,\mathbf{u})^d \in L^q(\Omega)^{n\times n}_{sym}\},$$

with the norm

$$\|\mathbf{u}\|_{1,(q,*)} = \|\mathbf{u}\|_q + \|(\mathcal{E}\,\mathbf{u})^d\|_q.$$

The spaces from the Definition 4.4 are Banach spaces. Korn's inequality and miscellaneous results of duality, traces, density and orthogonality for these spaces were established in Geymonat et al. (1986) in the context of the analysis of Norton-Hoff materials. Some additional results regarding these spaces can be found in Fuchs – Seregin (2000).

Definition 4.5 (Standard domain properties). *Recall that by Ω we understand an open, bounded, simply connected subset of $\mathbb{R}^n$, $n \in \{2, 3\}$. From now on, we make the following additional assumption that $\Omega \in C^{0,1}$, $\partial\Omega = \overline{\Gamma_D \cup \Gamma_N}$, where Γ_D and Γ_N are open, disjoint parts of the boundary $\partial\Omega$.*

We will denote by $|\Gamma_D| > 0$ the requirement that $(n-1)$-dimensional Hausdorff measure of Γ_D is positive.

Lemma 4.6 (Korn's inequality). *Let $\Omega \in C^{0,1}$, $q \in (1, \infty)$, then there exists a constant $C(\Omega, q) > 0$, so that*

$$\forall \mathbf{u} \in W^{1,q}(\Omega)^n, \quad \|\mathbf{u}\|_{1,q} \leq C(\Omega, q)(\|\mathbf{u}\|_q + \|\mathcal{E}\,\mathbf{u}\|_q).$$

Proof. See Korn (1907). □

Lemma 4.7 (Generalized Korn's inequality). *Let $n \geq 3$, $\Omega \in C^{0,1}$, $q \in (1, \infty)$. Then the spaces $W^{1,(q,*)}(\Omega)$ and $W^{1,q}(\Omega)^n$ are equivalent in the sense of Definition A.77, (p. 137) and there exists a constant $C(\Omega, q) > 0$ such that*

$$\|\mathbf{u}\|_{1,q} \leq C(\Omega, q)(\|\mathbf{u}\|_q + \|(\mathcal{E}\,\mathbf{u})^d\|_q), \quad \forall \mathbf{u} \in W^{1,(q,*)}(\Omega).$$

Proof. See Schirra (2012). □

For $n = 2$, Lemma 4.7 holds in the space of tracefree functions $W_0^{1,q}(\Omega)^2$. However, it does not hold in general, see (Schirra, 2012, p. 150).

Theorem 4.8. *Let $\Omega \in C^{0,1}$, $q \in (1, \infty)$. Then the spaces $W^{1,(q,q)}(\Omega)$ and $W^{1,q}(\Omega)^n$ are equivalent in the sense of Definition A.77, (p. 137), and there exist two constants $C_1, C_2 > 0$ such that*

$$C_1\|\mathbf{u}\|_{1,q} \leq \|\mathbf{u}\|_{1,(q,q)} \leq C_2\|\mathbf{u}\|_{1,q}, \quad \forall \mathbf{u} \in W^{1,(q,q)}(\Omega).$$

Proof. See (Geymonat et al., 1986, Theorem 1). □

Theorem 4.9. *Let $\Omega \in C^{0,1}$. Let $q \in (1, \infty)$, $s \in [q, \infty)$. Then there exists a continuous linear operator $Tr : W^{1,(q,s)}(\Omega) \to W^{1-\frac{1}{q},q}(\partial\Omega)^n$ that is onto. Moreover, there exists a continuous lifting operator $Lf : W^{1-\frac{1}{q},q}(\partial\Omega)^n \to W^{1,(q,s)}(\Omega)$.*

Proof. See (Geymonat et al., 1986, Proposition 2). □

We may now define the meaning of the trace operator in $W^{1,(p,q,s)}(\Omega)$.

Definition 4.10 (Trace). *Let $p, q, s \in (1, \infty)$. In $W^{1,(p,q,s)}(\Omega)$, we understand the trace Tr as the operator defined by Theorem 4.9 on the space $W^{1,(min(p,q,s),min(p,q,s))}(\Omega)$.*

For the space $W^{1,(q,s)}(\Omega)$, we define the trace separately in $n = 2$ and $n = 3$.

Definition 4.11 (Trace in $n = 2$). *Let $n = 2$. Let $q, s \in (1, \infty)$. For the space $W^{1,(q,s)}(\Omega)$, we understand the trace Tr as the operator defined by Theorem 4.9 on $W^{1,(min(s,q),min(s,q))}(\Omega)$.*

Definition 4.12 (Trace in $n = 3$). *Let $n = 3$. Let $q, s \in (1, \infty)$. For the spaces $W^{1,(q,s)}(\Omega)$ and $W^{1,(q,*)}(\Omega)$, we understand the trace Tr as the operator defined by Theorem 4.9 on $W^{1,(q,q)}(\Omega)$.*

Lemma 4.7 and Theorem 4.8 establish the equivalence of spaces $W^{1,(q,*)}(\Omega)$, $W^{1,(q,q)}(\Omega)$ and $W^{1,q}(\Omega)^n$ for the spatial dimension $n = 3$ and $q \in (1, \infty)$. Considering a natural embedding $W^{1,(q,s)}(\Omega) \subset W^{1,(q,*)}(\Omega)$, Lemma 4.7 and Theorem 4.8 may be summarized by saying that for $s \in (1, \infty)$, there exists a constant $C > 0$ such that

$$\|\mathbf{u}\|_{1,q} \leq C\|\mathbf{u}\|_{1,(q,s)}, \quad \forall \mathbf{u} \in W^{1,(q,s)}(\Omega).$$

We have also the hierarchy

$$W^{1,(q,s)}(\Omega) \subset W^{1,(q,*)}(\Omega) \subset W^{1,(q,q)}(\Omega). \tag{4.3}$$

With the help of (4.3), we clarify that the trace operator in Definition 4.12 is well defined.

Definition 4.13 (Boundary spaces). *Let Ω satisfy the assumptions of Definition 4.5 of standard domain properties, $\Gamma \subset \partial\Omega$, Γ open. Let $r \in (0, 1)$, $q \in (1, \infty)$. We define the space $W^{r,q}(\Gamma)$ as a subspace of $W^{r,q}(\partial\Omega)$, which contains only the functions vanishing on $\partial\Omega \setminus \overline{\Gamma}$.*

Now, we have all the tools in place to define natural spaces for the weak solutions.

Definition 4.14 (Natural spaces for the weak solutions). *Let Ω satisfy the assumptions of Definition 4.5 of standard domain properties with $|\Gamma_D| > 0$, let $p, q, s \in (1, \infty)$, then we define the natural spaces for the weak solutions as follows*

$$W^{(p,q,s)}_{\Gamma_D}(\Omega) = \{\mathbf{u} : \mathbf{u} \in W^{1,(p,q,s)}(\Omega), \mathbf{u}|_{\Gamma_D} = 0\},$$

and

$$W^{(q,s)}_{\Gamma_D}(\Omega) = \{\mathbf{u} : \mathbf{u} \in W^{1,(q,s)}(\Omega), \mathbf{u}|_{\Gamma_D} = 0\}.$$

Lemma 4.15 (Korn-Poincaré inequality). *Let Ω satisfy the assumptions of Definition 4.5 of standard domain properties with $|\Gamma_D| > 0$. Let $q \in (1, \infty)$. Then there exists a constant $C > 0$ such that*

$$\|\mathbf{u}\|_q \leq C(\Omega, q)\|\mathcal{E}\,\mathbf{u}\|_q, \quad \forall \mathbf{u} \in W^{1,q}(\Omega)^n, \quad \mathbf{u}|_{\Gamma_D} = \mathbf{0}.$$

Proof. Suppose the lemma was false. Then there exists a sequence $\{\mathbf{u}_k\} \subset L^q(\Omega)^n$, $\|\mathbf{u}_k\|_q = 1$ for $k \in \mathbb{N}$, such that

$$\|\mathbf{u}_k\|_q > k\|\mathcal{E}\,\mathbf{u}_k\|_q,$$

from which follows

$$\|\mathcal{E}\,\mathbf{u}_k\|_q < \frac{1}{k}. \tag{4.4}$$

From (4.4), it may be concluded that

$$\mathcal{E}\,\mathbf{u}_k \to \mathbf{0} \quad \text{in } L^q(\Omega)^{n\times n}_{sym}. \tag{4.5}$$

Using Korn's inequality (Lemma 4.6) and Eberlein-Šmulian Theorem A.75, (p. 136), it can be seen that

$$\mathbf{u}_{k_i} \rightharpoonup \mathbf{u} \quad \text{in } W^{1,q}(\Omega)^n.$$

From compact embedding Theorem A.89, (p. 138), we have that $\mathbf{u} \in W^{1,q}(\Omega)^n \subset\subset L^q(\Omega)^n$ and thus

$$\mathbf{u}_{k_i} \to \mathbf{u} \quad \text{in } L^q(\Omega)^n, \quad \|\mathbf{u}\|_q = 1.$$

We obtain $\mathcal{E}\,\mathbf{u} = 0$ from (4.5). Employing the result from Hlaváček – Nečas (1970), $\mathbf{u}$ has the structure

$$u_i = W_{ij}x_j + c_i, \quad W_{ij} = -W_{ji}, \quad i,j \in \{1,\dots,n\}, \tag{4.6}$$

where W_{ij}, c_i are constants. Since $\Omega \in C^{0,1}$, we can assume that there exists $\alpha > 0$ such that some part of Γ_D is described by the Lipschitz mapping a, where

$$\begin{aligned} &x'_k \in (-\alpha,\alpha), \quad k \in \{1,\dots,n-1\},\\ &x_n = a(x'_1,\dots,x'_{n-1}), \end{aligned}$$

and $(x'_1,\dots,x'_{n-1},a(x'_1,\dots,x'_{n-1})) \subset \Gamma_D$. This involves no loss of generality. On the assumed part of the boundary we have that

$$u_n = \sum_{j=1}^{n-1} W_{nj}x'_j + W_{nn}a(x'_1,\dots,x'_{n-1}) + c_n. \tag{4.7}$$

Since $\mathbf{u} = \mathbf{0}$ on Γ_D and $W_{nn} = 0$, we can rewrite (4.7) as

$$0 = \sum_{j=1}^{n-1} W_{nj}x'_j + c_n, \quad x'_j \in (-\alpha,\alpha),$$

which yields $c_n = 0$ and $W_{nj} = 0$ for $j \in \{1,\dots,n\}$. We now turn to the case $i \in \{1,\dots,n-1\}$ where

$$u_i = \sum_{j=1}^{n-1} W_{ij}x'_j + W_{in}a(x'_1,\dots,x'_{n-1}) + c_i.$$

Since $W_{in} = -W_{ni} = 0$ and $u_i = 0$, following the previous argument, we obtain $W_{ij} = 0$, $c_i = 0$ for all $i,j \in \{1,\dots,n\}$. As the $\mathbf{u}$ is of the form (4.6), we conclude that $\mathbf{u} = \mathbf{0}$ in Ω, which contradicts $\|\mathbf{u}\|_q = 1$. □

Theorem 4.16. *Let Ω satisfy the assumptions of Definition 4.5 of standard domain properties with $|\Gamma_D| > 0$. Let $s,q \in (1,\infty)$. There exists a positive constant C, such that for every $\mathbf{u} \in W^{(min(s,q),q,s)}_{\Gamma_D}(\Omega)$, we have that*

$$\|\mathbf{u}\|_{min(s,q)} \le C(\|(\mathcal{E}\,\mathbf{u})^d\|_q + \|\mathrm{div}\,\mathbf{u}\|_s).$$

Proof. Proof is a consequence of Lemma 4.15. □

Theorem 4.17. *Let $n = 3$, let Ω satisfy the assumptions of Definition 4.5 of standard domain properties with $|\Gamma_D| > 0$. Let $s, q \in (1, \infty)$. There exists a positive constant $C > 0$ such that for every $\mathbf{u} \in W^{(q,s)}_{\Gamma_D}(\Omega)$, we have that*

$$\|\mathbf{u}\|_q \leq C(\|(\mathcal{E}\,\mathbf{u})^d\|_q + \|\operatorname{div}\mathbf{u}\|_s).$$

Proof. Assume the opposite. Then there exists a sequence $\{\mathbf{u}_k\} \subset L^q(\Omega)^n$,

$$\|\mathbf{u}_k\|_q = 1, \tag{4.8}$$

for $k \in \mathbb{N}$, such that

$$\|\mathbf{u}_k\|_q > k(\|(\mathcal{E}\,\mathbf{u}_k)^d\|_q + \|\operatorname{div}\mathbf{u}_k\|_s),$$

and therefore

$$\|(\mathcal{E}\,\mathbf{u}_k)^d\|_q + \|\operatorname{div}\mathbf{u}_k\|_s < \frac{1}{k}. \tag{4.9}$$

The equation (4.9) yields

$$\begin{aligned} (\mathcal{E}\,\mathbf{u}_k)^d &\to \mathbf{0} \quad \text{in } L^q(\Omega)^{3\times 3}_{sym}, \\ \operatorname{div}\mathbf{u}_k &\to 0 \quad \text{in } L^s(\Omega) \end{aligned} \tag{4.10}$$

Applying Lemma 4.7 on (4.8) and (4.9) yields that $\mathbf{u}_k$ is a bounded sequence in $W^{1,q}(\Omega)^3$. Therefore,

$$\nabla\mathbf{u}_k \in L^q(\Omega)^{3\times 3}, \quad \|\nabla\mathbf{u}_k\|_q \leq C(\Omega, q)$$

and specially

$$\operatorname{div}\mathbf{u}_k \in L^q(\Omega), \quad \|\operatorname{div}\mathbf{u}_k\|_q \leq C(\Omega, q). \tag{4.11}$$

Moreover, by Eberlein-Šmulian Theorem A.75 and by the compact embedding theorem Theorem A.89, (p. 138), there is a subsequence $\{k_i, i \in \mathbb{N}\}$ such that

$$\begin{aligned} \mathbf{u}_{k_i} &\rightharpoonup \mathbf{u} \quad \text{in } W^{1,q}(\Omega)^3, \\ \mathbf{u}_{k_i} &\to \mathbf{u} \quad \text{in } L^q(\Omega)^n, \quad \|\mathbf{u}\|_q = 1. \end{aligned} \tag{4.12}$$

Combining (4.10) and (4.12) yields $\|\mathcal{E}\,\mathbf{u}\|_{min(s,q)} = 0$ and therefore $\mathcal{E}\,\mathbf{u} = \mathbf{0}$. Using Lemma 4.15, we have $\mathbf{u} = \mathbf{0}$, which contradicts $\|\mathbf{u}\|_q = 1$. □

We shall remark that for $n = 3$ in case of $s < q$, Theorem 4.17 was proven as a consequence of Lemma 4.7. For $n = 2$, Lemma 4.7 does not hold, thus to prove a variant of Theorem 4.17 we need to employ compact embedding. It yields the claim of the type stated in Theorem 4.7 for $q \in (1, \infty)$ and $s \in (\frac{2q}{2+q}, \infty)$.

Theorem 4.18. *Let $n = 2$, let Ω satisfy the assumptions of Definition 4.5 of standard domain properties with $|\Gamma_D| > 0$. Let $q \in (1, \infty)$, $s \in (max(1, \frac{2q}{2+q}), \infty)$. There exists a positive constant C such that for every $\mathbf{u} \in W^{(q,s)}_{\Gamma_D}(\Omega)$, we have that*

$$\|\mathbf{u}\|_q \leq C(\|(\mathcal{E}\,\mathbf{u})^d\|_q + \|\operatorname{div}\mathbf{u}\|_s).$$

Proof. For contradiction, as in Theorem 4.17, we assume that there exists a sequence $\{\mathbf{u}_k\} \subset L^q(\Omega)^n$ that satisfies

$$\|\mathbf{u}_k\|_q = 1, \tag{4.13}$$

for $k \in \mathbb{N}$, such that

$$\|(\mathcal{E}\,\mathbf{u}_k)^d\|_q + \|\operatorname{div}\mathbf{u}_k\|_s < \frac{1}{k}. \tag{4.14}$$

The equation (4.14) yields

$$\begin{aligned} (\mathcal{E}\,\mathbf{u}_k)^d &\to \mathbf{0} \quad \text{in } L^q(\Omega)^{2\times 2}_{sym}, \\ \operatorname{div}\mathbf{u}_k &\to 0 \quad \text{in } L^s(\Omega). \end{aligned} \tag{4.15}$$

Applying Korn's inequality, Lemma 4.6, on (4.13) and (4.14) yields that $\mathbf{u}_k$ is a bounded sequence in $W^{1,s}(\Omega)^2$. Since $s \in (max(1, \frac{2q}{2+q}), \infty)$, we can apply Rellich-Kondrachov Compactness Theorem A.89, (p. 138), which yields

$$\begin{aligned} &\mathbf{u}_{k_i} \rightharpoonup \mathbf{u} \quad \text{in } W^{1,s}(\Omega)^2, \\ &\mathbf{u}_{k_i} \to \mathbf{u} \quad \text{in } L^q(\Omega)^n, \quad \|\mathbf{u}\|_q = 1. \end{aligned} \tag{4.16}$$

Combining (4.15) and (4.16) yields $\|\mathcal{E}\,\mathbf{u}\|_{min(s,q)} = 0$ and therefore $\mathcal{E}\,\mathbf{u} = \mathbf{0}$. Using Lemma 4.15, we have $\mathbf{u} = \mathbf{0}$, which contradicts $\|\mathbf{u}\|_q = 1$. □

Note that Theorem 4.18 holds for every $s \in [2, \infty)$. Rephrasing the results of Theorems 4.16–4.18, we obtain the following result.

Theorem 4.19. *Let Ω satisfy the assumptions of Definition 4.5 of standard domain properties with $|\Gamma_D| > 0$. Let $p, q \in (1, \infty)$, then*

$$\|\mathbf{u}\|_{1,(min(q,s),q,s)} \le C(\|(\mathcal{E}\,\mathbf{u})^d\|_q + \|\operatorname{div}\mathbf{u}\|_s), \quad \forall \mathbf{u} \in W^{1,(min(q,s),q,s)}_{\Gamma_D}, \tag{4.17}$$

Moreover, for $n = 3$ and for $n = 2$, when $q \in (1, \infty)$, $s \in (max(1, \frac{2q}{2+q}), \infty)$, there exists a $C > 0$ such that

$$\|\mathbf{u}\|_{1,(q,s)} \le C(\|(\mathcal{E}\,\mathbf{u})^d\|_q + \|\operatorname{div}\mathbf{u}\|_s), \quad \forall \mathbf{u} \in W^{1,(q,s)}_{\Gamma_D}. \tag{4.18}$$

Proof. The inequality (4.17) follows from Theorem 4.16. The inequality (4.18) is in case of $n = 3$ a consequence of Theorem 4.17 and in case of $n = 2$ a consequence of Lemma 4.18 . □

4.2 Variational formulation of boundary value problem

This section is intended to establish the weak variational version of the Problem (P), see Definition 1.1, (p. 7). Throughout this chapter, we will be using the following notation. Let $f \in L^p(\Omega)$, $g \in L^{p'}(\Omega)$, $\mathbf{u} \in L^p(\Omega)^n$, $\mathbf{v} \in L^{p'}(\Omega)^n$, $\mathbf{U} \in L^p(\Omega)^{n\times n}$ and $\mathbf{V} \in L^{p'}(\Omega)^{n\times n}$, then

$$(f, g) = \int_\Omega fg \,\mathrm{d}x, \quad (\mathbf{u}, \mathbf{v}) = \int_\Omega \mathbf{u}\cdot\mathbf{v} \,\mathrm{d}x, \quad (\mathbf{U}, \mathbf{V}) = \int_\Omega \mathbf{U} : \mathbf{V} \,\mathrm{d}x.$$

When deriving the variational formulation of the Problem (P) with the constitutive equation (2.20) of the power-law type, see Definition 2.11, (p. 24), we have the exponents $q, s \in (1, \infty)$. A natural space for solutions to this problem is $(\mathbf{u}, \mathbf{T}) \in (W^{1,(p,q,s)}(\Omega), L^{(q',s')}(\Omega))$, where in the full generality $p = min(q, s)$. We assume that for the function $\mathbf{u}_0 \in W^{1-\frac{1}{p},p}(\Gamma_D)^n$, there exists the function $\hat{\mathbf{u}} \in W^{1,(p,q,s)}(\Omega)$ such that $\hat{\mathbf{u}}|_{\Gamma_D} = \mathbf{u}_0$. We can rephrase the Dirichlet boundary condition (1.1c) by requiring that the solution satisfies $\mathbf{u} - \hat{\mathbf{u}} \in W^{1,(p,q,s)}_{\Gamma_D}(\Omega)$. By multiplying the constitutive equation (1.1b) by the test function $\mathbf{S} \in L^{(q',s')}(\Omega)$ and by integrating over Ω, we obtain the weak form of (1.1b) that is $(\mathcal{E}\,\mathbf{u}, \mathbf{S}) = (\mathbf{G}(\mathbf{T}), \mathbf{S})$. To deal with the equilibrium equation, consider a general $\mathbf{f} \in (W^{1,(p,q,s)}_{\Gamma_D}(\Omega))^*$, then multiply (1.1a) by the test function $\boldsymbol{\chi} \in W^{1,(p,q,s)}_{\Gamma_D}(\Omega)$ and integrate over Ω. According to Theorem 4.9, the test function $\boldsymbol{\chi}$ has the trace in the space $W^{1-\frac{1}{p},p}(\Gamma_N)^n$. In the most general case, the Neumann boundary condition (1.1d) can be reformulated by requiring $\mathbf{g} \in (W^{1-\frac{1}{p},p}(\Gamma_N)^n)^*$. Integrating by parts and using the assertion

$$(\mathbf{T}, \mathcal{E}\,\boldsymbol{\chi}) = (\mathbf{T}, \nabla\boldsymbol{\chi}), \quad \forall \boldsymbol{\chi} \in W^{1,(p,q,s)}_{\Gamma_D}(\Omega)$$

due to Lemma 4.3, we get the weak form of the equilibrium equation (1.1a) in the form $(\mathbf{T}, \mathcal{E}\,\boldsymbol{\chi}) = \langle \mathbf{g}, \boldsymbol{\chi}\rangle_{\Gamma_N} + \langle \mathbf{f}, \boldsymbol{\chi}\rangle$. The weak formulation of the Problem (P) is established in the following definition.

Definition 4.20 (Weak Problem (P)). *Let Ω satisfy the assumptions of Definition 4.5 of standard domain properties with $|\Gamma_D| > 0$. Let $b, p, s, q \in (1, \infty)$. Let functions $\hat{\mathbf{u}}$, $\mathbf{g}$, $\mathbf{f}$ be from the following spaces*

$$(\hat{\mathbf{u}}, \mathbf{g}, \mathbf{f}) \in (W^{1,(p,q,s)}(\Omega), (W^{1-\frac{1}{b},b}(\Gamma_N)^n)^*, (W^{1,(p,q,s)}_{\Gamma_D}(\Omega))^*)$$

and $\mathbf{G} : L^{(q',s')}(\Omega) \to L^{(q,s)}(\Omega)$ be a monotone, radially continuous operator. We call the pair $(\mathbf{u}, \mathbf{T}) \in (W^{1,(p,q,s)}(\Omega), L^{(q',s')}(\Omega))$ a solution to the weak Problem (P), if $\mathbf{u}_H = \mathbf{u} - \hat{\mathbf{u}} \in W^{1,(p,q,s)}_{\Gamma_D}(\Omega)$ and if

$$\begin{aligned} (\mathcal{E}\,\mathbf{u}, \mathbf{S}) &= (\mathbf{G}(\mathbf{T}), \mathbf{S}), \\ (\mathbf{T}, \mathcal{E}\,\boldsymbol{\chi}) &= \langle \mathbf{g}, \boldsymbol{\chi}\rangle_{\Gamma_N} + \langle \mathbf{f}, \boldsymbol{\chi}\rangle \end{aligned} \tag{4.19}$$

hold for every pair $(\mathbf{S}, \boldsymbol{\chi}) \in (L^{(q',s')}(\Omega), W^{1,(p,q,s)}_{\Gamma_D}(\Omega)$.

According to Theorem 4.9 for the function $\hat{\mathbf{u}}$ from Definition 4.20, there exists some $\mathbf{u}_0 \in W^{1-\frac{1}{min(p,q,s)},min(p,q,s)}(\Gamma_D)^n$ such that $\hat{\mathbf{u}}|_{\Gamma_D} = \mathbf{u}_0$. In order to establish the existence of the solution to the weak Problem (P) in $W^{1,(p,q,s)}_{\Gamma_D}(\Omega)$, we define a regularizing operator.

Definition 4.21. *Let the operator $\mathbf{H} : W^{1,(p,q,s)}_{\Gamma_D}(\Omega) \times W^{1,(p,q,s)}_{\Gamma_D}(\Omega) \to \mathbb{R}$, for any $\mathbf{u}, \mathbf{v} \in W^{1,(p,q,s)}_{\Gamma_D}(\Omega)$, be defined as*

$$\mathbf{H}(\mathbf{u}, \mathbf{v}) = (|\operatorname{div}\mathbf{u}|^{s-2}\operatorname{div}\mathbf{u}, \operatorname{div}\mathbf{v}) + (\left|(\mathcal{E}\,\mathbf{u})^d\right|^{q-2}(\mathcal{E}\,\mathbf{u})^d, (\mathcal{E}\,\mathbf{v})^d). \tag{4.20}$$

Now we can us define an ε regularized weak Problem (P).

Definition 4.22 (ε-regularized weak Problem (P)). *Let Ω satisfy the assumptions of Definition 4.5 of standard domain properties with $|\Gamma_D| > 0$. Let $b, p, s, q \in (1, \infty)$. Let functions $\hat{\mathbf{u}}$, $\mathbf{g}$, $\mathbf{f}$ be from the following spaces*

$$(\hat{\mathbf{u}}, \mathbf{g}, \mathbf{f}) \in (W^{1,(p,q,s)}(\Omega), (W^{1-\frac{1}{b},b}(\Gamma_N)^n)^*, (W^{1,(p,q,s)}_{\Gamma_D}(\Omega))^*),$$

and $\mathbf{G} : L^{(q',s')}(\Omega) \to L^{(q,s)}(\Omega)$ be a monotone, radially continuous operator. We call the pair $(\mathbf{u}, \mathbf{T}) \in (W^{1,(p,q,s)}(\Omega), L^{(q',s')}(\Omega))$ a solution to the ε regularized weak Problem (P), if $\mathbf{u}_H = \mathbf{u} - \hat{\mathbf{u}} \in W^{1,(p,q,s)}_{\Gamma_D}(\Omega)$ and if

$$\begin{aligned} (\mathcal{E}\,\mathbf{u}, \mathbf{S}) &= (\mathbf{G}(\mathbf{T}), \mathbf{S}), \\ (\mathbf{T}, \mathcal{E}\,\boldsymbol{\chi}) &= \langle \mathbf{g}, \boldsymbol{\chi} \rangle_{\Gamma_N} + \langle \mathbf{f}, \boldsymbol{\chi} \rangle - \varepsilon \mathbf{H}(\mathbf{u}_H, \boldsymbol{\chi}), \end{aligned} \tag{4.21}$$

where $\mathbf{H}$ is given by (4.20)*, hold for every pair $(\mathbf{S}, \boldsymbol{\chi}) \in (L^{(q',s')}(\Omega), W^{1,(p,q,s)}_{\Gamma_D}(\Omega))$.*

Note that for $\varepsilon = 0$, the regularized weak problem reduces to the weak problem.

4.3 Existence of solutions

Prior to proving the existence of solutions to the weak Problem (P), we need to impose some restrictions on the form of the operator $\mathbf{G}$. The following assumption on the constitutive function $\mathbf{G}$ is coherent with the constitutive equation (2.20) for the power-law model from Definition 2.11, (p. 24). It will be shown in Section 4.4.

Definition 4.23. *Let $s, q \in (1, \infty)$. We assume that $\mathbf{G} : L^{(q',s')}(\Omega) \to L^{(q,s)}(\Omega)$ is a monotone, radially continuous operator for which there exist constants $C_1 > 0$, $C_2 > 0$ such that for all $\mathbf{T} \in L^{(q',s')}(\Omega)$, the following is true*

$$(\mathbf{G}(\mathbf{T}), \mathbf{T}) \geq C_1(\|\mathbf{T}^d\|^{q'}_{q'} + \|\mathbf{G}(\mathbf{T})^d\|^q_q + \|\operatorname{tr}\mathbf{T}\|^{s'}_{s'} + \|\operatorname{tr}\mathbf{G}(\mathbf{T})\|^s_s) - C_2|\Omega|. \tag{4.22}$$

The following theorem establishes the existence of solutions to the ε regularised weak problem for any $\mathbf{G}$ that fulfils (4.22). As for prerequisites, some important results from the theory of monotone operators are formulated in Section A.2.4, (p. 139).

Theorem 4.24 (Existence of a weak solution to the regularized problem). *Let $\varepsilon > 0$. Let Ω satisfy the assumptions of Definition 4.5 of standard domain properties with $|\Gamma_D| > 0$. Let $s, q \in (1, \infty)$, $p = b = \min(s, q)$. Let functions $\hat{\mathbf{u}}$, $\mathbf{g}$, $\mathbf{f}$ be from the following spaces*

$$(\hat{\mathbf{u}}, \mathbf{g}, \mathbf{f}) \in (W^{1,(p,q,s)}(\Omega), (W^{1-\frac{1}{b},b}(\Gamma_N)^n)^*, (W^{1,(p,q,s)}_{\Gamma_D}(\Omega))^*), \tag{4.23}$$

and $\mathbf{G} : L^{(q',s')}(\Omega) \to L^{(q,s)}(\Omega)$ be a monotone, radially continuous operator that satisfies (4.22)*. Then there exists a pair*

$$(\mathbf{u}, \mathbf{T}) \in (W^{1,(p,q,s)}(\Omega), L^{(q',s')}(\Omega)), \tag{4.24}$$

which solves (4.21)*. In other words, $(\mathbf{u}, \mathbf{T})$ is a solution to the ε regularized weak problem (P).*

When $n = 3$, then there exists a solution (4.24) *to the ε regularized weak problem (P) even under the assumption $p = b = q$ in* (4.23)*. Moreover, such a solution satisfies* $\operatorname{div} \mathbf{u} \in L^{max(s,q)}(\Omega)$.

When $n = 2$, $q \in (1, \infty)$, $s \in (max(1, \frac{2q}{2+q}), \infty)$, then there exists a solution (4.24) *to the ε regularized weak problem (P) even under the assumption $p = q$ and $b = min(s, q)$ in* (4.23)*.*

Proof. Note that since we have $p \leq max(q, s)$, then according to Theorem 4.9 for the function $\mathbf{u}_0 \in W^{1-\frac{1}{q},q}(\Gamma_D)^n$, we can always find the function $\hat{\mathbf{u}} \in W^{1,(q,max(q,s))}(\Omega) \subset W^{1,(p,q,s)}(\Omega)$ such that $\hat{\mathbf{u}}|_{\Gamma_D} = \mathbf{u}_0$, therefore the function $\hat{\mathbf{u}}$ satisfying (4.23) can be constructed from boundary data. We proceed with the proof in the following steps:

- Derivation of the Galerkin system
- Showing the existence of solutions to the Galerkin system
- Deriving apriori estimates
- Passing to the limit in $\mathbf{T}$ and $\mathbf{u}$

Step 1 - Derivation of the Galerkin system

Let $\{\bar{\mathbf{S}}_i, i \in \mathbb{N}\}$ represent a sequence which is dense in $L^{(q',s')}(\Omega)$ and $\{\bar{\boldsymbol{\chi}}_j, j \in \mathbb{N}\}$ represent a sequence which is dense in $W^{1,(p,q,s)}_{\Gamma_D}(\Omega)$. We construct the sequence $\{\mathbf{S}_i, i \in \mathbb{N}\}$ such that in the k-th step we pick $\bar{\mathbf{S}}_k$ and check whether $\bar{\mathbf{S}}_k \in \operatorname{span}\{\bar{\mathbf{S}}_i, i = 1, \dots, k-1\}$. If this assertion is true, we exclude it from the sequence. If the assertion is false, we add the element $\bar{\mathbf{S}}_k / \|\bar{\mathbf{S}}_k\|_{(q',s')}$ at the end of the sequence. We construct the sequence $\{\boldsymbol{\chi}_j, j \in \mathbb{N}\}$ from the sequence $\{\bar{\boldsymbol{\chi}}_j, j \in \mathbb{N}\}$ by an analogous procedure.

For $(n, m) \in \mathbb{N}^2$, we define finite-dimensional vector spaces V_n, U_m and the direct sum space $Z_{n,m} = V_n \oplus U_m$ so that any element $(\mathbf{S}, \boldsymbol{\chi}) \in Z_{n,m}$ could be written as

$$\mathbf{S} = \sum_{i=1}^{n} \alpha_i \mathbf{S}_i, \quad \boldsymbol{\chi} = \sum_{j=1}^{m} \beta_j \boldsymbol{\chi}_j, \tag{4.25}$$

where $\alpha_i, \beta_j \in \mathbb{R}$. We also define spaces

$$V_\infty = \bigcup_{i \in \mathbb{N}} V_i, \quad U_\infty = \bigcup_{i \in \mathbb{N}} U_i, \quad Z_{\infty,\infty} = V_\infty \oplus U_\infty. \tag{4.26}$$

Note that V_∞, U_∞ and $Z_{\infty,\infty}$ defined by (4.26) are actually vector spaces since they are nested in a way that $V_1 \subseteq V_2 \dots V_\infty \subseteq L^{(q',s')}(\Omega)$ and $U_1 \subseteq U_2 \dots U_\infty \subseteq W^{1,(p,q,s)}_{\Gamma_D}(\Omega)$. Moreover, V_∞ is dense in $L^{(q',s')}(\Omega)$ and U_∞ is dense in $W^{1,(p,q,s)}_{\Gamma_D}(\Omega)$.

For $(n, m) \in \mathbb{N}^2$, we seek a pair $(\mathbf{T}^n, \mathbf{u}^m_H) \in Z_{n,m}$ such that for any pair of test functions $(\mathbf{S}, \boldsymbol{\chi}) \in Z_{n,m}$, the following is true

$$\begin{aligned} (\mathcal{E}\,\hat{\mathbf{u}}, \mathbf{S}) + (\mathcal{E}\,\mathbf{u}^m_H, \mathbf{S}) &= (\mathbf{G}(\mathbf{T}^n), \mathbf{S}), \\ \varepsilon \mathbf{H}(\mathbf{u}^m_H, \boldsymbol{\chi}) + (\mathbf{T}^n, \mathcal{E}\,\boldsymbol{\chi}) &= \langle \mathbf{g}, \boldsymbol{\chi} \rangle_{\Gamma_N} + \langle \mathbf{f}, \boldsymbol{\chi} \rangle. \end{aligned} \tag{4.27}$$

Since the elements $\mathbf{S} \in V_n$, $\boldsymbol{\chi} \in U_m$ can be written as a sum (4.25), it is sufficient to use $\mathbf{S} \in \{\mathbf{S}_i, i = 1, \dots, n\}$ and $\boldsymbol{\chi} \in \{\boldsymbol{\chi}_j, j = 1, \dots, m\}$ as test functions in (4.27).

It is convenient to consider $(\mathbf{T}^n, \mathbf{u}_H^m)$ to be of the form (4.25), such that

$$\mathbf{T}^n(\mathbf{y}) = \sum_{i=1}^{n} y_i \mathbf{S}_i, \quad \mathbf{u}_H^m(\mathbf{y}) = \sum_{j=1}^{m} y_{n+j} \boldsymbol{\chi}_j, \tag{4.28}$$

where $\mathbf{y} \in \mathbb{R}^{n+m}$. The system of equations (4.27) when combined with (4.28) can be understood as a system of nonlinear algebraic equations for unknown coefficients $y_i \in \mathbb{R}, i \in \{1, \dots, n, n+1, \dots, n+m\}$, we call it the Galerkin system.

Step 2 - Showing the existence of solutions to the Galerkin system

We will construct the function $\mathbf{h} : \mathbb{R}^{n+m} \to \mathbb{R}^{n+m}$ such that

$$\begin{aligned} h_i(\mathbf{y}) &= (\mathbf{G}(\mathbf{T}^n(\mathbf{y})), \mathbf{S}_i) - (\mathcal{E}\,\hat{\mathbf{u}}, \mathbf{S}_i) - (\mathcal{E}\,\mathbf{u}_H^m(\mathbf{y}), \mathbf{S}_i), \quad i \in \{1, \dots, n\}, \\ h_i(\mathbf{y}) &= \varepsilon \mathbf{H}(\mathbf{u}_H^m(\mathbf{y}), \boldsymbol{\chi}_i) + (\mathbf{T}^n(\mathbf{y}), \mathcal{E}\,\boldsymbol{\chi}_i), \\ &\quad - \langle \mathbf{g}, \boldsymbol{\chi}_i \rangle_{\Gamma_N} - \langle \mathbf{f}, \boldsymbol{\chi}_i \rangle, \qquad\qquad i \in \{n+1, \dots, n+m\}. \end{aligned}$$

Using (4.28), we get the scalar product $\mathbf{h}(\mathbf{y}) \cdot \mathbf{y}$ of the form

$$\begin{aligned} \mathbf{h}(\mathbf{y}) \cdot \mathbf{y} = (\mathbf{G}(\mathbf{T}^n(\mathbf{y})), \mathbf{T}^n(\mathbf{y})) + \varepsilon \|(\mathcal{E}\,\mathbf{u}_H^m)^d\|_q^q + \varepsilon \|\operatorname{div} \mathbf{u}_H^m\|_s^s \\ - (\mathcal{E}\,\hat{\mathbf{u}}, \mathbf{T}^n(\mathbf{y})) - \langle \mathbf{g}, \mathbf{u}_H^m(\mathbf{y}) \rangle_{\Gamma_N} - \langle \mathbf{f}, \mathbf{u}_H^m(\mathbf{y}) \rangle. \end{aligned} \tag{4.29}$$

In order to apply Lemma 4.2, we need to estimate the scalar product (4.29) from below. To get a lower bound on the first term on the right in (4.29), we use (4.22), which yields

$$\begin{aligned} (\mathbf{G}(\mathbf{T}^n(\mathbf{y})), \mathbf{T}^n(\mathbf{y})) \geq C_1 (\|(\mathbf{T}^n(\mathbf{y}))^d\|_{q'}^{q'} + \|\mathbf{G}(\mathbf{T}^n(\mathbf{y}))^d\|_q^q \\ + \|\operatorname{tr} \mathbf{T}^n(\mathbf{y})\|_{s'}^{s'} + \|\operatorname{tr} \mathbf{G}(\mathbf{T}^n(\mathbf{y}))\|_s^s) - C_2 |\Omega|. \end{aligned} \tag{4.30}$$

To obtain a lower bound on the second and the third term on the right in (4.29), we apply Theorem 4.19 to conclude the existence of a constant $C_3 > 0$ such that

$$\|(\mathcal{E}\,\mathbf{u}_H^m)^d\|_q^q + \|\operatorname{div} \mathbf{u}_H^m\|_s^s \geq C_3 min(\|\mathbf{u}_H^m\|_{1,(p,q,s)}^q, \|\mathbf{u}_H^m\|_{1,(p,q,s)}^s). \tag{4.31}$$

Now, we wish to construct a lower bound on the last three terms on the right in (4.29), which can be reformulated as constructing an upper bound on the expression

$$(\mathcal{E}\,\hat{\mathbf{u}}, \mathbf{T}^n(\mathbf{y})) + \langle \mathbf{g}, \mathbf{u}_H^m(\mathbf{y}) \rangle_{\Gamma_N} + \langle \mathbf{f}, \mathbf{u}_H^m(\mathbf{y}) \rangle. \tag{4.32}$$

The first term in (4.32) can be estimated using the Hölder inequality and the Young's inequality. Therefore there exist constants $C_4, C_5 > 0$ such that

$$(\mathcal{E}\,\hat{\mathbf{u}}, \mathbf{T}^n(\mathbf{y})) \leq \frac{C_1}{2} \|(\mathbf{T}^n(\mathbf{y}))^d\|_{q'}^{q'} + \frac{C_1}{2} \|\operatorname{tr} \mathbf{T}^n(\mathbf{y})\|_{s'}^{s'} + C_4 \|(\mathcal{E}\,\hat{\mathbf{u}})^d\|_q^q + C_5 \|\operatorname{div} \hat{\mathbf{u}}\|_s^s. \tag{4.33}$$

We proceed to show an upper bound on the boundary term $\langle \mathbf{g}, \mathbf{u}_H^m(\mathbf{y}) \rangle_{\Gamma_N}$. Notice that $\mathbf{u}_H^m(\mathbf{y})$ is understood as an element of $W_{\Gamma_D}^{1,(b,b,b)}(\Omega)$. Therefore it has the trace established by Theorem 4.9 in the space $W^{1-\frac{1}{b},b}(\Gamma_N)^n$. It is clear that there exists a constant $C_6 > 0$ such that

$$\langle \mathbf{g}, \mathbf{u}_H^m(\mathbf{y}) \rangle_{\Gamma_N} \leq \|\mathbf{g}\| \|Tr(\mathbf{u}_H^m(\mathbf{y}))\| \leq C_6 \|\mathbf{g}\| \|\mathbf{u}_H^m(\mathbf{y})\|_{1,(b,b,b)}, \tag{4.34}$$

where $\|\mathbf{g}\|$ denotes the norm of $\mathbf{g}$ in $(W^{1-\frac{1}{b},b}(\Gamma_N)^n)^*$ and $\|Tr(\mathbf{u}_H^m(\mathbf{y}))\|$ denotes the norm of the trace Tr of $\mathbf{u}_H^m(\mathbf{y})$ in $W^{1-\frac{1}{b},b}(\Gamma_N)^n$. It remains to show that

$$W_{\Gamma_D}^{1,(p,q,s)}(\Omega) \subset W_{\Gamma_D}^{1,(b,b,b)}(\Omega). \tag{4.35}$$

When $b = min(s, q)$, $p > b$, it is easy to check that (4.35) is true. We now turn to the case of the only exception, which is the spatial dimension $n = 3$, $p = b = q$ and $s < q$, for which we apparently don't have the embedding (4.35). To show that (4.35) is true, we combine the natural embedding $W_{\Gamma_D}^{1,(q,s)}(\Omega) \subset W_{\Gamma_D}^{1,(q,*)}(\Omega)$ with the equivalence of the spaces $W^{1,(q,*)}(\Omega)$ and $W^{1,(q,q)}(\Omega)$ in the sense of Definition A.77, (p. 137) that follows from Lemma 4.7 and Theorem 4.8. Therefore for $n = 3$, $s < q$, the spaces $W_{\Gamma_D}^{1,(q,q,s)}(\Omega)$ and $W_{\Gamma_D}^{1,(q,q,q)}(\Omega)$ are also equivalent, which yields (4.35). Summarizing (4.35) and (4.34), we have a constant $C_7 > 0$, such that

$$\langle \mathbf{g}, \mathbf{u}_H^m(\mathbf{y})\rangle_{\Gamma_N} \leq C_7\|\mathbf{g}\|\|\mathbf{u}_H^m(\mathbf{y})\|_{1,(p,q,s)}. \tag{4.36}$$

In fact, for $n = 3$, $b = p = q$ we have even more powerful estimate than (4.35) of the form

$$W_{\Gamma_D}^{1,(q,*)}(\Omega) \subset W_{\Gamma_D}^{1,(q,q)}(\Omega). \tag{4.37}$$

That means, when having (4.37), we don't even need to consider the divergence term in $\|\mathbf{u}_H^m\|_{1,(q,s)}$ and we can use the norm $\|\mathbf{u}_H^m\|_{1,(q,*)}$ in (4.36) instead. In order to unify the treatment of all cases in this theorem, we use the estimate (4.36) universally. By applying Young's inequality on (4.36), we conclude that there exists a constant $C_8 > 0$, which depends on ε, such that

$$\langle \mathbf{g}, \mathbf{u}_H^m(\mathbf{y})\rangle_{\Gamma_N} \leq \varepsilon\frac{C_3}{3}min(\|\mathbf{u}_H^m(\mathbf{y})\|_{1,(p,q,s)}^q, \|\mathbf{u}_H^m(\mathbf{y})\|_{1,(p,q,s)}^s) + C_8max(\|\mathbf{g}\|^{q'}, \|\mathbf{g}\|^{s'}). \tag{4.38}$$

It remains to construct an upper bound on the third term in (4.32). Using Young's inequality, we have the constant $C_9 > 0$, which depends on ε, such that

$$\langle \mathbf{f}, \mathbf{u}_H^m(\mathbf{y})\rangle \leq \varepsilon\frac{C_3}{3}min(\|\mathbf{u}_H^m(\mathbf{y})\|_{1,(p,q,s)}^q, \|\mathbf{u}_H^m(\mathbf{y})\|_{1,(p,q,s)}^s) + C_9max(\|\mathbf{f}\|^{q'}, \|\mathbf{f}\|^{s'}), \tag{4.39}$$

where by $\|\mathbf{f}\|$, we understand the norm in $(W_{\Gamma_D}^{1,(p,q,s)}(\Omega))^*$.

It follows immediately from estimates (4.30), (4.31), (4.33), (4.38) and (4.39) that there exist constants C_1, C_2, C_3, C_4, C_5, C_8, $C_9 > 0$ such that

$$\begin{aligned}\mathbf{h}(\mathbf{y}).\mathbf{y} \geq\ & \frac{C_1}{2}\|(\mathbf{T}^n(\mathbf{y}))^d\|_{q'}^{q'} + \frac{C_1}{2}\|\mathrm{tr}\,\mathbf{T}^n(\mathbf{y})\|_{s'}^{s'} \\ & + \varepsilon\frac{C_3}{3}min(\|\mathbf{u}_H^m(\mathbf{y})\|_{1,(p,q,s)}^q, \|\mathbf{u}_H^m(\mathbf{y})\|_{1,(p,q,s)}^s) - C_4\|(\mathcal{E}\,\hat{\mathbf{u}})^d\|_q^q \\ & - C_5\|\mathrm{div}\,\hat{\mathbf{u}}\|_s^s - C_8max(\|\mathbf{g}\|^{q'}, \|\mathbf{g}\|^{s'}) - C_9max(\|\mathbf{f}\|^{q'}, \|\mathbf{f}\|^{s'}) - C_2|\Omega|. \end{aligned} \tag{4.40}$$

Employing standard tools (Observation A.18, Theorem A.9, Lemma 4.1), we can show there is a constant $C_{10} > 0$, which depends on ε, such that

$$\begin{aligned}\frac{C_1}{2}\|(\mathbf{T}^n(\mathbf{y}))^d\|_{q'}^{q'} + \frac{C_1}{2}\|\mathrm{tr}\,\mathbf{T}^n(\mathbf{y})\|_{s'}^{s'} + \varepsilon\frac{C_3}{3}min(\|\mathbf{u}_H^m(\mathbf{y})\|_{1,(p,q,s)}^q, \|\mathbf{u}_H^m(\mathbf{y})\|_{1,(p,q,s)}^s) \\ \geq C_{10}\min\left(|\mathbf{y}|^q, |\mathbf{y}|^s, |\mathbf{y}|^{q'}, |\mathbf{y}|^{s'}\right). \end{aligned} \tag{4.41}$$

Combining (4.41) and (4.40) we have a constant $C(\Omega, \varepsilon, \mathbf{g}, \mathbf{f}, \hat{\mathbf{u}}) > 0$ such that

$$\mathbf{h}(\mathbf{y}) \cdot \mathbf{y} \geq C_{10} \min\left(|\mathbf{y}|^q, |\mathbf{y}|^s, |\mathbf{y}|^{q'}, |\mathbf{y}|^{s'}\right) - C(\Omega, \varepsilon, \mathbf{g}, \mathbf{f}, \hat{\mathbf{u}}). \tag{4.42}$$

The inequality (4.42) fulfils the assumptions of Lemma 4.2 by assuring that there exists $r > 0$ such that for all $\mathbf{y}$ for which $|\mathbf{y}| = r$ we have $\mathbf{h}(\mathbf{y}) \cdot \mathbf{y} \geq 0$. Therefore there exists $\bar{\mathbf{y}} \in \mathbb{R}^{n+m}$ such that $\mathbf{h}(\bar{\mathbf{y}}) = \mathbf{0}$. We can conclude that the discrete system (4.27) has the solution $(\mathbf{T}^n(\bar{\mathbf{y}}), \mathbf{u}_H^m(\bar{\mathbf{y}})) \in Z_{n,m}$ for any pair $(n, m) \in \mathbb{N}^2$.

Step 3 - Deriving apriori estimates

Let $\{(\mathbf{T}^n, \mathbf{u}_H^m) \in Z_{n,m}, (n, m) \in \mathbb{N}^2\}$ be the set of solutions to the Galerkin system. We can use $(\mathbf{T}^n, \mathbf{u}_H^m) \in Z_{n,m}$ as test functions in (4.27) to obtain the system

$$\begin{aligned} (\mathcal{E}\,\hat{\mathbf{u}}, \mathbf{T}^n) + (\mathcal{E}\,\mathbf{u}_H^m, \mathbf{T}^n) &= (\mathbf{G}(\mathbf{T}^n), \mathbf{T}^n) \\ \varepsilon \mathbf{H}(\mathbf{u}_H^m, \mathbf{u}_H^m) + (\mathbf{T}^n, \mathcal{E}\,\mathbf{u}_H^m) &= \langle \mathbf{g}, \mathbf{u}_H^m \rangle_{\Gamma_N} + \langle \mathbf{f}, \mathbf{u}_H^m \rangle. \end{aligned} \tag{4.43}$$

Summing up the equations in (4.43), we get

$$(\mathbf{G}(\mathbf{T}^n), \mathbf{T}^n) + \varepsilon(\|(\mathcal{E}\,\mathbf{u}_H^m)^d\|_q^q + \|\operatorname{div} \mathbf{u}_H^m\|_s^s) = \langle \mathbf{g}, \mathbf{u}_H^m \rangle_{\Gamma_N} + \langle \mathbf{f}, \mathbf{u}_H^m \rangle + (\mathcal{E}\,\hat{\mathbf{u}}, \mathbf{T}^n). \tag{4.44}$$

Combining (4.44) and (4.22), we have that

$$\begin{aligned} C_1(\|(\mathbf{T}^n)^d\|_{q'}^{q'} + \|\mathbf{G}(\mathbf{T}^n)^d\|_q^q + \|\operatorname{tr} \mathbf{T}^n\|_{s'}^{s'} + \|\operatorname{tr} \mathbf{G}(\mathbf{T}^n)\|_s^s) + \varepsilon(\|(\mathcal{E}\,\mathbf{u}_H^m)^d\|_q^q + \|\operatorname{div} \mathbf{u}_H^m\|_s^s) \\ \leq \langle \mathbf{g}, \mathbf{u}_H^m \rangle_{\Gamma_N} + \langle \mathbf{f}, \mathbf{u}_H^m \rangle + (\mathcal{E}\,\hat{\mathbf{u}}, \mathbf{T}^n) + C_2|\Omega|. \end{aligned} \tag{4.45}$$

Applying the estimates (4.30), (4.31), (4.33), (4.38) and (4.39) to the formula (4.45), we deduce that there exists a positive constant $C(\Omega, \varepsilon, \mathbf{f}, \mathbf{g}, \hat{\mathbf{u}})$ such that

$$\begin{aligned} \|(\mathbf{T}^n)^d\|_{q'}^{q'} + \|\mathbf{G}(\mathbf{T}^n)^d\|_q^q + \|\operatorname{tr} \mathbf{T}^n\|_{s'}^{s'} + \|\operatorname{tr} \mathbf{G}(\mathbf{T}^n)\|_s^s + \|(\mathcal{E}\,\mathbf{u}_H^m)^d\|_q^q + \|\operatorname{div} \mathbf{u}_H^m\|_s^s \\ \leq C(\Omega, \varepsilon, \mathbf{f}, \mathbf{g}, \hat{\mathbf{u}}). \end{aligned} \tag{4.46}$$

Note that the constant $C(\Omega, \varepsilon, \mathbf{f}, \mathbf{g}, \hat{\mathbf{u}})$ is independent of a particular $(n, m) \in \mathbb{N}^2$. We may improve the estimate (4.46) by noting that $(\mathcal{E}\,\mathbf{u}_H^m)^d \in L^q(\Omega)^{n \times n}_{sym}$ and $\operatorname{div} \mathbf{u}_H^m \in L^s(\Omega)$ are bounded functions in respective spaces and

$$\left|(\mathcal{E}\,\mathbf{u}_H^m)^d\right|^{q-2} (\mathcal{E}\,\mathbf{u}_H^m)^d \in L^{q'}(\Omega)^{n \times n}_{sym}, \quad |\operatorname{div} \mathbf{u}_H^m|^{s-2} \operatorname{div} \mathbf{u}_H^m \in L^{s'}(\Omega). \tag{4.47}$$

Using that $q' = q/(q-1)$, norms of the functions (4.47) can be rewritten to the form

$$\|\left|(\mathcal{E}\,\mathbf{u}_H^m)^d\right|^{q-2} (\mathcal{E}\,\mathbf{u}_H^m)^d\|_{q'}^{q'} = \|(\mathcal{E}\,\mathbf{u}_H^m)^d\|_q^q, \quad \||\operatorname{div} \mathbf{u}_H^m|^{s-2} \operatorname{div} \mathbf{u}_H^m\|_{s'}^{s'} = \|\operatorname{div} \mathbf{u}_H^m\|_s^s,$$

therefore (4.46) yields an upper bound on the functions (4.47) in the form

$$\|\left|(\mathcal{E}\,\mathbf{u}_H^m)^d\right|^{q-2} (\mathcal{E}\,\mathbf{u}_H^m)^d\|_{q'}^{q'} + \||\operatorname{div} \mathbf{u}_H^m|^{s-2} \operatorname{div} \mathbf{u}_H^m\|_{s'}^{s'} \leq C(\Omega, \varepsilon, \mathbf{f}, \mathbf{g}, \hat{\mathbf{u}}). \tag{4.48}$$

Step 4 - Limit passage in T and u

So far, for each $(n, m) \in \mathbb{N}^2$ we have established the existence of the discrete solution $(\mathbf{T}^n, \mathbf{u}_H^m) \in Z_{n,m} \subseteq L^{(q',s')}(\Omega) \oplus W^{1,(p,q,s)}_{\Gamma_D}(\Omega)$ that solves the system (4.27) for any pair of test functions $(\mathbf{S}, \boldsymbol{\chi}) \in Z_{n,m}$. Now we define a sequence $\{(\mathbf{T}^k, \mathbf{u}_H^k), k \in \mathbb{N}\}$ in $L^{(q',s')}(\Omega) \oplus W^{1,(p,q,s)}_{\Gamma_D}(\Omega)$ such that for $(k, k) \in \mathbb{N}^2$, the pair $(\mathbf{T}^k, \mathbf{u}_H^k)$ is the

discrete solution to the system (4.27), where $n = k$ and $m = k$. Therefore the pair $(\mathbf{T}^k, \mathbf{u}_H^k)$ solves the system

$$\forall (\mathbf{S}, \boldsymbol{\chi}) \in Z_{k,k} \begin{cases} (\mathcal{E}\,\hat{\mathbf{u}}, \mathbf{S}) + (\mathcal{E}\,\mathbf{u}_H^k, \mathbf{S}) = (\mathbf{G}(\mathbf{T}^k), \mathbf{S}), \\ \varepsilon \mathbf{H}(\mathbf{u}_H^k, \boldsymbol{\chi}) + (\mathbf{T}^k, \mathcal{E}\,\boldsymbol{\chi}) = \langle \mathbf{g}, \boldsymbol{\chi} \rangle_{\Gamma_N} + \langle \mathbf{f}, \boldsymbol{\chi} \rangle. \end{cases} \tag{4.49}$$

Applying Eberlein–Šmulian theorem on apriori estimates (4.46) and (4.48), there exist functions $\mathbf{T} \in L^{(q',s')}(\Omega)$, $\mathbf{Y} \in L^{(q,s)}(\Omega)$, $\mathbf{u}_H \in W^{1,(p,q,s)}_{\Gamma_D}(\Omega)$, $\mathbf{v} \in L^{q'}(\Omega)^{n\times n}_{sym}$, $e \in L^{s'}(\Omega)$ and a subsequence $\{k_i, i \in \mathbb{N}\}$ such that for $i \to \infty$,

$$\begin{aligned} \mathbf{T}^{k_i} &\rightharpoonup \mathbf{T} && \text{in } L^{(q',s')}(\Omega), \\ \mathbf{G}(\mathbf{T}^{k_i}) &\rightharpoonup \mathbf{Y} && \text{in } L^{(q,s)}(\Omega), \\ \mathbf{u}_H^{k_i} &\rightharpoonup \mathbf{u}_H && \text{in } W^{1,(p,q,s)}_{\Gamma_D}(\Omega), \\ (\mathcal{E}\,\mathbf{u}_H^{k_i})^d &\rightharpoonup (\mathcal{E}\,\mathbf{u}_H)^d && \text{in } L^q(\Omega)^{n\times n}_{sym}, \\ \operatorname{div} \mathbf{u}_H^{k_i} &\rightharpoonup \operatorname{div} \mathbf{u}_H && \text{in } L^s(\Omega), \\ \left|(\mathcal{E}\,\mathbf{u}_H^{k_i})^d\right|^{q-2} (\mathcal{E}\,\mathbf{u}_H^{k_i})^d &\rightharpoonup \mathbf{v} && \text{in } L^{q'}(\Omega)^{n\times n}_{sym}, \\ \left|\operatorname{div} \mathbf{u}_H^{k_i}\right|^{s-2} \operatorname{div} \mathbf{u}_H^{k_i} &\rightharpoonup e && \text{in } L^{s'}(\Omega). \end{aligned} \tag{4.50}$$

Consider the operator $\mathbf{O} : L^{(q',s')}(\Omega) \oplus W^{1,(p,q,s)}_{\Gamma_D}(\Omega) \to (L^{(q',s')}(\Omega) \oplus W^{1,(p,q,s)}_{\Gamma_D}(\Omega))^*$ such that for $(\bar{\mathbf{T}}, \bar{\mathbf{u}}_H) \in L^{(q',s')}(\Omega) \oplus W^{1,(p,q,s)}_{\Gamma_D}(\Omega)$, $(\mathbf{S}, \boldsymbol{\chi}) \in L^{(q',s')}(\Omega) \oplus W^{1,(p,q,s)}_{\Gamma_D}(\Omega)$

$$\langle \mathbf{O}((\bar{\mathbf{T}}, \bar{\mathbf{u}}_H)), (\mathbf{S}, \boldsymbol{\chi}) \rangle = (\mathbf{G}(\bar{\mathbf{T}}), \mathbf{S}) + \varepsilon \mathbf{H}(\bar{\mathbf{u}}_H, \boldsymbol{\chi}),$$

which can be expanded into the form

$$\begin{aligned} \langle \mathbf{O}((\bar{\mathbf{T}}, \bar{\mathbf{u}}_H)), (\mathbf{S}, \boldsymbol{\chi}) \rangle = (\mathbf{G}(\bar{\mathbf{T}}), \mathbf{S}) &+ \varepsilon(|\operatorname{div} \bar{\mathbf{u}}_H|^{s-2} \operatorname{div} \bar{\mathbf{u}}_H, \operatorname{div} \boldsymbol{\chi}) \\ &+ \varepsilon(\left|(\mathcal{E}\,\bar{\mathbf{u}}_H)^d\right|^{q-2} (\mathcal{E}\,\bar{\mathbf{u}}_H)^d, (\mathcal{E}\,\boldsymbol{\chi})^d). \end{aligned}$$

The operator $\mathbf{O}$ contains the nonlinear terms from (4.49). It is clear that $\mathbf{O}$ is radially continuous and monotone because it is a sum of two radially continuous monotone operators $\mathbf{G}$ and $\varepsilon\mathbf{H}$. Therefore, for all $(\mathbf{S}, \boldsymbol{\chi}) \in L^{(q',s')}(\Omega) \oplus W^{1,(p,q,s)}_{\Gamma_D}(\Omega)$ we have that

$$\lim_{i\to\infty} \langle \mathbf{O}((\mathbf{T}^{k_i}, \mathbf{u}_H^{k_i})) - \mathbf{O}((\mathbf{S}, \boldsymbol{\chi})), (\mathbf{T}^{k_i}, \mathbf{u}_H^{k_i}) - (\mathbf{S}, \boldsymbol{\chi}) \rangle \geq 0. \tag{4.51}$$

Before we can apply Lemma A.92, (p. 139) on the equation (4.51), we need to evaluate this limit. We begin by evaluating the expression

$$\lim_{i\to\infty} \langle \mathbf{O}((\mathbf{T}^{k_i}, \mathbf{u}_H^{k_i})), (\mathbf{T}^{k_i}, \mathbf{u}_H^{k_i}) \rangle = \lim_{i\to\infty} (\mathbf{G}(\mathbf{T}^{k_i}), \mathbf{T}^{k_i}) + \varepsilon(\|(\mathcal{E}\,\mathbf{u}_H^{k_i})^d\|_q^q + \|\operatorname{div} \mathbf{u}_H^{k_i}\|_s^s).$$

We substitute the pair $(\mathbf{T}^{k_i}, \mathbf{u}_H^{k_i}) \in Z_{k_i,k_i}$ into the system (4.49), and sum up the results to obtain

$$(\mathbf{G}(\mathbf{T}^{k_i}), \mathbf{T}^{k_i}) + \varepsilon(\|(\mathcal{E}\,\mathbf{u}_H^{k_i})^d\|_q^q + \|\operatorname{div} \mathbf{u}_H^{k_i}\|_s^s) = \langle \mathbf{g}, \mathbf{u}_H^{k_i} \rangle_{\Gamma_N} + \langle \mathbf{f}, \mathbf{u}_H^{k_i} \rangle + (\mathcal{E}\,\hat{\mathbf{u}}, \mathbf{T}^{k_i}). \tag{4.52}$$

Let for a moment fix a particular test function $(\mathbf{S}, \boldsymbol{\chi}) \in Z_{\infty,\infty}$ in (4.49). According to (4.26), there exists $i_0 \in \mathbb{N}$, such that $(\mathbf{S}, \boldsymbol{\chi}) \in Z_{k_i,k_i}$ for all $i > i_0$. Thus we can let

$i \to \infty$ in the system (4.49), where $k = k_i$, and use the convergence results (4.50) to conclude that

$$\begin{aligned} (\mathcal{E}\,\hat{\mathbf{u}}, \mathbf{S}) + (\mathcal{E}\,\mathbf{u}_H, \mathbf{S}) &= (\mathbf{Y}, \mathbf{S}), \\ \varepsilon(e, \operatorname{div}\boldsymbol{\chi}) + \varepsilon(\mathbf{v}, (\mathcal{E}\,\boldsymbol{\chi})^d) + (\mathbf{T}, \mathcal{E}\,\boldsymbol{\chi}) &= \langle \mathbf{g}, \boldsymbol{\chi}\rangle_{\Gamma_N} + \langle \mathbf{f}, \boldsymbol{\chi}\rangle. \end{aligned} \tag{4.53}$$

As we have chosen an arbitrary $(\mathbf{S}, \boldsymbol{\chi}) \in Z_{\infty,\infty}$, the (4.53) is true for every pair $(\mathbf{S}, \boldsymbol{\chi}) \in Z_{\infty,\infty}$. Moreover, since $Z_{\infty,\infty}$ is dense in $L^{(q',s')}(\Omega) \oplus W^{1,(p,q,s)}_{\Gamma_D}(\Omega)$, the (4.53) remains valid for every pair $(\mathbf{S}, \boldsymbol{\chi}) \in L^{(q',s')}(\Omega) \oplus W^{1,(p,q,s)}_{\Gamma_D}(\Omega)$. Using that fact, we substitute $(\mathbf{S}, \boldsymbol{\chi}) = (\mathbf{T}, \mathbf{u}_H)$ into (4.53) and sum the results up to get the expression

$$(\mathbf{Y}, \mathbf{T}) + \varepsilon(e, \operatorname{div}\mathbf{u}_H) + \varepsilon(\mathbf{v}, (\mathcal{E}\,\mathbf{u}_H)^d) = \langle \mathbf{g}, \mathbf{u}_H\rangle_{\Gamma_N} + \langle \mathbf{f}, \mathbf{u}_H\rangle + (\mathcal{E}\,\hat{\mathbf{u}}, \mathbf{T}). \tag{4.54}$$

For $i \to \infty$, the right-hand sides of (4.54) and (4.52) coincide, and therefore we have shown that

$$\lim_{i\to\infty} \langle \mathbf{O}((\mathbf{T}^{k_i}, \mathbf{u}_H^{k_i})), (\mathbf{T}^{k_i}, \mathbf{u}_H^{k_i})\rangle = (\mathbf{Y}, \mathbf{T}) + \varepsilon(e, \operatorname{div}\mathbf{u}_H) + \varepsilon(\mathbf{v}, (\mathcal{E}\,\mathbf{u}_H)^d). \tag{4.55}$$

Let $(\mathbf{S}, \boldsymbol{\chi}) \in L^{(q',s')}(\Omega) \oplus W^{1,(p,q,s)}_{\Gamma_D}(\Omega)$. We use the convergence results (4.50) to show that

$$\lim_{i\to\infty} \langle \mathbf{O}((\mathbf{T}^{k_i}, \mathbf{u}_H^{k_i})), (\mathbf{S}, \boldsymbol{\chi})\rangle = (\mathbf{Y}, \mathbf{S}) + \varepsilon(e, \operatorname{div}\boldsymbol{\chi}) + \varepsilon(\mathbf{v}, (\mathcal{E}\,\boldsymbol{\chi})^d), \tag{4.56}$$

and also that

$$\begin{aligned} \lim_{i\to\infty} \langle \mathbf{O}((\mathbf{S}, \boldsymbol{\chi})), (\mathbf{T}^{k_i}, \mathbf{u}_H^{k_i})\rangle = (\mathbf{G}(\mathbf{S}), \mathbf{T}) &+ \varepsilon\,|\operatorname{div}\boldsymbol{\chi}|^{s-2}(\operatorname{div}\boldsymbol{\chi}, \operatorname{div}\mathbf{u}_H) \\ &+ \varepsilon\left|(\mathcal{E}\,\boldsymbol{\chi})^d\right|^{q-2}((\mathcal{E}\,\boldsymbol{\chi})^d, (\mathcal{E}\,\mathbf{u}_H)^d). \end{aligned} \tag{4.57}$$

For all $(\mathbf{S}, \boldsymbol{\chi}) \in L^{(q',s')}(\Omega) \oplus W^{1,(p,q,s)}_{\Gamma_D}(\Omega)$, we combine (4.55), (4.56) and (4.57) to rewrite the limit (4.51) into the form

$$\begin{aligned} (\mathbf{Y} - \mathbf{G}(\mathbf{S}), \mathbf{T} - \mathbf{S}) + \varepsilon(e - |\operatorname{div}\boldsymbol{\chi}|^{s-2}\operatorname{div}\boldsymbol{\chi}, \operatorname{div}(\mathbf{u}_H - \boldsymbol{\chi})) \\ + \varepsilon(\mathbf{v} - \left|(\mathcal{E}\,\boldsymbol{\chi})^d\right|^{q-2}(\mathcal{E}\,\boldsymbol{\chi})^d, (\mathcal{E}(\mathbf{u}_H - \boldsymbol{\chi}))^d) \geq 0. \end{aligned}$$

Lemma A.92, (p. 139) yields

$$\begin{aligned} (\mathbf{G}(\mathbf{T}), \mathbf{S}) + \varepsilon(|\operatorname{div}\mathbf{u}|^{s-2}\operatorname{div}\mathbf{u}, \operatorname{div}\boldsymbol{\chi}) + \varepsilon(\left|(\mathcal{E}\,\mathbf{u})^d\right|^{q-2}(\mathcal{E}\,\mathbf{u})^d, (\mathcal{E}\,\boldsymbol{\chi})^d) \\ = (\mathbf{Y}, \mathbf{S}) + \varepsilon(e, \operatorname{div}\boldsymbol{\chi}) + \varepsilon(\mathbf{v}, (\mathcal{E}\,\boldsymbol{\chi})^d). \end{aligned} \tag{4.58}$$

From (4.58) we conclude, by gradually taking $\boldsymbol{\chi} = \mathbf{0}$ and $\mathbf{S}$ arbitrary, $\mathbf{S} = \mathbf{0}$ and $\boldsymbol{\chi}$ arbitrary with $(\mathcal{E}\,\boldsymbol{\chi})^d = \mathbf{0}$, and finally $\mathbf{S} = \mathbf{0}$ and $\boldsymbol{\chi}$ arbitrary with $\operatorname{div}\boldsymbol{\chi} = 0$, that

$$\mathbf{G}(\mathbf{T}) = \mathbf{Y}, \quad |\operatorname{div}\mathbf{u}_H|^{s-2}\operatorname{div}\mathbf{u}_H = e, \quad \left|(\mathcal{E}\,\mathbf{u}_H)^d\right|^{q-2}(\mathcal{E}\,\mathbf{u}_H)^d = \mathbf{v}. \tag{4.59}$$

By substituting (4.59) into (4.53), we obtain the weak formulation of the problem. Now, it is easy to show that the pair $(\mathbf{u}_H + \hat{\mathbf{u}}, \mathbf{T}) \in (W^{1,(p,q,s)}(\Omega), L^{(q',s')}(\Omega))$ is a solution the the ε regularized weak problem, which proves the theorem. For $n = 3$, $b = q$, $p = q$ we have the solution in $W^{1,(q,s)}(\Omega)$. From the embedding (4.3) we have that $\operatorname{div}\mathbf{u} \in L^q(\Omega)$.

□

For each $\varepsilon > 0$, we have proved the existence of the solution to the ε regularized weak Problem (P), see Definition 4.20. It remains to show that as $\varepsilon \to 0$, the sequence of the solutions to the regularized problem converges to the weak solution of the original problem. This is the objective of the following result.

Theorem 4.25 (Existence of a weak solution to the Problem (P)). *Under the hypotheses of Theorem 4.24, there exists a solution to the weak Problem (P) in the sense of Definition 4.20.*

Proof. We proceed with the proof in the following steps:

- Finding a sequence of approximate solutions
- Deriving apriori estimates
- Passing to the limit

Step 1 - Finding a sequence of approximate solutions

We apply the Theorem 4.24 on $\varepsilon = 1/k$, $k \in \mathbb{N}$. Therefore, for each $k \in \mathbb{N}$, there exists a pair $(\mathbf{u}_H^k, \mathbf{T}^k) \in (W^{1,(p,q,s)}_{\Gamma_D}(\Omega), L^{(q',s')}(\Omega))$ such that $(\mathbf{u}_H^k + \hat{\mathbf{u}}, \mathbf{T}^k) \in (W^{1,(p,q,s)}(\Omega), L^{(q',s')}(\Omega))$ is a $1/k$-regularized weak solution. We have that

$$\forall \mathbf{S} \in L^{(q',s')}(\Omega) \qquad (\mathcal{E}\,\hat{\mathbf{u}}, \mathbf{S}) + (\mathcal{E}\,\mathbf{u}_H^k, \mathbf{S}) = (\mathbf{G}(\mathbf{T}^k), \mathbf{S}), \tag{4.60a}$$

$$\forall \boldsymbol{\chi} \in W^{1,(p,q,s)}_{\Gamma_D}(\Omega) \qquad \varepsilon_k \mathbf{H}(\mathbf{u}_H^k, \boldsymbol{\chi}) + (\mathbf{T}^k, \mathcal{E}\,\boldsymbol{\chi}) = \langle \mathbf{g}, \boldsymbol{\chi} \rangle_{\Gamma_N} + \langle \mathbf{f}, \boldsymbol{\chi} \rangle, \tag{4.60b}$$

Step 2 - Deriving apriori estimates

For each k, we can substitute the pair $(\boldsymbol{\chi}, \mathbf{S}) = (\mathbf{u}_H^k, \mathbf{T}^k)$ into (4.60) as test functions. Summing up the results, we have that

$$\frac{1}{k}\mathbf{H}(\mathbf{u}_H^k, \mathbf{u}_H^k) + (\mathbf{G}(\mathbf{T}^k), \mathbf{T}^k) = (\mathcal{E}\,\hat{\mathbf{u}}, \mathbf{T}^k) + \langle \mathbf{g}, \mathbf{u}_H^k \rangle_{\Gamma_N} + \langle \mathbf{f}, \mathbf{u}_H^k \rangle. \tag{4.61}$$

Combining (4.61) with (4.22) yields

$$\begin{aligned} \frac{1}{k}(\|(\mathcal{E}\,\mathbf{u}_H^k)^d\|_q^q + \|\operatorname{div} \mathbf{u}_H^k\|_s^s) \\ + C_1(\|(\mathbf{T}^k)^d\|_{q'}^{q'} + \|\mathbf{G}(\mathbf{T}^k)^d\|_q^q + \|\operatorname{tr} \mathbf{T}^k\|_{s'}^{s'} + \|\operatorname{tr} \mathbf{G}(\mathbf{T}^k)\|_s^s) \\ \leq (\mathcal{E}\,\hat{\mathbf{u}}, \mathbf{T}^k) + \langle \mathbf{g}, \mathbf{u}_H^k \rangle_{\Gamma_N} + \langle \mathbf{f}, \mathbf{u}_H^k \rangle + C_2|\Omega|. \end{aligned} \tag{4.62}$$

Analogously to deriving the estimates (4.46) and (4.48) in Theorem 4.24, we show the existence of a constant $C(\Omega, k, \mathbf{f}, \mathbf{g}, \hat{\mathbf{u}})$ that depends on the data and k such that

$$\begin{aligned} \|(\mathbf{T}^k)^d\|_{q'}^{q'} + \|\mathbf{G}(\mathbf{T}^k)^d\|_q^q + \|\operatorname{tr} \mathbf{T}^k\|_{s'}^{s'} + \|\operatorname{tr} \mathbf{G}(\mathbf{T}^k)\|_s^s + \|(\mathcal{E}\,\mathbf{u}_H^k)^d\|_q^q + \|\operatorname{div} \mathbf{u}_H^k\|_s^s \\ \leq C(\Omega, k, \mathbf{f}, \mathbf{g}, \hat{\mathbf{u}}) \end{aligned} \tag{4.63}$$

and that

$$\| \left|(\mathcal{E}\,\mathbf{u}_H^k)^d\right|^{q-2} (\mathcal{E}\,\mathbf{u}_H^k)^d \|_{q'}^{q'} + \| \left|\operatorname{div} \mathbf{u}_H^k\right|^{s-2} \operatorname{div} \mathbf{u}_H^k \|_{s'}^{s'} \leq C(\Omega, k, \mathbf{f}, \mathbf{g}, \hat{\mathbf{u}}). \tag{4.64}$$

According to (4.64), for the functions

$$\mathbf{S}_1^k = \left|(\mathcal{E}\,\mathbf{u}_H^k)^d\right|^{q-2}(\mathcal{E}\,\mathbf{u}_H^k)^d, \quad \mathbf{S}_2^k = \left|\operatorname{div}\mathbf{u}_H^k\right|^{s-2}\operatorname{div}\mathbf{u}_H^k\mathbf{I} \tag{4.65}$$

it holds that $\mathbf{S}_1^k \in L^{(q',s')}(\Omega)$ and $\mathbf{S}_2^k \in L^{(q',s')}(\Omega)$. Therefore, they are suitable test functions in (4.60a) for every $k \in \mathbb{N}$. Testing by them in (4.60a) yields

$$\begin{aligned} \|(\mathcal{E}\,\mathbf{u}_H^k)^d\|_q^q &= (\mathbf{G}(\mathbf{T}^k)^d, \mathbf{S}_1^k) - ((\mathcal{E}\,\hat{\mathbf{u}})^d, \mathbf{S}_1^k), \\ \|\operatorname{div}\mathbf{u}_H^k\|_s^s &= (\mathbf{G}(\mathbf{T}^k), \mathbf{S}_2^k) - (\mathcal{E}\,\hat{\mathbf{u}}, \mathbf{S}_2^k). \end{aligned} \tag{4.66}$$

Now, we estimate (4.66) using the Hölder inequality to obtain

$$\begin{aligned} \|(\mathcal{E}\,\mathbf{u}_H^k)^d\|_q^q &\le \|\mathbf{G}(\mathbf{T}^k)^d\|_q\|(\mathcal{E}\,\mathbf{u}_H^k)^d\|_q^{q-1} + \|(\mathcal{E}\,\hat{\mathbf{u}})^d\|_q\|(\mathcal{E}\,\mathbf{u}_H^k)^d\|_q^{q-1}, \\ \|\operatorname{div}\mathbf{u}_H^k\|_s^s &\le \|\operatorname{tr}\mathbf{G}(\mathbf{T}^k)\|_s\|\operatorname{div}\mathbf{u}_H^k\|_s^{s-1} + \|\operatorname{div}\hat{\mathbf{u}}\|_s\|\operatorname{div}\mathbf{u}_H^k\|_s^{s-1}. \end{aligned} \tag{4.67}$$

We can combine the two inequalities in (4.67) to conclude that

$$\|(\mathcal{E}\,\mathbf{u}_H^k)^d\|_q + \|\operatorname{div}\mathbf{u}_H^k\|_s \le \|\mathbf{G}(\mathbf{T}^k)^d\|_q + \|(\mathcal{E}\,\hat{\mathbf{u}})^d\|_q + \|\operatorname{tr}\mathbf{G}(\mathbf{T}^k)\|_s + \|\operatorname{div}\hat{\mathbf{u}}\|_s. \tag{4.68}$$

Rewriting (4.62) to a reduced form, where first two terms are excluded, we have that

$$\begin{aligned} C_1(\|(\mathbf{T}^k)^d\|_{q'}^{q'} + \|\mathbf{G}(\mathbf{T}^k)^d\|_q^q + \|\operatorname{tr}\mathbf{T}^k\|_{s'}^{s'} + \|\operatorname{tr}\mathbf{G}(\mathbf{T}^k)\|_s^s) \\ \le (\mathcal{E}\,\hat{\mathbf{u}}, \mathbf{T}^k) + \langle\mathbf{g}, \mathbf{u}_H^k\rangle_{\Gamma_N} + \langle\mathbf{f}, \mathbf{u}_H^k\rangle + C_2|\Omega|. \end{aligned} \tag{4.69}$$

We use the improved estimate (4.68) to formulate estimates analogous to (4.30), (4.31), (4.33), (4.34) and (4.36) from Theorem 4.24 that doesn't depend on k. By this procedure, we show the existence of a positive constant $C(\Omega, \mathbf{f}, \mathbf{g}, \hat{\mathbf{u}})$ that does not depend on k such that

$$\begin{aligned} \|(\mathbf{T}^k)^d\|_{q'}^{q'} + \|\mathbf{G}(\mathbf{T}^k)^d\|_q^q + \|\operatorname{tr}\mathbf{T}^k\|_{s'}^{s'} + \|\operatorname{tr}\mathbf{G}(\mathbf{T}^k)\|_s^s \\ + \|(\mathcal{E}\,\mathbf{u}_H^k)^d\|_q^q + \|\operatorname{div}\mathbf{u}_H^k\|_s^s + \|\mathbf{u}\|_{(q,s)}^q \le C(\Omega, \mathbf{f}, \mathbf{g}, \hat{\mathbf{u}}), \end{aligned} \tag{4.70}$$

and hence also

$$\|\left|(\mathcal{E}\,\mathbf{u}_H^k)^d\right|^{q-2}(\mathcal{E}\,\mathbf{u}_H^k)^d\|_{q'}^{q'} + \|\left|\operatorname{div}\mathbf{u}_H^k\right|^{s-2}\operatorname{div}\mathbf{u}_H^k\|_{s'}^{s'} \le C(\Omega, \mathbf{f}, \mathbf{g}, \hat{\mathbf{u}}). \tag{4.71}$$

Step 3 - Passing to the limit

By application of the Eberlein–Šmulian theorem to (4.70) and (4.71), we conclude that there exist functions $\mathbf{T} \in L^{(q',s')}(\Omega)$, $\mathbf{Y} \in L^{(q,s)}(\Omega)$, $\mathbf{u}_H \in W^{1,(p,q,s)}_{\Gamma_D}(\Omega)$, $\mathbf{v} \in L^{q'}(\Omega)^{n\times n}_{sym}$, $e \in L^{s'}(\Omega)$ and a subsequence $\{k_i, i \in \mathbb{N}\}$ such that, for $i \to \infty$,

$$\begin{aligned} \mathbf{T}^{k_i} &\rightharpoonup \mathbf{T} && \text{in } L^{(q',s')}(\Omega), \\ \mathbf{G}(\mathbf{T}^{k_i}) &\rightharpoonup \mathbf{Y} && \text{in } L^{(q,s)}(\Omega), \\ \mathbf{u}_H^{k_i} &\rightharpoonup \mathbf{u}_H && \text{in } W^{1,(p,q,s)}_{\Gamma_D}(\Omega), \\ (\mathcal{E}\,\mathbf{u}_H^{k_i})^d &\rightharpoonup (\mathcal{E}\,\mathbf{u}_H)^d && \text{in } L^q(\Omega)^{n\times n}_{sym}, \\ \operatorname{div}\mathbf{u}_H^{k_i} &\rightharpoonup \operatorname{div}\mathbf{u}_H && \text{in } L^s(\Omega), \\ \left|(\mathcal{E}\,\mathbf{u}_H^{k_i})^d\right|^{q-2}(\mathcal{E}\,\mathbf{u}_H^{k_i})^d &\rightharpoonup \mathbf{v} && \text{in } L^{q'}(\Omega)^{n\times n}_{sym}, \\ \left|\operatorname{div}\mathbf{u}_H^{k_i}\right|^{s-2}\operatorname{div}\mathbf{u}_H^{k_i} &\rightharpoonup e && \text{in } L^{s'}(\Omega). \end{aligned} \tag{4.72}$$

Substituting the pair of test functions $(\mathbf{u}_H^{k_i}, \mathbf{T}^{k_i}) \in (W^{1,(p,q,s)}_{\Gamma_D}(\Omega), L^{(q',s')}(\Omega))$ into the system (4.60), where $k = k_i$, and summing up the results yields

$$(\mathbf{G}(\mathbf{T}^{k_i}), \mathbf{T}^{k_i}) = -\frac{1}{k_i}\mathbf{H}(\mathbf{u}_H^{k_i}, \mathbf{u}_H^{k_i}) + (\mathcal{E}\,\hat{\mathbf{u}}, \mathbf{T}^{k_i}) + \langle \mathbf{g}, \mathbf{u}_H^{k_i}\rangle_{\Gamma_N} + \langle \mathbf{f}, \mathbf{u}_H^{k_i}\rangle, \tag{4.73}$$

where it is easy to check using (4.70) that the limit of the first term on the right in (4.73) is zero

$$\lim_{i\to\infty} \frac{1}{k_i}\mathbf{H}(\mathbf{u}_H^{k_i}, \mathbf{u}_H^{k_i}) = \frac{1}{k_i}(\|(\mathcal{E}\,\mathbf{u}_H^{k_i})^d\|_q^q + \|\operatorname{div}\mathbf{u}_H^{k_i}\|_s^s) = 0.$$

Now, let substitute test functions $(\mathbf{u}_H, \mathbf{T}) \in (W^{1,(p,q,s)}_{\Gamma_D}(\Omega), L^{(q',s')}(\Omega))$ into (4.60), where $k = k_i$, and pass to the limit $i \to \infty$. From (4.72), we have that

$$(\mathbf{Y}, \mathbf{T}) = -\lim_{i\to\infty} \frac{1}{k_i}\mathbf{H}(\mathbf{u}_H^{k_i}, \mathbf{u}_H) + (\mathcal{E}\,\hat{\mathbf{u}}, \mathbf{T}) + \langle \mathbf{g}, \mathbf{u}_H\rangle_{\Gamma_N} + \langle \mathbf{f}, \mathbf{u}_H\rangle. \tag{4.74}$$

By (4.71), it is easy to check that

$$\lim_{i\to\infty} \frac{1}{k_i}\mathbf{H}(\mathbf{u}_H^{l_i}, \mathbf{u}_H) = 0.$$

Comparing (4.73) with (4.74), we obtain

$$\lim_{i\to\infty} (\mathbf{G}(\mathbf{T}^{k_i}), \mathbf{T}^{k_i}) = (\mathbf{Y}, \mathbf{T}). \tag{4.75}$$

Using the same reasoning as when showing (4.59) in Theorem 4.24, we have that

$$\mathbf{G}(\mathbf{T}) = \mathbf{Y}. \tag{4.76}$$

These results enable us to pass to the limit $k_i \to \infty$ in the system (4.60) to show that

$$\begin{aligned} &\forall \mathbf{S} \in L^{(q',s')}(\Omega), && (\mathcal{E}\,\hat{\mathbf{u}}, \mathbf{S}) + (\mathcal{E}\,\mathbf{u}_H, \mathbf{S}) = (\mathbf{G}(\mathbf{T}), \mathbf{S}),\\ &\forall \boldsymbol{\chi} \in W^{1,(p,q,s)}_{\Gamma_D}(\Omega), && (\mathbf{T}, \mathcal{E}\,\boldsymbol{\chi}) = \langle \mathbf{g}, \boldsymbol{\chi}\rangle_{\Gamma_N} + \langle \mathbf{f}, \boldsymbol{\chi}\rangle \end{aligned}$$

The pair $(\mathbf{u}_H + \hat{\mathbf{u}}, \mathbf{T}) \in (W^{1,(p,q,s)}(\Omega), L^{(q',s')}(\Omega))$ is a solution of the weak Problem (P) in the sense of Definition 4.20, which completes the proof. □

4.4 Existence of solutions for power-law models

To show that Theorem 4.25 guarantees the existence of a solution for a particular constitutive function $\mathbf{G}$, we have to show that assumptions of Theorem 4.25 about $\mathbf{G}$ are met. For $s, q \in (1, \infty)$, it is sufficient to show that the constitutive function $\mathbf{G} : \mathbb{R}^{n\times n}_{sym} \to \mathbb{R}^{n\times n}_{sym}$ in (1.1b), see Definition 1.1, (p. 7), is continuous, monotone and has the following property. There exist constants $C_1 > 0$, $C_2 > 0$ such that for all $\mathbf{X} \in \mathbb{R}^{n\times n}_{sym}$, the following is true

$$\begin{aligned} \mathbf{G}(\mathbf{X})^d : \mathbf{X}^d &\geq C_1(|\mathbf{X}^d|^{q'} + |\mathbf{G}(\mathbf{X})^d|^q) - \frac{C_2}{2},\\ \operatorname{tr}\mathbf{G}(\mathbf{X}) \cdot \operatorname{tr}\mathbf{X} &\geq 3C_1(|\operatorname{tr}\mathbf{X}|^{s'} + |\operatorname{tr}\mathbf{G}(\mathbf{X})|^s) - 3\frac{C_2}{2}. \end{aligned} \tag{4.77}$$

It is easy to check that when $\mathbf{G}$ satisfies (4.77), then the related operator $\mathbf{G} : L^{(q',s')}(\Omega) \to L^{(q,s)}(\Omega)$ in the sense of Observation A.94, (p. 139) fulfils the coercivity condition (4.22) imposed by Definition 4.23. In this section, we show that the power-law model (2.20), see Definition 2.11, (p. 24), satisfies (4.77). Therefore according to Theorem 4.25, there exists the weak solution to the Problem (P) with power-law response.

In order to easily test that a particular constitutive function $\mathbf{G}$ is monotone, we formulate a few auxiliary lemmas.

Auxiliary lemmas

Let $\mathbf{G}_1, \mathbf{G}_2, \mathbf{G}_3 : \mathbb{R}^{n\times n}_{sym} \to \mathbb{R}^{n\times n}_{sym}$ be tensor-valued functions with the structure

$$\begin{aligned} \mathbf{G}_1(\mathbf{T}) &= \mathbf{I}\sigma_1(\operatorname{tr}\mathbf{T})\operatorname{tr}\mathbf{T}, \\ \mathbf{G}_2(\mathbf{T}) &= \sigma_2(|\mathbf{T}|)\mathbf{T}, \\ \mathbf{G}_3(\mathbf{T}) &= \sigma_3(|\mathbf{T}^d|)\mathbf{T}^d, \end{aligned} \tag{4.78}$$

where σ_i are scalar functions, $\sigma_i : \mathbb{R} \to \mathbb{R}$.

Next three lemmas show that when σ_i are monotone scalar functions, then the corresponding $\mathbf{G}_i(\mathbf{T})$ are also monotone tensor-valued functions.

Lemma 4.26 (Monotonicity of tensor-valued functions 1). *Let $\mathbf{G} : \mathbb{R}^{n\times n}_{sym} \to \mathbb{R}^{n\times n}_{sym}$ be a tensor-valued function of the form $\mathbf{G}(\mathbf{T}) = \mathbf{I}\sigma_1(\operatorname{tr}\mathbf{T})\operatorname{tr}\mathbf{T}$, where $\sigma_1 : \mathbb{R} \to \mathbb{R}$. Then the scalar function $g(t) = \sigma_1(t)t$ is nondecreasing if and only if $\mathbf{G}$ is a monotone tensor-valued function.*

Proof. It is sufficient to show that for all $\mathbf{T}_1, \mathbf{T}_2 \in \mathbb{R}^{n\times n}_{sym}$, the following equalities are true

$$\begin{aligned} (\mathbf{I}\sigma_1(\operatorname{tr}\mathbf{T}_1)\operatorname{tr}\mathbf{T}_1 - \mathbf{I}\sigma_1(\operatorname{tr}\mathbf{T}_2)\operatorname{tr}\mathbf{T}_2) : (\mathbf{T}_1 - \mathbf{T}_2) \\ = (g(\operatorname{tr}\mathbf{T}_1) - g(\operatorname{tr}\mathbf{T}_2))\mathbf{I} : (\mathbf{T}_1 - \mathbf{T}_2) \\ = (g(\operatorname{tr}\mathbf{T}_1) - g(\operatorname{tr}\mathbf{T}_2))(\operatorname{tr}\mathbf{T}_1 - \operatorname{tr}\mathbf{T}_2). \end{aligned}$$

□

Lemma 4.27 (Monotonicity of tensor-valued functions 2). *Let $\mathbf{G} : \mathbb{R}^{n\times n}_{sym} \to \mathbb{R}^{n\times n}_{sym}$ be a tensor-valued function of the form $\mathbf{G}(\mathbf{T}) = \sigma_2(|\mathbf{T}|)\mathbf{T}$, where $\sigma_2 : \mathbb{R}^+_0 \to \mathbb{R}^+_0$. The function $g(t) = \sigma_2(|t|)t$ is nondecreasing if and only if the $\mathbf{G}$ is a monotone tensor-valued function.*

Proof. Assumption of g being nondecreasing function can be rephrased as that for any $t_1, t_2 \in \mathbb{R}$, we have the inequality

$$(\sigma_2(|t_1|)t_1 - \sigma_2(|t_2|)t_2)(t_1 - t_2) \geq 0, \tag{4.79}$$

which is the same as

$$\sigma_2(|t_1|)t_1^2 + \sigma_2(|t_2|)t_2^2 - \sigma_2(|t_1|)t_1t_2 - \sigma_2(|t_2|)t_1t_2 \geq 0. \tag{4.80}$$

$\mathbf{G}$ being monotone means that

$$\forall \mathbf{T}_1, \mathbf{T}_2 \in \mathbb{R}^{n\times n}_{sym}, \quad (\sigma_2(|\mathbf{T}_1|)\mathbf{T}_1 - \sigma_2(|\mathbf{T}_2|)\mathbf{T}_2) : (\mathbf{T}_1 - \mathbf{T}_2) \geq 0. \tag{4.81}$$

Expanding the formula above, we get

$$\sigma_2(|\mathbf{T}_1|)\,|\mathbf{T}_1|^2 + \sigma_2(|\mathbf{T}_2|)\,|\mathbf{T}_2|^2 - \sigma_2(|\mathbf{T}_1|)\mathbf{T}_1 : \mathbf{T}_2 - \sigma_2(|\mathbf{T}_2|)\mathbf{T}_1 : \mathbf{T}_2 \geq 0. \quad (4.82)$$

Applying the Cauchy-Schwartz inequality in the form

$$-\mathbf{A} : \mathbf{B} \geq -|\mathbf{A}|\,|\mathbf{B}|, \quad \forall \mathbf{A}, \mathbf{B} \in \mathbb{R}^{n\times n}_{sym}$$

to the left-hand side of (4.82) yields

$$\begin{aligned}&(\sigma_2(|\mathbf{T}_1|)\mathbf{T}_1 - \sigma_2(|\mathbf{T}_2|)\mathbf{T}_2) : (\mathbf{T}_1 - \mathbf{T}_2) \geq \\ &\quad \sigma_2(|\mathbf{T}_1|)\,|\mathbf{T}_1|^2 + \sigma_2(|\mathbf{T}_2|)\,|\mathbf{T}_2|^2 - \sigma_2(|\mathbf{T}_1|)\,|\mathbf{T}_1|\,|\mathbf{T}_2| - \sigma_2(|\mathbf{T}_2|)\,|\mathbf{T}_1|\,|\mathbf{T}_2|. \quad (4.83)\end{aligned}$$

When g is nondecreasing, we combine (4.83) with (4.80), where $t_1 = |\mathbf{T}_1|$ and $t_2 = |\mathbf{T}_2|$ for any $\mathbf{T}_1, \mathbf{T}_2 \in \mathbb{R}^{n\times n}_{sym}$, which yields (4.81). In other words $\mathbf{G}$ is monotone.

Let's prove the opposite implication. We set

$$\mathbf{T}_1 = t_1\mathbf{e_1} \otimes \mathbf{e_1}, \quad \mathbf{T}_2 = t_2\mathbf{e_1} \otimes \mathbf{e_1}, \quad \mathbf{T}_1, \mathbf{T}_2 \in \mathbb{R}^{n\times n}_{sym}. \quad (4.84)$$

If $\mathbf{G}$ is monotone, then setting (4.84) in (4.81) yields (4.79), which means that $g(t)$ is nondecreasing. □

Lemma 4.28 (Monotonicity of tensor-valued functions 3). *Let $\mathbf{G} : \mathbb{R}^{n\times n}_{sym} \to \mathbb{R}^{n\times n}_{sym}$ be a tensor-valued function of the form $\mathbf{G}(\mathbf{T}) = \sigma_3(|\mathbf{T}^d|)\mathbf{T}^d$, where $\mathbf{T}^d$ is the deviatoric part of the tensor $\mathbf{T}$ and $\sigma_3 : \mathbb{R}^+_0 \to \mathbb{R}^+_0$. The function $g(t) = \sigma_3(|t|)t$ is nondecreasing if and only if $\mathbf{G}$ is a monotone tensor-valued function.*

Proof. If $\mathbf{G}$ is a monotone tensor-valued function, then

$$(\sigma_3(|\mathbf{T}^d_1|)\mathbf{T}^d_1 - \sigma_3(|\mathbf{T}^d_2|)\mathbf{T}^d_2) : (\mathbf{T}_1 - \mathbf{T}_2) \geq 0, \quad \forall \mathbf{T}_1, \mathbf{T}_2 \in \mathbb{R}^{n\times n}_{sym}. \quad (4.85)$$

We use the decomposition

$$\mathbf{T}_1 = \mathbf{T}^d_1 + \frac{\operatorname{tr}\mathbf{T}_1}{3}\mathbf{I} \quad \text{and} \quad \mathbf{T}_2 = \mathbf{T}^d_2 + \frac{\operatorname{tr}\mathbf{T}_2}{3}\mathbf{I}$$

and the fact that $\mathbf{Y} : \mathbf{I} = \mathbf{0}$ for any traceless tensor $\mathbf{Y}$, in particular for $\mathbf{T}^d$. Using these manipulations, the condition (4.85) can be rewritten as

$$(\sigma_3(|\mathbf{T}^d_1|)\mathbf{T}^d_1 - \sigma_3(|\mathbf{T}^d_2|)\mathbf{T}^d_2) : (\mathbf{T}^d_1 - \mathbf{T}^d_2) \geq 0, \quad \forall \mathbf{T}_1, \mathbf{T}_2 \in \mathbb{R}^{n\times n}_{sym}. \quad (4.86)$$

If g is nondecreasing, then $\mathbf{G}$ is monotone by Lemma 4.27.

The opposite implication can be proven by constructing tracefree matrices

$$\mathbf{T}_1 = \frac{t_1}{\sqrt{2}}(\mathbf{e_1}\otimes\mathbf{e_2}+\mathbf{e_2}\otimes\mathbf{e_1}), \quad \mathbf{T}_2 = \frac{t_2}{\sqrt{2}}(\mathbf{e_1}\otimes\mathbf{e_2}+\mathbf{e_2}\otimes\mathbf{e_1}), \quad \mathbf{T}_1, \mathbf{T}_2 \in \mathbb{R}^{n\times n}_{sym}. \quad (4.87)$$

If $\mathbf{G}$ is monotone, then setting (4.87) in (4.86) yields

$$(\sigma_3(t_1)t_1 - \sigma_3(t_2)t_2)(t_1 - t_2) \geq 0, \quad \forall t_1, t_2 \in \mathbb{R},$$

which means that $g(t)$ is nondecreasing. □

Lemma 4.26, Lemma 4.27 and Lemma 4.28 reduce the problem whether the given tensor-valued function with the structure (4.78) is monotone, to the problem whether the scalar function σ is monotone. Note that the structure (4.78) is typical for most constitutive responses studied in this thesis. Conditions for monotonicity of the scalar functions related to the power-law models from Definition 2.11, (p. 24) are established in the following lemma.

Lemma 4.29 (Monotonicity of a scalar power-law function). *Let $c, \gamma, \kappa, a, q > 0$ be parameters of function $g : \mathbb{R} \to \mathbb{R}$ such that*

$$g(t) = c\left(\gamma + \kappa|t|^a\right)^{\frac{q-2}{a}} t. \tag{4.88}$$

If $q \geq 1$, then g is monotone for every set of parameters $c, \gamma, \kappa, a > 0$.

Proof. Taking the derivative of g with respect to t, we have that

$$\begin{aligned} g'(t) &= c\kappa(q-2)\left(\gamma + \kappa|t|^a\right)^{\frac{q-2}{a}-1}|t|^a + c\left(\gamma + \kappa|t|^a\right)^{\frac{q-2}{a}} \\ &= c\left(\gamma + \kappa|t|^a\right)^{\frac{q-2}{a}}\left(\frac{\kappa(q-2)|t|^a}{\gamma + \kappa|t|^a} + 1\right) \\ &= c\left(\gamma + \kappa|t|^a\right)^{\frac{q-2}{a}}\left(\frac{\gamma + \kappa(q-1)|t|^a}{\gamma + \kappa|t|^a}\right), \end{aligned}$$

where for $q \geq 1$, there is $g'(t) > 0$, so the function $g(t)$ is strictly monotone. □

Observation 4.30 (Radial continuity of constitutive relation). *If functions σ_1, σ_2 and σ_3 from* (4.78) *are continuous, then related operators $\mathbf{G}_1$, $\mathbf{G}_2$, $\mathbf{G}_3$, in the sense of Observation A.94, (p. 139) are radially continuous.*

Existence of solutions for power-law models

We are now prepared to show that the power-law response (2.20) from Definition 2.11, (p. 24) fulfils the assumptions of Theorem 4.25 for the existence of the solutions to the weak problem. For simpler algebraic manipulations, we show that these assumptions hold for $\mathbf{G}$ of the reduced form where some material moduli are normalized. Let $s' \in (1, \infty)$ and $q' \in (1, \infty)$. We define the normalized form of power-law response $\mathbf{G}$, where $\mathbf{G}$ is split to the mean normal part and the deviatoric part by

$$\operatorname{tr}\mathbf{G}(\mathbf{T}) = \left(1 + |\operatorname{tr}\mathbf{T}|^2\right)^{\frac{s'-2}{2}} \operatorname{tr}\mathbf{T}, \tag{4.89a}$$

$$\mathbf{G}(\mathbf{T})^d = \left(1 + |\mathbf{T}^d|^2\right)^{\frac{q'-2}{2}} \mathbf{T}^d. \tag{4.89b}$$

Theorem 4.31. *Let $s' \in (1, \infty)$ and $q' \in (1, \infty)$. Function $\mathbf{G} : \mathbb{R}^{n\times n}_{sym} \to \mathbb{R}^{n\times n}_{sym}$ of the form* (4.89) *fulfils the requirements of Theorem 4.25 on the existence of the weak solutions. In other words, $\mathbf{G}$ is a monotone, radially continuous operator in the sense of Observation A.94, (p. 139), and there exist constants $C_1 > 0$, $C_2 \geq 0$ such that the condition* (4.22) *is fulfilled.*

Proof. The proof of the theorem can be split into three steps. First is to show that $\mathbf{G}$ is a radially continuous operator, second is that $\mathbf{G}$ is monotone and in the third step we show that $\mathbf{G}$ satisfies (4.22).

The function $\mathbf{G}$ can be reformulated as being a sum of functions of the type (4.78) such that

$$\mathbf{G}(\mathbf{T}) = \mathbf{G}_1(\mathbf{T}) + \mathbf{G}_3(\mathbf{T}), \quad \mathbf{G}_1(\mathbf{T}) = \mathbf{I}\sigma_1(\operatorname{tr}\mathbf{T})\operatorname{tr}\mathbf{T}, \quad \mathbf{G}_3(\mathbf{T}) = \sigma_3(\left|\mathbf{T}^d\right|)\mathbf{T}^d,$$

where

$$\sigma_1(t) = \frac{1}{3}\left(1+t^2\right)^{\frac{s'-2}{2}}, \quad \sigma_3 = \left(1+t^2\right)^{\frac{q'-2}{2}}. \tag{4.90}$$

We may also understand $\mathbf{G}$ as being an operator $\mathbf{G} : L^{(q',s')}(\Omega) \to L^{(q,s)}(\Omega)$ such that

$$\langle \mathbf{G}(\mathbf{T}), \mathbf{W}\rangle = (\sigma_1(\operatorname{tr}\mathbf{T})\operatorname{tr}\mathbf{T}, \operatorname{tr}\mathbf{W}) + (\sigma_3(\left|\mathbf{T}^d\right|)\mathbf{T}^d, \mathbf{W}^d), \quad \text{for } \mathbf{T}, \mathbf{W} \in L^{(q',s')}(\Omega). \tag{4.91}$$

Since σ_1 and σ_3 in (4.90) are continuous functions, it is straightforward that $\mathbf{G}$ of the form (4.91) is a radially continuous operator.

To show monotonicity of the operator $\mathbf{G}$, we first show the conditions for monotonicity of the functions $\sigma_1(t)t$ and $\sigma_3(|t|)t$. According to Lemma 4.29, function $\sigma_1(t)t$ is monotone for $s' \in [1,\infty)$, and function $\sigma_3(|t|)t$ is monotone for $q' \in [1,\infty)$. Using Lemma 4.26 and Lemma 4.28, we conclude that functions $\mathbf{G}_1$ and $\mathbf{G}_3$ are monotone tensor-valued functions. It is a simple matter to show that monotonicity, in the sense of tensors, implies monotonicity in the sense of operators, and that the sum of two monotone operators is again a monotone operator. Therefore, we have established monotonicity of the operator $\mathbf{G}$.

The last step of the proof is showing that the operator $\mathbf{G}$ satisfies (4.22). It is easy to check that (4.77) is a stronger form of the condition (4.22), which works with tensor-valued functions instead of operators. We proceed to show that $\mathbf{G}$ fulfils the condition (4.77). The proof falls naturally into two parts of showing the coercivity condition (4.77) for the deviatoric part and showing it for traces.

We begin with showing the coercivity of $\mathbf{G}$ for the deviatoric part. It suffices to show that there exist constants c_1, c_2, c_3 such that

$$\begin{aligned} &\mathbf{G}(\mathbf{T})^d : \mathbf{T}^d \geq c_1|\mathbf{T}^d|^{q'} - c_3, && \forall \mathbf{T} \in \mathbb{R}^{n\times n}_{sym}, \\ &\mathbf{G}(\mathbf{T})^d : \mathbf{T}^d \geq c_2|\mathbf{G}(\mathbf{T})^d|^{q} - c_3, && \forall \mathbf{T} \in \mathbb{R}^{n\times n}_{sym}. \end{aligned} \tag{4.92}$$

Combining (4.92) and the particular form of $\mathbf{G}$ given by (4.90), we have that

$$\left(1+t^2\right)^{\frac{q'-2}{2}} t^2 \geq c_1|t|^{q'} - c_3, \qquad \forall t \in \mathbb{R}, \tag{4.93a}$$

$$\left(1+t^2\right)^{\frac{q'-2}{2}} t^2 \geq c_2\left|\left(1+t^2\right)^{\frac{q'-2}{2}} t\right|^{q} - c_3, \qquad \forall t \in \mathbb{R}. \tag{4.93b}$$

Let us see that the problem of showing coercivity of $\mathbf{G}$ was reduced to showing the algebraic property of (4.93) for a general $q' \in (1,\infty)$. We can easily show the property (4.93a) from the inequality

$$\left(1+t^2\right)^{\frac{q'-2}{2}} \geq |t|^{q'-2}.$$

Now, we prove the property (4.93b). Using $q = q'/(q'-1)$, we rewrite the first term on the right side of (4.93b) into the form

$$\left|\left(1+t^2\right)^{\frac{q'-2}{2}} t\right|^{q} = \left(1+|t|^2\right)^{\frac{q'-2}{2}} |t|^2 \left(1+|t|^2\right)^{\frac{q'-2}{2(q'-1)}} |t|^{\frac{2-q'}{q'-1}}. \tag{4.94}$$

We split the further estimation of (4.94) into two cases. When

$$\frac{q'-2}{2(q'-1)} \leq 0 \Leftrightarrow q' < 2,$$

then the inequality

$$\left(1+|t|^2\right)^{\frac{q'-2}{2(q'-1)}} \leq |t|^{\frac{q'-2}{(q'-1)}} \tag{4.95}$$

holds. Substitution of (4.95) into (4.94) yields (4.93b) with $c_2 = 1$, $c_3 = 0$. Let consider the case

$$\frac{q'-2}{2(q'-1)} > 0 \Leftrightarrow q' > 2.$$

We investigate its two subcases. First, when $|t| > 1$, we have that

$$\left(1+|t|^2\right)^{\frac{q'-2}{2(q'-1)}} \leq \left(\sqrt{2}|t|\right)^{\frac{q'-2}{(q'-1)}}. \tag{4.96}$$

Second, when $|t| \leq 1$, we construct the estimate

$$\left(1+|t|^2\right)^{\frac{q'-2}{2(q'-1)}} \leq \sqrt{2}^{\frac{q'-2}{(q'-1)}} \leq \frac{\sqrt{2}^{\frac{q'-2}{(q'-1)}} 2^{\frac{q'-2}{2}}}{\left(1+|t|^2\right)^{\frac{q'-2}{2}} |t|^2 |t|^{\frac{2-q'}{q'-1}}}. \tag{4.97}$$

Combining the estimates (4.96) and (4.97), we deduce the estimate

$$\left(1+|t|^2\right)^{\frac{q'-2}{2(q'-1)}} \leq \left(\sqrt{2}|t|\right)^{\frac{q'-2}{(q'-1)}} + \frac{\sqrt{2}^{\frac{q'(q'-2)}{q'-1}}}{\left(1+|t|^2\right)^{\frac{q'-2}{2}} |t|^{\frac{q'}{q'-1}}}, \tag{4.98}$$

which holds for all $t \in \mathbb{R}$. By inserting (4.98) into (4.94), we obtain

$$\left| \left(1+t^2\right)^{\frac{q'-2}{2}} t \right|^q \leq 2^{\frac{q'-2}{2(q'-1)}} \left(1+|t|^2\right)^{\frac{q'-2}{2}} |t|^2 + 2^{\frac{q'(q'-2)}{2(q'-1)}}. \tag{4.99}$$

From (4.99), we deduce that the estimate (4.93b) holds with parameters

$$c_2 = 2^{\frac{2-q'}{2(q'-1)}}, \quad c_3 = 2^{\frac{(q'-1)(q'-2)}{2(q'-1)}}.$$

Proving that the second equation in (4.77) holds, reduces to showing the property (4.93b), which has already been proven. Concluding that the operator $\mathbf{G}$ fulfils the coercivity condition (4.22) completes the proof. □

It is a simple matter to see that the constitutive equation (2.20) of the power-law solid from Definition 2.11, (p. 24) is of the same form as the reduced relation (4.89). Using the full relation (2.20) would obscure the proof of Theorem 4.31 by additional constants that could be, however, handled with some care.

We shall also comment on proving the existence of solutions to the Problem (P) with the constitutive equation of the form

$$\mathbf{G}(\mathbf{T}) = \left(1+|\mathbf{T}|^2\right)^{\frac{q'-2}{2}} \mathbf{T}, \tag{4.100}$$

where $q' \in (1,\infty)$. The equation (4.100) comes without separation of the mean normal term from the deviatoric part of the constitutive relation. Simple modifications to the ideas provided in this chapter would establish the existence of a weak solution to (4.100). Since this is an easier task than showing the existence for a separated system with different power-law exponents, we are not including the corresponding analysis here.

5. Computer simulations

In Chapter 3, we identified the parameters of the power-law model (2.20), see Definition 2.11, (p. 24), for four different beta phase titanium alloys. Using these models, we perform computer simulations to study the shearing behavior of titanium alloys. We use anti-plane stress, which is a geometrical setting of stress, strain and displacement of the body, where all quantities depend only on plane coordinates (x_1 and x_2) and the only nonzero components of the stress tensor are T_{13} and T_{23}. A material that is subject to the anti-plane stress setting can be loaded only at the anti-plane direction perpendicular to the (x_1, x_2) plane, see Figure 5.1[1]. These assumptions allow us to rephrase the Problem (P) (1.1), see Definition 1.1, (p. 7), as a variational problem on a discrete space of finite elements to find an unknown Airy's stress function, which plays the role of a potential.

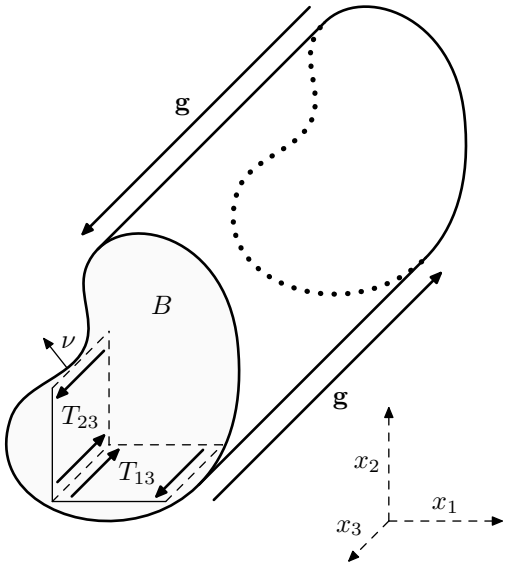

Figure 5.1: Anti-plane stress setting. The only nonzero components of the stress tensor are T_{13} and T_{23}.

We are interested in the behavior of studied materials in a geometry of a square plate with a V-shaped notch. According to the asymptotic analysis, there is a singularity of stress and strain at the tip of the notch. Therefore we study how the presence of the singularity affects the stability of numeric solutions with respect to the opening angle of the V-notch α. We further investigate the solutions in the two geometries where the V-notch tip is smoothened by an arc or by an end hole with a diameter r_c. By solving the problem on the set of 6 gradually refined meshes, we achieve a very good stability of the solutions even in the areas of high stress concentration.

The software implementation for solving these problems in Python is a part of this thesis and can be found in supplementary materials. Solver of the discretized problem on the FEM space uses the damped Newton method and utilizes FEniCS software library, see Logg et al. (2012).

[1]When visualising the anti-plane stress geometry, we use the right-handed coordinate system and sign convention, where positive face is a face with a normal in the positive axis direction. The shear stress acting in the positive axis direction on the positive face has a positive sign.

In a separate paper, see Kulvait et al. (2013), the computational simulations for the strain-limiting model can be found.

5.1 Boundary value problem

The geometry and the type of the deformation of anti-plane stress, see Figure 5.1, allows us to assume that $\Omega = B \times \mathbb{R}$, $\mathbf{u} = (0, 0, u(x_1, x_2))$, $\partial B = \Gamma_N$, $\mathbf{g} = (0, 0, g)$ and $\mathbf{f} = \mathbf{0}$. The stress tensor $\mathbf{T}$ has two nontrivial components and can be represented by vector $\mathbf{T}_v = (T_{13}, T_{23})$. The trace and the norm of the deviatoric part of the stress tensor can be expressed as

$$\operatorname{tr}(\mathbf{T}) = 0, \quad |\mathbf{T}^d| = \sqrt{2}|\mathbf{T}_v|.$$

We apply the model (2.15), see Definition 2.8, (p. 23), into the anti-plane stress setting. Then the strain tensor $\boldsymbol{\varepsilon}$ has also only two nontrivial components ε_{13} and ε_{23} and can be represented by the vector $\boldsymbol{\varepsilon}_v = (\varepsilon_{13}, \varepsilon_{23})$. Constitutive relation (2.15) reduces to the form

$$\boldsymbol{\varepsilon}_v = \sigma_2(\sqrt{2}|\mathbf{T}_v|)\mathbf{T}_v \equiv \sigma(|\mathbf{T}_v|)\mathbf{T}_v,$$

and Problem (P), see Definition 1.1, (p. 7), can be reformulated as:

Definition 5.1 (Problem (P) in anti-plane stress setting). *Let $\Omega = B \times \mathbb{R}$, where $B \subset \mathbb{R}^2$ is an open, bounded, simply connected domain. Let $\sigma : \mathbb{R} \to \mathbb{R}$ represent constitutive response of the material and let $g : \partial B \to \mathbb{R}$ be a given function. We say that a pair of functions $(\boldsymbol{\varepsilon}_v, \mathbf{T}_v)$ is the solution of Problem (P) in the anti-plane stress setting* [2] *when the following is true*

$$-\frac{\partial T_{13}}{\partial x_1} - \frac{\partial T_{23}}{\partial x_2} = 0 \qquad \text{in } B, \tag{5.1a}$$

$$\varepsilon_{13} = \sigma(|\mathbf{T}_v|)\,T_{13}, \quad \varepsilon_{23} = \sigma(|\mathbf{T}_v|)\,T_{23} \qquad \text{in } B, \tag{5.1b}$$

$$T_{13}\nu_1 + T_{23}\nu_2 = g \qquad \text{on } \partial B. \tag{5.1c}$$

In the remainder of this chapter, we use the following particular forms of the constitutive function σ. For the power-law model (2.20), see Definition 3.1, (p. 40), we have the response

$$\sigma(|\mathbf{T}_v|) = \frac{1}{2\mu}\left(\frac{\tau_0^2 + 3\,|\mathbf{T}_v|^2}{\tau_0^2}\right)^{\frac{q'-2}{2}}. \tag{5.2}$$

The linear Hooke's law is characterized by the response (5.2), where $q' = 2$, that is

$$\sigma(|\mathbf{T}_v|) = \frac{1}{2\mu_L}. \tag{5.3}$$

In the case of strain-limiting model (2.32), see Definition 2.15, (p. 26), which was used in Kulvait et al. (2013) we have that

$$\sigma(|\mathbf{T}_v|) = \frac{\tau_\mu}{2\mu_I\left(\tau_\mu^a + \left(\sqrt{2}\,|\mathbf{T}_v|\right)^a\right)^{1/a}}.$$

[2] Since we consider constitutive relations of the type (5.1b), the anti-plane stress state is equivalent to the classical definition of anti-plane strain, see Rice (1967).

5.1.1 Compatibility conditions

The Saint-Venant compatibility conditions for ε, see (A.17), are reduced to the two nontrivial equations

$$\frac{\partial^2 \varepsilon_{13}}{\partial x_1 \partial x_2} - \frac{\partial^2 \varepsilon_{23}}{\partial x_1 \partial x_1} = 0, \quad \frac{\partial^2 \varepsilon_{23}}{\partial x_1 \partial x_2} - \frac{\partial^2 \varepsilon_{13}}{\partial x_2 \partial x_2} = 0, \tag{5.4}$$

which implies the existence of a constant C such that

$$\frac{\partial \varepsilon_{13}}{\partial x_2} - \frac{\partial \varepsilon_{23}}{\partial x_1} = C. \tag{5.5}$$

Expressing (5.5) in terms of $\mathbf{u}$, we obtain

$$\frac{\partial^2 u_1}{\partial x_3 \partial x_2} - \frac{\partial^2 u_3}{\partial x_1 \partial x_2} - \frac{\partial^2 u_2}{\partial x_3 \partial x_1} + \frac{\partial^2 u_3}{\partial x_2 \partial x_1} = C. \tag{5.6}$$

Since $\mathbf{u} = (0, 0, u(x_1, x_2))$, we conclude that $C = 0$ and thus (5.4) leads to

$$\frac{\partial \varepsilon_{13}}{\partial x_2} - \frac{\partial \varepsilon_{23}}{\partial x_1} = 0. \tag{5.7}$$

The condition (5.7) is the necessary and sufficient condition for the existence of the displacement $u(x_1, x_2)$ fulfilling

$$\varepsilon_{13} = \frac{1}{2}\frac{\partial u}{\partial x_1}, \quad \varepsilon_{23} = \frac{1}{2}\frac{\partial u}{\partial x_2}.$$

5.1.2 Airy's function

Airy's stress function A is a scalar function, whose derivatives are components of the vector $\mathbf{T}_v$

$$T_{13} = \frac{\partial A}{\partial x_2}, \quad T_{23} = -\frac{\partial A}{\partial x_1}. \tag{5.8}$$

Every stress field of the type (5.8) fulfils the equilibrium equation (5.1a). From (5.8), we have that $|\mathbf{T}_v| = |\nabla A|$, and thus $\sigma(|\mathbf{T}_v|) = \sigma(|\nabla A|)$. Substituting the constitutive relation (5.1b) into the compatibility condition (5.7) leads to

$$-\frac{\partial}{\partial x_1}\left(\sigma(|\nabla A|)\frac{\partial A}{\partial x_1}\right) - \frac{\partial}{\partial x_2}\left(\sigma(|\nabla A|)\frac{\partial A}{\partial x_2}\right) = 0 \quad \text{in } B. \tag{5.9}$$

Let denote $\mathbf{t} = (-\nu_2, \nu_1)$ the tangential vector to the boundary ∂B. Then the boundary condition (5.1c) takes the form

$$\frac{\partial A}{\partial x_2}\nu_1 - \frac{\partial A}{\partial x_1}\nu_2 = \frac{\partial A}{\partial x_1}t_1 + \frac{\partial A}{\partial x_2}t_2 = g \qquad \text{on } \partial B. \tag{5.10}$$

We parametrize the boundary by the counterclockwise oriented closed curve $\boldsymbol{\xi} : [0, h] \to \mathbb{R}^2$, $\boldsymbol{\xi}(0) = \boldsymbol{\xi}(h)$, such that $\boldsymbol{\xi}([0, h]) = \partial B$ and

$$t_1(\boldsymbol{\xi}(b)) = \boldsymbol{\xi}_1'(b), \quad t_2(\boldsymbol{\xi}(b)) = \boldsymbol{\xi}_2'(b). \tag{5.11}$$

Substituting (5.11) into (5.10) and using the chain rule, we conclude that g is equal to the tangential derivative of A. We have that

$$g(\boldsymbol{\xi}(b)) = \nabla A . \frac{d\boldsymbol{\xi}(b)}{db} = \frac{dA(\boldsymbol{\xi}(b))}{db}, \quad b \in [0, h). \tag{5.12}$$

Integrating (5.12) along the boundary, we obtain the Dirichlet boundary condition

$$A_0^g(\boldsymbol{\xi}(b)) = A(\boldsymbol{\xi}(0)) + \int_0^b g(\boldsymbol{\xi}(b))\,\mathrm{d}b, \quad b \in [0, h). \tag{5.13}$$

Note that the value of the function A_0^g does not depend (up to a constant) on the parametrization of the boundary. By introducing Airy's stress function via (5.8), the boundary value problem, see Definition 5.1, takes the form summarized in the following definition.

Definition 5.2 (Airy's function solving Problem (P) in anti-plane stress setting). *Let the domain $B \subset \mathbb{R}^2$ and the functions (g, σ) fulfil the assumptions of Definition 5.1. We say that the function A is the Airy's function solving Problem (P) in the anti-plane stress setting if the following is true*

$$\begin{aligned} -\operatorname{div}(\sigma(|\nabla A|)\nabla A) &= 0 && \text{in } B, \\ A(\mathbf{x}) &= A_0^g(\mathbf{x}) && \text{on } \partial B, \end{aligned} \tag{5.14}$$

where A_0^g is the function defined by (5.13).

5.2 Asymptotic solutions for notched domains

Let focus, for a moment, on the asymptotic behavior of solutions in notched domains. As the geometry of the plate with a V-notch, see Figure 5.5, is closely related to the problem of fracture, a lot of research has been done regarding computation of asymptotic solutions in infinite domains. It has been observed that when studying the Problem (P) in the anti-plane stress setting, see Definition 5.1, in the geometry of the infinite plate with a V-notch, then the singularity of stress occurs for either the linear (5.3) or the power-law constitutive equations (5.2), the singularity is present at the tip C of the V-notch, see Neuber (1961); Rice (1967).

Asymptotic solutions can be understood as the first order estimate of the behavior of solution and can also supplement numerical simulations in the close vicinity of the V-notch tip, where the finite numerical solution is not able to capture the singular behavior.

5.2.1 Cylindrical coordinate system

When studying the behavior of the solution around the V-notch tip C, it is useful to introduce the cylindrical coordinate system (r, φ) centered at C, see Figure 5.2. Vectors $\boldsymbol{\varepsilon}_v$ and $\mathbf{T}_v$ can be transformed between Cartesian and polar coordinate systems by means of the formula

$$\begin{pmatrix} T_{rz} \\ T_{\varphi z} \end{pmatrix} = \begin{pmatrix} \cos\varphi & \sin\varphi \\ -\sin\varphi & \cos\varphi \end{pmatrix} \begin{pmatrix} T_{13} \\ T_{23} \end{pmatrix}.$$

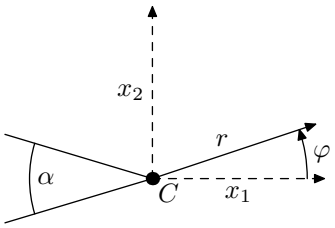

Figure 5.2: Cylindrical coordinate system.

5.2.2 Linear constitutive relation

Asymptotic solutions for the linear elastic model (5.3) in the anti-plane stress setting for an infinite geometry with a V-notch with an end hole, see Figure 5.6, were derived in Zappalorto – Lazzarin (2011). In polar coordinates centered at the center of the end hole C, the leading term of the asymptotic solution takes the form

$$T_{rz} = \frac{K^{IF}}{\sqrt{2\pi}} r^{k_T} \sin(\lambda_L \varphi) \left[1 - \left(\frac{r_c}{r}\right)^{2\lambda_L}\right], \quad T_{\varphi z} = \frac{K^{IF}}{\sqrt{2\pi}} r^{k_T} \cos(\lambda_L \varphi) \left[1 + \left(\frac{r_c}{r}\right)^{2\lambda_L}\right], \tag{5.15}$$

where

$$\lambda_L = \frac{\pi}{2\pi - \alpha}, \quad k_T = \frac{\alpha - \pi}{2\pi - \alpha}, \tag{5.16}$$

the constant K^{IF} is a stress intensity factor, α is the opening angle of the V-notch and r_c is the diameter of the end hole.

Asymptotic solution in the geometry of infinite plate with a V-notch, can be obtained by setting $r_c = 0$ in (5.15). We get that

$$T_{rz} = \frac{K^{IF}}{\sqrt{2\pi}} r^{k_T} \sin(\lambda_L \varphi), \quad T_{\varphi z} = \frac{K^{IF}}{\sqrt{2\pi}} r^{k_T} \cos(\lambda_L \varphi), \tag{5.17}$$

where λ_L and k_T are of the form (5.16), K^{IF} is a stress intensity factor and α is an angle of the V-notch.

When α varies from 0 to π, the exponent of the singularity k_T is changing from $-1/2$ to 0. In Neuber (1961), it was noted that *'As the notch angle influence indeed is insignificant, relation for $\alpha = 0$ can be used approximately for any deformation law and any notch angle'*. This observation is utilized in computer simulations where we use small V-notch angle $\alpha = 1°$ to approximate the solution for the crack geometry where $\alpha = 0$.

5.2.3 Power law materials

The power law solid with the constitutive equation of the type

$$\sigma(|\mathbf{T}_v|) = |\mathbf{T}_v|^{q'-2}, \tag{5.18}$$

which can be understood as a simplified relationship (5.2) for $|\mathbf{T}_v| \to \infty$, when subject to the anti-plane strain setting[3] in the infinite V-notch geometry, was first studied in Neuber (1961). Derivation of asymptotic solutions involves using hodograph transformation, see Atkinson – Champion (1984). This problem was studied

[3] Anti-plane strain setting is in this situation equal to the anti-plane stress setting.

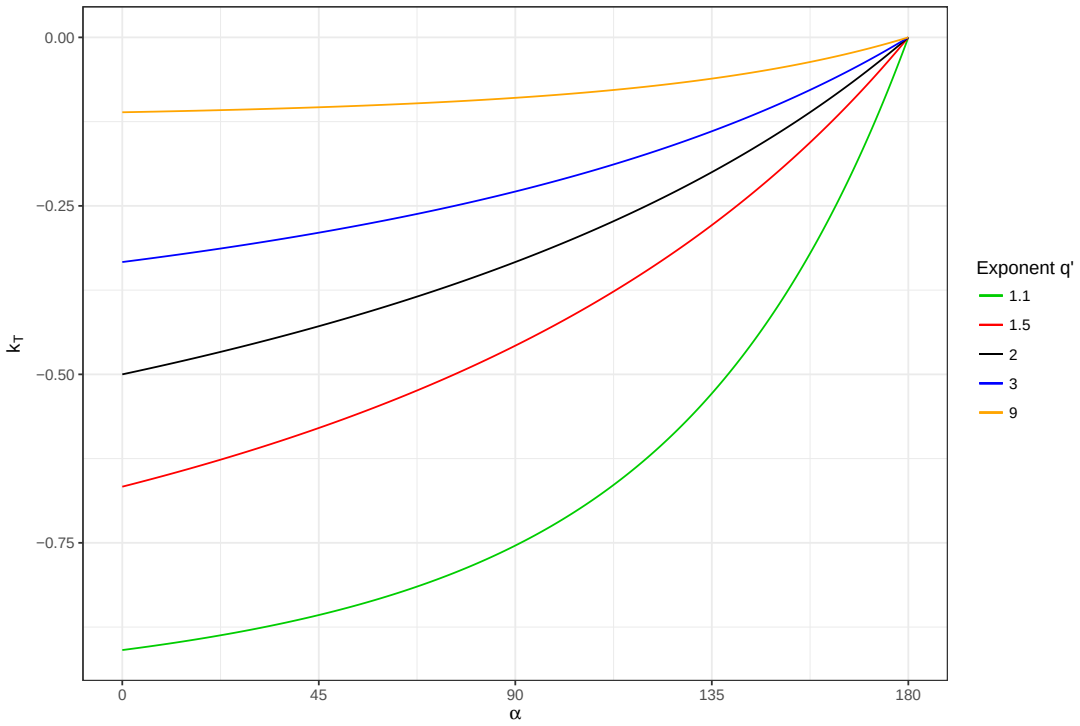

Figure 5.3: Dependence of the exponent k_T on α.

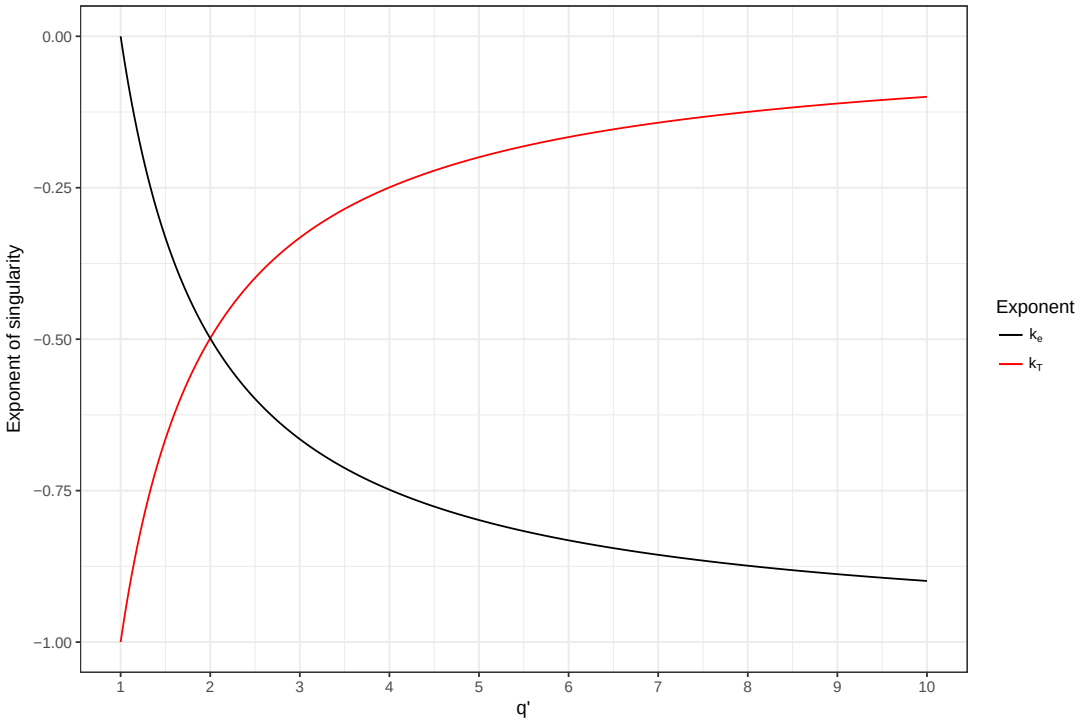

Figure 5.4: Dependence of the exponents k_T and k_e on q' for $\alpha = 0$.

in a number of works including Ore – Durban (1988); Gross – Yu (1987); Shaorui – Chao (1990). Asymptotic formulas in the polar coordinates centered at the V-notch tip C, which include implicit functional relationships for φ, can be found in Bassani (1984). Here we include the dependence of stress on the distance from the V-notch tip, which is of the form

$$\mathbf{T}_v \sim r^{k_T}, \quad k_T = \frac{-1}{\frac{q'}{2} + \left[\left(\frac{q'-2}{2}\right)^2 + \lambda^2(q'-1)\right]^{\frac{1}{2}}}, \quad \lambda = \frac{\pi}{\pi - \alpha}. \tag{5.19}$$

Figure 5.3 shows the dependence of the exponent of the singularity k_T on α for various q'. When considering the constitutive equation (5.18), the singularity of strain is of the form

$$\varepsilon_v \sim r^{k_e}, \quad k_e = (q'-1)k_T. \tag{5.20}$$

Upon setting $q' = 2$, we obtain $k_T = k_e$ and the exponent of singularity is the same as for the linear model (5.16). Note that for $q' \neq 2$, the singularities of stress and strain are not equal. For $\alpha = 0$, the dependence of the exponents k_T and k_e on q' is shown in Figure 5.4.

5.3 Setting of finite element simulations

In this section, we delineate the concrete setting that we follow when performing computer simulations. First, we depict geometries of the computational domains and describe boundary conditions that we use. Then, we define variational formulation of the problem on finite dimensional spaces. Finally, we tabulate the parameters of the models of the titanium alloys that we simulate.

5.3.1 Computational domains

We use three types of geometries of the computational domain B, each geometry consists of the unit square with a notch on its left side, see Figures 5.5, 5.6 and 5.7. We use SI units, therefore the edge length of the square is 1 m.

V geometry

V geometry of a computational domain, see Figure 5.5, consists of the unit square plate with a V shaped notch and the opening angle α, where $0 < \alpha < \pi$. When $\alpha < \pi/2$, the left part of the boundary consists of four segments $\Gamma_4 = \Gamma_4^A \cup \Gamma_4^B \cup \Gamma_4^C \cup \Gamma_4^D$ and the tip of the V notch is at point $C = (0.5, 0.5)$. When $\pi/2 \leq \alpha < \pi$, the left part of the boundary consists of two segments $\Gamma_4 = \Gamma_4^A \cup \Gamma_4^B$ and the tip of the V notch is at point

$$C = \left(\frac{0.5}{\tan(\frac{\alpha}{2})}, 0.5\right).$$

VO geometry

VO geometry of a computational domain, see Figure 5.6, is a modified V geometry where a circle of radius $r_c < 0.5$ centered at the tip of the V-notch C is subtracted

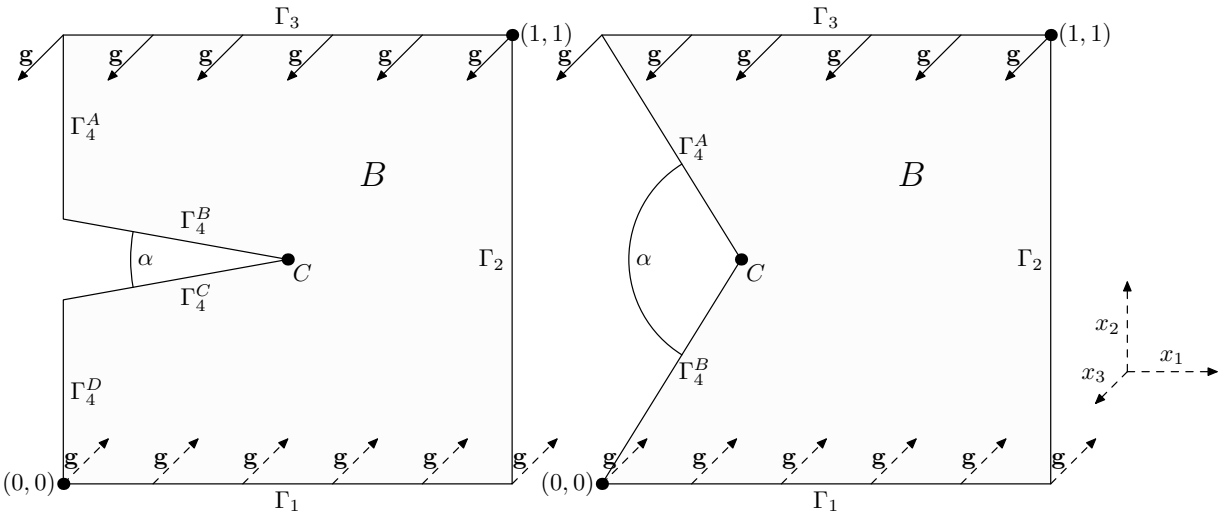

Figure 5.5: V geometry of a computational domain. On the left, the domain is depicted when $\alpha < \pi/2$. On the right, when $\pi/2 \leq \alpha < \pi$.

from the domain. The geometry is parametrized by angle α and the radius of circle r_c. When $\alpha < \pi/2$, the left part of the boundary consists of five parts $\Gamma_4 = \Gamma_4^A \cup \Gamma_4^B \cup \Gamma_4^C \cup \Gamma_4^D \cup \Gamma_4^E$. When $\pi/2 \leq \alpha < \pi$, the left part of the boundary consists of three parts $\Gamma_4 = \Gamma_4^A \cup \Gamma_4^B \cup \Gamma_4^C$.

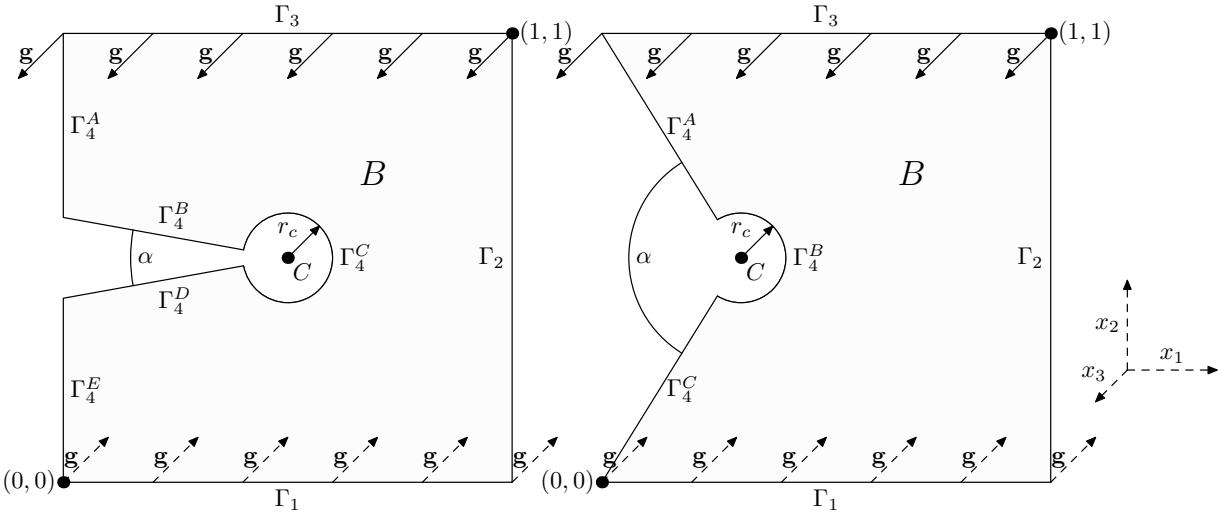

Figure 5.6: VO geometry of a computational domain. On the left, the domain is depicted when $\alpha < \pi/2$. On the right, when $\pi/2 \leq \alpha < \pi$.

VC geometry

VC geometry of a computational domain, see Figure 5.7, is a modified V geometry such that the tip of the V notch is smoothened by the circle arc of radius r_c that is tangent to the V-notch. The geometry is parametrized by angle α and the radius of arc r_c. When $\alpha < \pi/2$, then the left part of the boundary consists of five parts

$\Gamma_4 = \Gamma_4^A \cup \Gamma_4^B \cup \Gamma_4^C \cup \Gamma_4^D \cup \Gamma_4^E$. There is a restriction that the arc fits inside the unit square, which imposes a condition

$$0 < r_c < \frac{0.5 \sin(\frac{\alpha}{2})}{\cos^2(\frac{\alpha}{2})}.$$

The center of the arc is at point

$$C = \left(0.5 - \frac{r_c}{\sin(\frac{\alpha}{2})}, 0.5\right).$$

When $\pi/2 \leq \alpha < \pi$, the left part of the boundary consists of three parts $\Gamma_4 = \Gamma_4^A \cup \Gamma_4^B \cup \Gamma_4^C$. The restriction that the arc fits into the unit square takes the form

$$0 < r_c < \frac{0.5}{\cos(\frac{\alpha}{2})}$$

and the center of the arc is at point

$$C = \left(\frac{0.5}{\tan(\frac{\alpha}{2})} - \frac{r_c}{\sin(\frac{\alpha}{2})}, 0.5\right).$$

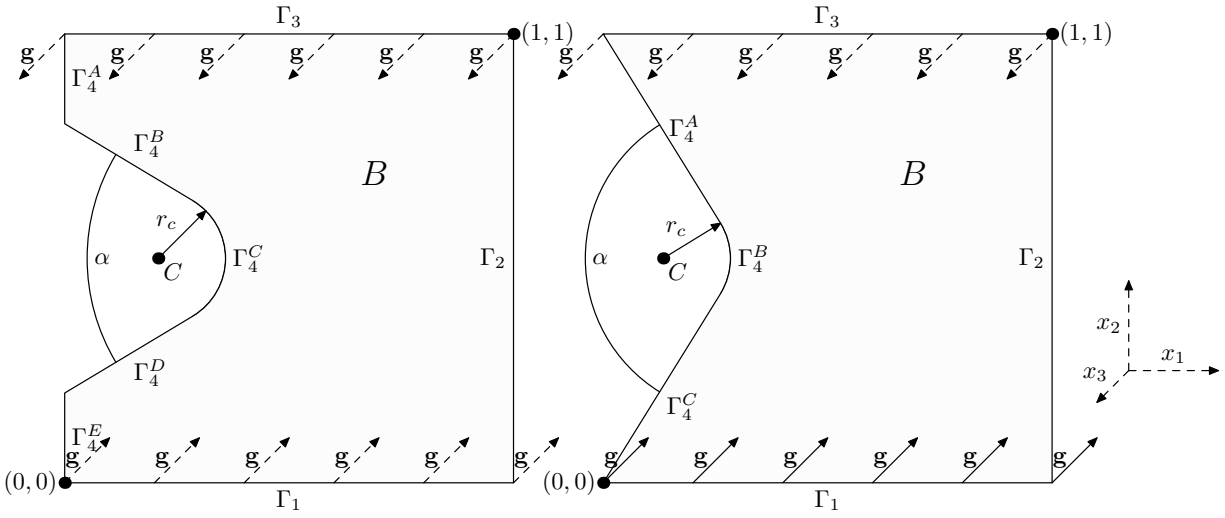

Figure 5.7: VC geometry of a computational domain. On the left, the domain is depicted when $\alpha < \pi/2$. On the right, when $\pi/2 \leq \alpha < \pi$.

5.3.2 Boundary conditions

We impose the same boundary conditions on all computational domains. The domain is loaded by the shearing force $F = 100\,\text{MPa}$ that acts on the top and on the bottom edge of the unit square. Therefore $g = F$ on Γ_3 (top), $g = -F$ on Γ_1 (down) and $g = 0$ on the remaining parts of the boundary. The boundary condition (5.13) takes the form

$$A_0^g(x_1, x_2) = \begin{cases} -Fx_1 & \text{on } \Gamma_1, \\ -F & \text{on } \Gamma_2, \\ -Fx_1 & \text{on } \Gamma_3, \\ 0 & \text{on } \Gamma_4, \end{cases}$$

where $F = 1 \times 10^8$ Pa.

5.3.3 Variational problem on the space of finite elements

Now we formulate the boundary value problem from Definition 5.2 as a variational problem on the space of finite elements. To derive the weak formulation, we multiply the first equation in (5.14) by a test function $\phi \in C_c^\infty(B)$, integrate over B and use the integration by parts. For the power-law solid (5.2) where σ has the form

$$\sigma(|\mathbf{T}|) \sim \left(1 + |\mathbf{T}|^2\right)^{\frac{q'-2}{2}},$$

we seek the function $A \in W^{1,q'}(B)$ that satisfies the formulation

$$\begin{aligned} \int_B \sigma(|\nabla A|)\nabla A.\nabla\phi \,\mathrm{d}x = 0 \quad & \forall \phi \in C_c^\infty(B), \\ A = A_0^g \quad & \text{on } \partial B, \end{aligned} \tag{5.21}$$

where A_0^g is defined by (5.13). When the response is given by Hooke's law (5.3), where σ is a constant, we set $q' = 2$ and seek Airy's function in the space $A \in W^{1,2}(B)$.

In Section A.2.6, (p. 141), important definitions and results from numerical analysis are summarized. To find numerical solutions, we first construct triangulation $\mathcal{T}_h$ of the computational domain B. We employ a finite dimensional space V_h over $\mathcal{T}_h$ and its counterpart with zero trace

$$V_h^0 = \{u \in V_h, u|_{\partial B} = 0\}.$$

Definition 5.3 (Airy's solution to discrete Problem (P) in anti-plane stress setting). *Let $B \subset \mathbb{R}^2$ be a computational domain described in Figure 5.5, 5.6 or 5.7. Let $\mathcal{T}_h$ be a triangulation over $\overline{B}$. Let the functions (σ, g) represent the problem data. We say that the function $A_h \in V_h$ is Airy's solution to the discrete Problem (P) in the anti-plane stress setting, if*

$$\begin{aligned} \sum_{T\in\mathcal{T}_h} \int_T \sigma(|\nabla A_h|)\nabla A_h.\nabla\phi_h \,\mathrm{d}x = 0 \quad & \forall \phi_h \in V_h^0, \\ A_h = A_0^g \quad & \text{on } \partial B, \end{aligned} \tag{5.22}$$

where A_0^g is the function defined by (5.13).

As V_h we use the space of piece-wise continuous second order polynomials $V_h = X_h^2$, where

$$X_h^2 = \{u_h \subset C^0(\overline{B}), u_h|_T \in P^2(T), \forall T \in \mathcal{T}_h\},$$

for details, see Definition A.108, (p. 142). We use Langrange elements of second order, which form the space X_h^2 and that are conforming. Lemma A.110, (p. 142) yields $X_h^2 \subseteq W^{1,q'}(B)$ and therefore we might omit the sum over elements in (5.22). For the problems of the type (5.22), the quasi-norm interpolation error estimates were established, see Ebmeyer – Liu (2005).

For solving the problem computationally, we have developed software in Python that utilize FEniCS library, see Alnæs et al. (2015). To find a solution for nonlinear power-law problems, we use damped Newton method, where the convergence criterion was based on the L^2 norm of the residuum. Computationally intensive tasks were performed using a cluster infrastructure supported by the Charles university, see http://cluster.karlin.mff.cuni.cz/.

5.3.4 Parameters of models for simulations of titanium alloys

We study the shear behavior of three different titanium alloys, namely Gum Metal, *Ti-30Nb-10Ta-5Zr* alloy and *Ti-24Nb-4Zr-7.9Sn* alloy. For each alloy, we compare four different models identified in Chapter 3. The model labelled NLB is the power law model with parameters obtained as the best fit under highly nonlinear bulk response condition (3.27). The model NLS is a model with parameters obtained under the highly nonlinear shear response condition (3.28) and the model NLO is the model obtained when maximizing the objective function (3.30). The model LIN is a linear model (5.3), where the shear modulus is given by Voigt-Reuss-Hill approximation, see Section 3.3.1. Original model (3.19) has the parameters (τ_0, s', K, q', μ). In the anti-plane stress setting, the parameters s' and K do not enter the model (5.2), and therefore we work with a reduced set of parameters (τ_0, q', μ). Parameters of computations are summarized in Table 5.1.

Material	Model	μ_L[GPa]	τ_0[GPa]	q'	μ[GPa]
Gum Metal	LIN1	23.5	-	-	-
Gum Metal	NLO1	-	0.5	1.92	20.9
Gum Metal	NLB1	-	0.5	2.23	20.2
Gum Metal	NLS1	-	0.5	7.65	18 668
Ti-30Nb-10Ta-5Zr	LIN2	21.75	-	-	-
Ti-30Nb-10Ta-5Zr	NLO2	-	0.5	1.88	24.5
Ti-30Nb-10Ta-5Zr	NLB2	-	0.5	2.49	22.3
Ti-30Nb-10Ta-5Zr	NLS2	-	0.5	9.15	1001
Ti-24Nb-4Zr-7.9Sn	LIN3	22.05	-	-	-
Ti-24Nb-4Zr-7.9Sn	NLO3	-	0.5	2.14	18.6
Ti-24Nb-4Zr-7.9Sn	NLB3	-	0.5	2.99	16.5
Ti-24Nb-4Zr-7.9Sn	NLS3	-	0.5	15.68	3378

Table 5.1: Parameters of computer simulations. Linear model LIN with the response (5.3) is parametrized by the shear modulus μ_L, from Table 3.6. Power law models NLB, NLS and NLO with the response (5.2) are parametrized by τ_0, q' and μ. Data for model NLB are based on Table 3.9, data for model NLS are based on Table 3.11. Data for model NLO are based on Table 3.13

5.4 Results

We have performed the following set of simulations. For each domain type, we computed solutions for $\alpha \in \{1°, 2°, \dots 70°, 80° \dots 180°\}$. For domains *VO* and *VC* and for each angle α, we considered $r_c \in \{0.05, 0.01, 0.005, 0.001\}$. In total, we use 712 different geometries of the computational domain. For each geometry, we generate one basic mesh and use its 5 adaptive refinements. In total, we use 4272 different meshes. Meshes were adaptively refined according to the local error estimator for the linear problem, this process is illustrated in Figures 5.8, 5.9 and 5.10 for three different geometries. Mesh construction and refinement was performed using COMSOL Multiphysics software, version 3.5*a*, see COMSOL AB (2008). On each mesh, we performed computer simulations for 12 different model settings

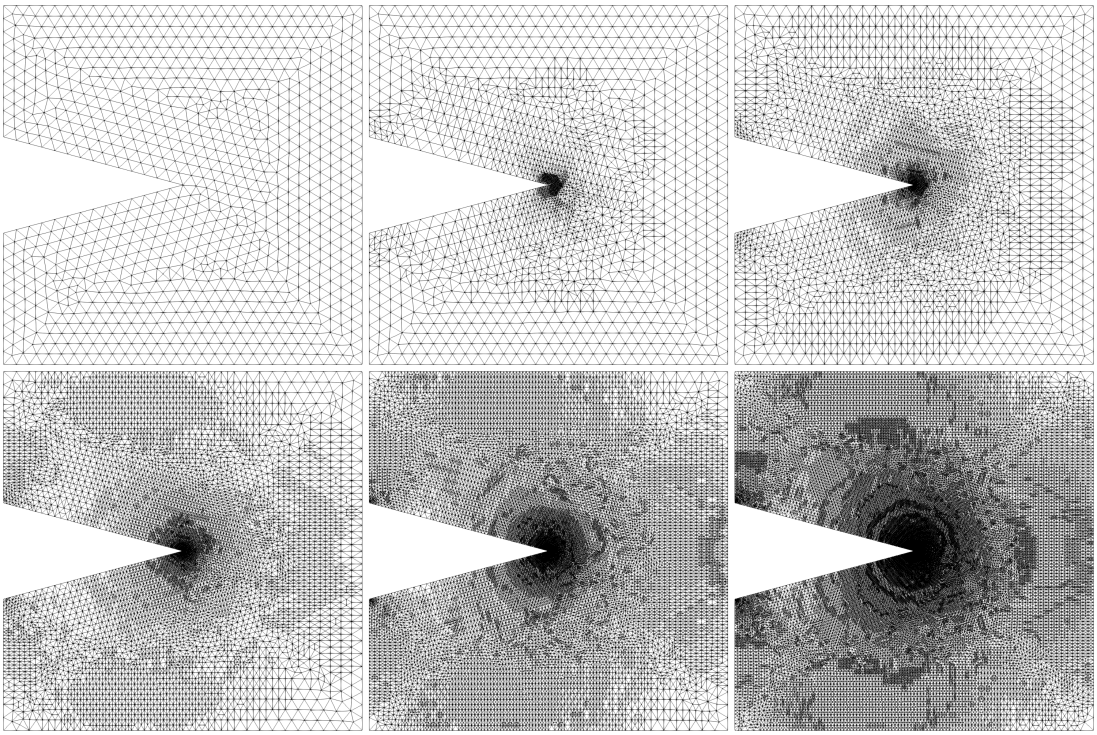

Figure 5.8: Visualization of the adaptive refinement of the mesh in 5 steps. In upper left, there is the unrefined mesh and in lower right, there is the mesh after 5 refinemet steps. Visualisation for V geometry, $\alpha = 30°$.

described in Table 5.1, see Section 5.3.4. Therefore, in total we generated solutions of 51 264 problems.

5.4.1 Global convergence of solutions

The primary goal of computer simulations is to study distributions of strains and stresses for each model in each studied geometry and to find differences between linear and nonlinear solutions and between solutions of problems NLO, NLB and NLS that differ in the magnitude of the shear response exponent q'.

Prior to studying this, we investigate how accurate and reliable the solutions are. In this section, we study the global stability of solutions with respect to a refinement level. To measure the relative error of solution with respect to the reference solution, we define the relative error norm.

Definition 5.4 (Relative error norm). *Let A_{ref} be a function (reference solution) on a finite dimensional space V_h. Let A be a function (solution) on a finite dimensional space $Q_h \subseteq V_h$. Let $\|.\|$ denote a norm on V_h. Then the relative error norm of A with respect to A_{ref} is defined through*

$$\|A\|^{rel} = \frac{\|A - A_{ref}\|}{\|A_{ref}\|}. \tag{5.23}$$

For a sequence of adaptively refined meshes, the triangulation on one level is a subset of triangulations on levels above. Let V_h^i be a finite dimensional space of solutions on the i-th refinement level, then $V_h^0 \subseteq V_h^1 ... \subseteq V_h^5$. When analysing adaptively refined problems, we use a solution on the densest mesh, that is on the

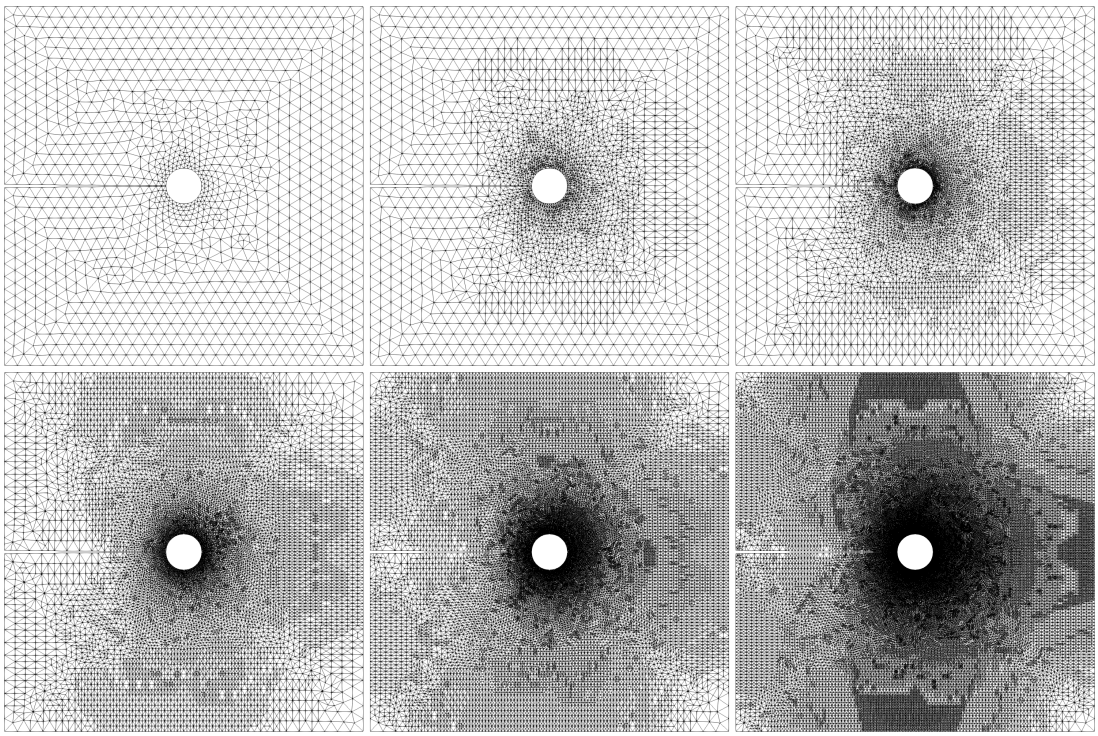

Figure 5.9: Visualization of the adaptive refinement of the mesh in 5 steps. In upper left, there is the unrefined mesh and in lower right, there is the mesh after 5 refinemet steps. Visualisation for VO geometry, $\alpha = 1°$, $r_c = 0.05$.

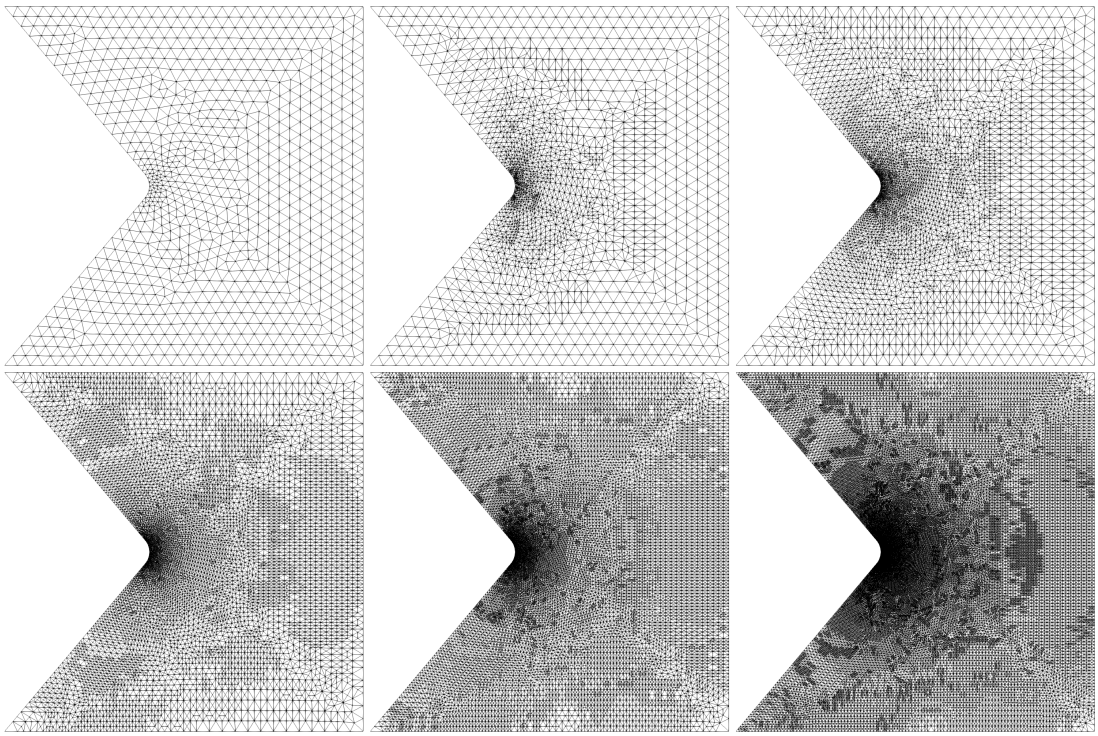

Figure 5.10: Visualization of the adaptive refinement of the mesh in 5 steps. In upper left, there is the unrefined mesh and in lower right, there is the mesh after 5 refinemet steps. Visualisation for VC geometry, $\alpha = 100°$, $r_c = 0.05$.

5-th refinement level, as the reference solution. Then we compute the relative error norm for the solutions computed on croaser meshes. Our spaces V_h^i consists of piece-wise continuous quadratic polynomials. Since $V_h^i \subseteq W^{1,2}(B)$ for $i \in \{0 \dots 5\}$, we use the norm $\|.\| = \|.\|_{1,2}$ in (5.23) for all problems.

Tables of mesh properties and error norms

In Tables 5.2–5.10 we list some important parameters of computations with respect to the mesh refinement. In particular, we list number of elements, number of degrees of freedom, mesh size parameters h_{min} and h_{max} and relative error norms for each problem listed in Table 5.1. For example, $\|A_{NLB2}\|_{1,2}^{rel}$ in a table row denotes the error norms with respect to the mesh refinement for the solution of the problem NLB2. In each table, the error norms for all linear problem are compressed to the single row with a label $\|A_{LIN}\|_{1,2}^{rel}$, because for every mesh, the solution A_{LIN} to a linear problem does not depend on shear modulus μ_L. It means that all linear problems have identical Airy's functions and consequently error norms are identical as well. We have that

$$\|A_{LIN}\|_{1,2}^{rel} = \|A_{LIN1}\|_{1,2}^{rel} = \|A_{LIN2}\|_{1,2}^{rel} = \|A_{LIN3}\|_{1,2}^{rel}. \tag{5.24}$$

We have chosen the following illustrative set of geometries to include in tables. For V geometry, we include data for $\alpha \in \{1°, 90°, 170°\}$, see Tables 5.2–5.4. For VO geometry, we include data for $\alpha = 2°$ and $r_c \in \{0.001, 0.01, 0.05\}$, see Tables 5.5–5.7. For VC geometry, we include data for $\alpha = 100°$ and $r_c \in \{0.001, 0.01, 0.05\}$, see Tables 5.8–5.10.

Refinement	0	1	2	3	4	5
Elements	1982	4571	9767	20 550	43 181	88 777
DOFs	4105	9314	19 746	41 411	86 922	178 284
h_{min}	0.02	0.002	0.0006	0.0001	3×10^{-5}	2×10^{-5}
h_{max}	0.04	0.04	0.04	0.04	0.04	0.04
$\|A_{LIN}\|_{1,2}^{rel}$	0.06	0.02	0.01	0.004	0.002	0.0
$\|A_{NLB1}\|_{1,2}^{rel}$	0.05	0.02	0.007	0.003	0.001	0.0
$\|A_{NLB2}\|_{1,2}^{rel}$	0.04	0.01	0.005	0.002	0.0009	0.0
$\|A_{NLB3}\|_{1,2}^{rel}$	0.03	0.008	0.003	0.001	0.0005	0.0
$\|A_{NLO1}\|_{1,2}^{rel}$	0.07	0.03	0.01	0.005	0.003	0.0
$\|A_{NLO2}\|_{1,2}^{rel}$	0.07	0.03	0.01	0.006	0.003	0.0
$\|A_{NLO3}\|_{1,2}^{rel}$	0.05	0.02	0.008	0.003	0.002	0.0
$\|A_{NLS1}\|_{1,2}^{rel}$	0.01	0.003	0.0008	0.0002	0.0001	0.0
$\|A_{NLS2}\|_{1,2}^{rel}$	0.01	0.002	0.0007	0.0002	0.000 09	0.0
$\|A_{NLS3}\|_{1,2}^{rel}$	0.01	0.002	0.0006	0.0002	0.0001	0.0

Table 5.2: Mesh properties and error norms of the solutions with respect to the refinement level for computational domain V with $\alpha = 1°$. For detailed description of row labels, see Section 5.4.1 and Table 5.1.

Refinement	0	1	2	3	4	5
Elements	1510	3709	8221	17 243	35 404	73 569
DOFs	3145	7564	16 644	34 820	71 325	147 826
h_{min}	0.02	0.002	0.0006	0.0001	6×10^{-5}	2×10^{-5}
h_{max}	0.04	0.04	0.04	0.04	0.04	0.04
$\|A_{LIN}\|_{1,2}^{rel}$	0.02	0.005	0.002	0.0008	0.0003	0.0
$\|A_{NLB1}\|_{1,2}^{rel}$	0.02	0.004	0.001	0.0006	0.0002	0.0
$\|A_{NLB2}\|_{1,2}^{rel}$	0.02	0.003	0.001	0.0004	0.0002	0.0
$\|A_{NLB3}\|_{1,2}^{rel}$	0.01	0.002	0.0007	0.0003	0.0001	0.0
$\|A_{NLO1}\|_{1,2}^{rel}$	0.02	0.005	0.002	0.0009	0.0003	0.0
$\|A_{NLO2}\|_{1,2}^{rel}$	0.02	0.005	0.002	0.0009	0.0004	0.0
$\|A_{NLO3}\|_{1,2}^{rel}$	0.02	0.004	0.001	0.0006	0.0002	0.0
$\|A_{NLS1}\|_{1,2}^{rel}$	0.007	0.001	0.0003	0.0002	0.000 06	0.0
$\|A_{NLS2}\|_{1,2}^{rel}$	0.007	0.0009	0.0003	0.0001	0.000 06	0.0
$\|A_{NLS3}\|_{1,2}^{rel}$	0.006	0.0008	0.0003	0.0002	0.000 09	0.0

Table 5.3: Mesh properties and error norms of the solutions with respect to the refinement level for computational domain V with $\alpha = 90°$. For detailed description of row labels, see Section 5.4.1 and Table 5.1.

Refinement	0	1	2	3	4	5
Elements	1956	4491	9348	18 920	38 053	74 764
DOFs	4025	9128	18 909	38 163	76 588	150 153
h_{min}	0.02	0.002	0.001	0.0003	0.0002	8×10^{-5}
h_{max}	0.04	0.04	0.04	0.04	0.04	0.03
$\|A_{LIN}\|_{1,2}^{rel}$	0.0007	0.0001	0.000 03	0.000 01	0.000 005	0.0
$\|A_{NLB1}\|_{1,2}^{rel}$	0.0007	0.0001	0.000 03	0.000 01	0.000 005	0.0
$\|A_{NLB2}\|_{1,2}^{rel}$	0.0007	0.0001	0.000 03	0.000 01	0.000 005	0.0
$\|A_{NLB3}\|_{1,2}^{rel}$	0.0007	0.0001	0.000 03	0.000 01	0.000 005	0.0
$\|A_{NLO1}\|_{1,2}^{rel}$	0.0007	0.0001	0.000 03	0.000 01	0.000 005	0.0
$\|A_{NLO2}\|_{1,2}^{rel}$	0.0008	0.0001	0.000 03	0.000 01	0.000 005	0.0
$\|A_{NLO3}\|_{1,2}^{rel}$	0.0007	0.0001	0.000 03	0.000 01	0.000 005	0.0
$\|A_{NLS1}\|_{1,2}^{rel}$	0.0006	0.0001	0.000 02	0.000 01	0.000 004	0.0
$\|A_{NLS2}\|_{1,2}^{rel}$	0.0005	0.000 07	0.000 02	0.000 009	0.000 004	0.0
$\|A_{NLS3}\|_{1,2}^{rel}$	0.0005	0.000 07	0.000 02	0.000 009	0.000 004	0.0

Table 5.4: Mesh properties and error norms of the solutions with respect to the refinement level for computational domain V with $\alpha = 170°$. For detailed description of row labels, see Section 5.4.1 and Table 5.1.

Refinement	0	1	2	3	4	5
Elements	4303	11 738	26 091	54 303	116 802	251 434
DOFs	8858	23 749	52 620	109 212	234 445	504 129
h_{min}	0.0002	0.0002	0.0002	0.0001	6×10^{-5}	4×10^{-5}
h_{max}	0.04	0.04	0.04	0.04	0.04	0.02
$\|A_{LIN}\|_{1,2}^{rel}$	0.001	0.0009	0.0008	0.0007	0.0004	0.0
$\|A_{NLB1}\|_{1,2}^{rel}$	0.001	0.0007	0.0006	0.0006	0.0003	0.0
$\|A_{NLB2}\|_{1,2}^{rel}$	0.001	0.0006	0.0005	0.0005	0.0002	0.0
$\|A_{NLB3}\|_{1,2}^{rel}$	0.001	0.0005	0.0004	0.0003	0.0002	0.0
$\|A_{NLO1}\|_{1,2}^{rel}$	0.001	0.001	0.0009	0.0008	0.0004	0.0
$\|A_{NLO2}\|_{1,2}^{rel}$	0.001	0.001	0.001	0.0009	0.0005	0.0
$\|A_{NLO3}\|_{1,2}^{rel}$	0.001	0.0008	0.0007	0.0006	0.0003	0.0
$\|A_{NLS1}\|_{1,2}^{rel}$	0.001	0.0003	0.0002	0.0001	0.000 07	0.0
$\|A_{NLS2}\|_{1,2}^{rel}$	0.001	0.0003	0.0002	0.0001	0.000 07	0.0
$\|A_{NLS3}\|_{1,2}^{rel}$	0.001	0.0003	0.0002	0.0001	0.000 07	0.0

Table 5.5: Mesh properties and error norms of the solutions with respect to the refinement level for computational domain VO with $\alpha = 2°$ and $r_c = 0.001$. For detailed description of row labels, see Section 5.4.1 and Table 5.1.

Refinement	0	1	2	3	4	5
Elements	2786	6410	13 116	27 252	56 041	119 673
DOFs	5757	13 015	26 471	54 947	112 712	240 248
h_{min}	0.002	0.002	0.001	0.0007	0.0005	0.0003
h_{max}	0.04	0.04	0.04	0.04	0.04	0.04
$\|A_{LIN}\|_{1,2}^{rel}$	0.003	0.003	0.002	0.0008	0.0003	0.0
$\|A_{NLB1}\|_{1,2}^{rel}$	0.002	0.002	0.002	0.0007	0.0003	0.0
$\|A_{NLB2}\|_{1,2}^{rel}$	0.002	0.002	0.002	0.0006	0.0002	0.0
$\|A_{NLB3}\|_{1,2}^{rel}$	0.002	0.002	0.001	0.0005	0.0002	0.0
$\|A_{NLO1}\|_{1,2}^{rel}$	0.003	0.003	0.002	0.0009	0.0003	0.0
$\|A_{NLO2}\|_{1,2}^{rel}$	0.003	0.003	0.002	0.0009	0.0003	0.0
$\|A_{NLO3}\|_{1,2}^{rel}$	0.003	0.002	0.002	0.0008	0.0003	0.0
$\|A_{NLS1}\|_{1,2}^{rel}$	0.001	0.001	0.0008	0.0003	0.0001	0.0
$\|A_{NLS2}\|_{1,2}^{rel}$	0.001	0.0009	0.0008	0.0003	0.0001	0.0
$\|A_{NLS3}\|_{1,2}^{rel}$	0.001	0.0008	0.0007	0.0003	0.0001	0.0

Table 5.6: Mesh properties and error norms of the solutions with respect to the refinement level for computational domain VO with $\alpha = 2°$ and $r_c = 0.01$. For detailed description of row labels, see Section 5.4.1 and Table 5.1.

Refinement	0	1	2	3	4	5
Elements	2300	6008	12 644	25 906	53 252	111 118
DOFs	4771	12 213	25 549	52 231	107 097	223 117
h_{min}	0.01	0.003	0.002	0.001	0.001	0.0007
h_{max}	0.04	0.04	0.04	0.04	0.04	0.04
$\|A_{LIN}\|_{1,2}^{rel}$	0.006	0.003	0.001	0.0007	0.0006	0.0
$\|A_{NLB1}\|_{1,2}^{rel}$	0.006	0.003	0.001	0.0006	0.0005	0.0
$\|A_{NLB2}\|_{1,2}^{rel}$	0.005	0.003	0.0009	0.0006	0.0005	0.0
$\|A_{NLB3}\|_{1,2}^{rel}$	0.005	0.003	0.0009	0.0006	0.0005	0.0
$\|A_{NLO1}\|_{1,2}^{rel}$	0.006	0.003	0.001	0.0007	0.0006	0.0
$\|A_{NLO2}\|_{1,2}^{rel}$	0.006	0.003	0.001	0.0007	0.0006	0.0
$\|A_{NLO3}\|_{1,2}^{rel}$	0.006	0.003	0.001	0.0007	0.0006	0.0
$\|A_{NLS1}\|_{1,2}^{rel}$	0.003	0.002	0.0007	0.0004	0.0003	0.0
$\|A_{NLS2}\|_{1,2}^{rel}$	0.003	0.002	0.0007	0.0004	0.0003	0.0
$\|A_{NLS3}\|_{1,2}^{rel}$	0.003	0.002	0.0006	0.0004	0.0003	0.0

Table 5.7: Mesh properties and error norms of the solutions with respect to the refinement level for computational domain VO with $\alpha = 2°$ and $r_c = 0.05$. For detailed description of row labels, see Section 5.4.1 and Table 5.1.

Refinement	0	1	2	3	4	5
Elements	2504	6231	13 442	28 305	58 294	127 106
DOFs	5169	12 644	27 159	57 066	117 185	255 155
h_{min}	0.0002	0.0002	0.0002	0.0002	8×10^{-5}	6×10^{-5}
h_{max}	0.04	0.04	0.04	0.04	0.03	0.02
$\|A_{LIN}\|_{1,2}^{rel}$	0.0006	0.0003	0.0002	0.0002	0.0002	0.0
$\|A_{NLB1}\|_{1,2}^{rel}$	0.0006	0.0003	0.0002	0.0002	0.0001	0.0
$\|A_{NLB2}\|_{1,2}^{rel}$	0.0005	0.0003	0.0002	0.0002	0.0001	0.0
$\|A_{NLB3}\|_{1,2}^{rel}$	0.0005	0.0002	0.0002	0.0001	0.0001	0.0
$\|A_{NLO1}\|_{1,2}^{rel}$	0.0006	0.0003	0.0002	0.0002	0.0002	0.0
$\|A_{NLO2}\|_{1,2}^{rel}$	0.0006	0.0003	0.0003	0.0002	0.0002	0.0
$\|A_{NLO3}\|_{1,2}^{rel}$	0.0006	0.0003	0.0002	0.0002	0.0001	0.0
$\|A_{NLS1}\|_{1,2}^{rel}$	0.0004	0.0002	0.0001	0.000 08	0.000 06	0.0
$\|A_{NLS2}\|_{1,2}^{rel}$	0.0004	0.0002	0.0001	0.000 08	0.000 06	0.0
$\|A_{NLS3}\|_{1,2}^{rel}$	0.0004	0.0002	0.0001	0.000 08	0.000 05	0.0

Table 5.8: Mesh properties and error norms of the solutions with respect to the refinement level for computational domain VC with $\alpha = 100°$ and $r_c = 0.001$. For detailed description of row labels, see Section 5.4.1 and Table 5.1.

Refinement	0	1	2	3	4	5
Elements	2028	4681	9667	20 025	40 747	87 058
DOFs	4197	9518	19 550	40 428	82 038	174 841
h_{min}	0.002	0.001	0.001	0.0006	0.0003	0.0002
h_{max}	0.04	0.04	0.04	0.04	0.04	0.02
$\|A_{LIN}\|^{rel}_{1,2}$	0.001	0.001	0.0007	0.0003	0.0001	0.0
$\|A_{NLB1}\|^{rel}_{1,2}$	0.001	0.0009	0.0006	0.0002	0.000 09	0.0
$\|A_{NLB2}\|^{rel}_{1,2}$	0.001	0.0008	0.0006	0.0002	0.000 09	0.0
$\|A_{NLB3}\|^{rel}_{1,2}$	0.0009	0.0007	0.0005	0.0002	0.000 08	0.0
$\|A_{NLO1}\|^{rel}_{1,2}$	0.001	0.001	0.0007	0.0003	0.0001	0.0
$\|A_{NLO2}\|^{rel}_{1,2}$	0.001	0.001	0.0007	0.0003	0.0001	0.0
$\|A_{NLO3}\|^{rel}_{1,2}$	0.001	0.0009	0.0006	0.0002	0.0001	0.0
$\|A_{NLS1}\|^{rel}_{1,2}$	0.0007	0.0005	0.0004	0.0001	0.000 05	0.0
$\|A_{NLS2}\|^{rel}_{1,2}$	0.0006	0.0005	0.0003	0.0001	0.000 05	0.0
$\|A_{NLS3}\|^{rel}_{1,2}$	0.0006	0.0005	0.0003	0.0001	0.000 05	0.0

Table 5.9: Mesh properties and error norms of the solutions with respect to the refinement level for computational domain VC with $\alpha = 100°$ and $r_c = 0.01$. For detailed description of row labels, see Section 5.4.1 and Table 5.1.

Refinement	0	1	2	3	4	5
Elements	1758	4153	8481	17 287	34 819	70 086
DOFs	3645	8460	17 172	34 920	70 138	140 827
h_{min}	0.01	0.002	0.002	0.001	0.0008	0.0006
h_{max}	0.04	0.04	0.04	0.04	0.04	0.03
$\|A_{LIN}\|^{rel}_{1,2}$	0.003	0.001	0.0004	0.0003	0.0002	0.0
$\|A_{NLB1}\|^{rel}_{1,2}$	0.003	0.0009	0.0004	0.0003	0.0002	0.0
$\|A_{NLB2}\|^{rel}_{1,2}$	0.003	0.0009	0.0003	0.0003	0.0002	0.0
$\|A_{NLB3}\|^{rel}_{1,2}$	0.003	0.0008	0.0003	0.0003	0.0002	0.0
$\|A_{NLO1}\|^{rel}_{1,2}$	0.003	0.001	0.0004	0.0003	0.0002	0.0
$\|A_{NLO2}\|^{rel}_{1,2}$	0.003	0.001	0.0004	0.0003	0.0002	0.0
$\|A_{NLO3}\|^{rel}_{1,2}$	0.003	0.0009	0.0004	0.0003	0.0002	0.0
$\|A_{NLS1}\|^{rel}_{1,2}$	0.002	0.0006	0.0002	0.0002	0.0001	0.0
$\|A_{NLS2}\|^{rel}_{1,2}$	0.002	0.0006	0.0002	0.0002	0.0001	0.0
$\|A_{NLS3}\|^{rel}_{1,2}$	0.002	0.0006	0.0002	0.0002	0.0001	0.0

Table 5.10: Mesh properties and error norms of the solutions with respect to the refinement level for computational domain VC with $\alpha = 100°$ and $r_c = 0.05$. For detailed description of row labels, see Section 5.4.1 and Table 5.1.

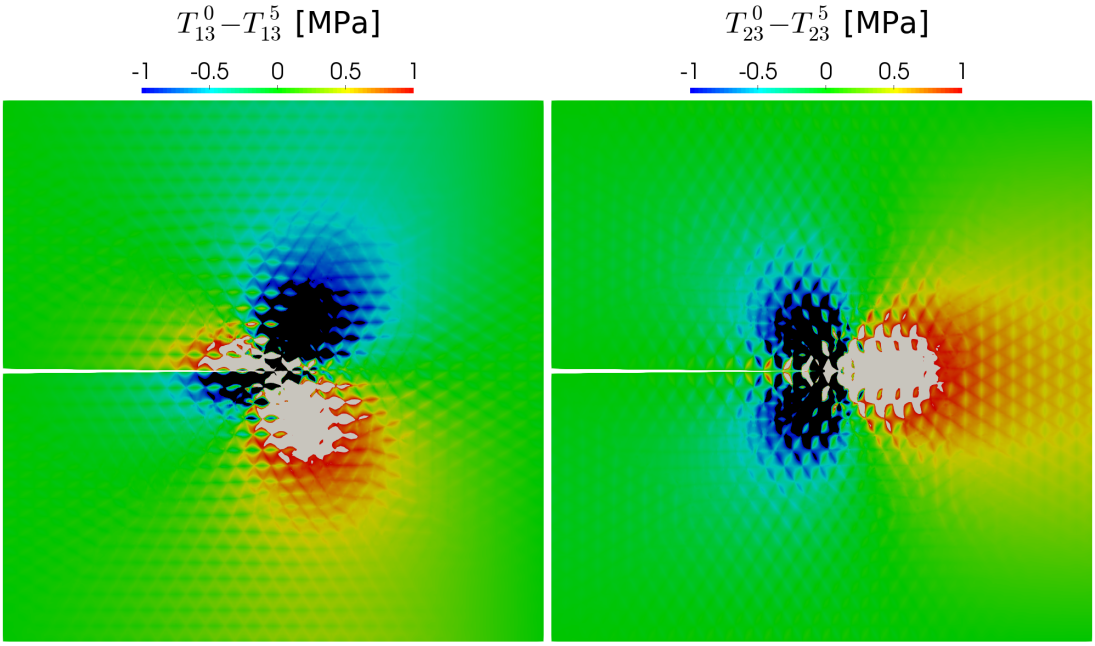

Figure 5.11: Visualization of a local error measured as a difference between the stress components of the solution on unrefined mesh and the solution on fully refined mesh. Visualisation for V geometry, $\alpha = 1°$, model NLB3. Grey areas are above the visualized range, while black areas are below the visualized range.

5.4.2 Local convergence and asymptotic behavior of solutions for V geometry

Let consider the problem of V geometry with $\alpha = 1°$. For this setting, we demonstrate how solutions converge to the reference solution with the mesh refinement and how close solutions to the linearized problem are to the asymptotic solution.

The local error of a solution is measured as the difference of the norm of the stress tensor, or its component, from its reference value on the finest mesh. As expected, the highest local error is in the vicinity of the V-notch tip, see Figure 5.11. With the mesh refinement, the local error is shrinking towards a small area around the V-notch tip, see Figure 5.12. Note that Figures 5.11 and 5.12 were created with a differences in stress ranging from -1 MPa to 1 MPa, while 1 MPa is one hundredth of the value T_{23} prescribed on the boundary.

To compare numerical solutions with asymptotic solutions, we have to determine stress intensity factor K^{IF} in (5.15). Stress intensity factor is a value of the stress T_{23} in the far field, therefore we set $K^{IF} = 100$ MPa, which is the value of the stress on the boundary. Comparison of the numeric solution for linearized problem with the asymptotic formula (5.15) in terms of stress distribution is in Figure 5.13. We can see that asymptotic solutions are a good predictors of the behavior of the numerical solution of linear problems.

5.4.3 Comparison of solutions in V domains

In the following two sections, we compare behavior of numerical solutions for different models and geometries. For simplicity and consistency, we consider only the

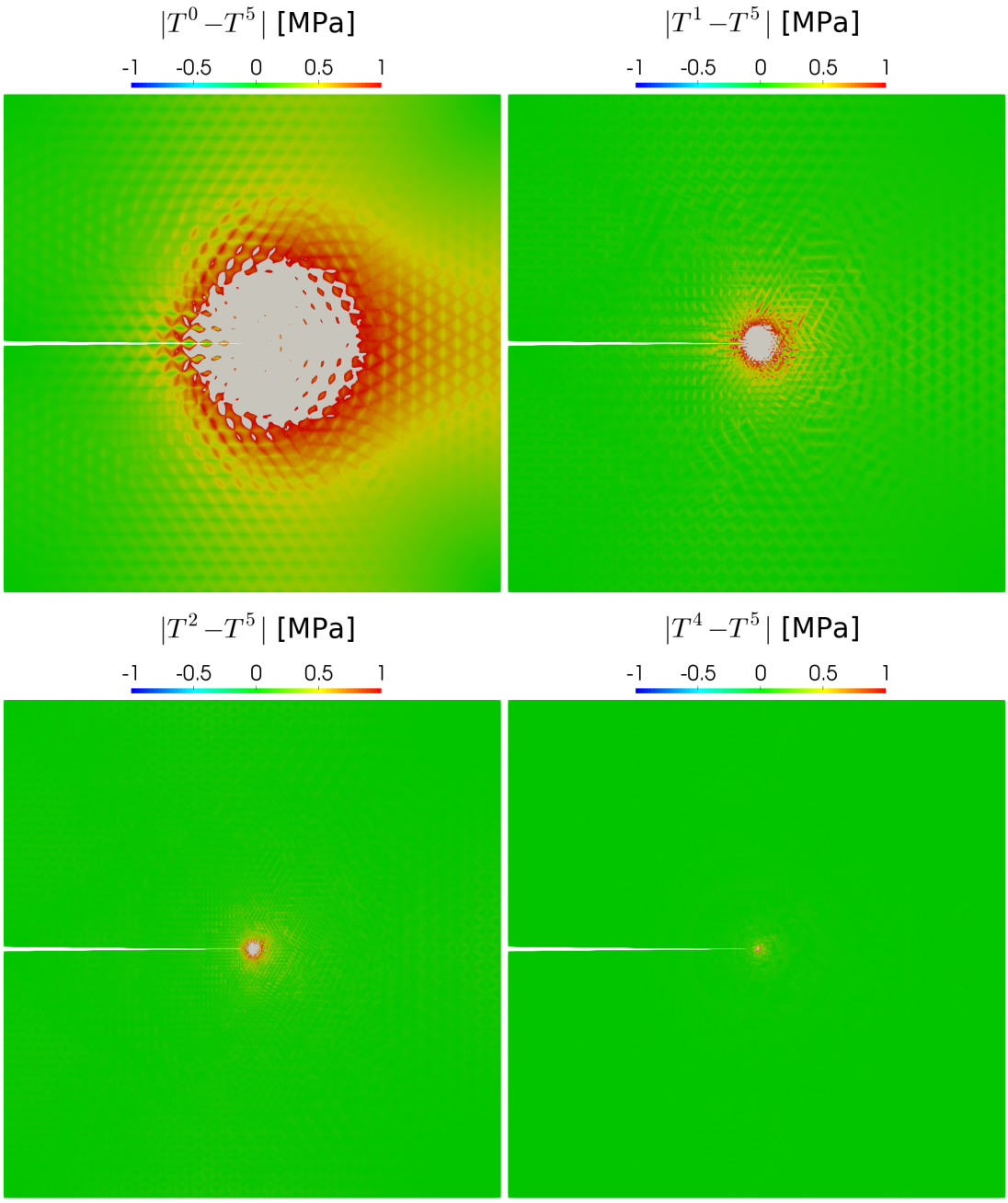

Figure 5.12: Decrease of a local error measured as a norm of difference between the stress tensor of the solution on partially refined mesh and the solution on fully refined mesh. Top left visualization describes difference with the solution on unrefined mesh while bottom right visualization describes difference with the solution on four times refined mesh. Visualisation for V geometry, $\alpha = 1°$, model NLB3. Grey areas are above the visualized range.

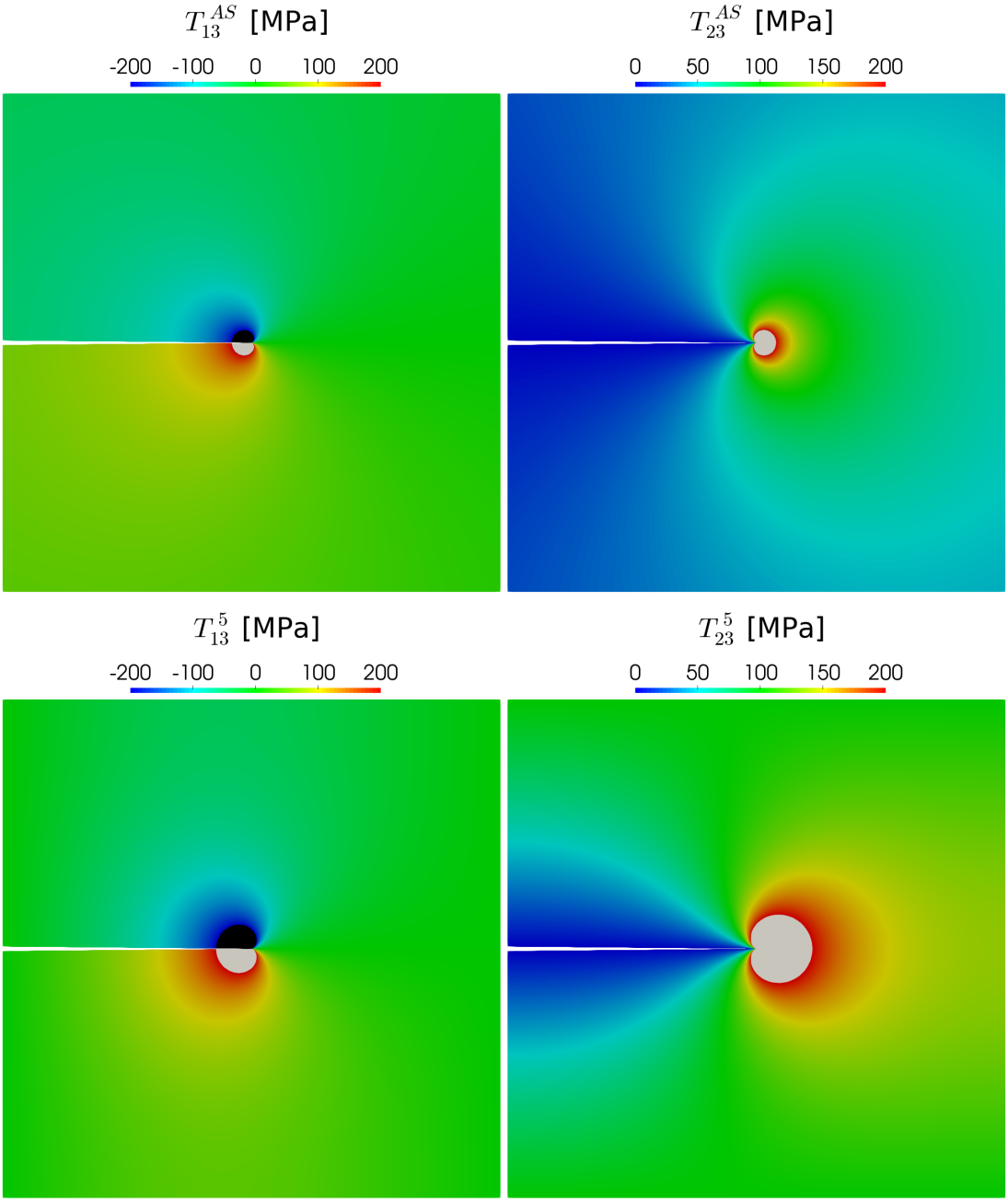

Figure 5.13: Comparison of the stress distribution for the first term of the linear asymptotic solution (5.15) (up) with the numeric solution (down). Computation was performed in V geometry with $\alpha = 1°$, grey areas are above the visualized range, while black areas are below the visualized range.

models NLO2, NLB2 and NLS2 and LIN2, which describe behavior of *Ti-30Nb-10Ta-5Zr* alloy, to perform all comparisons. We show how different exponents of the power-law dependence affect the solution in terms of stress and strain distributions. If we refer to numerical solutions, we refer to the solutions on the finest mesh, unless stated otherwise. In figures, we use the coloring convention, such that grey areas are above the visualized range and black areas are below the visualized range.

First, we consider V geometry with $\alpha = 1°$. In terms of the stress distribution, the size of effect is similar for all considered models, see Figure 5.14. The models NLO2 and NLB2 are close to each other and resemble the stress distribution for the linear model, while the model NLS2, with $q' = 9.15$, has notably different stress distribution from the former two. In terms of the distribution of strain, see Figure 5.15, there are clear differences between all studied models. Most prominent differences are in the strain distribution of the model NLS2, which is completely different from other two models. While the differences in the stress distribution can be entirely attributed to the high power-law exponent, the differences in the strain distribution are also due to the high shear modulus of the NLS2 model $\mu = 1001$ GPa. Therefore, although there is a high singularity (5.20) of the strain in case of the model NLS3, this singularity is concentrated in the close vicinity of the V-notch tip with a limited effect to the whole domain. Values of stress and strain over the line from the V-notch tip to the right, which is denoted $\varphi = 0°$ and to the top, which is denoted $\varphi = 90°$ are depicted in Figure 5.16.

5.4.4 Comparison of solutions in VO and VC domains

Now, we focus on geometries VO and VC that are smoothened by a circle or an arc of diameter r_c. We consider $\alpha = 90°$ and compare the behavior of the models LIN2, NLO2, NLB2 and NLS2.

In VO geometry, see Figure 5.7, we consider $r_c = 0.05$. The stress distribution is visualized in Figure 5.17. The distribution of strain is visualized in Figure 5.18. We also created plots of stress and strain over the line from the center of the end hole C to the right, which is denoted $\varphi = 0°$ and to the top, which is denoted $\varphi = 90°$, see Figure 5.19.

In VC geometry, see Figure 5.7, we consider $r_c = 0.01$. Visualizations of the stress and strain distributions are in Figure 5.20 and Figure 5.21 respectively. We construct plots of stress and strain over the line from the smothened tip, that is in case of VC geometry the point $C + (r_c, 0)$ to the right, which is denoted $\varphi = 0°$ and to the top, which is denoted $\varphi = 90°$, see Figure 5.22.

From stress and strain distributions for studied models, we confirm that there is no singularity of stress and strain. However, with shrinking r_c, there is still evident that there is a stress and strain concentration around the end hole or the end arc.

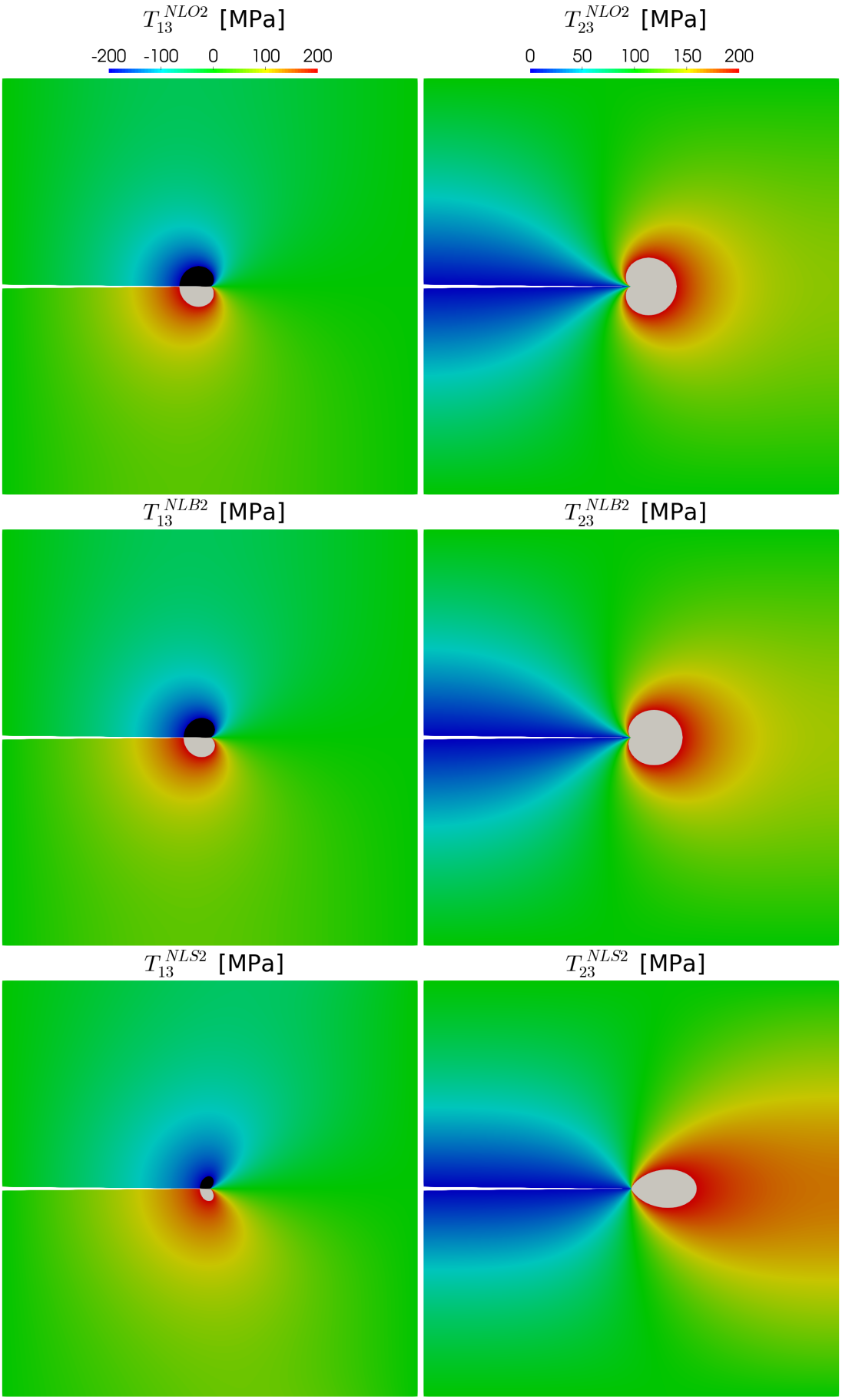

Figure 5.14: Comparison of the stress distributions in V geometry with $\alpha = 1°$ for models NLO2, NLB2, NLS2.

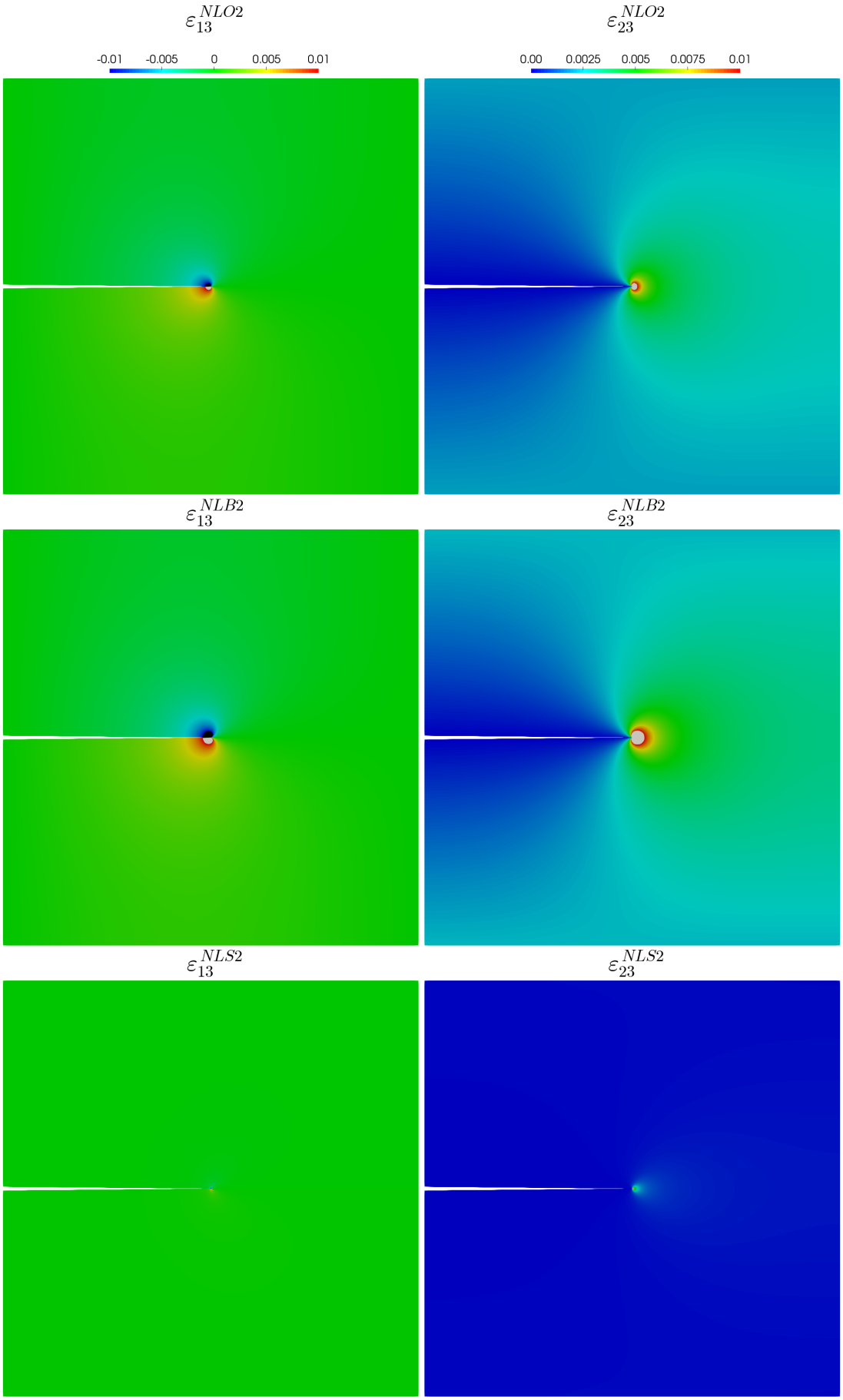

Figure 5.15: Comparison of the strain distributions in V geometry with $\alpha = 1°$ for models NLO2, NLB2, NLS2.

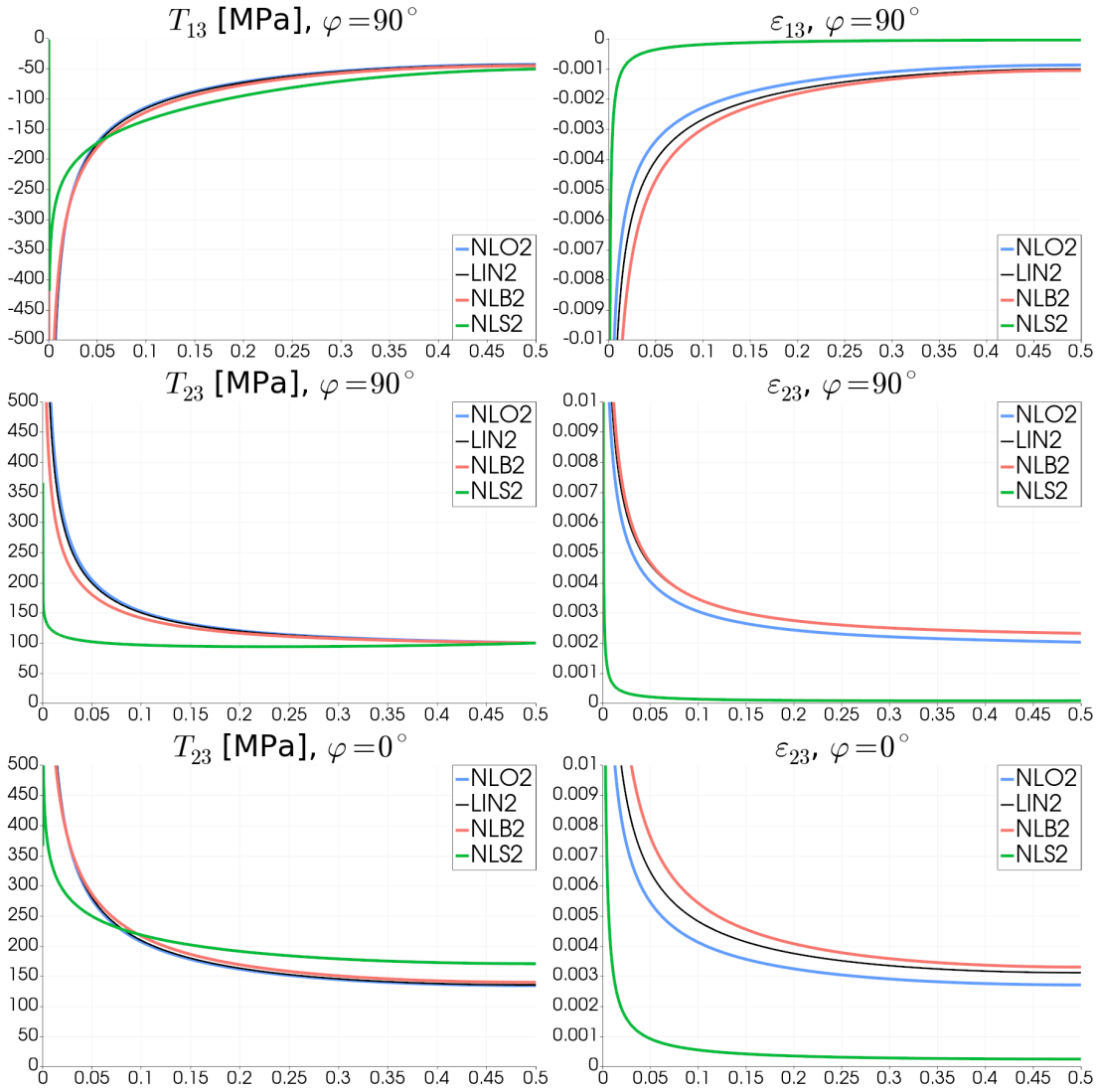

Figure 5.16: Asymptotic behavior of stress and strain for models LIN2, NLO2, NLB2 and NLS2 in V geometry with $\alpha = 1°$. The plots are created over the line starting at the V-notch tip and ending either at point $(1, 0.5)$, which is denoted $\varphi = 0°$, or at point $(0.5, 1)$, which corresponds to $\varphi = 90°$.

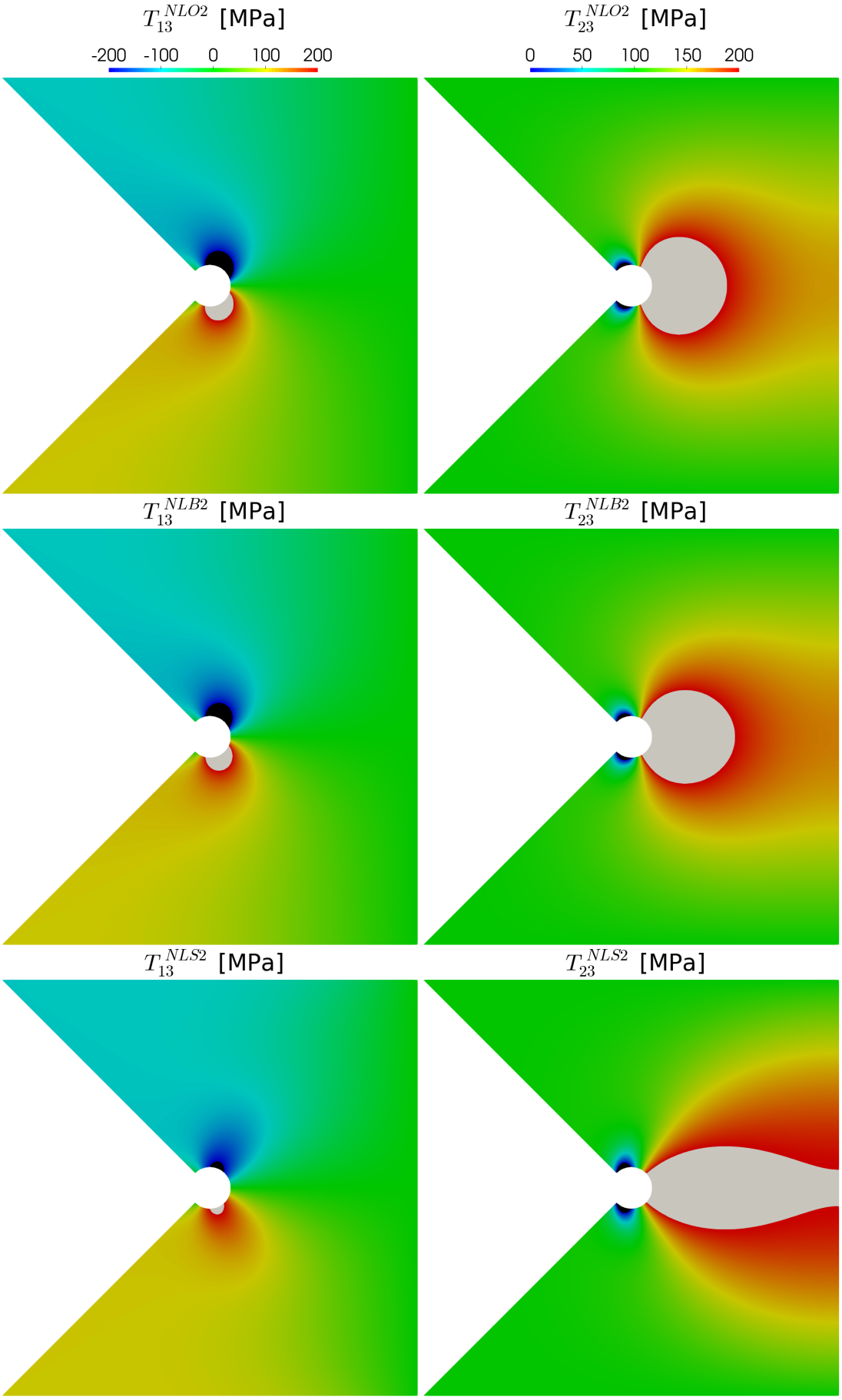

Figure 5.17: Comparison of stress distributions in VO geometry with $\alpha = 90°$ and $r_c = 0.05$ for models NLO2, NLB2, NLS2.

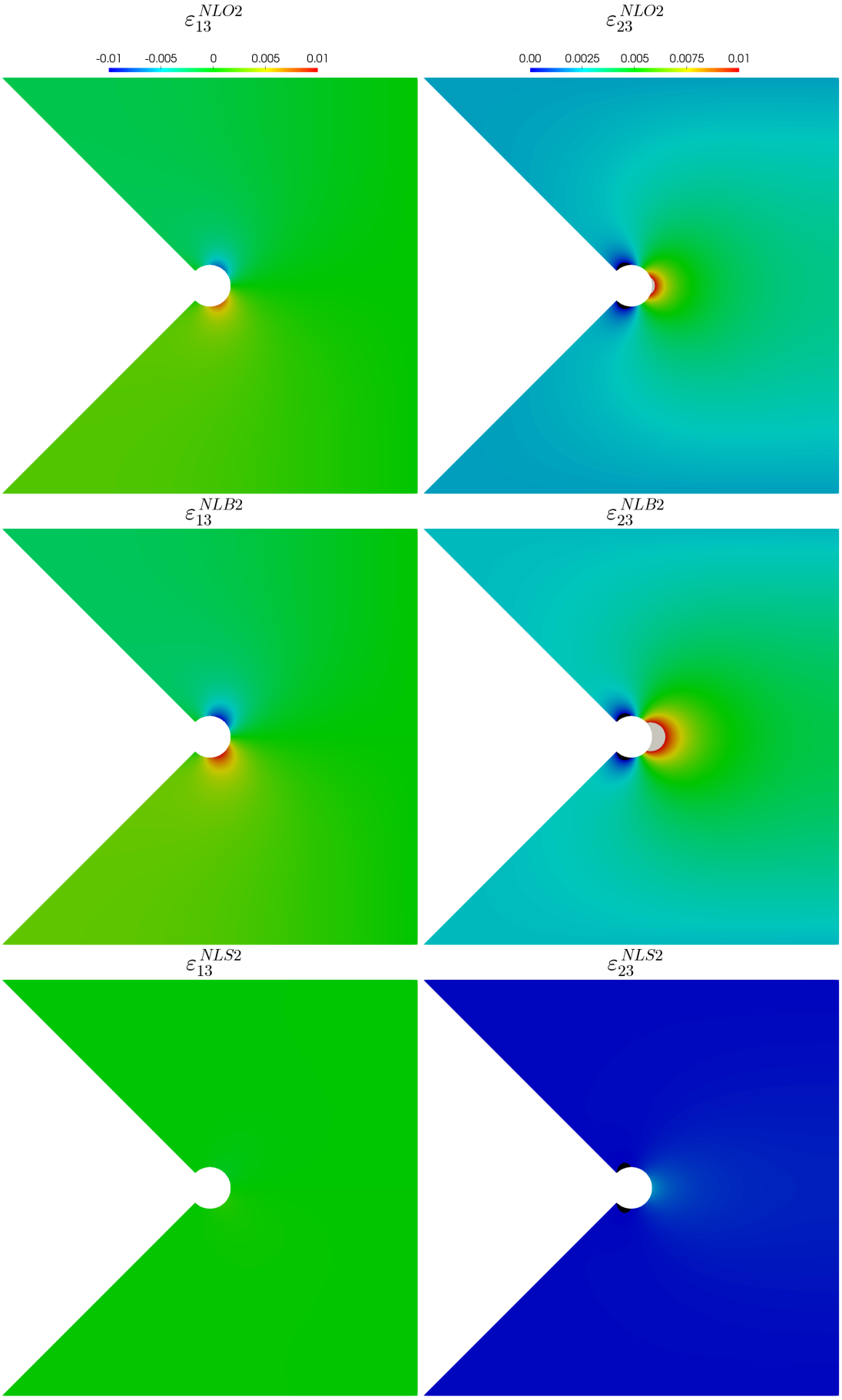

Figure 5.18: Comparison of strain distributions in VO geometry with $\alpha = 90°$ and $r_c = 0.05$ for models NLO2, NLB2, NLS2.

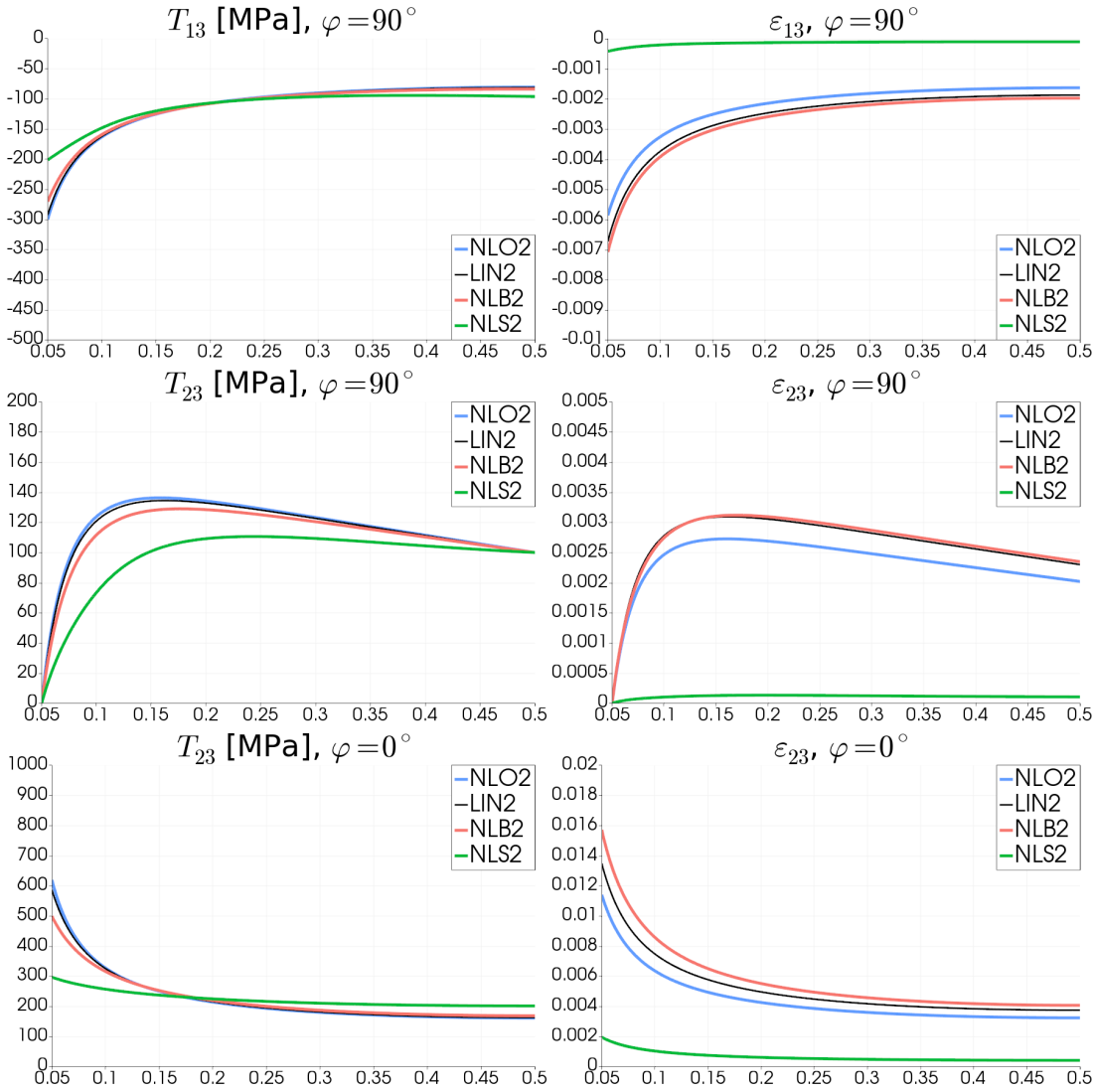

Figure 5.19: PLots of stress and strain for models LIN2, NLO2, NLB2 and NLS2 in VO geometry with $\alpha = 90°$ and $r_c = 0.05$. The plots are created over the line starting at the point C of the geometry and ending either at point $(1, 0.5)$, which is denoted $\varphi = 0°$, or at point $(0.5, 1)$, which corresponds to $\varphi = 90°$.

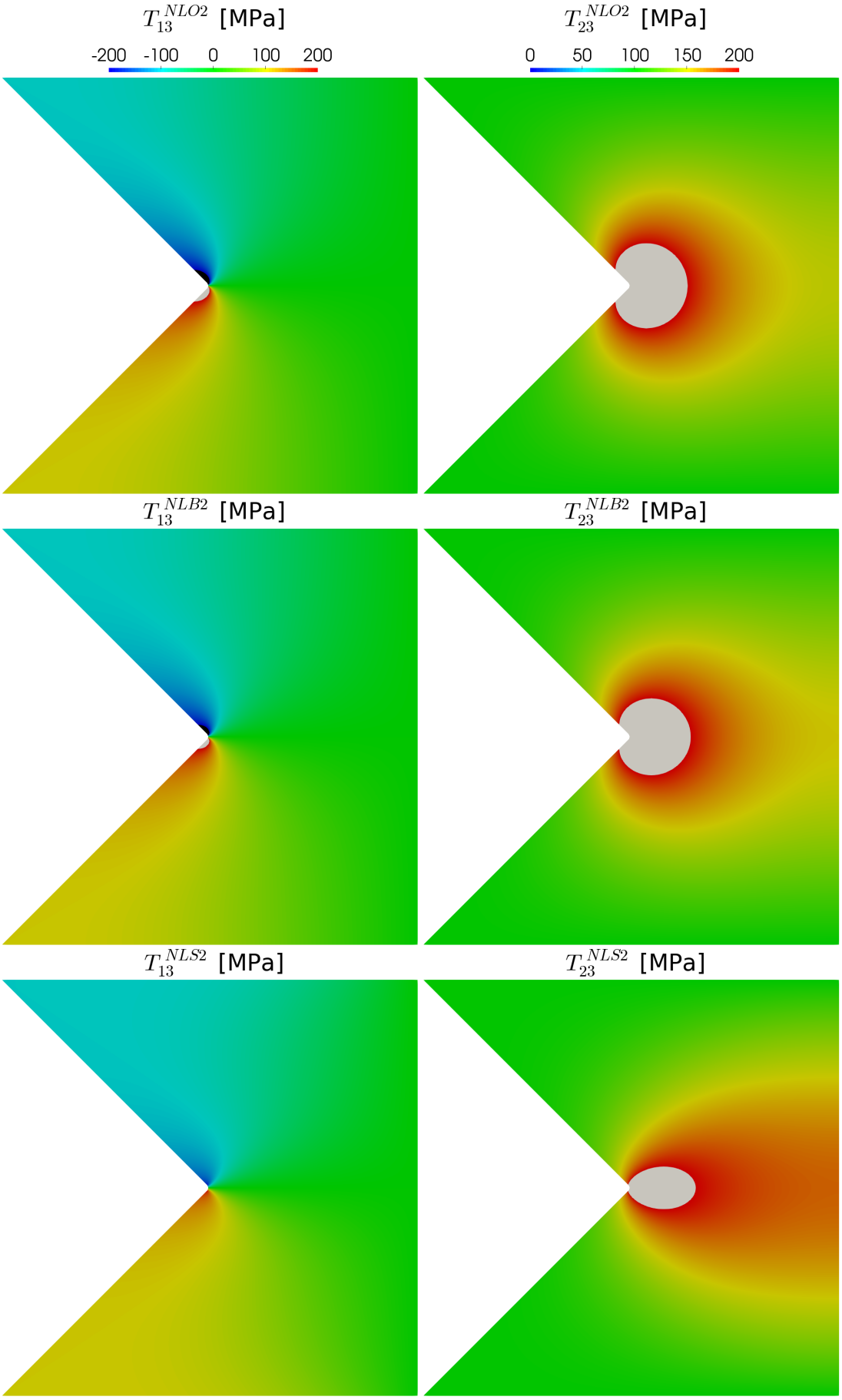

Figure 5.20: Comparison of stress distributions in VC geometry with $\alpha = 90°$ and $r_c = 0.01$ for models NLO2, NLB2, NLS2.

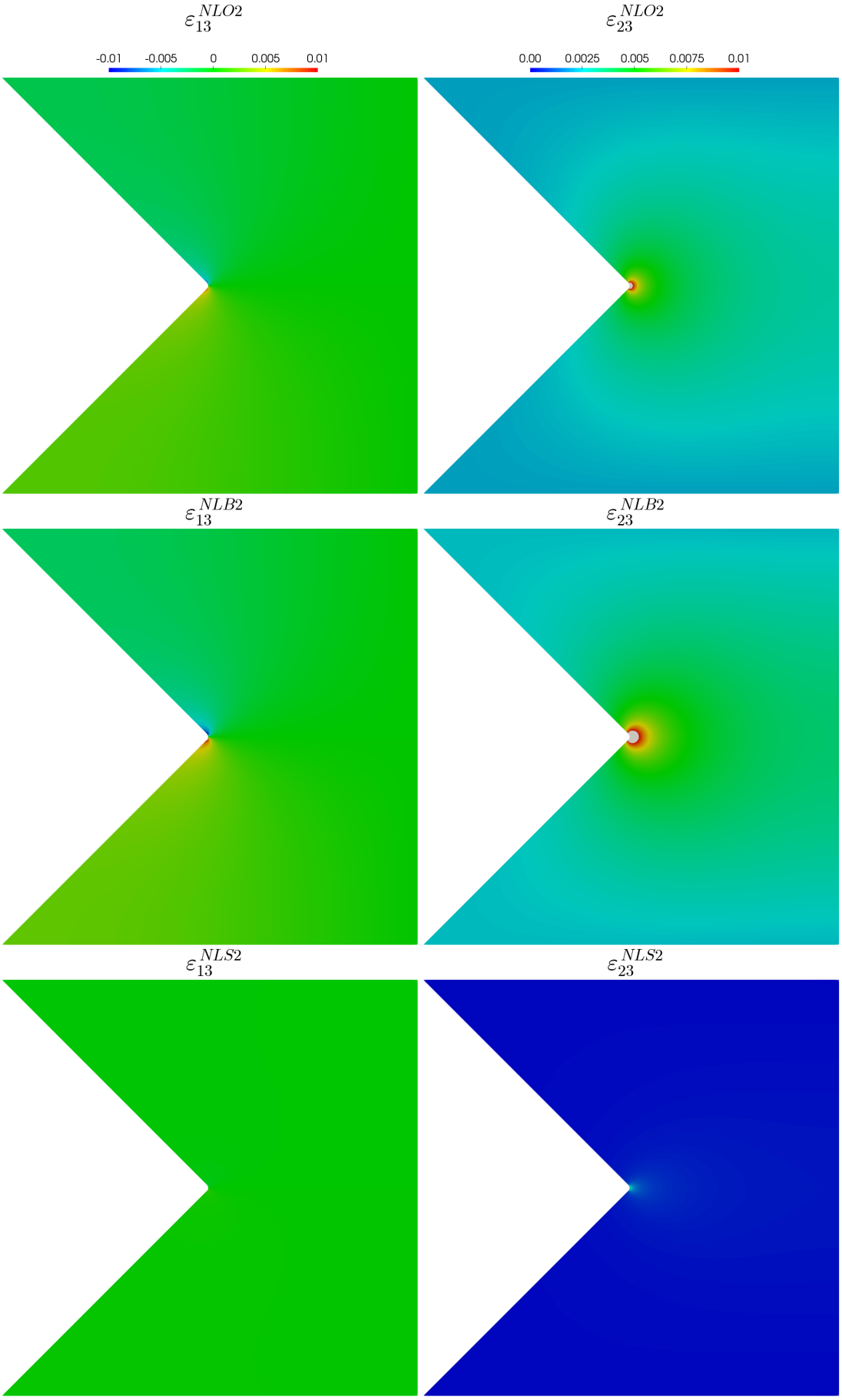

Figure 5.21: Comparison of strain distributions in VC geometry with $\alpha = 90°$ and $r_c = 0.01$ for models NLO2, NLB2, NLS2.

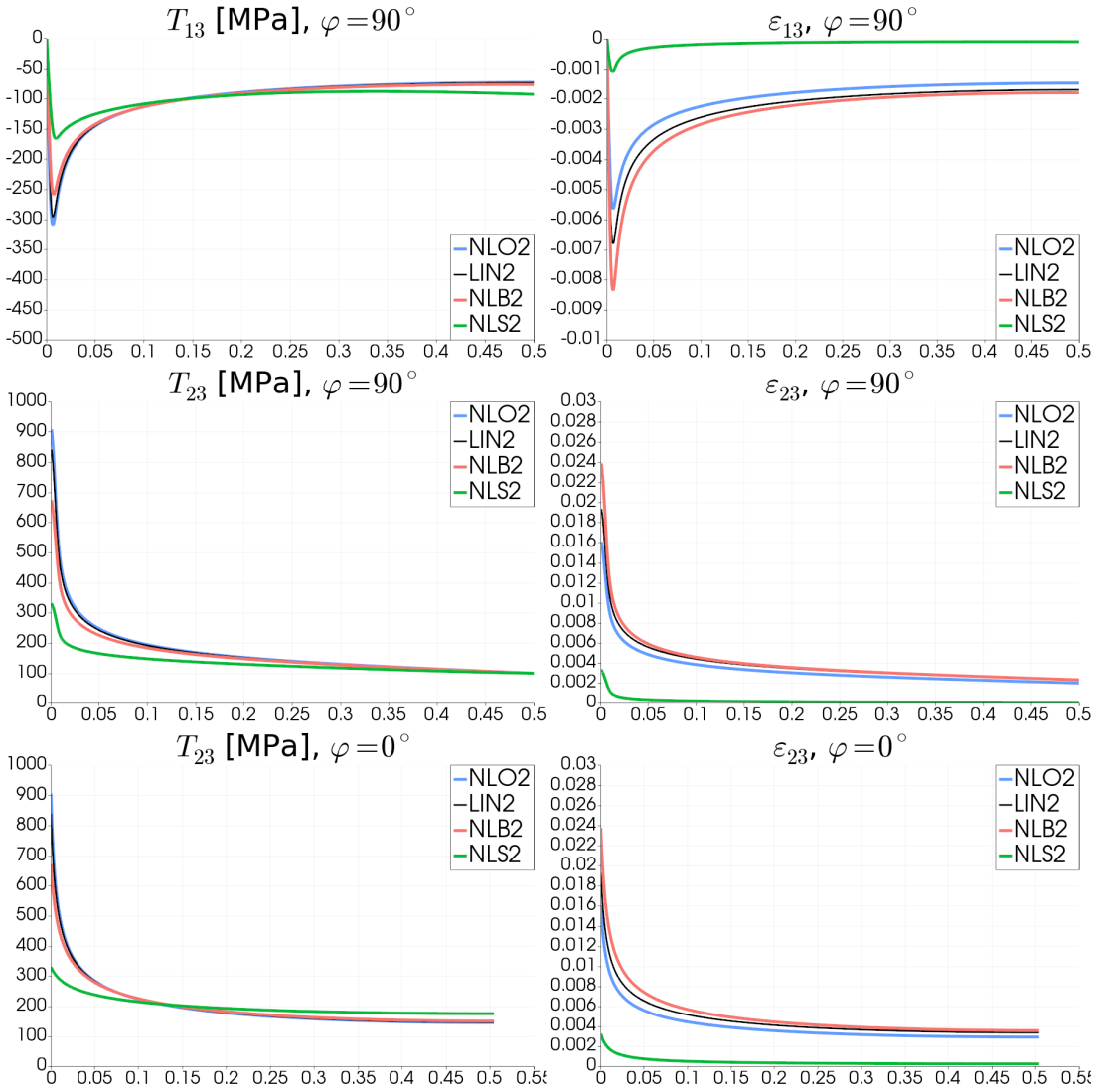

Figure 5.22: PLots of stress and strain for models LIN2, NLO2, NLB2 and NLS2 in VO geometry with $\alpha = 90°$ and $r_c = 0.01$. The plots are created over the line starting at the point $C + (r_c, 0)$ of the geometry and ending either at point $(1, 0.5)$, which is denoted $\varphi = 0°$, or at point $C + (r_c, 0.5)$, which corresponds to $\varphi = 90°$.

5.4.5 Dependence on α and r_c

So far, we have been comparing the solutions when the geometrical setting is fixed. In this section, we study how solutions depend on the parameters of geometries. We consider behavior of solutions when the diameter r_c is decreasing and when the opening angle α is increasing.

In Figure 5.23, we plot dependence of the highest value of T_{23} and ε_{23} in the whole computational domain for V geometries with respect to α for all studied models. Corresponding plots for the domains VO and VC are for LIN2 model in Figure 5.24, for NLO2 model in Figure 5.25, for NLB2 model in Figure 5.26 and for NLS2 model in Figure 5.27.

Stresses and strains are very high in the vicinity of the notch tip and with a distance they decrease, see Figures 5.22, 5.19 and 5.16. Distributions of T_{23} and ε_{23} over the line from the tip to the right, which is denoted $\varphi = 0°$, are monotone. It is therefore natural to ask how far from the tip stress or strain decreases to a particular value. Next we define the distance from the notch tip to the point, where T_{23} or ε_{23} acquires a particular value.

Definition 5.5 (Functions dst^T and dst^e). *Let (r, φ) be the cylindrical coordinate system, see Figure 5.2 centered at point C for V geometry and VO geometry or at point $C + (r_c, 0)$ for VC geometry. We define the functions $dst^T : [0, 2\pi) \times \mathbb{R} \to \mathbb{R}_0^+$ and $dst^e : [0, 2\pi) \times \mathbb{R} \to \mathbb{R}_0^+$ as follows*

$$dst^T(\varphi, T) = \begin{cases} \infty & \text{if } \forall r \geq 0 : T < T_{23}(r, \varphi), \\ -\infty & \text{if } \forall r \geq 0 : T > T_{23}(r, \varphi), \\ \min\{r \geq 0,\, T_{23}(r, \varphi) = T\} & \text{otherwise.} \end{cases}$$

$$dst^e(\varphi, e) = \begin{cases} \infty & \text{if } \forall r \geq 0 : e < \varepsilon_{23}(r, \varphi), \\ -\infty & \text{if } \forall r \geq 0 : e > \varepsilon_{23}(r, \varphi), \\ \min\{r \geq 0, \varepsilon_{23}(r, \varphi) = e\} & \text{otherwise.} \end{cases}$$

For visualizations, we define the three following distances called DT2, DT3 and DE1 such that

$$\begin{aligned} DT2 &= dst^T(0, 200\,\text{MPa}), \\ DT3 &= dst^T(0, 300\,\text{MPa}), \\ DE1 &= dst^e(0, 0.01). \end{aligned} \tag{5.25}$$

In V geometry, these distances are visualized for all considered models with respect to α in Figure 5.28. In VO and VC geometries, these distances are visualized for model LIN2 in Figure 5.29, for model NLO2 in Figure 5.30, for model NLB2 in Figure 5.31 and for model NLS2 in Figure 5.32.

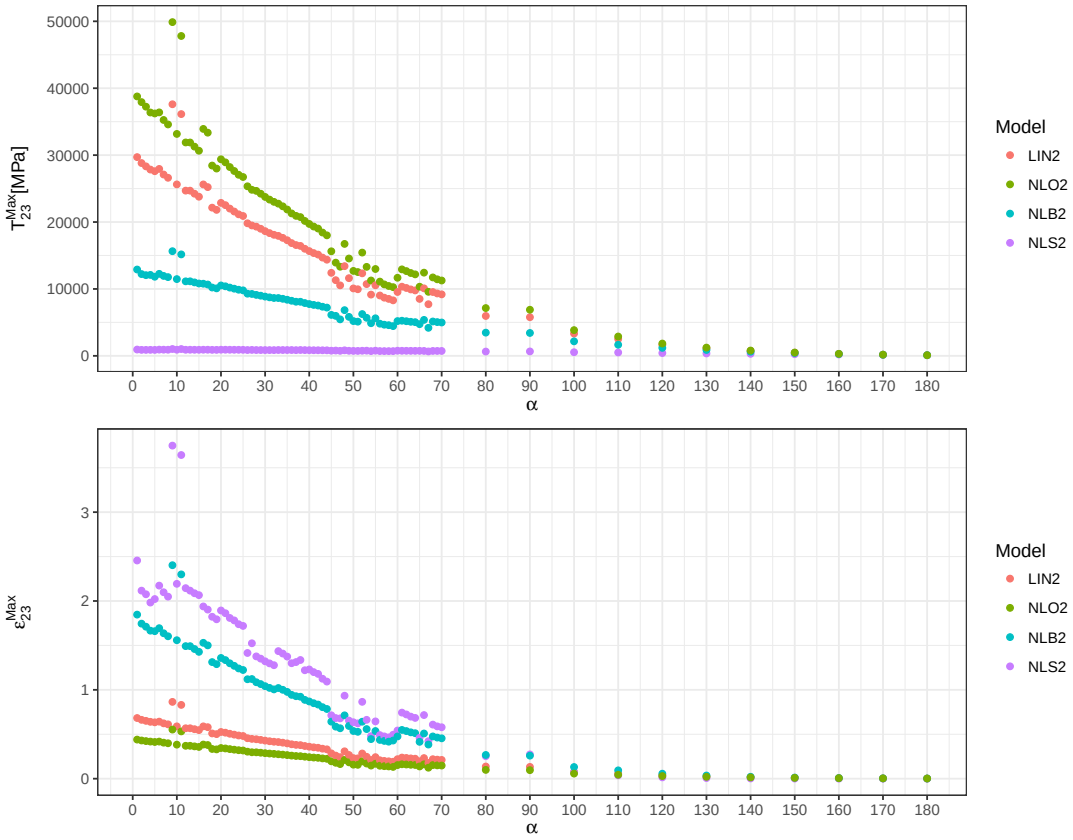

Figure 5.23: Maximal T_{23} and ε_{23} in V geometry with respect to α.

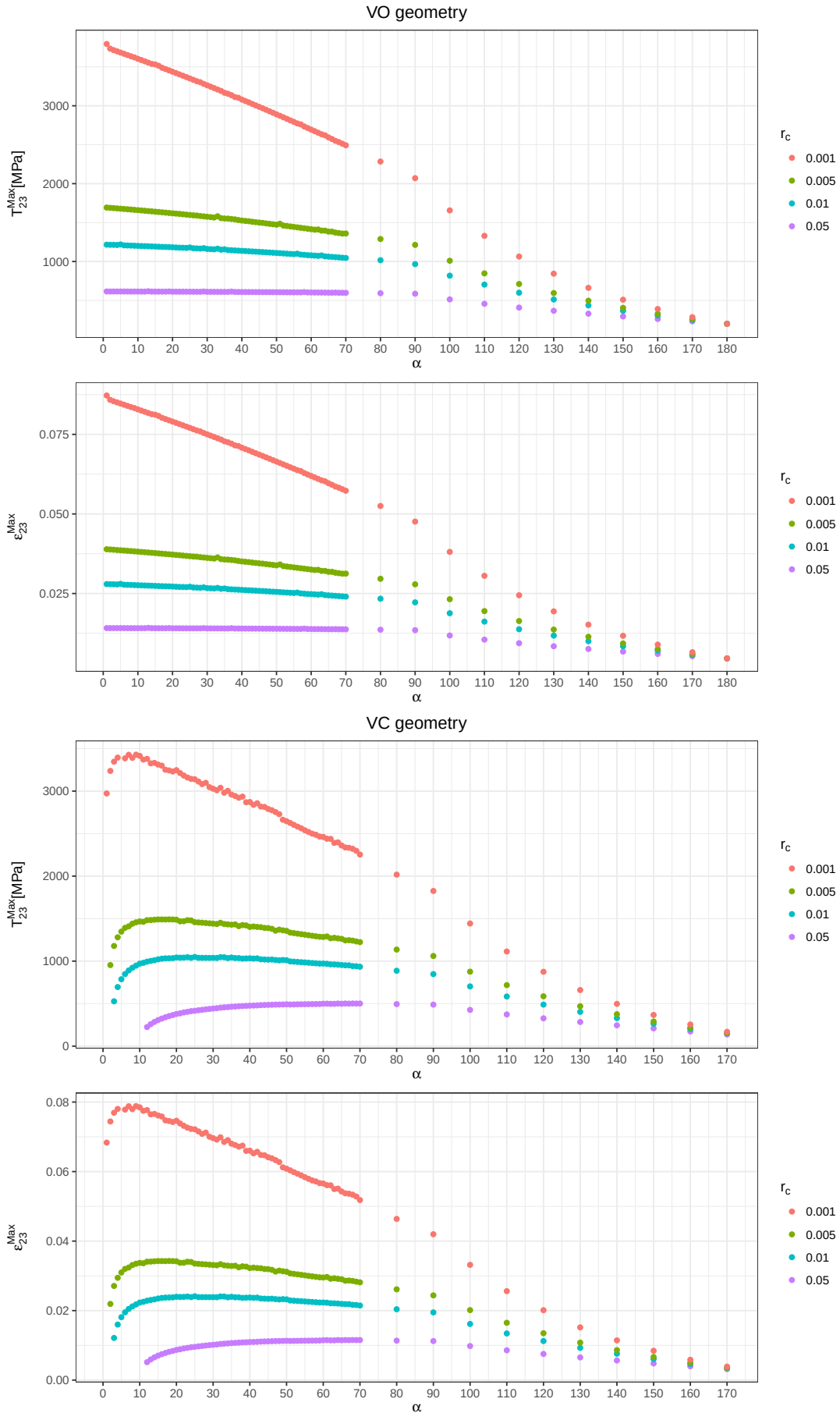

Figure 5.24: Maximal T_{23} and ε_{23} in VO geometry (top) and VC geometry (bottom) with respect to α for model LIN2.

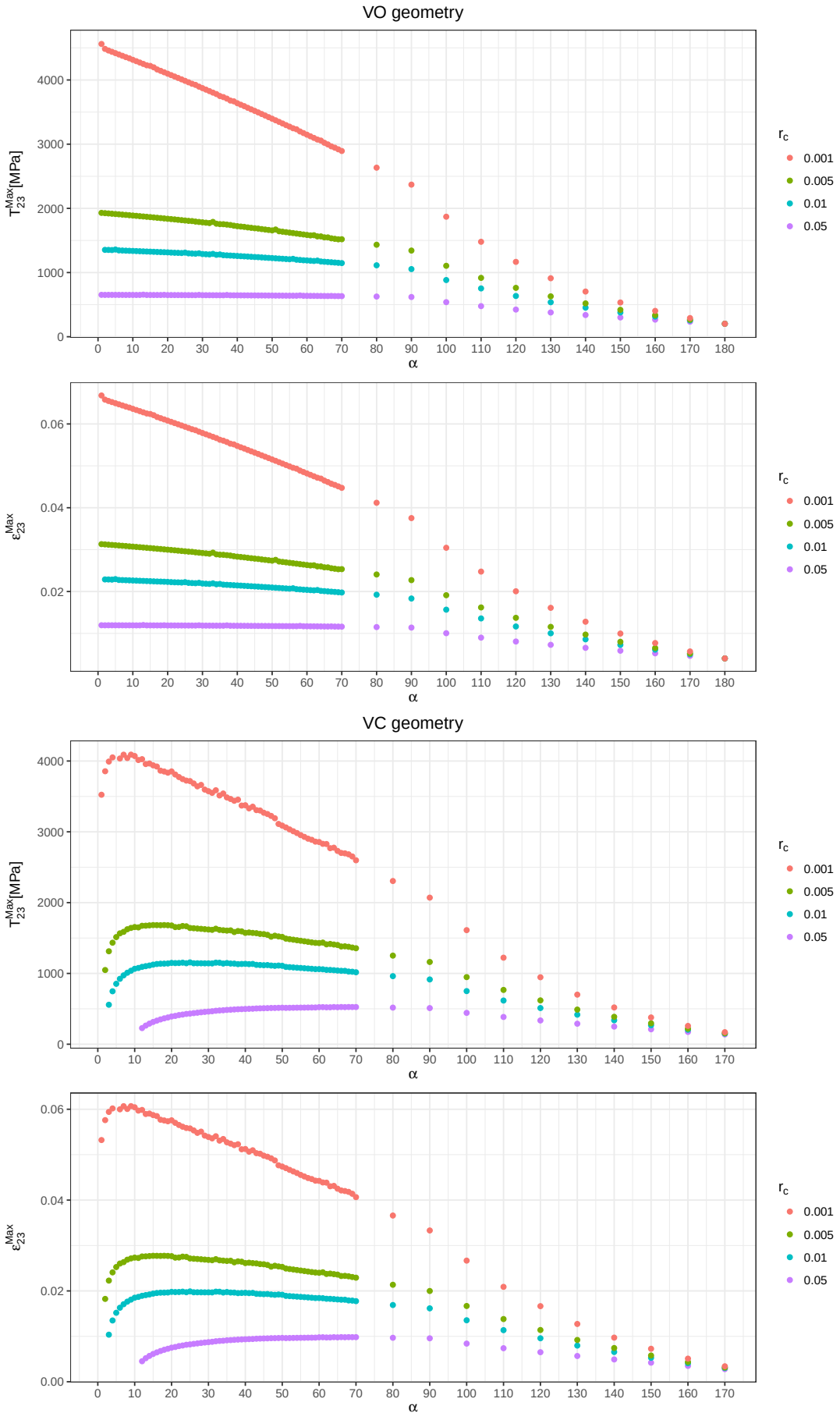

Figure 5.25: Maximal T_{23} and ε_{23} in VO geometry (top) and VC geometry (bottom) with respect to α for model NLO2.

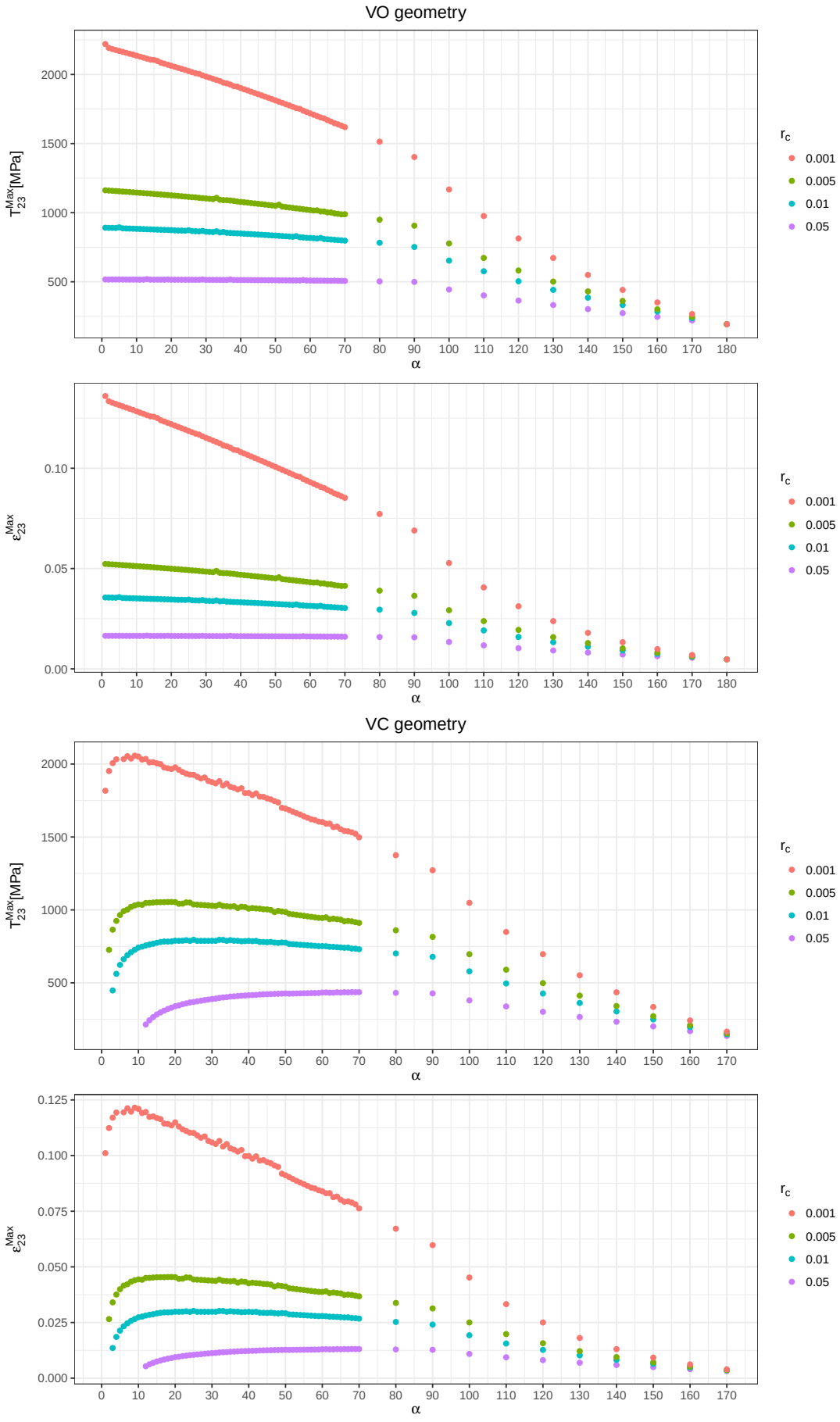

Figure 5.26: Maximal T_{23} and ε_{23} in VO geometry (top) and VC geometry (bottom) with respect to α for model NLB2.

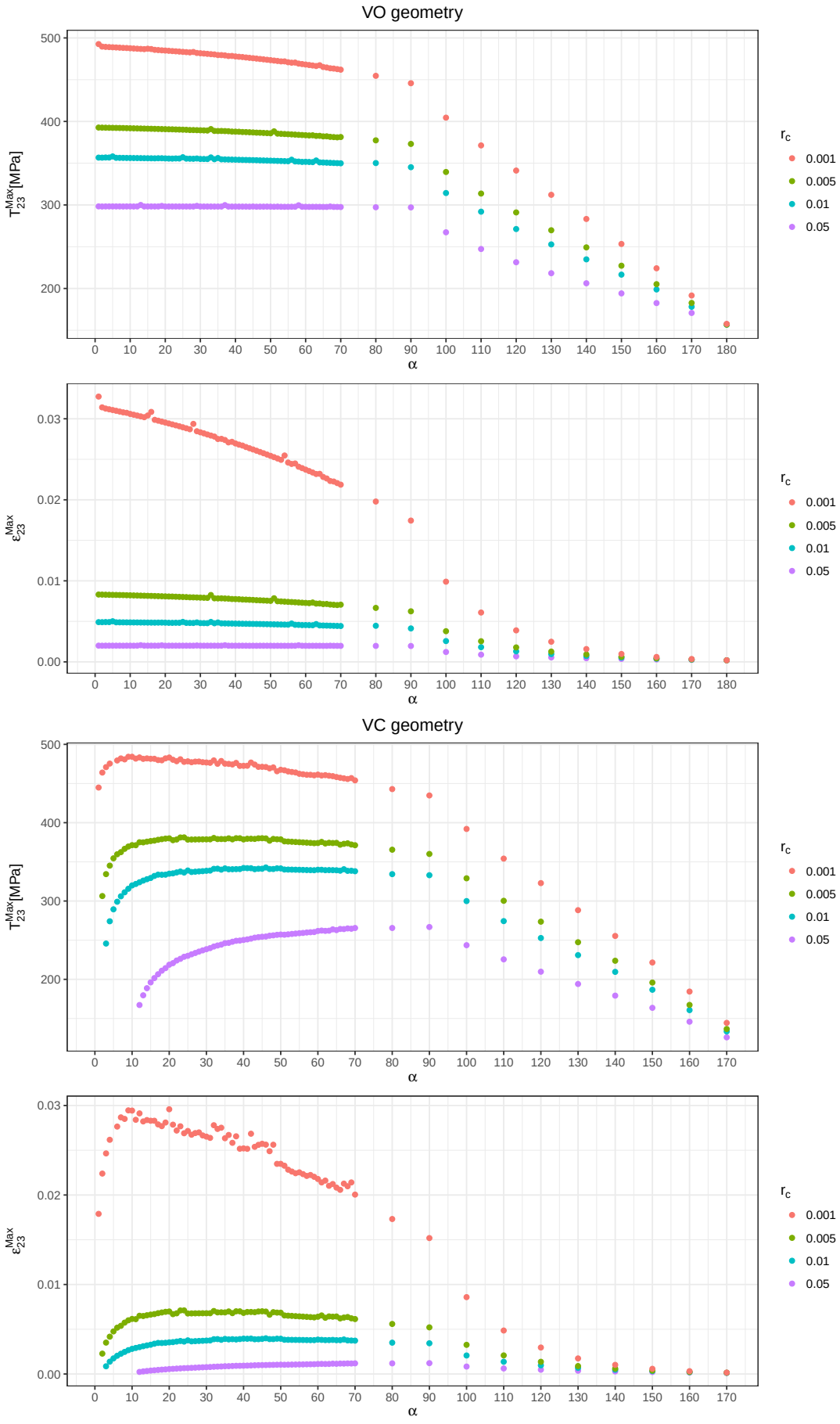

Figure 5.27: Maximal T_{23} and ε_{23} in VO geometry (top) and VC geometry (bottom) with respect to α for model NLS2.

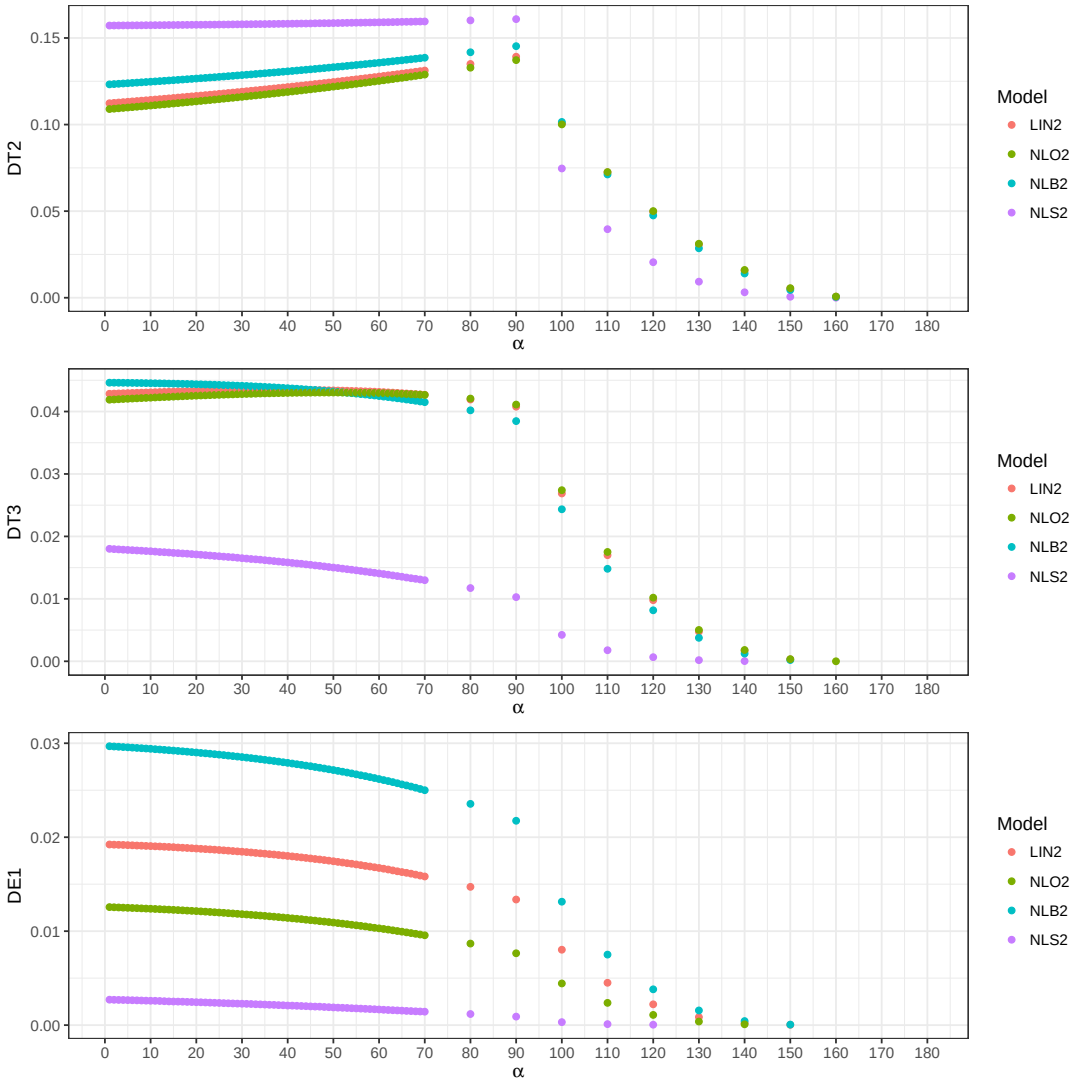

Figure 5.28: Distances DT2, DT3 and DE1, see (5.25), in V geometry with respect to α.

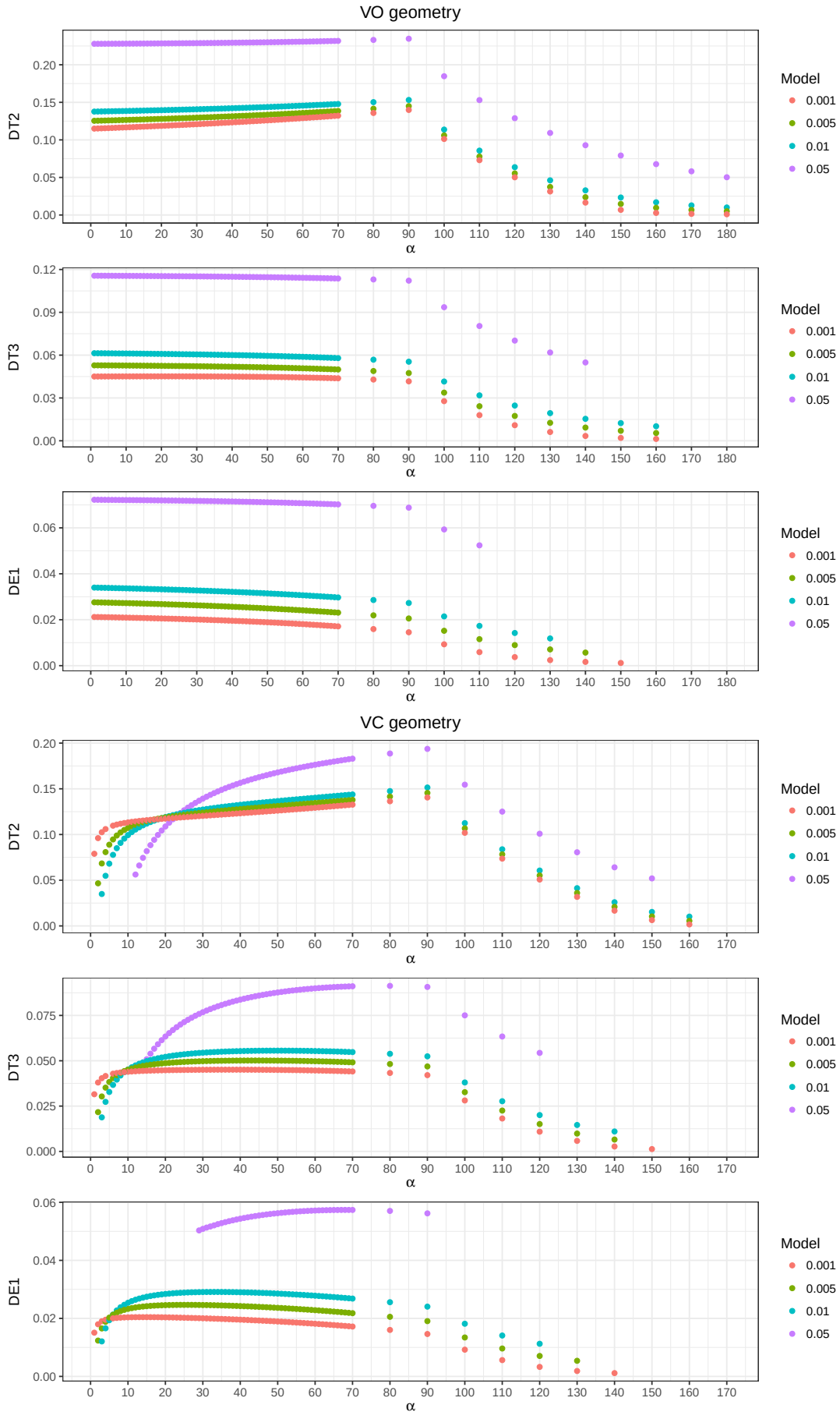

Figure 5.29: Distances DT2, DT3 and DE1, see (5.25), in VO and VC geometries with respect to α for model LIN2.

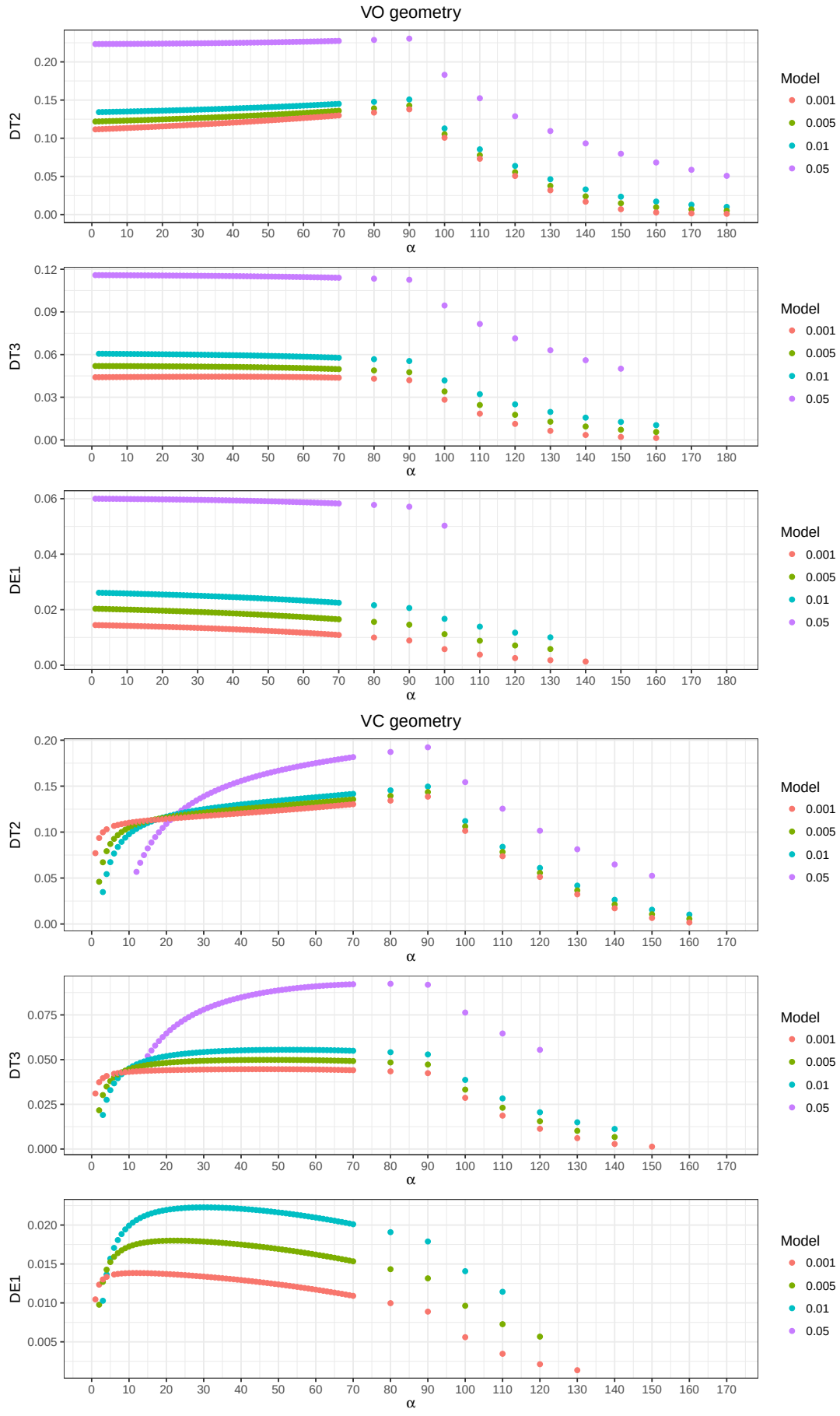

Figure 5.30: Distances DT2, DT3 and DE1, see (5.25), in VO and VC geometries with respect to α for model NLO2.

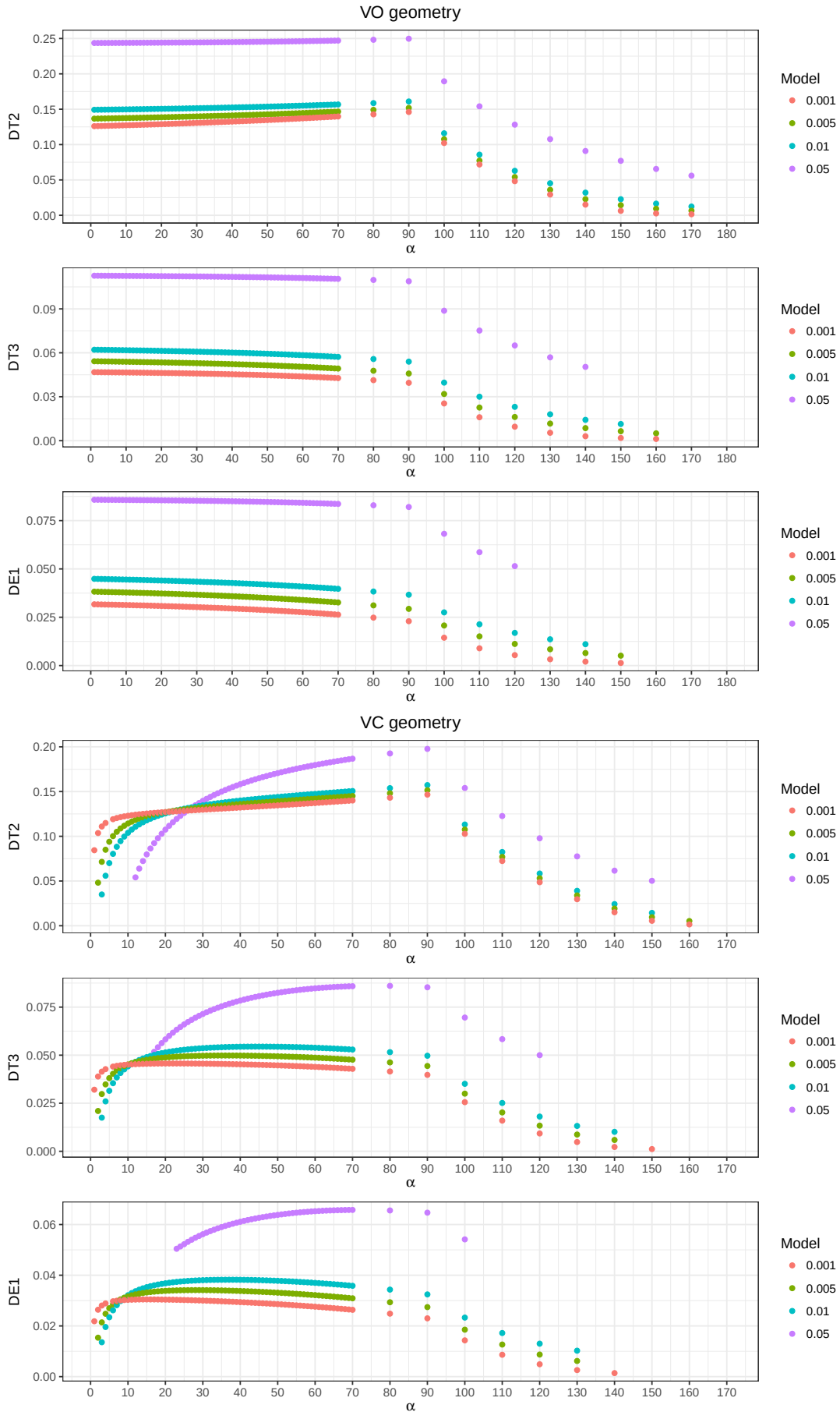

Figure 5.31: Distances DT2, DT3 and DE1, see (5.25), in VO and VC geometries with respect to α for model NLB2.

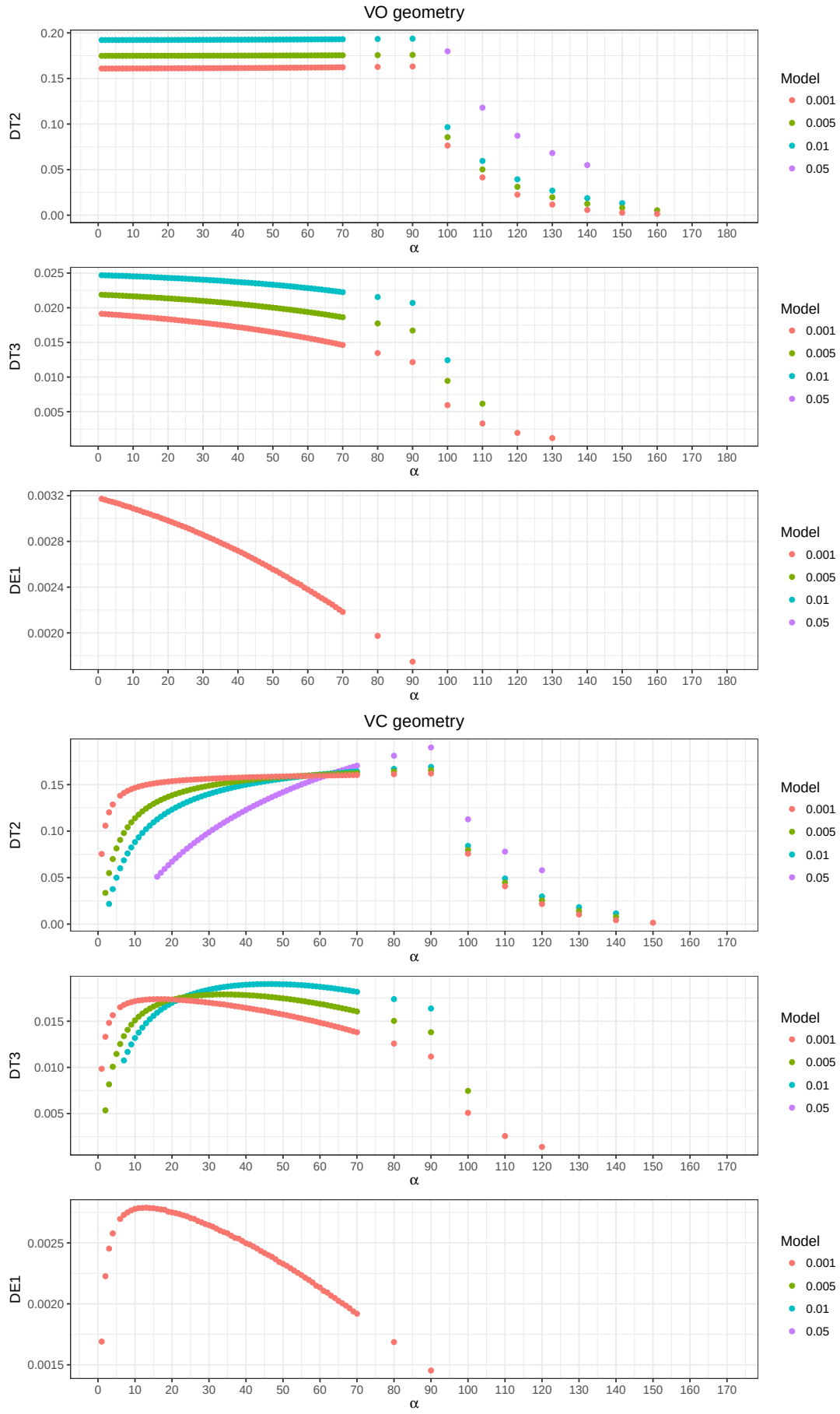

Figure 5.32: Distances DT2, DT3 and DE1, see (5.25), in VO and VC geometries with respect to α for model NLS2.

5.5 Discussion

We formulated Problem (P) as a variational problem on finite element spaces in a geometry of anti-plane stress. We simulated the response of three titanium alloys, described by the power-law models (5.2), with the material moduli identified in Chapter 3, see Table 5.1. Numerical simulations were performed on adaptively refined triangular meshes in a three basic geometries of a square plate with a V-notch, which are specified in the Section 5.3.1.

We have verified that the computed variational solutions are stable. In Tables 5.2–5.10, we list relative error norms (5.23) with respect to the refinement level for all studied problems in different geometries. The differences between computed solutions on the two most refined meshes are typically of order lower than 10^{-4}. The global stability measured by the error norms is for the power-law problems comparable to or even better than the global stability for a linear problem. The best results were obtained in the domains of types VO and VC where, despite the presence of stress concentration, there is no, expected or observed, singularity of stress and strain, see Figure 5.19 and Figure 5.22. For these geometries, we see that the error norms between the solution on once or twice refined mesh and the solution on the fully refined mesh are smaller than in case of V geometry. However, with a further refinements we can see a very limited improvement in the error norms. Thus, we can hypothesize that we converge to the close vicinity of the analytical solution.

For all geometries, it is evident that with increasing angle α, the solution is becoming even more stable due to the decrease of the magnitude of singularity or the severity of the stress concentration in case of smoothened domains. We observe that the solutions are more stable for higher values of the power law exponents q'. Namely the error norms for the model NLS2 with the highest q' are consistently smaller than the error norms for the NLO2 model with the lowest q'.

We measure the local error of computed solutions with respect to the refinement by the norm of the difference in the stress. In the V geometry, from Figures 5.11 and 5.12, we can see that the local error is the highest in the vicinity of the V-notch tip. With the mesh refinement, stress distributions converge to each other, and the local error shrinks towards negligible area around the V-notch tip, see Figure 5.12. Note that in Figures 5.11 and 5.12, the maximal visualised difference can be 1 MPa, which is hundred times less than the value of stress in the far field 100 MPa. Despite that, the error is very small after a few refinement steps.

When studying the behavior of the solutions with respect to parameters of geometries, see Figures 5.23–5.32, we see that there is substantial stability of the solution properties when comparing them across completely different meshes. We can clearly identify patterns in Figures 5.23–5.32 that arise with respect to the notch opening angle α. Even the properties such as the maximal value of the stress component T_{23} for V geometry, where the singularity is predicted, form interestingly stable patterns across discretizations, see Figure 5.23. As being expected, the most stability is present when comparing properties that lie in some distance from the notch tip, see Figures 5.28–5.32.

Let us further discuss the maximal values of T_{23} and ε_{23} in Figures 5.23–5.27. In V geometry, from Figure 5.23 we can see that the maximal values $max(T_{23})$ for considered models are ordered so that $max(T_{23}^{NLO2}) > max(T_{23}^{LIN2}) > max(T_{23}^{NLB2}) >$

$max(T_{23}^{NLS2})$, while the order of the maximal values of ε_{23} is reversed. We have that $max(\varepsilon_{23}^{NLO2}) < max(\varepsilon_{23}^{LIN2}) < max(\varepsilon_{23}^{NLB2}) < max(\varepsilon_{23}^{NLS2})$. This behavior corresponds very well to the predicted sizes of the singularities for asymptotic solutions. For our models, we have the order of the power law exponents $q'_{NLO2} < q'_{LIN2} < q'_{NLB2} < q'_{NLS2}$. Therefore, from equation (5.19) we get the following order of the sizes of stress singularities $|k_{NLO2}^T| > |k_{LIN2}^T| > |k_{NLB2}^T| > |k_{NLS2}^T|$. At the same time from equation (5.20) we have the reversed order of the singularities of the strain $|k_{NLO2}^e| < |k_{LIN2}^e| < |k_{NLB2}^e| < |k_{NLS2}^e|$. Figures 5.23–5.27 thus suggests that the size of the highest value of T_{23} and ε_{23} in computed solution correlates with the predicted magnitude of the singularity in the asymptotic solution, which is given by (5.19) and (5.20).

Another interesting aspect of our treatment of differences between solutions is the dependence of solutions on the diameter of smoothing circle r_c of the V-notch tip in the case of VO and VC geometries. We can see that maximal values of stress and strain grow with decreasing parameter r_c, see Figures 5.24–5.27. There is no singularity, but noticeably for $r_c = 0.001$, we have a high stress concentration around the smothened tip of the notch so that maximal values of strain clearly exceed the small strain range.

Finally, we can see very satisfactory stability results regarding the solution in the range of small strains. The values DT2, DT3 and DE1 were defined by (5.25) as distances from the (smothened) tip of the V-notch to the point, where the stress component T_{23} achieves the value of 200 MPa or 300 MPa or the strain component ε_{23} achieves the value 0.01 respectively. The dependence of these distances on the opening angle α is very smooth and stable, see Figures 5.28–5.32. In particular, the magnitude of component $\varepsilon_{23} = 0.01$ can be considered the elastic limit for most of studied materials. We can conclude that we achieved very good stability of solutions not only with respect to the mesh refinement but also across discretizations.

A. Review of the theory

In this chapter, we set the theoretical background of the thesis and introduce notation. First, we outline results and define notation from the field of calculus, linear algebra and tensor algebra. Then we review important results from functional analysis and analysis of PDE's. Afterwards, we review important parts of the theory of solid mechanics and elastostatics.

A.1 Vector spaces, tensor algebra and notation

In this section, we briefly review basic definitions from the field of vector spaces and calculus with second order tensors. We also set up basic notations used throughout the thesis. For the review of results from Real analysis, see Carothers (2000). For the review of the results from linear algebra and tensor manipulation, see Roman (2007); Itskov (2009).

Vector spaces

Definition A.1 (Real and natural numbers). *We denote the set of real numbers by* $\mathbb{R}$*, the set of positive real numbers by* $\mathbb{R}^+$ *and the set of positive real numbers including 0 by* $\mathbb{R}_0^+$*. We denote the set of natural numbers (positive integers) by* $\mathbb{N}$ *and the set of natural numbers including* 0 *by* $\mathbb{N}_0$*.*

Definition A.2 (Vector space (over $\mathbb{R}$)). *Vector space* $\mathbf{X}$ *is a set with operations addition (+), scalar multiplication and zero vector* $\mathbf{0} \in \mathbf{X}$ *such that* $\forall \mathbf{x}_1, \mathbf{x}_2, \mathbf{x}_3 \in \mathbf{X}$ *and* $\forall \alpha, \beta \in \mathbb{R}$*, the following is true:* $\mathbf{x}_1 + \mathbf{x}_2 \in \mathbf{X}$*,* $\alpha\mathbf{x}_1 \in \mathbf{X}$*,* $(\mathbf{x}_1 + \mathbf{x}_2) + \mathbf{x}_3 = \mathbf{x}_1 + (\mathbf{x}_2 + \mathbf{x}_3)$*,* $\mathbf{x}_1 + \mathbf{x}_2 = \mathbf{x}_2 + \mathbf{x}_1$*,* $\mathbf{x}_1 + \mathbf{0} = \mathbf{x}_1$*,* $\exists(-\mathbf{x}_1) \in \mathbf{X} : (-\mathbf{x}_1) + \mathbf{x}_1 = \mathbf{0}$*,* $\alpha(\beta\mathbf{x}_1) = (\alpha\beta)\mathbf{x}_1$*,* $1\mathbf{x}_1 = \mathbf{x}_1$*,* $\alpha\mathbf{x}_1 + \alpha\mathbf{x}_2 = \alpha(\mathbf{x}_1 + \mathbf{x}_2)$*,* $(\alpha + \beta)\mathbf{x}_1 = \alpha\mathbf{x}_1 + \beta\mathbf{x}_1$

Definition A.3 (Basis of vector space $\mathbf{X}$). *The basis of vector space* $\mathbf{B} \subset \mathbf{X}$ *is a set* $\mathbf{B} = \{\mathbf{v}_i, i \in I\}$ *that is linearly independent and generates* $\mathbf{X}$*. That means* [1]

- *For all* $n \in \mathbb{N}, n \leq |I|, \forall J \subseteq I, |J| = n$ *let* $\{\mathbf{v}_{J(1)}, \dots, \mathbf{v}_{J(n)}\} = \{\mathbf{v}_j, j \in J\}$ *then from* $\alpha_1\mathbf{v}_{J(1)} + \dots + \alpha_n\mathbf{v}_{J(n)} = 0$ *it follows that* $\alpha_1 = \dots \alpha_n = 0$*.*
- *For all* $\mathbf{v} \in \mathbf{X} \exists n \in \mathbb{N}, \exists J \subseteq I, |J| = n$ *and* $\alpha_1, \dots \alpha_n \in \mathbb{R}$ *such that if* $\{\mathbf{v}_{J(1)}, \dots, \mathbf{v}_{J(n)}\} = \{\mathbf{v}_j, j \in J\}$ *then* $\mathbf{v} = \alpha_1\mathbf{v}_{J(1)} + \dots + \alpha_n\mathbf{v}_{J(n)}$*.*

Definition A.4 (Linear span). *Let* P *represent an ordered set of vectors from the vector space* $\mathbf{X}$*.* P *could be finite or countable. We define the linear span of* P *as a set*

$$\text{span}\,(P) = \{\sum_{i=1}^{k} \alpha_i\mathbf{v}_i | k \in \mathbb{N}, \mathbf{v}_i \in P, \alpha_i \in \mathbb{R}\}.$$

Definition A.5 (Finite dimensional vector space and its dimension). *A vector space* $\mathbf{X}$ *is of finite dimension, if there exists its basis* $\mathbf{B}$*, which contains finite number of vectors. The dimension of* $\mathbf{X}$ *is a number of elements of* $\mathbf{B}$ [2]*.*

[1] By $|I|$ we mean cardinality of the set I, see (Carothers, 2000, p. 18). If the set I has a finite number of elements, then the cardinality is equal to the number of elements of I.

[2] All bases of the finite dimensional vector space have the same size, see (Itskov, 2009, p. 4).

Definition A.6 (Norm of vector space $\mathbf{X}$). *The norm $\|.\| : \mathbf{X} \to \mathbb{R}$ is a mapping, such that for all $\mathbf{x}, \mathbf{y} \in \mathbf{X}$ the following holds:*

- $\|\mathbf{x}\| \geq 0$, $\|\mathbf{x}\| = 0 \Leftrightarrow \mathbf{x} = \mathbf{0}$,
- $\|\alpha\mathbf{x}\| = |\alpha|\|\mathbf{x}\|$, *for* $\alpha \in \mathbb{R}$,
- $\|\mathbf{x} + \mathbf{y}\| \leq \|\mathbf{x}\| + \|\mathbf{y}\|$.

Definition A.7 (Normed vector space). *Vector space $\mathbf{X}$ with norm $\|.\|$ denoted by $(\mathbf{X}, \|.\|)$ is called a normed vector space.*

Definition A.8 (Equivalent norms). *Two norms $\|.\|_1$ and $\|.\|_2$ on vector space $\mathbf{X}$ are equivalent if there exists two constants $C_1, C_2 > 0$, such that*

$$\forall \mathbf{x} \in \mathbf{X} \quad C_1\|\mathbf{x}\|_1 \leq \|\mathbf{x}\|_2 \leq C_2\|\mathbf{x}\|_1.$$

Theorem A.9. *Any two norms on a finite dimensional vector space are equivalent.*

Proof. See (Carothers, 2000, p. 124). □

Definition A.10 (Direct sum of vector spaces). *Let $\mathbf{U}$ and $\mathbf{V}$ be vector spaces, the direct sum $\mathbf{W} = \mathbf{U} \oplus \mathbf{V}$ is a vector space of pairs $(\mathbf{u}, \mathbf{v})$, where $\mathbf{u} \in \mathbf{U}$ and $\mathbf{v} \in \mathbf{V}$. The addition and the scalar multiplication are defined as follows*

- $(\mathbf{u}_1, \mathbf{v}_1) + (\mathbf{u}_2, \mathbf{v}_2) = (\mathbf{u}_1 + \mathbf{u}_2, \mathbf{v}_1 + \mathbf{v}_2)$,
- $\alpha(\mathbf{u}, \mathbf{v}) = (\alpha\mathbf{u}, \alpha\mathbf{v})$, $\alpha \in \mathbb{R}$.

Observation A.11. *If $\mathbf{W} = \mathbf{U} \oplus \mathbf{V}$ and if $\|.\|_U$ is a norm on $\mathbf{U}$ and if $\|.\|_V$ is a norm on $\mathbf{V}$, then $\|(\mathbf{u}, \mathbf{v})\| = \|\mathbf{u}\|_U + \|\mathbf{v}\|_V$ is a norm on $\mathbf{W}$.*

Observation A.12. *If $\mathbf{W} = \mathbf{U} \oplus \mathbf{V}$ and if $\mathbf{U}$ has dimension n and if $\mathbf{V}$ has dimension m, then $\mathbf{W}$ has dimension $n + m$.*

We will discuss important examples of the normed vector spaces with a basis of finite dimension, which are Euclidean spaces.

Definition A.13 (Euclidean space $\mathbb{R}^n$). *Euclidean space of dimension $n \in \mathbb{N}$ is a set of n-tuples $\mathbf{v} = (v_1, v_2, \dots, v_n)$ such that $v_1, v_2, \dots, v_n \in \mathbb{R}$ equipped with the following operations:*

- *for $\mathbf{v}^1, \mathbf{v}^2 \in \mathbb{R}^n$: $\mathbf{v}^1 + \mathbf{v}^2 = (v_1^1 + v_1^2, v_2^1 + v_2^2, \dots, v_n^1 + v_n^2)$,*
- *for $\alpha \in R$, $\mathbf{v} \in \mathbb{R}^n$: $\alpha\mathbf{v} = (\alpha v_1, \alpha v_2, \dots, \alpha v_n)$,*
- $\mathbf{0} \in \mathbb{R}^n$ *:* $\mathbf{0} = (0, 0, \dots, 0)$.

Definition A.14 (Euclidean base). *The space $\mathbb{R}^n$ has a natural orthonormal basis consisting of vectors $\mathbf{e^1}, \dots \mathbf{e^n} \in \mathbb{R}^n$, of the form*

$$(\mathbf{e^i})_j = 1 \quad i = j$$
$$(\mathbf{e^i})_j = 0 \quad i \neq j$$

Matrix algebra and tensor algebra

Definition A.15 (Space of real matrices $\mathbb{R}^{n\times m}$). *Space of real matrices $n \times m$, where $n \in \mathbb{N}$, $m \in \mathbb{N}$ can be defined analogously to the Euclidean space as a space of m-tuples $\mathbf{A} = (\mathbf{A}_1, \mathbf{A}_2, \dots, \mathbf{A}_m)$ such that $\mathbf{A}_1, \mathbf{A}_2, \dots, \mathbf{A}_m \in \mathbb{R}^n$ equipped with the following operations:*

- *for $\mathbf{A}^1, \mathbf{A}^2 \in \mathbb{R}^{n\times m}$: $\mathbf{A}^1 + \mathbf{A}^2 = (\mathbf{A}^1_1 + \mathbf{A}^2_1, \mathbf{A}^1_2 + \mathbf{A}^2_2, \dots, \mathbf{A}^1_m + \mathbf{A}^2_m)$,*
- *for $\alpha \in R$, $\mathbf{A} \in \mathbb{R}^{n\times m}$: $\alpha\mathbf{A} = (\alpha\mathbf{A}_1, \alpha\mathbf{A}_2, \dots, \alpha\mathbf{A}_m)$,*
- $\mathbf{0} \in \mathbb{R}^{n\times m}$ *:* $\mathbf{0} = (\mathbf{0}, \mathbf{0}, \dots, \mathbf{0})$.

Matrix from the space $\mathbb{R}^{n\times m}$ is represented by its elements a_{ij}, $i \in \{1, \dots, n\}, j \in \{1, \dots m\}$.

Definition A.16 (p-norm of vector or matrix). *Let $p \geq 1$ and $\mathbf{A} \in \mathbb{R}^{n\times m}$, then the p-norm of $\mathbf{A}$ is*

$$|\mathbf{A}|_p = \left(\sum_{i=1}^{n} \sum_{j=1}^{m} |a_{ij}|^p \right)^{\frac{1}{p}}. \tag{A.1}$$

By (A.1) the p-norm $|\mathbf{v}|_p$ for vectors $\mathbf{v} \in \mathbb{R}^n$ was also defined, since vectors $\mathbf{v} \in \mathbb{R}^n$ can be understood as matrices from $\mathbb{R}^{n\times 1}$.

Definition A.17 (Euclidean norm of vector, Frobenius norm of matrix). *Let $\mathbf{A} \in \mathbb{R}^{n\times m}$, $\mathbf{v} \in \mathbb{R}^n$, then the symbol $|.|$ denotes 2-norm*

$$|\mathbf{A}| \equiv |\mathbf{A}|_2, \qquad |\mathbf{v}| \equiv |\mathbf{v}|_2.$$

Euclidean spaces $\mathbb{R}^n$ and $\mathbb{R}^{n\times m}$ are normed vector spaces with the norm $|.|$.

Observation A.18. *Let $n \in \mathbb{N}$. Let $\mathbf{V}$ be an n-dimensional vector space with a norm $\|.\|$. Let $\mathbf{B} = \{\mathbf{v}_i,\ i \in 1 \dots n\}$ be a basis of $\mathbf{V}$. We can uniquely define $\mathbf{y} : \mathbf{V} \to \mathbb{R}^n$ such that*

$$\mathbf{v} = \sum_{i=0}^{n} \mathbf{y}(\mathbf{v})_i \mathbf{v}_i, \quad \mathbf{v} \in \mathbf{V}. \tag{A.2}$$

Using (A.2), we can show that the Euclidean norm $|\mathbf{y}(\mathbf{v})|$ is a norm on $\mathbf{V}$. By Theorem A.9 this norm is equivalent to $\|.\|$. Thus, there exist $C_1, C_2 \in \mathbb{R}^+$ such that $C_1|\mathbf{y}(\mathbf{v})| \leq \|\mathbf{v}\| \leq C_2|\mathbf{y}(\mathbf{v})|$.

In the thesis, we reserve the symbol $\|.\|$ to denote norms on, typically infinite dimensional, functional spaces.

Definition A.19 (Inner product). *Inner product of vector space $\mathbf{X}$ is a mapping $(\cdot,\cdot) : \mathbf{X} \times \mathbf{X} \to \mathbb{R}$ that for all $\mathbf{x}, \mathbf{y}, \mathbf{z} \in \mathbb{X}$ fulfils*

- $(\mathbf{x}, \mathbf{x}) \geq 0$, $(\mathbf{x}, \mathbf{x}) = 0 \Leftrightarrow \mathbf{x} = \mathbf{0}$,
- $(\alpha\mathbf{x}, \mathbf{y}) = \alpha(\mathbf{x}, \mathbf{y})$, *for* $\alpha \in \mathbb{R}$,
- $(\mathbf{x}, \mathbf{y}) = (\mathbf{y}, \mathbf{x})$

- $(\mathbf{x}+\mathbf{y},\mathbf{z}) = (\mathbf{x},\mathbf{z}) + (\mathbf{y},\mathbf{z})$.

Definition A.20 (Natural norm). *Let* $\mathbf{X}$ *be a vector space with inner product* $(\cdot,\cdot)$. *Then the norm*

$$\|\mathbf{x}\| = \sqrt{(\mathbf{x},\mathbf{x})}, \quad \mathbf{x} \in \mathbf{X},$$

is called natural norm of space $\mathbf{X}$ *relative to* $(\cdot,\cdot)$.

Lemma A.21 (Cauchy-Schwarz inequality). *Let* $\mathbf{X}$ *be a vector space with inner product* $(\cdot,\cdot)$. *Let* $\|.\|$ *be its natural norm. Then*

$$\forall \mathbf{x},\mathbf{y} \in \mathbf{X}, \quad |(\mathbf{x},\mathbf{y})|^2 \leq (\mathbf{x},\mathbf{x})(\mathbf{y},\mathbf{y}) = \|\mathbf{x}\|^2\|\mathbf{y}\|^2.$$

Proof. See (Roman, 2007, p. 208). □

Definition A.22 (Inner product on the Euclidean space $\mathbb{R}^n$). *Let* $\mathbf{v}^1, \mathbf{v}^2 \in \mathbb{R}^n$, *then the inner product (denoted by .) is a mapping* $\mathbb{R}^n \times \mathbb{R}^n \to \mathbb{R}$ *defined as*

$$\mathbf{v}^1.\mathbf{v}^2 = \sum_{i=1}^{n} v_i^1 v_i^2.$$

Definition A.23 (Inner product on the space of real matrices $\mathbb{R}^{n\times m}$). *Let* $\mathbf{A}^1, \mathbf{A}^2 \in \mathbb{R}^{n\times m}$, *then the inner product (denoted by :) is a mapping* $\mathbb{R}^{n\times m} \times \mathbb{R}^{n\times m} \to \mathbb{R}$ *defined as*

$$\mathbf{A}^1 : \mathbf{A}^2 = \sum_{i=1}^{n}\sum_{j=1}^{m} a_{ij}^1 a_{ij}^2.$$

We can see that $|.|$ is a natural norm on $\mathbb{R}^n$ and $\mathbb{R}^{n\times m}$ relative to inner products on these spaces.

Definition A.24 (Identity matrix, the Kronecker delta). *We denote identity matrix by* $\mathbf{I}$ *and the Kronecker delta by* δ_{ij}.

Definition A.25 (Square matrix, symmetric matrix, singular matrix, orthogonal vectors, orthogonal matrices, eigenvalues, eigenvectors). *For these definitions, see Abadir – Magnus (2005).*

- *We denote the space of symmetric (square) matrices of the dimension n by* $\mathbb{R}^{n\times n}_{sym}$.
- *We denote the group of orthogonal (square) matrices of the dimension n (orthogonal group) by* $OG(n)$.

Definition A.26 (Matrix multiplication, Determinant of square matrix, Transposed matrix, Inverse matrix, Trace of the matrix). *These basic definitions can be found for example in Abadir – Magnus (2005).*

- *For* $\mathbf{A} \in \mathbb{R}^{n\times m}$, $\mathbf{B} \in \mathbb{R}^{m\times p}$, *matrix multiplication is denoted by* $\mathbf{AB} = \mathbf{C}$, *where* $C \in \mathbb{R}^{n\times p}$.
- *For* $\mathbf{A} \in \mathbb{R}^{n\times n}$, *the determinant is denoted by* $\det\mathbf{A}$.
- *For* $\mathbf{A} \in \mathbb{R}^{n\times n}$, $\det \mathbf{A} \neq 0$, *the inverse matrix is denoted by* $\mathbf{A}^{-1}$.
- *For* $\mathbf{A} \in \mathbb{R}^{n\times m}$, *the transposed matrix is denoted by* $\mathbf{A}^\top$.

- *For* $\mathbf{A} \in \mathbb{R}^{n\times n}$*, the trace of* $\mathbf{A}$ *is denoted by* $\operatorname{tr}\mathbf{A}$*.*

Tensors are in general defined as multilinear maps acting on vector spaces and their duals. In this thesis, we work primarily with second order tensors acting on $\mathbb{R}^n$, where $n = 2$ or $n = 3$. In this light, we identify square matrices $\mathbf{A} \in \mathbb{R}^{n\times n}$ with bilinear mappings $\mathbf{A} : \mathbb{R}^n \times \mathbb{R}^n \to \mathbb{R}$ defined by the equation

$$\mathbf{A}(\mathbf{v}, \mathbf{w}) = (\mathbf{A}\mathbf{w})^\top \mathbf{v}. \tag{A.3}$$

Conversely to (A.3), we also identify bilinear mappings $\mathbf{A} : \mathbb{R}^n \times \mathbb{R}^n \to \mathbb{R}$ with square matrices, by requiring that

$$A_{ij} = \mathbf{A}(\mathbf{e_i}, \mathbf{e_j}), \quad i, j \in \{1 \dots n\}. \tag{A.4}$$

Definition A.27 (Second order tensor over $\mathbb{R}^n$)**.** *Let* $n \in \mathbb{N}$*. Second order tensor is a bilinear mapping* $\mathbf{T} : \mathbb{R}^n \times \mathbb{R}^n \to \mathbb{R}$*, that is understood as a square matrix* $\mathbf{T} \in \mathbb{R}^{n\times n}$ *in the sense of* (A.4)*.*

For an abstract treatment of Tensor algebra, see Yokonuma (1992).

Definition A.28 (Tensor product)**.** *Let* $\mathbf{v}^1, \mathbf{v}^2 \in \mathbb{R}^n$*, then the tensor product (denoted by* $\otimes$*) is a mapping* $\mathbb{R}^n \times \mathbb{R}^n \to \mathbb{R}^{n\times n}$ *defined as*

$$(\mathbf{v}^1 \otimes \mathbf{v}^2)_{ij} = v^1_i v^2_j, \qquad i, j \in \{1 \dots n\}.$$

Definition A.29 ($\mathbf{A}^d$ - Deviatoric part of square matrix $\mathbf{A}$)**.** *For a square matrix* $\mathbf{A} \in \mathbb{R}^{n\times n}$ *we define its deviatoric part, by the formula*

$$\mathbf{A}^d = \mathbf{A} - \frac{1}{3}(\operatorname{tr}\mathbf{A})\mathbf{I}.$$

Theorem A.30 (Polar decomposition)**.** *For every matrix* $\mathbf{F} \in \mathbb{R}^{n\times n}$*,* $\det\mathbf{F} \neq 0$*, there exist an orthogonal matrix* $\mathbf{R} \in OG(n)$ *and symmetric matrices* $\mathbf{U} \in \mathbb{R}^{n\times n}_{sym}$*,* $\mathbf{V} \in \mathbb{R}^{n\times n}_{sym}$ *with* $\det\mathbf{U} = \det\mathbf{V} = |\det\mathbf{F}|$ *such that*

$$\mathbf{F} = \mathbf{R}\mathbf{U} = \mathbf{V}\mathbf{R}.$$

Proof. Proof can be found in (Abadir – Magnus, 2005, p. 226). □

Definition A.31 (Characteristic polynomial of square matrix)**.** *Characteristic polynomial of square matrix* $\mathbf{A} \in \mathbb{R}^{n\times n}$ *is a polynomial*

$$P(\lambda) = \det(\lambda\mathbf{I} - \mathbf{A})$$

Definition A.32 (Invariants of 3 dimensional matrix)**.** *Characteristic polynomial of matrix* $\mathbf{A} \in \mathbb{R}^{3\times 3}$ *has a form*

$$P(\lambda) = \lambda^3 - \mathrm{I}_A\lambda^2 + \mathrm{II}_A\lambda - \mathrm{III}_A.$$

Scalar coefficients I_A*,* II_A*,* III_A *are called invariants of matrix* $\mathbf{A}$ *and are given by the following identities*

$$\begin{aligned} \mathrm{I}_A &= \operatorname{tr}\mathbf{A}, \\ \mathrm{II}_A &= \frac{1}{2}\left((\operatorname{tr}\mathbf{A})^2 - \operatorname{tr}(\mathbf{A}^2)\right), \\ \mathrm{III}_A &= \det\mathbf{A}. \end{aligned} \tag{A.5}$$

In particular, when $\mathbf{A} = \mathbf{I}$*, then* (A.5) *yields that*

$$\mathrm{I}_I = 3, \qquad \mathrm{II}_I = 3, \qquad \mathrm{III}_I = 1.$$

Lemma A.33 (Derivatives of invariants). *The derivatives of invariants take the following values*

$$\frac{\partial \mathrm{I}_A}{\partial A_{ij}} = \delta_{ij}, \qquad \frac{\partial \mathrm{II}_A}{\partial A_{ij}} = \mathrm{I}_A \delta_{ij} - A_{ji}, \qquad \frac{\partial \mathrm{III}_A}{\partial A_{ij}} = \mathbf{A}_{jk}\mathbf{A}_{ki} - \mathrm{I}_A \mathbf{A}_{ji} + \mathrm{II}_A \delta_{ij}. \tag{A.6}$$

The values of the derivatives of invariants (A.6) *evaluated at the identity matrix* $\mathbf{I}$ *are*

$$\left.\frac{\partial \mathrm{I}_A}{\partial A_{ij}}\right|_{\mathbf{I}} = \delta_{ij}, \qquad \left.\frac{\partial \mathrm{II}_A}{\partial A_{ij}}\right|_{\mathbf{I}} = 2\delta_{ij}, \qquad \left.\frac{\partial \mathrm{III}_A}{\partial A_{ij}}\right|_{\mathbf{I}} = \delta_{ij}.$$

Proof. See (Zienkiewicz – Taylor, 2013, p. 607). □

Definition A.34 (Isotropic tensor function). *Let* $\mathbf{G} : \mathbb{R}^{n\times n} \to \mathbb{R}^{n\times n}$ *be a tensor-valued function.* $\mathbf{G}$ *is called isotropic when for all* $\mathbf{A} \in \mathbb{R}^{n\times n}$ *and* $\mathbf{Q} \in SO(n)$*, it is true that*

$$\mathbf{G}(\mathbf{Q}\mathbf{A}\mathbf{Q}^\top) = \mathbf{Q}\mathbf{G}(\mathbf{A})\mathbf{Q}^\top.$$

Theorem A.35 (Rivlin Ericksen Representation Theorem). *Let* $\mathbf{G}$ *be the function* $\mathbf{G} : \mathbb{R}^{3\times 3}_{sym} \to \mathbb{R}^{3\times 3}_{sym}$*, then the following two statements are equivalent*

- $\mathbf{G}$ *is an isotropic function.*
- *Function* $\mathbf{G}$ *can be represented as*

$$\mathbf{G}(\mathbf{A}) = a_0(\mathrm{I}_A, \mathrm{II}_A, \mathrm{III}_A)\mathbf{I} + a_1(\mathrm{I}_A, \mathrm{II}_A, \mathrm{III}_A)\mathbf{A} + a_2(\mathrm{I}_A, \mathrm{II}_A, \mathrm{III}_A)\mathbf{A}^2,$$

  where a_0*,* a_1 *and* a_2 *are scalar functions of invariants of matrix* $\mathbf{A}$*.*

Proof. See Liu (2013). □

A.2 Analysis of PDEs

In this section, we summarize the most important theoretical results regarding the analysis of PDEs. For the review of the background from the theory of Topology, see Armstrong (2010). For the review of the results from the Real analysis, see Carothers (2000). For the review of the results from the Functional analysis, see Yosida (1995). For textbooks on the analysis of PDEs, see Evans (2010) and Roubíček (2013).

A.2.1 Real analysis, Topology

Definition A.36 (Open ball of radius r). *Let* $(\mathbf{X}, \|.\|)$ *be a normed vector space,* $\mathbf{x} \in \mathbf{X}$*,* $r > 0$*, the ball of radius* r *is the set*

$$B_r(\mathbf{x}) = \{\mathbf{y} \in \mathbf{X} : \|\mathbf{y} - \mathbf{x}\| < r\}.$$

Definition A.37 (Bounded set). *Let* $\mathbf{X}$ *be a normed vector space. Set* $A \subset \mathbf{X}$ *is bounded when there exists* $d > 0$*, such that* $A \subset B_d(\mathbf{0})$*.*

Definition A.38 (Open set). *Let* $\mathbf{X}$ *be a normed vector space. Set* $A \subset \mathbf{X}$ *is open when for each point* $\mathbf{x} \in A$ *there exists* $\varepsilon > 0$*, such that* $B_\varepsilon(\mathbf{x}) \subset A$*.*

Definition A.39 (Closed set). *Let* $\mathbf{X}$ *be a normed vector space. Set* $A \subset \mathbf{X}$ *is closed when its complement* $\mathbf{X} \setminus A$ *is an open set.*

Definition A.40 (Closure of the set). *Let* $\mathbf{X}$ *be a normed vector space. The closure of the set* $A \subset \mathbf{X}$ *denoted by* $\overline{A}$ *is the intersection of all closed sets* $B \subset \mathbf{X}$*, such that* $A \subset B$*.*

Definition A.41 (Compact subset of normed vector space). *Let* $(\mathbf{X}, \|.\|)$ *be a normed vector space. We say that the subset* $\mathbf{K} \subset \mathbf{X}$ *is compact when for every collection of (possibly uncountable many) open sets*

$$\{U_\alpha\}_{\alpha \in A},$$

such that

$$\mathbf{K} = \bigcup_{\alpha \in A} U_\alpha,$$

there exists finite set $I \subset A$*, such that*

$$\mathbf{K} = \bigcup_{\alpha \in I} U_\alpha.$$

Definition A.42 (Precompact subset of normed vector space). *Let* $(\mathbf{X}, \|.\|)$ *be a normed vector space. We say that the subset* $\mathbf{P} \subset \mathbf{X}$ *is precompact if the closure* $\overline{\mathbf{P}}$ *is compact subset of* $\mathbf{X}$*.*

Lemma A.43 (Compact subset of $\mathbb{R}^n$). *The set* $A \subset \mathbf{R}^n$ *is compact if and only if* A *is closed and bounded set.*

Proof. See Armstrong (2010). □

For a broader discussion of the topological concepts, see Armstrong (2010). For the review of the use of these in the context of real analysis, see (Carothers, 2000, p.51-62).

Definition A.44 (Countable set). *Set* A *is countable if there exists one to one and onto function (bijection)* $f : A \to B$*, where* $B \subset \mathbb{N}$*.*

Definition A.45 (Separable space). *Let* $(\mathbf{X}, \|.\|)$ *be a normed vector space. Space* $(\mathbf{X}, \|.\|)$ *is separable if there exists a countable set* $A \subset \mathbf{X}$*, such that* $\overline{A} = \mathbf{X}$*.*

Definition A.46 (Convergence of sequence in the norm). *Let* $(\mathbf{X}, \|.\|)$ *be a normed vector space. Sequence* $(\mathbf{x}_n) \subset \mathbf{X}$ *converges in the norm* $\|.\|$ *to the limit* $\mathbf{L} \in \mathbf{X}$ *when*

$$\forall \varepsilon > 0, \exists N \in \mathbb{N} : \forall i > N \quad \mathbf{x}_i \in B_\varepsilon(\mathbf{L}).$$

Convergence in the norm is denoted by

$$\lim_{i \to \infty} \|\mathbf{x}_i - \mathbf{L}\| = 0, \quad \text{or} \quad \lim_{i \to \infty} \mathbf{x}_i = \mathbf{L}, \quad \text{or} \quad \mathbf{x}_i \to \mathbf{L}.$$

Definition A.47 (Cauchy sequence). *Let* $(\mathbf{X}, \|.\|)$ *be a normed vector space. Sequence* $(\mathbf{x}_n) \subset \mathbf{X}$ *is called Cauchy sequence if*

$$\forall \varepsilon > 0, \exists N \in \mathbb{N} : \forall i, j > N \quad \|\mathbf{x}_i - \mathbf{x}_j\| < \varepsilon.$$

Definition A.48 (Function). *Let* $\mathbf{X}$, $\mathbf{Y}$ *be normed spaces,* $\Omega \subset \mathbf{X}$. *Function* $f : \Omega \to \mathbf{Y}$ *is a mapping that assigns one particular value* $\mathbf{y} \in \mathbf{Y}$ *to each* $\mathbf{x} \in \Omega$.

Definition A.49 (Bounded function). *Let* $\mathbf{X}$, $\mathbf{Y}$ *be normed spaces,* $\Omega \subset \mathbf{X}$. *Function* $f : \Omega \to \mathbf{Y}$ *is bounded when* $f(\Omega)$ *is a bounded set in* $\mathbf{Y}$.

Definition A.50 (Support of function). *Let* $\mathbf{X}$, $\mathbf{Y}$ *be normed spaces,* $\Omega \subset \mathbf{X}$. *For function* $f : \Omega \to \mathbf{Y}$, *the support is a set*

$$\operatorname{supp} f = \overline{\{\mathbf{x} \in \Omega, f(\mathbf{x}) \neq \mathbf{0})\}}.$$

Definition A.51 (Continuous function). *Let* $\mathbf{X}$, $\mathbf{Y}$ *be normed spaces,* $\Omega \subset \mathbf{X}$. *Function* $f : \Omega \to \mathbf{Y}$ *is continuous if for each open set* $A \subset \mathbf{Y}$, *the set* $f^{-1}(A)$ *is open in* $\mathbf{X}$, *where* f^{-1} *is the preimage of* f.

We work mainly with scalar valued $\mathbf{Y} = \mathbb{R}$, vector-valued $\mathbf{Y} = \mathbb{R}^n$ or matrix valued $\mathbf{Y} = \mathbb{R}^{n \times m}$ functions, where the domain Ω is an open and bounded subset of the Euclidean space $\mathbf{X} = \mathbb{R}^n$. We state some important definitions and results for scalar valued functions. Most of these can be applied to vector or matrix valued functions.

Definition A.52 (Limit of function at point). *Let* $f : \mathbb{R} \to \mathbb{R}$. *We say that* L *is a limit of* f *at* $a \in \mathbb{R}$ *if*

$$\forall \varepsilon > 0, \exists \delta > 0, \forall x \in \{B_\delta(a) \setminus a\} : f(x) \in B_\varepsilon(L),$$

we write that

$$\lim_{x \to a} f(x) = L.$$

Definition A.53 (Continuous function). *Let* $\Omega \subset \mathbb{R}^n$, *the function* $f : \Omega \to \mathbb{R}$ *is continuous if the following is true*

$$\forall \varepsilon > 0, \forall \mathbf{x} \in \Omega, \exists \delta > 0, \forall \mathbf{y} \in B_\delta(\mathbf{x}) : f(\mathbf{y}) \in B_\varepsilon(f(\mathbf{x})).$$

More topological Definition A.51 and more analytical Definition A.53 of continuous function coincide, see (Armstrong, 2010, p. 32).

Definition A.54 (Uniformly continuous function). *Let* $\Omega \subset \mathbb{R}^n$, *the function* $f : \Omega \to \mathbb{R}$ *is uniformly continuous, if*

$$\forall \varepsilon > 0, \exists \delta > 0, \forall \mathbf{x} \in \Omega, \forall \mathbf{y} \in B_\delta(\mathbf{x}) : f(\mathbf{y}) \in B_\varepsilon(f(\mathbf{x})).$$

Definition A.55 (The Lipchitz continuous function). *Let* $\Omega \subset \mathbb{R}^n$, *the function* $f : \Omega \to \mathbb{R}$ *is the Lipschitz continuous if there exists a constant* $C_L > 0$, *so that*

$$\forall \mathbf{x}, \mathbf{y} \in \Omega, \quad |f(\mathbf{x}) - f(\mathbf{y})| \leq C_L |\mathbf{x} - \mathbf{y}|.$$

Definition A.56 (Partial derivative of function at point). *Let* $f : \mathbb{R}^n \to \mathbb{R}$, *we say that* P *is i-th partial derivative of* f *at point* $\mathbf{a} \in \mathbb{R}^n$ *with respect to* x_i, *when is true that*

$$\lim_{h \to 0} \frac{f(a_1, \ldots, a_i + h, \ldots, a_n) - f(a_1, \ldots, a_i, \ldots, a_n)}{h} = P.$$

Partial derivative with respect to x_i *is denoted by*

$$\frac{\partial f}{\partial x_i}(\mathbf{a}) = P.$$

Definition A.57 (Multiindex). *Multiindex, that is used to index dimensions in $\mathbb{R}^n$, is an ordered n-tuple of form $\alpha = (\alpha_1, \dots, \alpha_n)$, where $\alpha_i \in \mathbb{N}_0$. The order of multiindex is a number $|\alpha| = \sum_{i=1}^{n} \alpha_i$.*

Definition A.58 (Partial derivative with respect to multiindex). *Let f be a function $f : \Omega \to \mathbb{R}$, we define the partial derivative of f with respect to multiindex α as*

$$f^{\alpha} = \frac{\partial^{|\alpha|} f}{\partial x_1^{\alpha_1} \dots \partial x_n^{\alpha_n}}.$$

We define important classes of continuous functions.

Definition A.59 ($C^k(\Omega)$, $k \in \mathbb{N}$). *Let $\Omega \subset \mathbb{R}^n$ be an open, bounded set. Then*

$$\begin{aligned} C(\Omega) &= \{f : \Omega \to \mathbb{R} | f \text{ continuous } \}, \\ C^k(\Omega) &= \{f : \Omega \to \mathbb{R} | f^{\alpha} \in C(\Omega), |\alpha| \leq k\}, \\ C^{\infty}(\Omega) &= \bigcap_{k \in \mathbb{N}} C^k(\Omega). \end{aligned}$$

Definition A.60 ($C^k(\bar{\Omega})$, $k \in \mathbb{N}$). *Let $\Omega \subset \mathbb{R}^n$ be an open, bounded set. Then*

$$\begin{aligned} C(\bar{\Omega}) &= \{f : \Omega \to \mathbb{R} | f \text{ uniformly continuous, bounded } \}, \\ C^k(\bar{\Omega}) &= \{f : \Omega \to \mathbb{R} | f^{\alpha} \in C(\bar{\Omega}), |\alpha| \leq k\}, \\ C^{\infty}(\bar{\Omega}) &= \bigcap_{k \in \mathbb{N}} C^k(\bar{\Omega}). \end{aligned}$$

Definition A.61 ($C_c^k(\bar{\Omega})$, $k \in \mathbb{N}$). *Let $\Omega \subset \mathbb{R}^n$ be an open, bounded set. Then*

$$\begin{aligned} C_c(\Omega) &= \{f \in C(\Omega) \mid \operatorname{supp} f \text{ is compact}, \operatorname{supp} f \subset \Omega\}, \\ C_c^k(\Omega) &= \{f \in C^k(\Omega) | \operatorname{supp} f \text{ is compact}, \operatorname{supp} f \subset \Omega\}, \\ C_c^{\infty}(\Omega) &= \{f \in C^{\infty}(\Omega) | \operatorname{supp} f \text{ is compact}, \operatorname{supp} f \subset \Omega\}. \end{aligned}$$

Symmetric gradient operator

Definition A.62 (Symmetric gradient operator $\mathcal{E}$). *Let $\mathbf{u} : \mathbb{R}^n \to \mathbb{R}^n$ be a vector-valued function, then*

$$\mathcal{E}\,\mathbf{u} = \frac{1}{2}\left(\nabla \mathbf{u} + (\nabla \mathbf{u})^{\top}\right), \quad (\mathcal{E}\,\mathbf{u})_{ij} = \frac{1}{2}\left(\frac{\partial u_i}{\partial x_j} + \frac{\partial u_j}{\partial x_i}\right).$$

Observation A.63. *$\mathcal{E}$ is a linear operator, let $\mathbf{f}_1, \mathbf{f}_2 : \mathbb{R}^n \to \mathbb{R}^n$ be vector-valued functions, then*

$$\mathcal{E}(\mathbf{f}_1 + \alpha \mathbf{f}_2) = \mathcal{E}\,\mathbf{f}_1 + \alpha\,\mathcal{E}\,\mathbf{f}_2, \text{ for all } \alpha \in \mathbb{R}.$$

A.2.2 Functional analysis

Definition A.64 (Banach space). *A normed vector space $(\mathbf{X}, \|.\|)$ is called Banach space (or complete normed vector space) if each Cauchy sequence $(\mathbf{x}_n) \subset \mathbf{X}$ converges in the norm to some $\mathbf{x} \in \mathbf{X}$.*

Definition A.65 (Linear operator). *Let* $(\mathbf{X}, \|.\|_X)$, $(\mathbf{Y}, \|.\|_Y)$ *be normed vector spaces. Function* $A : \mathbf{X} \to \mathbf{Y}$ *is called a linear operator if*

$$\forall \mathbf{u}, \mathbf{v} \in \mathbf{X} : \alpha \in \mathbb{R}, \quad A(\mathbf{u} + \alpha\mathbf{v}) = A(\mathbf{u}) + \alpha A(\mathbf{v}).$$

Definition A.66 (Bounded linear operator). *Let* $(\mathbf{X}, \|.\|_X)$, $(\mathbf{Y}, \|.\|_Y)$ *be normed vector spaces. Let* $A : \mathbf{X} \to \mathbf{Y}$ *be a linear operator. A is bounded if*

$$\exists C > 0, \forall \mathbf{u} \in \mathbf{X} : \quad \|A\mathbf{u}\|_Y \leq C\|\mathbf{u}\|_X.$$

Lemma A.67. *Let* $(\mathbf{X}, \|.\|_X)$, $(\mathbf{Y}, \|.\|_Y)$ *be normed vector spaces. Linear operators* $A : \mathbf{X} \to \mathbf{Y}$ *are bounded if and only if they are continuous mappings.*

Proof. See (Yosida, 1995, p. 42). □

Definition A.68 (Space of bounded linear operators). *Let* $(\mathbf{X}, \|.\|_X)$, $(\mathbf{Y}, \|.\|_Y)$ *be normed vector spaces. By* $B(\mathbf{X}, \mathbf{Y})$ *we define the space of all bounded linear operators* $A : \mathbf{X} \to \mathbf{Y}$*, that is equipped with operator norm*

$$\|A\| = \sup\{\|A\mathbf{u}\|_Y : \mathbf{u} \in \mathbf{X}, \|\mathbf{u}\|_X \leq 1\}.$$

Lemma A.69. *Let* $(\mathbf{X}, \|.\|_X)$, $(\mathbf{Y}, \|.\|_Y)$ *be normed vector spaces. Space* $B(\mathbf{X}, \mathbf{Y})$ *with the operator norm is a normed vector space. If the space* $(\mathbf{Y}, \|.\|_Y)$ *is a Banach space, then* $B(\mathbf{X}, \mathbf{Y})$ *is also a Banach space.*

Proof. See (Yosida, 1995, p. 110). □

Definition A.70 (Dual space). *Let* $(\mathbf{X}, \|.\|)$ *be a normed vector space. Banach space* $\mathbf{X}^* = B(\mathbf{X}, \mathbb{R})$ *with operator norm is called dual space to* $\mathbf{X}$*.*

Definition A.71 (Duality pairing). *Let* $(\mathbf{X}, \|.\|)$ *be a normed vector space. For* $\mathbf{u} \in \mathbf{X}$*,* $\mathbf{u}^* \in \mathbf{X}^*$*, the duality pairing is denoted as*

$$\langle \mathbf{u}^*, \mathbf{u} \rangle = \mathbf{u}^*(\mathbf{u}).$$

Definition A.72 (Compact operator). *Let* $(\mathbf{X}, \|.\|_X)$, $(\mathbf{Y}, \|.\|_Y)$ *be a normed vector spaces,* $K : \mathbf{X} \to \mathbf{Y}$ *is linear operator. K is compact if for every bounded* $A \subset \mathbf{X}$*,* $K(A)$ *is precompact.*

Definition A.73 (Reflexive space). *Let* $(\mathbf{X}, \|.\|)$ *be normed vector space. Space* $\mathbf{X}$ *is reflexive if*

$$\forall \mathbf{u}^{**} \in \mathbf{X}^{**}, \exists \mathbf{u} \in \mathbf{X}, \forall \mathbf{u}^* \in \mathbf{X}^* : \quad \langle \mathbf{u}^{**}, \mathbf{u}^* \rangle = \langle \mathbf{u}^*, \mathbf{u} \rangle.$$

Definition A.74 (Weak convergence). *Let* $(\mathbf{X}, \|.\|)$ *be a normed vector space. Sequence* $(\mathbf{x}_n) \subset \mathbf{X}$ *converges weekly to limit* $\mathbf{L} \in \mathbf{X}$ *when*

$$\forall \phi \in X^*, \lim_{i \to \infty} \langle \phi, \mathbf{x_i} \rangle = \langle \phi, \mathbf{L} \rangle.$$

Weak convergence is denoted by

$$\mathbf{x_i} \rightharpoonup \mathbf{L}.$$

Theorem A.75 (Eberlein–Šmulian). *In the reflexive Banach space* $(\mathbf{X}, \|.\|)$*, each sequence that is bounded in the norm* $\|.\|$ *has a weakly convergent subsequence.*

Proof. See (Yosida, 1995, p.141-145). □

Definition A.76 (Continuous embedding). *Let* $(\mathbf{X}, \|.\|_X)$, $(\mathbf{Y}, \|.\|_Y)$ *be Banach spaces. We say that the space* $\mathbf{X}$ *is continuously embedded into the space* $\mathbf{Y}$*, when* $\mathbf{X} \subseteq \mathbf{Y}$ *and there exists a constant* C *such that*

$$\forall \mathbf{u} \in \mathbf{X} : \|\mathbf{u}\|_Y \leq C\|\mathbf{u}\|_X.$$

We denote continuous embedding by $\mathbf{X} \subset \mathbf{Y}$*.*

Definition A.77 (Equivalent spaces). *We say that the two Banach spaces* $(\mathbf{X}, \|.\|_X)$ *and* $(\mathbf{Y}, \|.\|_Y)$ *are equivalent when* $\mathbf{X} \subset \mathbf{Y}$ *and* $\mathbf{Y} \subset \mathbf{X}$*.*

Definition A.78 (Compact embedding). *Let* $(\mathbf{X}, \|.\|_X)$, $(\mathbf{Y}, \|.\|_Y)$ *be Banach spaces. We say that the space* $\mathbf{X}$ *is compactly embedded into the space* $\mathbf{Y}$*, when* $\mathbf{X} \subset \mathbf{Y}$ *and the identity mapping* $i : \mathbf{X} \to \mathbf{Y}$ *is a compact operator. We denote compact embedding by* $\mathbf{X} \subset\subset \mathbf{Y}$*.*

A.2.3 Lebesque spaces and Sobolev spaces

In the thesis, integral symbol, $\int$, is always used in the sense of the Lebesque integration. For the review of the theory of Lebesque integration, see (Carothers, 2000, p.263-379).

Definition A.79 (Size of the set). *Let* Ω *be a Lebesgue measurable set. Then we denote its size (Lebesgue measure) by*

$$|\Omega| = \int_\Omega 1 \, \mathrm{d}x.$$

Definition A.80 (L^p norm $\|.\|_p$). *Let* $p \geq 1$*.* L^p *norm* $\|.\|_p$ *is a mapping on the space of Lebesgue measurable functions* f *defined on* Ω*, given by*

$$\|f\|_p = \left(\int_\Omega |f|^p \, \mathrm{d}x \right)^{\frac{1}{p}}, \quad p \neq \infty$$
$$\|f\|_\infty = \operatorname*{ess\,sup}_\Omega |f|,$$

where $\operatorname{ess\,sup}_\Omega$ *denotes essential supremum. For definition, see Carothers (2000).*

Definition A.81 (L^p space).

$$L^p(\Omega) = \{f : \Omega \to \mathbb{R} | f \text{ is Lebesgue measurable}, \|f\|_p < \infty\}$$

Definition A.82 (L^p_{loc} space).

$$L^p_{loc}(\Omega) = \{f : \Omega \to \mathbb{R} | \forall K \subsetneq \Omega, K \text{ compact} : f(K) \in L^p(K)\}$$

Definition A.83 (Weak derivative). *Let* $u, v \in L^1_{loc}(\Omega)$*,* α *is a multiindex. We say that* v *is the weak derivative of* u *with respect to* α*, that is denoted by* $u^\alpha = v$*, when*

$$\int_\Omega u\phi^\alpha \, \mathrm{d}x = (-1)^{|\alpha|} \int_\Omega v\phi \, \mathrm{d}x, \quad \forall \phi \in C_c^\infty(\Omega).$$

If the strong derivative exists, it coincides with the weak derivative, see (Evans, 2010, p 257). Thus we understand Definition A.83 as an extension of Definition A.58. When working with Sobolev spaces, unless stated otherwise, we understand derivatives in the weak sense.

Definition A.84 (Sobolev space). *Let $k \in \mathbb{N}_0$, $p \geq 1$, then we define Sobolev space*

$$W^{k,p}(\Omega) = \{f \in L^1_{loc}(\Omega) | \forall \alpha, |\alpha| \leq k \ \exists f^\alpha, f^\alpha \in L^p(\Omega)\}.$$

Definition A.85 ($W^{k,p}$ norm $\|.\|_{k,p}$). *Let $k \in \mathbb{N}_0$, $p \geq 1$, $f \in W^{k,p}(\Omega)$. The norm $\|.\|_{k,p}$ is defined as*

$$\|f\|_{k,p} = \left(\sum_{|\alpha| \leq k} \|f^\alpha\|_p^p \right)^{\frac{1}{p}}, \quad p \neq \infty,$$
$$\|f\|_{k,\infty} = \sum_{|\alpha| \leq k} \|f^\alpha\|_\infty.$$

Definition A.86 (Sobolev space with zero trace). *Let $k \in \mathbb{N}_0$, $p \geq 1$, then we define*

$$W_0^{k,p}(\Omega) = \text{closure of } C_c^\infty(\Omega) \text{ in } \|.\|_{k,p}.$$

Theorem A.87. *Let $\Omega \subset \mathbb{R}^n$ be an open, bounded set. Let $1 < p < \infty$ and $k \in \mathbb{N}$. The spaces $(L^p(\Omega), \|.\|_p)$, $(W^{k,p}(\Omega), \|.\|_{k,p})$ and $(W_0^{k,p}(\Omega), \|.\|_{k,p})$ are then separable, reflexive Banach spaces.*

Proof. See for example (Adams – Fournier, 2003, p. 61). □

Definition A.88 (Boundary continuity and Lipschitz domains). *Let $\Omega \subset \mathbb{R}^n$ be open and bounded, for every $\mathbf{x} \in \partial\Omega$ let exist an open set U_x, $\mathbf{x} \in U_x$ and one to one and onto mapping $A_x : Q \to U_x$, where*

$$Q = \{\mathbf{x} \in \mathbb{R}^n : \ |x_j| < 1, j = 1 \dots n\},$$
$$Q^+ = \{\mathbf{x} \in Q : \ x_n > 0\},$$
$$Q^0 = \{\mathbf{x} \in Q : \ x_n = 0\},$$

such that $A_x(Q^+) = U_x \cap \Omega$, $A_x(Q^0) = U_x \cap \partial\Omega$. We say that $\Omega \in C^k$ if $A_x \in C^k(\overline{Q})$ and $A_x^{-1} \in C^k(\overline{U_x})$ for all $\mathbf{x} \in \Omega$. We say that the boundary is Lipschitz $\Omega \in C^{0,1}$ if A_x and A_x^{-1} are Lipschitz functions for all $\mathbf{x} \in \Omega$. For more details, see for example (Dacorogna, 2009, p. 34).

Theorem A.89 (Rellich-Kondrachov Compactness Theorem). *Let $\Omega \subset \mathbb{R}^n$ be an open, bounded domain, $\Omega \in C^{0,1}$. Let $1 \leq p < n$. Then*

$$\text{for } 1 \leq q < \frac{pn}{n-p}, \quad W^{1,p}(\Omega) \subset\subset L^q(\Omega).$$

Moreover when $p \in [n, \infty)$ it can be shown that

$$\forall q \in [1, \infty), \quad W^{1,p}(\Omega) \subset\subset L^q(\Omega).$$

Proof. See (Evans, 2010, p. 286), Rellich (1930). □

Definition A.90 (Spaces of vector and matrix valued functions). *To work with vector or matrix (tensor) valued functions, for $k \in \mathbb{N}_0$, $p \geq 1$ and $n \in \mathbb{N}_0$ we denote spaces of n dimensional vector-valued functions, by $C^k(\Omega)^n$, $L^p(\Omega)^n$, $W^{k,p}(\Omega)^n$, etc. Spaces of $n \times n$ dimensional matrix valued functions are denoted by by $C^k(\Omega)^{n \times n}$, $L^p(\Omega)^{n \times n}$, $W^{k,p}(\Omega)^{n \times n}$, etc. Spaces of $n \times n$ dimensional symmetric matrix valued functions are denoted by $C^k(\Omega)^{n \times n}_{sym}$, $L^p(\Omega)^{n \times n}_{sym}$, $W^{k,p}(\Omega)^{n \times n}_{sym}$, etc.*

A.2.4 Monotone operators

In this section, the symbol $\mathbf{X}$ denotes separable, reflexive Banach space and $\mathbf{X}^*$ is its dual.

Definition A.91 (Radial continuity). *Let* $\mathbf{F}$ *be an operator* $\mathbf{F} : \mathbf{X} \to \mathbf{X}^*$. *We say that* $\mathbf{F}$ *is radially continuous if for all* $\mathbf{x}, \mathbf{y} \in \mathbf{X}$, *the function* $f_{\mathbf{x},\mathbf{y}} : \mathbb{R} \to \mathbb{R}$ *defined by*

$$f_{\mathbf{x},\mathbf{y}}(t) = \langle \mathbf{F}(\mathbf{x} + t\mathbf{y}), \mathbf{y} \rangle$$

is a continuous function.

Lemma A.92 (Minty's lemma). *Let* $\mathbf{F}$ *be a radially continuous operator* $\mathbf{F} : \mathbf{X} \to \mathbf{X}^*$. *Let* $\mathbf{a} \in \mathbf{X}$, $\mathbf{g} \in \mathbf{X}^*$ *be such that*

$$\forall \mathbf{y} \in \mathbf{X}, \quad \langle \mathbf{g} - \mathbf{F}(\mathbf{y}), \mathbf{a} - \mathbf{y} \rangle \geq 0. \tag{A.7}$$

Then $\mathbf{F}(\mathbf{a}) = \mathbf{g}$, *see Minty (1963).*

Proof. Let $\varepsilon > 0$, $\phi \in \mathbf{X}$, setting $\mathbf{y} = \mathbf{a} + \varepsilon\phi$ in (A.7) yields

$$\langle \mathbf{g} - \mathbf{F}(\mathbf{a} + \varepsilon\phi), -\varepsilon\phi \rangle \geq 0. \tag{A.8}$$

We divide (A.8) by $-\varepsilon$ and take the limit $\varepsilon \to 0$. We have that

$$\lim_{\varepsilon \to 0} \langle \mathbf{g} - \mathbf{F}(\mathbf{a} + \varepsilon\phi), \phi \rangle = \langle \mathbf{g} - \mathbf{F}(\mathbf{a}), \phi \rangle \leq 0. \tag{A.9}$$

As we have chosen $\phi \in \mathbf{X}$ arbitrarily, the inequality holds also for $-\phi$ and by multiplication by -1 we get the opposite inequality to (A.9). Therefore we obtain

$$\langle \mathbf{F}(\mathbf{a}), \phi \rangle = \langle \mathbf{g}, \phi \rangle \quad \forall \phi \in \mathbf{X},$$

which means $\mathbf{F}(\mathbf{a}) = \mathbf{g}$. □

There is an important class of operators for which we are able to establish the inequality (A.7), these are monotone operators.

Definition A.93 (Monotone operator). *Let* $\mathbf{F}$ *be an operator* $\mathbf{F} : \mathbf{X} \to \mathbf{X}^*$. *We say that* $\mathbf{F}$ *is monotone if it satisfies*

$$\langle \mathbf{F}(\mathbf{x}_1) - \mathbf{F}(\mathbf{x}_2), \mathbf{x}_1 - \mathbf{x}_2 \rangle \geq 0 \quad \textit{for all} \quad \mathbf{x}_1, \mathbf{x}_2 \in \mathbf{X}.$$

Observation A.94. *To represent constitutive equation, we work with a tensor valued functions of the type*

$$\mathbf{G}(\mathbf{T}) : \mathbb{R}^{n\times n}_{sym} \to \mathbb{R}^{n\times n}_{sym}. \tag{A.10}$$

For $q \in (1, \infty)$, *let* $\mathbf{X} = L^q(\Omega)^{n\times n}_{sym}$ *and* $\mathbf{X}^* = L^{q'}(\Omega)^{n\times n}_{sym}$. *We define operator* $\mathbf{G} : L^q(\Omega)^{n\times n}_{sym} \to L^{q'}(\Omega)^{n\times n}_{sym}$, *which is related to the constitutive equation* (A.10) *by the formula*

$$\forall \mathbf{T}, \mathbf{W} \in L^q(\Omega)^{n\times n}_{sym}, \quad \langle \mathbf{G}(\mathbf{T}), \mathbf{W} \rangle = \int_\Omega \mathbf{G}(\mathbf{T}) : \mathbf{W} \, \mathrm{d}x. \tag{A.11}$$

The representation of a tensor-valued function $\mathbf{G}(\mathbf{T})$ as an operator in the sense of Observation A.94 is useful when $\mathbf{G}(\mathbf{T})$ is poitwise monotone.

Definition A.95 (Monotone tensor-valued function). *Let* $\mathbf{G}(\mathbf{T})$ *be a tensor-valued function* $\mathbf{G} : \mathbb{R}^{n\times n}_{sym} \to \mathbb{R}^{n\times n}_{sym}$. *We say that* $\mathbf{G}$ *is monotone if it satisfies*

$$\forall \mathbf{T}_1, \mathbf{T}_2 \in \mathbb{R}^{n\times n}_{sym}, \quad (\mathbf{G}(\mathbf{T}_1) - \mathbf{G}(\mathbf{T}_2)) : (\mathbf{T}_1 - \mathbf{T}_2) \geq 0.$$

Observation A.96. *Let* $\mathbf{G}(\mathbf{T})$ *be a monotone tensor-valued function. Then the operator* $\mathbf{G}$ *from* (A.11) *is a monotone operator.*

Observation A.97. *Let* $\mathbf{G}_1$ *and* $\mathbf{G}_2$ *be a monotone functions or operators with the same signature. The sum* $\mathbf{G}_1 + \mathbf{G}_2$ *is then also a monotone function or operator.*

A.2.5 Important inequalities

Definition A.98 (Hölder conjugates). *Let* $q \in [1, \infty]$, *then we define the Hölder conjungate* q' *by*

$$q' = \begin{cases} \frac{q}{q-1}, & \text{when} \quad q \in (1, \infty), \\ 1, & \text{when} \quad q = \infty, \\ \infty, & \text{when} \quad q = 1. \end{cases}$$

Lemma A.99 (Young's inequality). *Let* $\varepsilon > 0$, $a, b > 0$, p, q *by the Hölder conjungates* $p, q \in (1, \infty)$, *then the following is true*

$$ab \leq \varepsilon a^p + C(\varepsilon) b^q, \quad C(\varepsilon) = \frac{(\varepsilon p)^{-q/p}}{q}.$$

Proof. See (Evans, 2010, page 706) □

Lemma A.100 (Hölder inequality). *Let* $q, q' \in [1, \infty]$ *be the Hölder conjungates,* $\mathbf{u} \in L^q(\Omega)$ *and* $\mathbf{v} \in L^{q'}(\Omega)$. *Then we have the following inequality*

$$\int_\Omega \mathbf{u}\mathbf{v} \, \mathrm{d}x \leq \|\mathbf{u}\|_q \|\mathbf{v}\|_{q'}.$$

Proof. See (Evans, 2010, page 706) □

Observation A.101. *Let* $p \in [1, \infty]$, $\mathbf{u} \in W^{1,p}(\Omega)^n$, *it holds that*

$$\|\mathcal{E}\,\mathbf{u}\|_p \leq \|\nabla \mathbf{u}\|_p.$$

Proof. By triangle inequality. □

Theorem A.102 (Poincaré-Friedrichs inequality). *Let* $\Omega \subset \mathbb{R}^n$, $\Gamma \subset \partial\Omega$, $(n-1)$*-dimensional Hausdorff measure of* Γ *is positive and* $p \in [1, \infty)$. *Then there exists a constant* $C > 0$, *such that for all* $\mathbf{u} \in W^{1,p}(\Omega)$ *we have that*

$$\|\mathbf{u}\|^p_{1,p} \leq C(\|\nabla \mathbf{u}\|^p_p + \int_\Gamma |\mathbf{u}|^p \, \mathrm{d}S).$$

Proof. See Poincaré (1890). □

Theorem A.103 (Interpolation inequality for Lebesque spaces). *Let $\Omega \subset \mathbb{R}^n$ be an open, bounded set. Let $1 \leq s \leq r \leq t \leq \infty$ and*

$$\frac{1}{r} = \frac{\theta}{s} + \frac{1-\theta}{t}.$$

Let $u \in L^s(\Omega) \cap L^t(\Omega)$. Then $u \in L^r(\Omega)$ and

$$\|u\|_r \leq \|u\|_s^{\theta} \|u\|_t^{1-\theta}.$$

Proof. See (Evans, 2010, page 707) □

Theorem A.104 (Trace theorem). *Let $\Omega \in C^{0,1}$ be an open, bounded set, let $p \in [1, \infty)$. Then there exists a bounded linear operator*

$$\mathrm{Tr} : W^{1,p} \to L^p(\partial\Omega),$$

and a constant $C > 0$, which depends on Ω and p, so that

$$\forall \mathbf{u} \in W^{1,p} \quad \|\mathrm{Tr}\,\mathbf{u}\|_p \leq C\|\mathbf{u}\|_{1,p},$$

and

$$\forall \mathbf{u} \in W^{1,p} \cap C(\overline{\Omega}) \quad \mathrm{Tr}\,\mathbf{u} = \mathbf{u}|_{\partial\Omega}.$$

Proof. See (Evans, 2010, page 772) □

A.2.6 Finite element method

In this part, we outline some important definitions and results from the theory of the finite element method. For a detailed overview, we refer to a classical book Ciarlet (2002). For the mathematical theory of the finite element method, see Brenner – Scott (2002). For the application oriented book, that comes free of charge, with a focus on FEniCS software library, see Logg et al. (2012).

Definition A.105 (Subdivision of Ω). *Let $\Omega \subset \mathbb{R}^n$ be an open, bounded domain. A subdivision of Ω is a finite collection of open sets $\mathcal{K}_h = \{K_i, i = 1 \dots N\}$, such that:*

- $K_i \cap K_j = \emptyset$ *for* $i \neq j$,
- $\bigcup_{i=1}^{N} \overline{K_i} = \overline{\Omega}$.

Definition A.106 (Triangulation of Ω). *Let $\Omega \subset \mathbb{R}^n$ be an open, bounded domain. The subdivision $\mathcal{T}_h = \{T_i, i = 1 \dots N\}$ is a triangulation if $\overline{T_i}$, $i \in \{1 \dots N\}$ are all triangles and each two different triangles has either*

- *one common edge and two common vertices,*
- *no common edges and one common vertex,*
- *no common edges nor vertices.*

Definition A.107 (Space of polynomials up to degree k). *Let $\Omega \subset \mathbb{R}^n$ be an open, bounded domain, $k \in \mathbb{N}$. We denote $P^k(\Omega)$ the space of polynomials up to degree k on Ω. Each element of $P^k(\Omega)$ has a form*

$$p = \sum_{|\alpha| \leq k} \gamma_\alpha x^\alpha, \quad \gamma_\alpha \in \mathbb{R},$$

where α is a multiindex and x to the power of α is defined as

$$x^\alpha = x_1^{\alpha_1} \dots x_n^{\alpha_n}.$$

Definition A.108 (Piece-wise polynomial space). *Let $\Omega \subset \mathbb{R}^n$ be an open, bounded domain. Let $\mathcal{T}_h$ be a triangulation of Ω. We define the following space of piece-wise polynomials of degree k.*

$$X_h^k = \{u_h \subset C^0(\overline{\Omega}), u_h|_T \in P^k(T), \forall T \in \mathcal{T}_h\}.$$

Theorem A.109. *Let $\Omega \subset \mathbb{R}^n$ be an open, bounded domain. Let $\mathcal{T}_h$ be a triangulation of Ω. Let $q \in (1, \infty)$. The function $u : \Omega \to \mathbb{R}$ belongs to $W^{1,q}(\Omega)$ if and only if the following is true:*

- *$u|_T \in W^{1,q}(T), \forall T \in \mathcal{T}_h$,*
- *For each common edge e of the two triangles $e = \overline{T_i} \cup \overline{T_j}$, the traces of u in $W^{1,q}(T_i)$ and $W^{1,q}(T_j)$ coincide on e. We have that $u|_{e_{T_i}} = u|_{e_{T_j}}$.*

Proof. See (Kwak, 2014, Proposition 3.2.1.). □

Lemma A.110 (Conformity of X_h^k). *Let $\Omega \subset \mathbb{R}^n$ be an open, bounded domain. Let $\mathcal{T}_h$ be a triangulation of Ω. For $k \in \mathbb{N}$, the space $X_h^k \subseteq W^{1,q}(\Omega)$.*

Proof. We can easily see that $u|_T \in W^{1,q}(T), \forall T \in \mathcal{T}_h$. Traces of polynomials are well defined, since they are from the space $C^\infty(\bar{T})$. Therefore using Theorem A.109 we get the claim. □

Definition A.111 (Finite element). *Finite element is a triple $(K, \mathcal{P}, \mathcal{N})$, where*

- *$K \subset \mathbb{R}^n$ is a domain with piecewise smooth boundary.*
- *$\mathcal{P}$ is a finite-dimensional space of functions on K.*
- *$\mathcal{N} = \{N_1, \dots, N_k\}$ is a basis of a $\mathcal{P}^*$.*

A.3 Solid mechanics

In this section, we review essential Solid mechanics principles and definitions. We focus on small strain elastostatics. Further discussion of the concepts of Solid mechanics including dynamic effects can be found in Liu (2013, 2006), Truesdell – Noll (1969), Oden (2008), Sadd (2009).

A.3.1 Kinematics

Let $\mathbb{E}$ represent a vector space that abstracts a physical space. $\mathbb{E}$ is two or three dimensional Euclidean space $\mathbb{E} = \mathbb{R}^2$ or $\mathbb{E} = \mathbb{R}^3$. We project representations of the body $\mathcal{B}$ at different points of time to $\mathbb{E}$.

Definition A.112 (Configuration). *The representation of a body at particular time t is called its configuration and is mathematically represented by mapping*

$$\kappa_t : \mathcal{B} \to \mathbb{E}.$$

There is one important configuration called reference configuration κ_R. Reference configuration might not be connected with any time but in practice it usually coincides with the configuration of the body κ_0 at initial time $t = 0$. Current configuration κ_t is a configuration of the body at time t. For evolutionary problems, time is continuous, $t \in [0, T]$, and we have infinitely many current configurations κ_t. For the static problems, time is discrete, $t \in \{0, \infty\}$. By κ_∞, we understand the deformed steady state of the material after the application of forces to the body at initial state. For the purpose of the thesis, we identify the reference configuration κ_R with the initial state of the body κ_0. The deformed configuration is κ_∞.

Definition A.113 (Reference and deformed configuration). *Let κ_R be the reference configuration and κ_∞ the deformed configuration. Point $\mathbf{X} \in \kappa_R(\mathcal{B})$ denotes the body particle in the reference configuration and $\mathbf{x} \in \kappa_\infty(\mathcal{B})$ denotes the body particle at a deformed configuration.*

Deformation and strain

Definition A.114 (Deformation). *Deformation described by the mapping χ,*

$$\chi : \kappa_R(\mathcal{B}) \to \kappa_\infty(\mathcal{B}), \quad \chi(\mathbf{X}) = \kappa_\infty(\kappa_R^{-1}(\mathbf{X})).$$

Definition A.115 (Displacement). *Body motion relative to the initial state of the body is described by the displacement vector*

$$\mathbf{u} = \chi(\mathbf{X}) - \mathbf{X}.$$

Definition A.116 (Deformation gradient and its determinant).

$$\mathbf{F} = \nabla_{\mathbf{X}} \chi = \mathbf{I} + \nabla_{\mathbf{X}} \mathbf{u}, \qquad J = \det \mathbf{F}. \tag{A.12}$$

We assume that mapping $\chi : \kappa_R(\mathcal{B}) \to \kappa_\infty(\mathcal{B})$ has differentiable inversion χ^{-1} and that $\det \mathbf{F} > 0$, which can be interpreted such that the body can not penetrate itself. The deformation gradient $\mathbf{F}$ (Jacobian matrix of χ) then exists. Inverse function theorem, see (Corwin, 1982, p. 225), yields that the inverse mapping χ^{-1} has Jacobian matrix $\mathbf{F}^{-1}$.

From Theorem A.30, there is a polar decomposition of $\mathbf{F}$ of the form

$$\mathbf{F} = \mathbf{RU} = \mathbf{VR}, \tag{A.13}$$

where $\mathbf{R} \in OG(n)$, $\mathbf{U} \in \mathbb{R}^{n\times n}_{sym}$, $\mathbf{V} \in \mathbb{R}^{n\times n}_{sym}$ with $\det \mathbf{U} = \det \mathbf{V} = \det \mathbf{F}$.

Definition A.117 (Right and left stretch tensors, rotation tensor). *We call* $\mathbf{R}$ *from* (A.13) *a rotation tensor. The tensors* $\mathbf{U}$ *and* $\mathbf{V}$ *are right and left stretches.*

Definition A.118 (Right and left Cauchy-Green strain tensors). *The tensor* $\mathbf{C} = \mathbf{U}^2 = \mathbf{F}^\top\mathbf{F}$ *is called the right Cauchy-Green strain tensor. The tensor* $\mathbf{B} = \mathbf{V}^2 = \mathbf{F}\mathbf{F}^\top$ *is the left Cauchy-Green strain tensor.*

Definition A.119 (Small strain tensor). *Small strain tensor* ε *is defined as a symmetric gradient of the displacement vector*

$$\varepsilon = \mathcal{E}\,\mathbf{u} = \frac{1}{2}\left(\nabla\mathbf{u} + (\nabla\mathbf{u})^\top\right).$$

Small displacement gradinet assumption

In the small displacement gradient range, the square of the norm of the displacement gradient can be neglected in comparison to the norm of the displacement gradient. In other words, it is possible to neglect quadratic terms that are present in Cauchy-Green strain tensors. In case of left Cauchy-Green strain tensor $\mathbf{B} = \mathbf{F}\mathbf{F}^\top = (\mathbf{I} + \nabla_{\mathbf{X}}\,\mathbf{u})(\mathbf{I} + \nabla_{\mathbf{X}}\,\mathbf{u})^\top = \mathbf{I} + \nabla_{\mathbf{X}}\,\mathbf{u} + (\nabla_{\mathbf{X}}\,\mathbf{u})^\top + \nabla_{\mathbf{X}}\,\mathbf{u}(\nabla_{\mathbf{X}}\,\mathbf{u})^\top$, we neglect the last term and approximate $\nabla_{\mathbf{X}}\,\mathbf{u} \approx \nabla\mathbf{u}$.

Definition A.120 (Small displacement gradient assumption). *In small strain theory we work with materials in the regimen where* $|\nabla_{\mathbf{X}}\,\mathbf{u}| < \delta \ll 1$.

The following proposition is important for the derivation of small strain approximations of constitutive relations in the theory of elasticity (small strain elasticity). It is also utilized in the framework of Implicit constitutive theory, see Rajagopal (2003, 2007, 2011a), to derive constitutive relations in the small strain regimen.

Proposition A.121 (Small strain proposition). *Under the Small displacement gradient assumption, see Definition A.120, it is possible to approximate* $\mathbf{B} - \mathbf{I} \approx 2\varepsilon$.

Proof. In this proof, we follow Liu (2013). Using (A.12), we obtain

$$\mathbf{B} - \mathbf{I} = \mathbf{F}\mathbf{F}^\top - \mathbf{I} = \nabla_{\mathbf{X}}\,\mathbf{u} + (\nabla_{\mathbf{X}}\,\mathbf{u})^\top + \mathbf{h}(\nabla_{\mathbf{X}}\,\mathbf{u}),\ \text{where}\ \lim_{|\mathbf{A}|\to 0}\frac{|\mathbf{h}(\mathbf{A})|}{|\mathbf{A}|} = 0. \quad \text{(A.14)}$$

By the chain rule, we can write

$$\nabla_{\mathbf{X}}\,\mathbf{u} = (\nabla\mathbf{u})\mathbf{F} = \nabla\mathbf{u}(\mathbf{I} + \nabla_{\mathbf{X}}\,\mathbf{u}) \approx \nabla\mathbf{u}. \quad \text{(A.15)}$$

Last assumption holds since

$$\lim_{|\nabla_{\mathbf{X}}\,\mathbf{u}|\to 0}\frac{|\nabla\mathbf{u}\,\nabla_{\mathbf{X}}\,\mathbf{u}|}{|\nabla_{\mathbf{X}}\,\mathbf{u}|} \leq \lim_{|\nabla_{\mathbf{X}}\,\mathbf{u}|\to 0}|(\nabla_{\mathbf{X}}\,\mathbf{u})\mathbf{F}^{-1}| = 0. \quad \text{(A.16)}$$

In (A.16), we use approximation $\mathbf{F}^{-1} \approx \mathbf{I} - \nabla_{\mathbf{X}}\,\mathbf{u}$ as $\mathbf{F} = \mathbf{I} + \nabla_{\mathbf{X}}\,\mathbf{u}$. Combining equations (A.14) and (A.15), we finally obtain

$$\mathbf{B} - \mathbf{I} = \mathbf{F}\mathbf{F}^\top - \mathbf{I} = \nabla\mathbf{u} + (\nabla\mathbf{u})^\top + \hat{\mathbf{h}}(\nabla_{\mathbf{X}}\,\mathbf{u}),\ \text{where}\ \lim_{|\mathbf{A}|\to 0}\frac{|\hat{\mathbf{h}}(\mathbf{A})|}{|\mathbf{A}|} = 0,$$

which proves small strain proposition. □

Compatibility of small strain

For every sufficiently smooth function $\mathbf{u}$, there exists its symmetric gradient $\mathcal{E}\,\mathbf{u}$. The inverse problem is to find for a given symmetric tensor ε the function $\mathbf{u}$, so that $\varepsilon = \mathcal{E}\,\mathbf{u}$. The following theorem gives a necessary and sufficient condition to solve this problem.

Definition A.122 (Saint-Venant's compatibility tensor). *For a symmetric second order tensor* $\mathbf{E}$*, the Saint-Venant's compatibility tensor* $\mathbf{W}(\mathbf{E})$ *is the fourth order tensor of the form*

$$W_{ijkl}(\mathbf{E}) = \frac{\partial^2 E_{ij}}{\partial x_k \partial x_l} + \frac{\partial^2 E_{kl}}{\partial x_i \partial x_j} - \frac{\partial^2 E_{il}}{\partial x_j \partial x_k} - \frac{\partial^2 E_{jk}}{\partial x_i \partial x_l}. \tag{A.17}$$

Theorem A.123 (Saint-Venant's theorem). *For a given second order tensor* ε *defined over simply connected domain* Ω*, there exists vector* $\mathbf{u}$ *such that* $\varepsilon = \mathcal{E}\,\mathbf{u}$ *if and only if* $\mathbf{W}(\varepsilon) = \mathbf{0}$ *everywhere in* Ω*.*

Proof. The theorem has been proven for the first time in Beltrami (1886). It can be found also in Amrouche et al. (2006) or (Sadd, 2009, Chapter 2). For the proof of Saint-Venant's theorem in the weak sense, where only the Lebesgue integrability of ε is required, see Ciarlet – Ciarlet (2005). For non-simply connected domains, there is a result by Yavari (2013). □

A.3.2 Cauchy stress and equations of equilibrium

In this section, we define the Cauchy stress tensor and recall equations of the static equilibrium.

Surface traction $\mathbf{t}$ is defined as a force acting on an infinitesimal surface perpendicular to a given unit vector $\boldsymbol{\nu}$ at a point $\mathbf{x} \in \kappa_\infty(\mathcal{B})$ of the deformed configuration.

Definition A.124 (Surface traction). *Let* $\boldsymbol{\Delta}\mathbf{A}(\boldsymbol{\nu})$ *be a surface perpendicular to* $\boldsymbol{\nu}$*,* $\mathbf{x} \in \boldsymbol{\Delta}\mathbf{A}(\boldsymbol{\nu})$*. Let* $\mathbf{F}_\mathbf{A}(\mathbf{x}, \boldsymbol{\Delta}\mathbf{A}(\boldsymbol{\nu}))$ *be the force acting on that surface. Then the surface traction is defined as*

$$\mathbf{t} = \lim_{|\boldsymbol{\Delta}\mathbf{A}(\boldsymbol{\nu})| \to 0} \frac{\mathbf{F}_\mathbf{A}(\mathbf{x}, \boldsymbol{\Delta}\mathbf{A}(\boldsymbol{\nu}))}{|\boldsymbol{\Delta}\mathbf{A}(\boldsymbol{\nu})|}.$$

Definition A.125 (Cauchy postulate). *Surface traction only depends on the position* $\mathbf{x}$ *and the normal vector to the surface* $\boldsymbol{\nu}$*. It does not depend on a particular choice of the surface.*

$$\mathbf{t} = \mathbf{t}(\mathbf{x}, \boldsymbol{\nu})$$

Definition A.126 (Body force density per volume). *Let* $\mathbf{x} \in \kappa_\infty(\mathcal{B})$ *and* $\Delta V \subset \kappa_\infty(\mathcal{B})$ *be a volume element, so that* $\mathbf{x} \in \Delta V$*. Let* $\mathbf{F}(\Delta V)$ *be the force acting on the volume element* ΔV*. Then body force density per volume is defined as a limit*

$$\mathbf{f}(\mathbf{x}) = \lim_{|\Delta V| \to 0} \frac{\mathbf{F}(\Delta V)}{|\Delta V|}.$$

Equations of static equilibrium

The surface force, caused by the surface traction $\mathbf{t}(\mathbf{x}, \boldsymbol{\nu})$ and the body force caused by the force density $\mathbf{f}$ must be in equilibrium on each part of the body $B \subset \kappa_\infty(\mathcal{B})$. That can be mathematically expressed by the following integral equation

$$\int_{\partial B} \mathbf{t}(\mathbf{x}, \boldsymbol{\nu}) \, \mathrm{d}x + \int_B \mathbf{f}(\mathbf{x}) \, \mathrm{d}x = 0. \tag{A.18}$$

Theorem A.127 (Cauchy theorem). *Suppose that surface traction $\mathbf{t}(\mathbf{x}, \boldsymbol{\nu})$ and body force density $\mathbf{f}(\mathbf{x})$ are Lebesque integrable functions in $B \subset \kappa_\infty(\mathcal{B})$. Then there exists stress tensor $\mathbf{T}(\mathbf{x})$ that is Lebesque integrable in B and fully describes stress at any given point $\mathbf{x} \in B$. It holds that*

$$\mathbf{t}(\mathbf{x}, \boldsymbol{\nu}) = \mathbf{T}(\mathbf{x})\boldsymbol{\nu}. \tag{A.19}$$

Proof. For proof, see Gurtin et al. (1968). □

Definition A.128 (Cauchy stress tensor). *The Cauchy stress tensor $\mathbf{T}(\mathbf{x})$, that exists by the Cauchy theorem, fully describes stress in the deformed configuration of the body $\kappa_\infty(\mathcal{B})$. Cauchy stress can be represented by matrix*

$$\mathbf{T}(\mathbf{x}) = \left(\mathbf{t}(\mathbf{x}, \mathbf{e_1}), \mathbf{t}(\mathbf{x}, \mathbf{e_2}), \mathbf{t}(\mathbf{x}, \mathbf{e_3})\right),$$

where $\mathbf{e_i}$ are natural basis vectors of $\mathbb{R}^3$.

Using (A.19) and Divergence theorem, we can rewrite the equation (A.18) into the form

$$\int_B \operatorname{div} \mathbf{T} + \mathbf{f} \, \mathrm{d}x = \mathbf{0}. \tag{A.20}$$

As $B \subset \kappa_\infty(\mathcal{B})$ was chosen arbitrarily, the integral in (A.20) must be zero in $\kappa_\infty(\mathcal{B})$, therefore the local form of the equations of equilibrium (A.20) is

$$\operatorname{div} \mathbf{T} + \mathbf{f} = \mathbf{0}.$$

Theorem A.129 (Symmetry of Cauchy stress tensor). *The Cauchy stress tensor $\mathbf{T}$ is a symmetric second order tensor.*

Proof. This fact follows from the balance of angular momentum, the proof can be found for example in Shabana (2011). □

A.3.3 Constitutive theory

Constitutive relations between stress and deformation describe physical nature of the material. The models, which are used in the thesis were already defined in chapter 2. We always have to keep in mind the transformation properties that these relations explicitly or implicitly assume as a consequences of the physical principles of objectivity and frame indifference and material symmetries such as isotropy. Therefore, in this thesis, we decided to define particular constitutive relations together with their transformation properties. This approach brings clarity when dealing with constitutive relations and their transformations in a mathematical manner. Here we briefly recall the meaning of objectivity, frame indiference and isotropy.

Objectivity

When two observers measure kinematic quantities or the Cauchy stress in different coordinate systems, measured quantities should be related in a particular way. Assume that we transform coordinate systems from one coordinate system (all quantities denoted without star) to another (all quantities are denoted with star).

Definition A.130 (Objective quantity). *Let the change of coordinate system (from* $\mathbf{x}$ *to* $\mathbf{x}^*$*) be given by the transformation*

$$\mathbf{x}^* = \mathbf{Q}(\mathbf{x} - \mathbf{x}_0) + \mathbf{a},$$

where $\mathbf{Q} \in OG(n)$, $\mathbf{x}_0 \in \mathbb{R}^n$, $\mathbf{a} \in \mathbb{R}^n$ *are fixed. For scalar* c*, vector* $\mathbf{v}$ *and tensor* $\mathbf{T}$ *(measured in non * coordinate system), we say that these quantities are objective if the corresponding quantities* c^*, $\mathbf{v}^*$ *and* $\mathbf{T}^*$ *(measured in * coordinate system), are related in the following way*

$$\begin{aligned} c^* &= c \\ \mathbf{v}^* &= \mathbf{Q}\mathbf{v} \\ \mathbf{T}^* &= \mathbf{Q}\mathbf{T}\mathbf{Q}^\top. \end{aligned}$$

It can be shown that the left stretch tensor $\mathbf{V}$ and the left Cauchy-Green strain tensor $\mathbf{B}$ are objective. For details, see Liu (2013). The objectivity of the Cauchy stress tensor is one of basic postulates of Continuum mechanics.

Postulate A.131 (Euclidean objectivity). *The Cauchy stress tensor* $\mathbf{T}$ *is an objective tensor quantity.*

Frame indifference

Principle of frame indifference is a formalization of the idea that when we change coordinate system, then the underlying physical system should behave independently of that change. This principle is formalized by stating that constitutive relations that relate objective quantities should behave in a specific way when subjected to the orthogonal transformation, see Liu (2013).

Isotropy

Isotropy is a property of material that behaves in the same manner regardless of its orientation. There is no directional preference in the constitutive relation.

For broader discussion of the concepts of objectivity, frame indifference and isotropy and their consequences on the constitutive relations, see Liu (2013).

A.3.4 Linearized elasticity

Probably, the most widely used class of models in Solid mechanics are models with a linear constitutive relation, Hooke's law. Linearized elastic models are capable to capture behavior of wide range of materials that have different underlying structure (metal, rock, wood, bone, numerous alloys, ...) with reasonable accuracy using the same basic approach.

Definition A.132 (Linearized elastic solid). *We define linearized elastic solid as a generally anisotropic material with a constitutive relation of the type*

$$\mathbf{T} = \mathbf{C}\varepsilon, \tag{A.21}$$

where $\mathbf{C}$ *is a fourth order tensor with the following properties*

$$C_{ijkl} = C_{jikl} = C_{ijlk}, \quad C_{ijkl} = C_{klij}, \quad i,j,k,l \in \{1,2,3\}. \tag{A.22}$$

Linearized elastic solid is an approximation of the Cauchy elastic solid under the Small displacement gradient assumption, see Definition A.120. For details of the derivation, see (Liu, 2006, section 5.2). The equation (A.22) yields that the tensor $\mathbf{C}$ has 21 independent values of elastic moduli. If we represent symmetric tensors $\mathbf{T}$ and ε as

$$\mathbf{T} = (T_{11}, T_{22}, T_{33}, T_{12}, T_{13}, T_{23})^\top, \quad \boldsymbol{\varepsilon} = (\varepsilon_{11}, \varepsilon_{22}, \varepsilon_{33}, \varepsilon_{12}, \varepsilon_{13}, \varepsilon_{23})^\top,$$

then we understand $\mathbf{C}$ as 6×6 symmetric matrix and the right hand side of the constitutive equation (A.21) as a classical matrix multiplication.

Hooke's law for isotropic solid

In this section, we derive Hooke's law for isotropic solid under the Small displacement gradient assumption, see Definition A.120, as an approximation of the constitutive model for the Isotropic Cauchy elastic solid, see Definition 2.3, (p. 19). For more details, see Liu (2006, 2013).

Proposition A.133. *Under the Small displacement gradient assumption, see Definition A.120, we can approximate the response* (2.6) *of isotropic Cauchy elastic solid, see Definition 2.3, (p. 19), by equation*

$$\mathbf{T} = \lambda(\operatorname{tr}\varepsilon)\mathbf{I} + 2\mu\varepsilon, \tag{A.23}$$

where λ *and* μ *are called Lamé constants. The linear equation* (A.23) *is called Hooke's law.*

Proof. We can approximate the function (2.6) by the linear term of its Taylor series. We have that

$$\widetilde{G}_{ij}(\mathbf{B}) = \widetilde{G}_{ij}(\mathbf{I}) + \left.\frac{\partial \widetilde{G}_{ij}}{\partial B_{kl}}\right|_{\mathbf{I}} (B_{kl} - \delta_{kl}) + H_{ij}(\mathbf{B}), \tag{A.24}$$

where

$$\lim_{\mathbf{B}\to\mathbf{I}} \frac{|\mathbf{H}(\mathbf{B})|}{|\mathbf{B}-\mathbf{I}|} = 0.$$

Under the small displacement gradient assumption the function $\mathbf{H}$ in (A.24) can be neglected. From small strain proposition A.121, we have that $\mathbf{B} - \mathbf{I} \approx 2\varepsilon$ and Definition 2.3, (p. 19) of isotropic Cauchy elastic solid assumes $\widetilde{\mathbf{G}}(\mathbf{I}) = \mathbf{0}$. Therefore we can approximate (A.24) as

$$\widetilde{G}_{ij}(\mathbf{B}) = 2 \left.\frac{\partial \widetilde{G}_{ij}}{\partial B_{kl}}\right|_{\mathbf{I}} \varepsilon_{kl}. \tag{A.25}$$

Since $\mathbf{B}$ is a objective, symmetric tensor, the Rivlin Ericksen Representation Theorem A.35 yields

$$\widetilde{\mathbf{G}}(\mathbf{B}) = \alpha_1(\mathrm{I}_B, \mathrm{II}_B, \mathrm{III}_B)\mathbf{I} + \alpha_2(\mathrm{I}_B, \mathrm{II}_B, \mathrm{III}_B)\mathbf{B} + \alpha_3(\mathrm{I}_B, \mathrm{II}_B, \mathrm{III}_B)\mathbf{B}^2.$$

Let denote

$$\bar{\alpha} = \alpha_1 + \alpha_2 + \alpha_3.$$

Using formulas for derivatives of invariants, see Lemma A.33, we obtain

$$\left.\frac{\partial \widetilde{G}_{ij}}{\partial B_{kl}}\right|_{\mathbf{I}} = \left(\left.\frac{\partial \bar{\alpha}}{\partial \mathrm{I}_B}\right|_{(3,3,1)} \delta_{kl} + \left.\frac{\partial \bar{\alpha}}{\partial \mathrm{II}_B}\right|_{(3,3,1)} 2\delta_{kl} + \left.\frac{\partial \bar{\alpha}}{\partial \mathrm{III}_B}\right|_{(3,3,1)} \delta_{kl} \right) \delta_{ij} + \alpha_1(3,3,1) \left.\frac{\partial \delta_{ij}}{\partial \mathbf{B}_{kl}}\right|_{\mathbf{I}} + \alpha_2(3,3,1) \left.\frac{\partial \mathbf{B}_{ij}}{\partial \mathbf{B}_{kl}}\right|_{\mathbf{I}} + \alpha_3(3,3,1) \left.\frac{\partial \mathbf{B}_{in}\mathbf{B}_{nj}}{\partial \mathbf{B}_{kl}}\right|_{\mathbf{I}}. \quad \text{(A.26)}$$

Let define

$$\lambda = 2 \left(\left.\frac{\partial \bar{\alpha}}{\partial \mathrm{I}_B}\right|_{(3,3,1)} + 2 \left.\frac{\partial \bar{\alpha}}{\partial \mathrm{II}_B}\right|_{(3,3,1)} + \left.\frac{\partial \bar{\alpha}}{\partial \mathrm{III}_B}\right|_{(3,3,1)} \right), \quad \text{(A.27)}$$

and

$$\mu = \alpha_2(3,3,1) + 2\alpha_3(3,3,1). \quad \text{(A.28)}$$

Inserting (A.27) and (A.28) into the equation (A.26), we get

$$2 \left.\frac{\partial \widetilde{\mathbf{G}}_{ij}}{\partial \mathbf{B}_{kl}}\right|_{\mathbf{I}} \varepsilon_{kl} = \lambda(\operatorname{tr}\boldsymbol{\varepsilon})\delta_{ij} + 2\mu\varepsilon_{ij}. \quad \text{(A.29)}$$

Combining (2.6) with (A.25) and (A.29), we obtain

$$\mathbf{T}_{ij} = \lambda(\operatorname{tr}\boldsymbol{\varepsilon})\delta_{ij} + 2\mu\boldsymbol{\varepsilon}_{ij},$$

which completes the proof. □

Hooke's law inversion

Hooke's law (A.23) can be inverted into the form

$$\boldsymbol{\varepsilon} = -\frac{\lambda \operatorname{tr}\mathbf{T}}{2\mu(2\mu + 3\lambda)}\mathbf{I} + \frac{\mathbf{T}}{2\mu}. \quad \text{(A.30)}$$

Material moduli

It is sometimes convenient to express Hooke's law in terms of other parameters than Lamé constants λ and μ. For example, we can rewrite Hooke's law (A.23) using bulk and shear moduli K and μ into the form

$$\mathbf{T} = K(\operatorname{tr}\boldsymbol{\varepsilon})\mathbf{I} + 2\mu\boldsymbol{\varepsilon}^d, \text{ where } K = \frac{3\lambda + 2\mu}{3},$$

or equivalently,

$$\boldsymbol{\varepsilon} = \frac{1}{9K}(\operatorname{tr}\mathbf{T})\mathbf{I} + \frac{1}{2\mu}\mathbf{T}^d. \quad \text{(A.31)}$$

Parameters characterising linear material response such as λ, μ or K are called elastic moduli. Typically, they have a particular physical meaning and each two of them may be used to fully describe a linearized isotropic elastic solid. Here we list important elastic moduli, which are first Lamé parameter λ, shear modulus μ, bulk modulus K, Young's modulus E and Poison's ratio ν.

Definition A.134 (First Lamé parameter). *First Lamé parameter λ is one of the two moduli present in Hooke's law* (A.23). *This modulus is hard to measure directly. Its SI unit is Pascal* [Pa].

Definition A.135 (Shear modulus). *Shear modulus or modulus of rigidity is denoted by μ, in some sources also by G. It is a ratio of the shear stress to the shear strain. Its SI unit is Pascal* [Pa].

From Hooke's law (A.23), *in a state of pure shear where $\varepsilon_{12} = \varepsilon_{21} = \gamma$, $T_{12} = T_{21} = \sigma$ and other components $T_{ij} = \varepsilon_{ij} = 0$, we can derive $\mu = \sigma/2\gamma$. We assume that the value of Shear modulus is strictly positive $\mu > 0$ as the shearing stress produces deformation in the direction of applied force.*

Definition A.136 (Bulk modulus). *Bulk modulus or modulus of compression is denoted by K and it is a measure of resistance to compression. Its SI unit is Pascal* [Pa].

Bulk modulus is defined as a negative proportion of hydrostatic pressure to the term $\varepsilon_{11} + \varepsilon_{22} + \varepsilon_{33}$, which is a first order estimate of the volume change of the specimen. In a state of pure hydrostatic pressure, when $T_{11} = T_{22} = T_{33} = \sigma$, we derive from Hooke's law (A.23) *that*

$$K = \frac{\sigma}{\varepsilon_{11} + \varepsilon_{22} + \varepsilon_{33}} = \frac{3\lambda + 2\mu}{3}. \tag{A.32}$$

We assume that the value of Bulk modulus is strictly positive, $K > 0$, as the hydrostatic pressure causes a decrease in volume.

Definition A.137 (Young's modulus). *Young's modulus or Elastic modulus is denoted by E. It is a ratio of tensile stress to tensile strain. Young's modulus is easy to measure and is often used in engineering. Its SI unit is Pascal* [Pa].

In a simple tension, where $T_{11} = \sigma$ and $T_{ij} = 0$ otherwise, from Hooke's law (A.30) *we have the formula*

$$E = \frac{\sigma}{\varepsilon_{11}} = \frac{\mu(3\lambda + 2\mu)}{\lambda + \mu}.$$

We assume that the value of Young's modulus is strictly positive, $E > 0$, as the tension causes elongation.

Definition A.138 (Poison's ratio). *Poison's ratio, denoted by ν, is a negative proportion of transverse axial strain to longitudinal strain in a direction of applied force in a simple tension. It is dimensionless.*

In a simple tension, where $T_{11} = \sigma$ and $T_{ij} = 0$ otherwise, combining Hooke's law (A.30) *with a formula for bulk modulus* (A.32) *yields that*

$$\nu = -\frac{\varepsilon_{22}}{\varepsilon_{11}} = \frac{\lambda}{2\lambda + 2\mu} = \frac{3K - 2\mu}{6K + 2\mu}. \tag{A.33}$$

From equation (A.33), *when assuming $K > 0$, $\mu > 0$, we have that $\nu > -1$, $\nu < 0.5$.*

In Table A.1, transformation relations between important elastic moduli are outlined.

	λ	μ	K	E	ν
(λ, μ)	-	-	$\frac{3\lambda+2\mu}{3}$	$\frac{\mu(3\lambda+2\mu)}{\lambda+\mu}$	$\frac{\lambda}{2(\lambda+\mu)}$
(λ, K)	-	$\frac{3(K-\lambda)}{2}$	-	$\frac{9K(K-\lambda)}{3K-\lambda}$	$\frac{\lambda}{3K-\lambda}$
(λ, E) [3]	-	$\frac{E-3\lambda+A}{4}$	$\frac{E+3\lambda+A}{6}$	-	$\frac{2\lambda}{E+\lambda+A}$
(λ, ν)	-	$\frac{\lambda(1-2\nu)}{2\nu}$	$\frac{\lambda(1+\nu)}{3\nu}$	$\frac{\lambda(1+\nu)(1-2\nu)}{\nu}$	-
(μ, K)	$\frac{3K-2\mu}{3}$	-	-	$\frac{9K\mu}{3K+\mu}$	$\frac{3K-2\mu}{2(3K+\mu)}$
(μ, E)	$\frac{\mu(E-2\mu)}{3\mu-E}$	-	$\frac{E\mu}{3(3\mu-E)}$	-	$\frac{E-2\mu}{2\mu}$
(μ, ν)	$\frac{2\mu\nu}{1-2\nu}$	-	$\frac{2\mu(1+\nu)}{3(1-2\nu)}$	$2\mu(1+\nu)$	-
(K, E)	$\frac{3K(3K-E)}{9K-E}$	$\frac{3KE}{9K-E}$	-	-	$\frac{3K-E}{6K}$
(K, ν)	$\frac{3K\nu}{1+\nu}$	$\frac{3K(1-2\nu)}{2(1+\nu)}$	-	$3K(1-2\nu)$	-
(E, ν)	$\frac{E\nu}{(1+\nu)(1-2\nu)}$	$\frac{E}{2(1+\nu)}$	$\frac{E}{3(1-2\nu)}$	-	-

Table A.1: Conversion relationships between elastic moduli: first Lamé parameter λ, shear modulus μ, bulk modulus K, Young's modulus E and Poisson's ratio ν.

Separating the bulk part from isochoric parts of deformation

Hooke's law (A.30) can be rewritten into the form

$$\operatorname{tr}\boldsymbol{\varepsilon} = \frac{1}{3K}\operatorname{tr}\mathbf{T}, \quad \boldsymbol{\varepsilon}^d = \frac{1}{2\mu}\mathbf{T}^d. \tag{A.34}$$

The decomposition (A.34) is in keeping with an idea in that the response is split into a part that describes volume changes in a response to normal stress and a part that represents the shear response. In the theory of the nonlinear isotropic compressible hyperelasticity, such decomposition was first proposed by Flory (1961). Let define a modified deformation gradient $\overline{\mathbf{F}}$ and a modified left Cauchy-Green deformation tensor $\overline{\mathbf{B}}$

$$\overline{\mathbf{F}} = J^{-1/3}\mathbf{F}, \qquad \overline{\mathbf{B}} = J^{-2/3}\mathbf{B},$$

where $\mathbf{F}$ is a deformation gradient, J is the determinant of $\mathbf{F}$ and $\mathbf{B}$ is a left Cauchy-Green deformation tensor. Modified deformation gradient $\overline{\mathbf{F}}$ and modified left Cauchy-Green deformation tensor $\overline{\mathbf{B}}$ represent the volume preserving part of the deformation with determinants $\det\overline{\mathbf{F}} = \det\overline{\mathbf{B}} = 1$. The stress strain relation for a compressible Neo-Hokean model with parameters $\hat{\mu}$ and $\hat{K}$ that correspond to the shear and bulk moduli is of the form

$$\mathbf{T} = \hat{K}(J-1)\mathbf{I} + \hat{\mu}J^{-5/3}\mathbf{B}^d,$$

see Holzapfel (2000). In the context of small strain theory, under the small displacement gradient assumption, see Definition A.120, we approximate

$$J \approx 1 + \operatorname{tr}\boldsymbol{\varepsilon}, \qquad J^{-5/3} \approx 1, \qquad \mathbf{B} \approx \mathbf{I} + 2\boldsymbol{\varepsilon},$$

[3] Here we set $A = \sqrt{E^2 + 9\lambda^2 + 2E\lambda}$.

and obtain

$$\mathbf{T} = \hat{K}(\operatorname{tr}\varepsilon)\mathbf{I} + 2\hat{\mu}\varepsilon^{d}.$$

Therefore the decomposition proposed by Flory (1961) is analogous to the decomposition (A.34).

B. Supplementary materials

Supplementary materials are organized by chapters and they can be found on DVD attached to this thesis. These materials contain source code of the algorithms described in the thesis and additional files described below.

If a chapter contains figures produced using MetaPost, see Hobby (2017), the sources of these figures are put into the `metapost` subfolder. If there are figures produced using R, see R Core Team (2016) or specifically using ggplot2 package, see Wickham (2009), the sources of these figures are put into the `rfigures` subfolder or `ggplot2` subfolder.

Supplementary materials concern Chapter 1, Chapter 3 and Chapter 5 and thus they are organized into the following directories.

```
/
├── 01Introduction
├── 03ModelingTitaniumAlloys
└── 05ComputerSimulations
```

Chapter 1 - Introduction

Subfolder `01Introduction` is organized as follows.

```
01Introduction
└── metapost
    └── computationalDomain.mp ..... Figure 1.1
```

Chapter 3 - Modeling of Gum Metal and other newly developed titanium alloys

Supplementary materials for Chapter 3 are in folder `03ModelingTitaniumAlloys`. In the subfolder `tables`, we enclose the tensile loading experimental data that were used in the algorithm to find the best fit. The source codes for this algorithm are included in the `R` subfolder. More precisely, the best fit can be computed using functions findBestFit or findObjectiveFit from the file `fittingAlgorithm.R`. The folder `03ModelingTitaniumAlloys` is organized as follows.

```
03ModelingTitaniumAlloys
├── tables
│   ├── saito2003.csv ..... Table 3.1.
│   ├── sakaguch2004.csv ..... Table 3.2.
│   ├── hao2005.csv ..... Table 3.3.
│   └── hou2010.csv ..... Table 3.4.
├── ggplot2
│   ├── tensileLoadingExperiments.R ..... Figure 3.2.
│   └── predictedResponses.R ..... Figures 3.18–3.23.
├── rfigures
│   ├── qualityOfFit.R ..... Figures 3.3–3.6.
│   └── bulkShear.R ..... Figures 3.7–3.17.
└── R ..... R source codes for the best fit algorithm.
    ├── fittingAlgorithm.R ..... Functions findBestFit and findObjectiveFit.
    └── IO.R ..... Input output management.
```

Chapter 5 - Computer simulations

Supplementary materials for Chapter 5 are in the folder `05ComputerSimulations`.

The subfolder `generatemesh` contains Matlab scripts[1], which we use to create adaptively refined triangular meshes on the geometries of computational domains specified in Section 5.3.1. In particular, the file `createMeshes.m` can be used to create structure, from which the triangulation data are exported. The file `ExportData.m` is an actual implementation of the export of the triangulation data. For each geometry and refinement level, it exports triangulation data into the two files named `*triangles.txt` and `*vertices.txt` in a format that fully describes a given triangulation.

The subfolder `meshtoxml` contains JAVA source code that performs conversion of the triangulation data into the XML format, which can be consumed by FEniCS component dolfin. More specifically, it takes files `*triangles.txt` and `*vertices.txt` and creates a new output file `*dolfin.xml`.

Actual implementation of the solver for the problem described in Section 5.3 is in the directory `solver`, which has two subdirectories. In the directory `classes` there are core classes that implements the solver and the manipulations with the solutions. In the directory `scripts` we put the programs that use aforementioned classes to solve particular problems described in this thesis. The main class to perform numerical simulations using FEniCS library is in the file `VNotchSolverPowerLaw.py`. It uses the class `Damping.py`, which is a implementation of damped Newton's method and the class `BoundaryConditions.py`, which encapsulates the boundary conditions. There is also a class `DirectoryVisitor.py`, which is able to browse the directory structure of the discretizations and call solver on yet unsolved problems. `DirectoryWrapper.py` is a class that manages solutions with respect to the refinement level in a single directory. The class `ErrorNorms.py` performs computations of error norms (5.23). The class `GeometryParams.py` encapsulates different geometries as they are defined in Section 5.3.1 and the class `MaterialModel.py` encapsulates the material models from Table 5.1. In the directory `classes/IO`, there are two classes for storing and loading solutions `SolutionExporter.py` and `SolutionImporter.py`. In the directory `solver/scripts`, are the following files. The scripts `SolvePowerLaw.py` and `SolveBatch.py` can be used to call the solver using command line or for solving multiple problems non-interactively. The script `paraviewMeshImages.py` can be used to create Figures 5.8–5.10, which visualize the adaptive mesh refinement process. Scripts `VCFigures.py`, `VFigures.py` and `VOFigures.py` can be used to create XDMF files that contain data regarding stress and strain components of the solutions that can be visualized, see Figures 5.14–5.22. The script `GenerateErrorNorms.py` can be used to generate Tables 5.2–5.10. And finally the script `TabulateMaxDist.py` can be used to tabulate distances (5.25) and in turn to generate the source file `solutions.csv`, which can be used to produce Figures 5.23–5.32.

In the subfolder `visualizations` we enclose XDMF files exported using scripts `VCFigures.py`, `VFigures.py` and `VOFigures.py`. Stress and strain distributions that are included in these XDMF files can be visualized in ParaView, see Ayachit

[1]Triangular meshes are created using COMOL, see COMSOL AB (2008). We use the LIVELINK interface to communicate with COMSOL from Matlab, see https://www.comsol.com/livelink-for-matlab. It allows us to write scripts that automate the task of creating the meshes.

(2016). The files contain solutions to the problems LIN2, NLO2, NLB2 and NLS2, see Table 5.1 on the most refined mesh. We include the visualizations for V geometry with $\alpha = 1°$. For VO and VC geometries we include the visualizations for $\alpha = 90°$ and $r_c \in \{0.05, 0.01, 0.005, 0.001\}$. Note that these are exactly the solutions that were used for visualizations in Figures 5.11–5.22.

We are including the described structure of the folder `05ComputerSimulations`.

```
05ComputerSimulations
├── metapost
│   ├── antiPlaneStress.mp ..... Figure 5.1.
│   ├── polarCoordinates.mp ..... Figure 5.2.
│   └── createGeometryFigures.mp ..... Figures 5.5, 5.6 and 5.7.
├── ggplot2
│   ├── plotExponents.R ..... Figures 5.3 and 5.4.
│   ├── plotDependences.R ..... Figures 5.23–5.32.
│   └── solutions.csv ..... Precomputed source data for Figures 5.23–5.32.
├── generatemesh ..... Matlab source files to generate meshes.
│   ├── createMeshes.m ..... Script to create adaptively refined meshes.
│   └── ExportData.m ..... Script for mesh export.
├── meshtoxml ..... XML format of triangulation data.
│   └── ComsolToXMLMeshFiles.java ..... Format converter.
├── solver ..... Implementation of the solver.
│   ├── classes
│   │   ├── VNotchSolverPowerLaw.py ..... Power law solver.
│   │   ├── BoundaryConditions.py ..... Boundary conditions.
│   │   ├── Damping.py ..... Damped Newton's method.
│   │   ├── DirectoryVisitor.py ..... Browse the directory structure.
│   │   ├── DirectoryWrapper.py .... Management of directory with solutions.
│   │   ├── ErrorNorms.py ..... Compute error norms.
│   │   ├── GeometryParams.py ..... Encapsulates geometries.
│   │   ├── MaterialModel.py ..... Encapsulates models.
│   │   └── IO
│   │       ├── SolutionExporter.py ..... Exporting solutions.
│   │       └── SolutionImporter.py ..... Importing solutions.
│   └── scripts
│       ├── SolvePowerLaw.py ..... Script to call solver.
│       ├── SolveBatch.py ..... Solve multiple problems.
│       ├── paraviewMeshImages.py ..... Visualize mesh refinement.
│       ├── VCFigures.py ..... XDMF export.
│       ├── VFigures.py ..... XDMF export.
│       ├── VOFigures.py ..... XDMF export.
│       ├── GenerateErrorNorms.py ..... Generate tables of error norms.
│       └── TabulateMaxDist.py ..... Tabulate distances (5.25).
└── visualizations ..... Selected stress and strain distributions.
```

List of Figures

1.1 Domain illustration. 7

2.1 Diagram of stress strain responses 16

3.1 Elastic properties of Gum Metal 32
3.2 Tensile loading data of beta phase titanium alloys 33
3.3 Tensile loading response of Gum Metal 45
3.4 Tensile loading response of *Ti-30Nb-10Ta-5Zr* alloy 45
3.5 Tensile loading response of *Ti-24Nb-4Zr-7.9Sn* alloy 46
3.6 Tensile loading response of *Ti-24Nb-4Zr-7.9Sn* alloy 46
3.7 Bulk and shear responses of Gum Metal 1 48
3.8 Bulk and shear responses of Gum Metal 2 48
3.9 Bulk and shear responses of Gum Metal 3 49
3.10 Bulk and shear responses of *Ti-30Nb-10Ta-5Zr* alloy 1 49
3.11 Bulk and shear responses of *Ti-30Nb-10Ta-5Zr* alloy 2 50
3.12 Bulk and shear responses of *Ti-30Nb-10Ta-5Zr* alloy 3 50
3.13 Bulk and shear responses of *Ti-24Nb-4Zr-7.9Sn* alloy 1 51
3.14 Bulk and shear responses of *Ti-24Nb-4Zr-7.9Sn* alloy 2 51
3.15 Bulk and shear responses of *Ti-24Nb-4Zr-7.9Sn* alloy 3 52
3.16 Bulk and shear responses of *Ti-30Nb-12Zr* alloy 1 52
3.17 Bulk and shear responses of *Ti-30Nb-12Zr* alloy 2 53
3.18 Bulk responses of all alloys 1 53
3.19 Bulk responses of all alloys 2 54
3.20 Bulk responses of all alloys 3 54
3.21 Generalized Poisson's ratio for all alloys 1 55
3.22 Generalized Poisson's ratio for all alloys 2 55
3.23 Strain component ε_{22} for all alloys 58

5.1 Anti-plane stress setting 83
5.2 Cylindrical coordinate system. 87
5.3 Dependence of the exponent k_T on α. 88
5.4 Dependence of the exponents k_T and k_e on q' for $\alpha = 0$. 88
5.5 V geometry of a computational domain 90
5.6 VO geometry of a computational domain 90
5.7 VC geometry of a computational domain 91
5.8 Visualization of adaptive mesh refinement, V geometry 94
5.9 Visualization of adaptive mesh refinement, VO geometry 95
5.10 Visualization of adaptive mesh refinement, VC geometry 95
5.11 Visualization of local error 101
5.12 Decrease of local error when refining mesh 102

5.13 Comparison of numerical to asymptotic solution in V geometry . . . 103
5.14 Comparison of stress distributions in V geometry 105
5.15 Comparison of strain distributions in V geometry 106
5.16 Asymptotic behavior of stress and strain in V geometry 107
5.17 Comparison of stress distributions in VO geometry 108
5.18 Comparison of strain distributions in VO geometry 109
5.19 Plots of stress and strain over the line in VO geometry 110
5.20 Comparison of stress distributions in VC geometry 111
5.21 Comparison of strain distributions in VC geometry 112
5.22 Plots of stress and strain over the line in VC geometry 113
5.23 Maximal T_{23} and ε_{23} in V geometry with respect to α. 115
5.24 Maximal T_{23} and ε_{23} in VO geometry and VC geometry, model LIN2 116
5.25 Maximal T_{23} and ε_{23} in VO geometry and VC geometry, model NLO2 117
5.26 Maximal T_{23} and ε_{23} in VO geometry and VC geometry, model NLB2 118
5.27 Maximal T_{23} and ε_{23} in VO geometry and VC geometry, model NLS2 119
5.28 Distances DT2, DT3 and DE1 in V geometry 120
5.29 Distances DT2, DT3 and DE1 in VO and VC geometries, model LIN2 . 121
5.30 Distances DT2, DT3 and DE1 in VO and VC geometries, model NLO2 122
5.31 Distances DT2, DT3 and DE1 in VO and VC geometries, model NLB2 123
5.32 Distances DT2, DT3 and DE1 in VO and VC geometries, model NLS2 124

List of Tables

3.1 Uniaxial tensile loading data of Gum Metal 34
3.2 Uniaxial tensile loading data of *Ti-30Nb-10Ta-5Zr* alloy 35
3.3 Uniaxial tensile loading data of *Ti-24Nb-4Zr-7.9Sn* alloy 36
3.4 Uniaxial tensile loading data of *Ti-30Nb-12Zr* alloy 37
3.5 Elastic moduli of various materials 38
3.6 Single crystal moduli of studied beta phase titanium alloys 39
3.7 VRH estimates of the elastic parameters of studied titanium alloys. 40
3.8 Estimates of Young's modulus for titanium alloys 40
3.9 The best fit, highly nonlinear bulk response, $\tau_0 = 0.5$ GPa 47
3.10 The best fit, highly nonlinear bulk response, $\tau_0 = \sigma_{max}$ 47
3.11 The best fit, highly nonlinear shear response, $\tau_0 = 0.5$ GPa 56
3.12 The best fit, highly nonlinear shear response, $\tau_0 = \sigma_{max}$ 56
3.13 The best fit, maximizing objective function, $\tau_0 = 0.5$ GPa 57
3.14 Parameters of existing models for titanium alloys 57

5.1 Parameters of computer simulations 93
5.2 Mesh properties and error norms V domain, $\alpha = 1°$ 96
5.3 Mesh properties and error norms V domain, $\alpha = 90°$ 97
5.4 Mesh properties and error norms V domain, $\alpha = 170°$ 97
5.5 Mesh properties and error norms, VO domain $\alpha = 2°$, $r_c = 0.001$ . . 98
5.6 Mesh properties and error norms, VO domain $\alpha = 2°$, $r_c = 0.01$ . . 98
5.7 Mesh properties and error norms, VO domain $\alpha = 2°$, $r_c = 0.05$ . . 99
5.8 Mesh properties and error norms, VC domain $\alpha = 2°$, $r_c = 0.001$ . . 99
5.9 Mesh properties and error norms, VC domain $\alpha = 2°$, $r_c = 0.01$ . . . 100
5.10 Mesh properties and error norms, VC domain $\alpha = 2°$, $r_c = 0.05$ . . . 100

A.1 Conversion relationships between elastic moduli 151

Acronyms

BVP	Boundary value problem
FEM	Finite element method
PDE	Partial differential equation

Bibliography

Abadir, K. M. – Magnus, J. R. *Matrix Algebra*. Cambridge University Press, 2005. ISBN 9780521822893.

Adams, R. A. – Fournier, J. J. F. *Sobolev Spaces*. Academic Press, 2003. ISBN 9780080541297.

Alnæs, M. et al. The FEniCS project version 1.5. *Archive of Numerical Software*. 2015, 3, 100, p. 9–23. doi: 10.11588/ans.2015.100.20553. [Available online].

Amrouche, C. et al. On Saint Venant's compatibility conditions and Poincaré's lemma. *Comptes Rendus Mathematique*. 2006, 342, 11, p. 887–891. doi: 10.1016/j.crma.2006.03.026. [Available online].

Argyris, J. H. Energy Theorems and Structural Analysis. *Aircraft Engineering and Aerospace Technology*. 1955, 27, 2, p. 42–58. doi: 10.1108/eb032525. [Available online].

Armstrong, M. A. *Basic Topology*. Springer New York, 2010. ISBN 9781441928191.

Atkinson, C. – Champion, C. R. Some boundary-value problems for the equation $\nabla.(|\nabla\Phi|^N\nabla\Phi) = 0$. *Quarterly journal of mechanics and applied mathematics*. 1984, 37, 3, p. 401–419. doi: 10.1093/qjmam/37.3.401. [Available online].

Ayachit, U. The Paraview Guide: Community Edition, Updated for ParaView version 5.0. https://www.paraview.org/paraview-guide/, 2016. [Available online].

AZoNetwork UK Ltd. AZoM.com - the A to Z of Materials. http://www.azom.com. [Available online].

Bassani, J. L. Notch-tip stresses in a creeping solid. *ASME, Transactions, Journal of Applied Mechanics*. 1984, 51, 3, p. 475–480. doi: 10.1115/1.3167660. [Available online].

Beck, L. et al. On the Existence of Integrable Solutions to Nonlinear Elliptic Systems and Variational Problems with Linear Growth. *Archive for Rational Mechanics and Analysis*. 2017, p. 1–53. doi: 10.1007/s00205-017-1113-4. [Available online].

Beltrami, E. Sull'interpretazione meccanica delle formole di Maxwell. *Il Nuovo Cimento*. 1886, 20, 1, p. 5–25. doi: 10.1007/bf02737284. [Available online].

Brenner, S. C. – Scott, L. R. *The Mathematical Theory of Finite Element Methods*. Springer New York, 2002. ISBN 9780387954516.

Bridges, C. – Rajagopal, K. R. Implicit constitutive models with a thermodynamic basis: a study of stress concentration. *Zeitschrift für angewandte Mathematik und Physik*. 2014, 66, 1, p. 1–18. doi: 10.1007/s00033-014-0398-5. [Available online].

Bulíček, M. et al. On elastic solids with limiting small strain: modelling and analysis. *EMS Surv. Math. Sci*. 2014, 1, 2, p. 283–332. doi: 10.4171/emss/7. [Available online].

Bulíček, M. et al. Existence of solutions for the anti-plane stress for a new class of strain-limiting elastic bodies. *Calculus of Variations and Partial Differential Equations*. 2015a, 54, 2, p. 2115–2147. doi: 10.1007/s00526-015-0859-5. [Available online].

Bulíček, M. – Málek, J. – Süli, E. Analysis and approximation of a strain-limiting nonlinear elastic model. *Mathematics and Mechanics of Solids*. 2015b, 20, 1, p. 92–118. doi: 10.1177/1081286514543601. [Available online].

Carothers, N. L. *Real Analysis*. Cambridge University Press, 2000. ISBN 9780521497565.

Cauchy, A. L. De la pression ou tension dans un corps solide. *Ex. de math*. 1827, 2, p. 42–56.

Chambers, J. M. – Hastie, T. *Statistical Models in S*. Wadsworth & Brooks/Cole Advanced Books & Software, 1992. ISBN 9780534167646.

Ciarlet, P. G. *The Finite Element Method for Elliptic Problems*. Society for Industrial and Applied Mathematics, 2002. ISBN 9780898715149.

Ciarlet, P. G. – Ciarlet, P. Another approach to linearized elasticity and a new proof of Korn's inequality. *Mathematical Models and Methods in Applied Sciences*. 2005, 15, 02, p. 259–271. doi: 10.1142/S0218202505000352. [Available online].

Clough, R. W. Early history of the finite element method from the view point of a pioneer. *International Journal for Numerical Methods in Engineering*. 2004, 60, 1, p. 283–287. doi: 10.1002/nme.962. [Available online].

Clough, R. W. The finite element method in plane stress analysis, 1960.

COMSOL AB. COMSOL multiphysics user's guide. http://www.comsol.com, 2008.

Corwin, L. J. *Multivariable Calculus*. CRC Press, 1982. ISBN 9780824769628.

Courant, R. Variational methods for the solution of problems of equilibrium and vibrations. *Bull. Amer. Math. Soc*. 1943, 49, 1, p. 1–23. doi: 10.1090/s0002-9904-1943-07818-4. [Available online].

Criscione, J. C. – Rajagopal, K. R. On the modeling of the non-linear response of soft elastic bodies. *International Journal of Non-Linear Mechanics*. 2013, 56, p. 20–24. doi: 10.1016/j.ijnonlinmec.2013.05.004. [Available online].

Criscione, J. C. et al. An invariant basis for natural strain which yields orthogonal stress response terms in isotropic hyperelasticity. *Journal of the Mechanics and Physics of Solids*. 2000, 48, 12, p. 2445–2465. doi: 10.1016/S0022-5096(00)00023-5. [Available online].

Dacorogna, B. *Introduction to the Calculus of Variations*. Imperial College Press, 2009. ISBN 9781848163331.

Devendiran, V. K. et al. A thermodynamically consistent constitutive equation for describing the response exhibited by several alloys and the study of a meaningful physical problem. *International Journal of Solids and Structures*. 2017, 108, p. 1–10. doi: 10.1016/j.ijsolstr.2016.07.036. [Available online].

Ebmeyer, C. – Liu, S. W. Quasi-Norm interpolation error estimates for the piecewise linear finite element approximation of p-Laplacian problems. *Numerische Mathematik*. 2005, 100, 2, p. 233–258. doi: 10.1007/s00211-005-0594-5. [Available online].

Erk, K. A. – Henderson, K. J. – Shull, K. R. Strain stiffening in synthetic and biopolymer networks. *Biomacromolecules*. 2010, 11, 5, p. 1358–1363. doi: 10.1021/bm100136y. [Available online].

Evans, L. C. *Partial Differential Equations, 2nd ed.* American Mathematical Society, 2010. ISBN 9780821849743.

Fefferman, C. L. Existence and smoothness of the Navier-Stokes equation. http://www.claymath.org/library/monographs/MPPc.pdf, 2000. [Available online].

Flory, P. J. Thermodynamic relations for high elastic materials. *Transactions of the Faraday Society*. 1961, 57, p. 829–838. doi: 10.1039/tf9615700829. [Available online].

Fook, S. J. L. et al. Elastic constants of inflated lobes of dog lungs. *Journal of Applied Physiology*. 1976, 40, 4, p. 508–513. [Available online].

Freed, A. D. – Einstein, D. R. An implicit elastic theory for lung parenchyma. *International Journal of Engineering Science*. 2013, 62, p. 31–47. doi: 10.1016/j.ijengsci.2012.08.003. [Available online].

Freed, A. D. – Liao, J. – Einstein, D. R. A membrane model from implicit elasticity theory: application to visceral pleura. *Biomechanics and Modeling in Mechanobiology*. 2013, 13, 4, p. 871–881. doi: 10.1007/s10237-013-0542-8. [Available online].

Fuchs, M. – Seregin, G. *Variational methods for problems from plasticity theory and for generalized Newtonian fluids*. Springer-Verlag Berlin Heidelberg, 2000. ISBN 9783540444428.

Fung, Y. C. Elasticity of soft tissues in simple elongation. *American Journal of Physiology*. 1967, 213, 6, p. 1532–1544. [Available online].

Gent, A. N. A new constitutive relation for rubber. *Rubber chemistry and technology*. 1996, 69, 1, p. 59–61. doi: 10.5254/1.3538357. [Available online].

Geymonat, G. – Suquet, P. – Nédélec, J. C. Functional spaces for Norton-Hoff materials. *Mathematical Methods in the Applied Sciences*. 1986, 8, 1, p. 206–222. doi: 10.1002/mma.1670080113. [Available online].

Gou, K. et al. Modeling fracture in the context of a strain-limiting theory of elasticity: A single plane-strain crack. *International Journal of Engineering Science*. 2015, 88, p. 73–82. doi: 10.1016/j.ijengsci.2014.04.018. [Available online].

Gross, D. – Yu, S. W. The singular field near a sharp notch with mixed boundary conditions for hardening materials under longitudinal shear. *Theoretical and applied fracture mechanics*. 1987, 8, 3, p. 199–203. doi: 10.1016/0167-8442(87)90046-2. [Available online].

Gurtin, M. E. – Mizel, V. J. – Williams, W. O. A note on Cauchy's stress theorem. *Journal of Mathematical Analysis and Applications*. 1968, 22, 2, p. 398–401. doi: 10.1016/0022-247X(68)90181-9. [Available online].

Hao, Y. L. et al. Super-elastic titanium alloy with unstable plastic deformation. *Applied Physics Letters*. 2005, 87, 9, p. 91906–91906. doi: 10.1063/1.2037192. [Available online].

Hill, R. The elastic behaviour of a crystalline aggregate. *Proceedings of the Physical Society. Section A*. 1952, 65, 5, p. 349–354. doi: 10.1088/0370-1298/65/5/307. [Available online].

Hlaváček, I. – Nečas, J. On inequalities of Korn's type. *Archive for Rational Mechanics and Analysis*. 1970, 36, 4, p. 312–334. doi: 10.1007/bf00249518. [Available online].

Hobby, J. D. MetaPost A user's manual. https://www.tug.org/docs/metapost/mpman.pdf, 2017. [Available online].

Holzapfel, G. A. *Nonlinear Solid Mechanics: A Continuum Approach for Engineering*. Wiley, 2000. ISBN 9780471823193.

Horgan, C. O. – Saccomandi, G. Anti-plane shear deformations for non-Gaussian isotropic, incompressible hyperelastic materials. *Proceedings of the Royal Society of London A: Mathematical, Physical and Engineering Sciences*. 2001, 457, 2012, p. 1999–2017. doi: 10.1098/rspa.2001.0798. [Available online].

Horgan, C. O. – Saccomandi, G. Constitutive Modelling of Rubber-Like and Biological Materials with Limiting Chain Extensibility. *Mathematics and Mechanics of Solids*. 2002, 7, 4, p. 353–371. doi: 10.1177/108128028477. [Available online].

Horgan, C. O. – Saccomandi, G. Constitutive Models for Compressible Nonlinearly Elastic Materials with Limiting Chain Extensibility. *Journal of Elasticity*. 2004, 77, 2, p. 123–138. doi: 10.1007/s10659-005-4408-x. [Available online].

Horgan, C. O. – Saccomandi, G. A description of arterial wall mechanics using limiting chain extensibility constitutive models. *Biomechanics and Modeling in Mechanobiology*. 2003, 1, 4, p. 251–266. doi: 10.1007/s10237-002-0022-z. [Available online].

Horgan, C. O. – Saccomandi, G. Phenomenological Hyperelastic Strain-Stiffening Constitutive Models for Rubber. *Rubber Chemistry and Technology*. 2006, 79, 1, p. 152–169. doi: 10.5254/1.3547924. [Available online].

Hou, F. Q. et al. Nonlinear elastic deformation behaviour of Ti-30Nb-12Zr alloys. *Scripta Materialia*. 2010, 63, 1, p. 54–57. doi: 10.1016/j.scriptamat.2010.03.011. [Available online].

Itou, H. – Kovtunenko, V. A. – Rajagopal, K. R. Nonlinear elasticity with limiting small strain for cracks subject to non-penetration. *Mathematics and Mechanics of Solids*. 2016, p. 1–13. doi: 10.1177/1081286516632380. [Available online].

Itskov, M. *Tensor Algebra and Tensor Analysis for Engineers: With Applications to Continuum Mechanics*. Springer Science & Business Media, 2009. ISBN 9783540939078.

Jun, Q. – Yuqiu, L. Sub-region mixed FEM for calculating stress intensity factor of antiplane notch in bi-material. *Engineering fracture mechanics*. 1992, 43, 6, p. 1003–1007. doi: 10.1016/0013-7944(92)90029-E. [Available online].

Knees, D. – Sändig, A.-M. *Multifield Problems in Solid and Fluid Mechanics*, Regularity of Elastic Fields in Composites, p. 331–360. Springer Berlin Heidelberg, 2006. ISBN 9783540349617.

Knees, D. – Sändig, A.-M. Stress behaviour in a power-law hardening material, 2004. [Available online].

Knowles, J. K. The finite anti-plane shear field near the tip of a crack for a class of incompressible elastic solids. *International Journal of Fracture*. 1977, 13, 5, p. 611–639. doi: 10.1007/BF00017296. [Available online].

Korn, M. A. Sur les équations de l'élasticité. *Annales scientifiques de l'École Normale Supérieure*. 1907, 24, p. 9–75. [Available online].

Kulvait, V. – Málek, J. – Rajagopal, K. R. Anti-plane stress state of a plate with a V-notch for a new class of elastic solids. *International Journal of Fracture*. 2013, 179, 1-2, p. 59–73. doi: 10.1007/s10704-012-9772-5. [Available online].

Kulvait, V. – Málek, J. – Rajagopal, K. R. Modeling Gum Metal and other newly developed titanium alloys within a new class of constitutive relations for elastic bodies. http://ncmm.karlin.mff.cuni.cz/db/attachments/single/411, 2017. Revised version submitted to Archives of Mechanics.

Kwak, D. Y. Finite Element Spaces, lecture notes. http://mathsci.kaist.ac.kr/~dykwak/Courses/Num765-08/FEM-theory.pdf, 2014. [Available online].

Little, R. W. S. History of Continuum Mechanics, 2007.

Liu, I. S. A Continuum Mechanics Primer On Constitutive Theories of Materials. www.im.ufrj.br/~liu/Papers/MCURS.pdf, 2006. [Available online].

Liu, I. S. *Continuum Mechanics*. Springer Science & Business Media, 2013. ISBN 9783662050569.

Logg, A. – Mardal, K. A. – Wells, G. *Automated Solution of Differential Equations by the Finite Element Method: The FEniCS Book*. Springer Science & Business Media, 2012. ISBN 9783642230998.

Love, A. E. H. *A Treatise on the Mathematical Theory of Elasticity*. Vol 1. Cambridge University Press, 1927. ISBN 9781107618091.

Machado, A. R. – Wallbank, A. J. Machining of titanium and its alloys a review. *Proceedings of the Institution of Mechanical Engineers, Part B: Journal of Engineering Manufacture*. 1990, 204, 1, p. 53–60. doi: 10.1007/978-3-662-43902-9_1. [Available online].

Minty, G. J. On a monotonicity method for the solution of nonlinear equations in Banach spaces. *Proceedings of the National Academy of Sciences of the United States of America*. 1963, 50, 6, p. 1038–1041. doi: 10.1073/pnas.50.6.1038. [Available online].

Morgan, A. J. A. Some properties of media defined by constitutive equations in implicit form. *International Journal of Engineering Science*. 1966, 4, 2, p. 155–178. doi: 10.1016/0020-7225(66)90021-8. [Available online].

Nagasako, N. – Asahi, R. – Hafner, J. First-principles Study of Gum-metal Alloys: Mechanism of Ideal Strength. *R&D Review of Toyota CRDL*. 2013, 44, 2, p. 61–68. [Available online].

Neal, C. et al. Titanium in UK rural, agricultural and urban/industrial rivers: Geogenic and anthropogenic colloidal/sub-colloidal sources and the significance of within-river retention. *Science of the Total Environment*. 2011, 409, 10, p. 1843–1853. doi: 10.1016/j.scitotenv.2010.12.021. [Available online].

Neuber, H. Theory of stress concentration for shear-strained prismatical bodies with arbitrary nonlinear stress-strain law. *Journal of Applied Mechanics*. 1961, 28, 4, p. 544–550. doi: 10.1115/1.3641780. [Available online].

Obbard, E. G. et al. Mechanics of superelasticity in Ti-30Nb-(8-10)Ta-5Zr alloy. *Acta Materialia*. 2010, 58, 10, p. 3557–3567. doi: 10.1016/j.actamat.2010.02.010. [Available online].

Oden, J. T. A short course on nonlinear continuum mechanics. http://users.ices.utexas.edu/~arbogast/cam397/oden0908.pdf, 2008. [Available online].

Ore, E. – Durban, D. Boundary effects at a notch tip in anti-plane shear. *International journal of fracture*. 1988, 38, 1, p. 15–24. doi: 10.1007/BF00034273. [Available online].

Ortiz, A. – Bustamante, R. – Rajagopal, K. R. A numerical study of a plate with a hole for a new class of elastic bodies. *Acta Mechanica*. 2012, 223, 9, p. 1971–1981. doi: 10.1007/s00707-012-0690-4. [Available online].

Ortiz, A. – Bustamante, R. – Rajagopal, K. R. A numerical study of elastic bodies that are described by constitutive equations that exhibit limited strains. *International Journal of Solids and Structures*. 2014, 51, 3, p. 875–885. doi: 10.1016/j.ijsolstr.2013.11.014. [Available online].

Penn, R. W. Volume Changes Accompanying the Extension of Rubber. *Transactions of The Society of Rheology (1957-1977)*. 1970, 14, 4, p. 509–517. doi: 10.1122/1.549176. [Available online].

Poincaré, H. Sur les Equations aux Dérivées Partielles de la Physique Mathématique. *American Journal of Mathematics*. 1890, 12, 3, p. 211–294. doi: 10.2307/2369620. [Available online].

R Core Team. R: A Language and Environment for Statistical Computing, Reference Index. http://cran.r-project.org/doc/manuals/r-release/fullrefman.pdf, 2016. [Available online].

Rajagopal, K. R. Conspectus of concepts of elasticity. *Mathematics and Mechanics of Solids*. 2011a, 16, 5, p. 536–562. doi: 10.1177/1081286510387856. [Available online].

Rajagopal, K. R. The elasticity of elasticity. *Zeitschrift für angewandte Mathematik und Physik*. 2007, 58, 2, p. 309–317. doi: 10.1007/s00033-006-6084-5. [Available online].

Rajagopal, K. R. On the Flows of Fluids Defined through Implicit Constitutive Relations between the Stress and the Symmetric Part of the Velocity Gradient. *Fluids*. 2016, 1, 2, p. 1–14. doi: 10.3390/fluids1020005. [Available online].

Rajagopal, K. R. On Implicit Constitutive Theories. *Applications of Mathematics*. 2003, 48, 4, p. 279–319. doi: 10.1023/A:1026062615145. [Available online].

Rajagopal, K. R. On a new class of models in elasticity. *Mathematical and Computational Applications*. 2010, 15, 4, p. 506–528. doi: 10.3390/mca15040506. [Available online].

Rajagopal, K. R. Non-linear elastic bodies exhibiting limiting small strain. *Mathematics and Mechanics of Solids*. 2011b, 16, 1, p. 122–139. doi: 10.1177/1081286509357272. [Available online].

Rajagopal, K. R. On the nonlinear elastic response of bodies in the small strain range. *Acta Mechanica*. 2014, 225, 6, p. 1545–1553. doi: 10.1007/s00707-013-1015-y. [Available online].

Rajagopal, K. R. – Srinivasa, A. R. On a class of non-dissipative materials that are not hyperelastic. *Proceedings of the Royal Society A: Mathematical, Physical and Engineering Sciences*. 2009, 465, 2102, p. 493–500. doi: 10.1098/rspa.2008.0319. [Available online].

Rajagopal, K. R. – Srinivasa, A. R. On the response of non-dissipative solids. *Proceedings of the Royal Society A: Mathematical, Physical and Engineering Sciences*. 2007, 463, 2078, p. 357–367. doi: 10.1098/rspa.2006.1760. [Available online].

Rajagopal, K. R. – Walton, J. R. Modeling fracture in the context of a strain-limiting theory of elasticity: a single anti-plane shear crack. *International Journal of Fracture*. 2011, 169, 1, p. 39–48. doi: 10.1007/s10704-010-9581-7. [Available online].

Ramberg, W. – Osgood, W. R. Description of stress-strain curves by three parameters. https://ntrs.nasa.gov/search.jsp?R=19930081614, 1943. [Available online].

Rasmussen, K. J. R. Full-range stress-strain curves for stainless steel alloys. *Journal of Constructional Steel Research*. 2003, 59, 1, p. 47–61. doi: 10.1016/S0143-974X(02)00018-4. [Available online].

Rellich, F. Ein Satz über mittlere Konvergenz. *Nachrichten von der Gesellschaft der Wissenschaften zu Göttingen, Mathematisch-Physikalische Klasse*. 1930, 408, p. 30–35. [Available online].

Reuss, A. Berechnung der Flieggrenze yon Mischkristallen auf Grund der Plastizithtsbedingung für Einkristalle. *Z. Angew. Math. Mech*. 1929, 9, 1, p. 49–58. doi: 10.1002/zamm.19290090104. [Available online].

Rice, J. R. Stresses Due to a Sharp Notch in a Work-Hardening Elastic-Plastic Material Loaded by Longitudinal Shear. *Journal of Applied Mechanics*. 1967, 34, 2, p. 287–298. doi: 10.1115/1.3607681. [Available online].

Rivlin, R. S. – Thomas, A. G. Large elastic deformations of isotropic materials. VIII. Strain distribution around a hole in a sheet. *Philosophical Transactions of the Royal Society of London A: Mathematical, Physical and Engineering Sciences*. 1951, 243, 865, p. 289–298. doi: 10.1098/rsta.1951.0005. [Available online].

Roman, S. *Advanced Linear Algebra*. Springer Science & Business Media, 2007. ISBN 9780387728315.

Roubíček, T. *Nonlinear Partial Differential Equations with Applications*. Springer Science & Business Media, 2013. ISBN 9783034805131.

Sadd, M. H. *Elasticity: Theory, Applications, and Numerics*. Academic Press, 2009. ISBN 9780123744463.

Saito, T. et al. Multifunctional Alloys Obtained via a Dislocation-Free Plastic Deformation Mechanism. *Science*. 2003, 300, 5618, p. 464–467. doi: 10.1126/science.1081957. [Available online].

Sakaguch, N. – Niinomi, M. – Akahori, T. Tensile deformation behavior of Ti-Nb-Ta-Zr biomedical alloys. *Materials transactions*. 2004, 45, 4, p. 1113–1119. doi: 10.2320/matertrans.45.1113. [Available online].

Schirra, O. D. New Korn-type inequalities and regularity of solutions to linear elliptic systems and anisotropic variational problems involving the trace-free part of the symmetric gradient. *Calculus of Variations and Partial Differential Equations*. 2012, 43, 1-2, p. 147–172. doi: 10.1007/s00526-011-0406-y. [Available online].

Sfyris, D. – Bustamante, R. On the treatment of non-solvable implicit constitutive relations in solid mechanics. *Zeitschrift für angewandte Mathematik und Physik*. 2014, 66, 3, p. 1165–1174. doi: 10.1007/s00033-014-0430-9. [Available online].

Shabana, A. A. *Computational Continuum Mechanics*. Cambridge University Press, 2011. ISBN 9781139505420.

Shaorui, Y. – Chao, Y. J. The singular field at the tip of a wedge-like rigid inclusion in a hardening material under longitudinal shear. *Engineering Fracture Mechanics*. 1990, 37, 2, p. 251–257. doi: 10.1016/0013-7944(90)90037-H. [Available online].

Talling, R. J. et al. Determination of (C11-C12) in Ti-36Nb-2Ta-3Zr-0.3O (wt.%) (Gum metal). *Scripta Materialia*. 2008, 59, 6, p. 669–672. doi: 10.1016/j.scriptamat.2008.05.022. [Available online].

Talling, R. J. et al. On the mechanism of superelasticity in Gum metal. *Acta Materialia*. 2009, 57, 4, p. 1188–1198. doi: 10.1016/j.actamat.2008.11.013. [Available online].

Truesdell, C. – Noll, W. *The Non-Linear Field Theories of Mechanics*. Springer Berlin Heidelberg, 1969. ISBN 9783662103883.

Truesdell, C. – Toupin, R. A. *Principles of Classical Mechanics and Field Theory / Prinzipien der Klassischen Mechanik und Feldtheorie*, The Classical Field Theories, p. 226–858. Springer Berlin Heidelberg, 1960. ISBN 9783642459436.

Turner, M. J. Stiffness and Deflection Analysis of Complex Structures. *Journal of the Aeronautical Sciences*. 1956, 23, 9, p. 805–823. doi: 10.2514/8.3664. [Available online].

Voigt, W. *Lehrbuch der kristallphysik (mit ausschluss der kristalloptik)*. B. G. Teubner Verlag, 1928.

Wickham, H. *ggplot2: Elegant Graphics for Data Analysis*. Springer-Verlag New York, 2009. ISBN 9780387981406.

Wikipedia. List of finite element software packages. https://en.wikipedia.org/wiki/List_of_finite_element_software_packages, 2017a. [Available online].

Wikipedia. Titanium alloy. http://en.wikipedia.org/w/index.php?title=Titanium_alloy, 2017b. [Available online].

Yavari, A. Compatibility equations of nonlinear elasticity for non-simply-connected bodies. *Archive for Rational Mechanics and Analysis*. 2013, 209, 1, p. 237–253. doi: 10.1007/s00205-013-0621-0. [Available online].

Yokonuma, T. *Tensor Spaces and Exterior Algebra*. American Mathematical Soc., 1992. ISBN 9780821827963.

Yosida, K. *Functional Analysis*. Springer Science & Business Media, 1995. ISBN 9783540586548.

Zappalorto, M. – Lazzarin, P. In-plane and out-of-plane stress field solutions for V-notches with end holes. *International journal of fracture*. 2011, 168, 2, p. 167–180. doi: 10.1007/s10704-010-9567-5. [Available online].

Zhang, S. Q. et al. Fatigue properties of a multifunctional titanium alloy exhibiting nonlinear elastic deformation behavior. *Scripta Materialia*. 2009, 60, 8, p. 733–736. doi: 10.1016/j.scriptamat.2009.01.007. [Available online].

Zhang, Y. W. et al. Elastic properties of Ti-24Nb-4Zr-8Sn single crystals with bcc crystal structure. *Acta Materialia*. 2011, 59, 8, p. 3081–3090. doi: 10.1016/j.actamat.2011.01.048. [Available online].

Zienkiewicz, O. C. – Cheung, Y. K. *The finite element method in structural and continuum mechanics: numerical solution of problems in structural and continuum mechanics*. McGraw-Hill, 1967.

Zienkiewicz, O. C. – Taylor, R. L. *The Finite Element Method for Solid and Structural Mechanics*. Butterworth-Heinemann, 2013. ISBN 9780080951362.